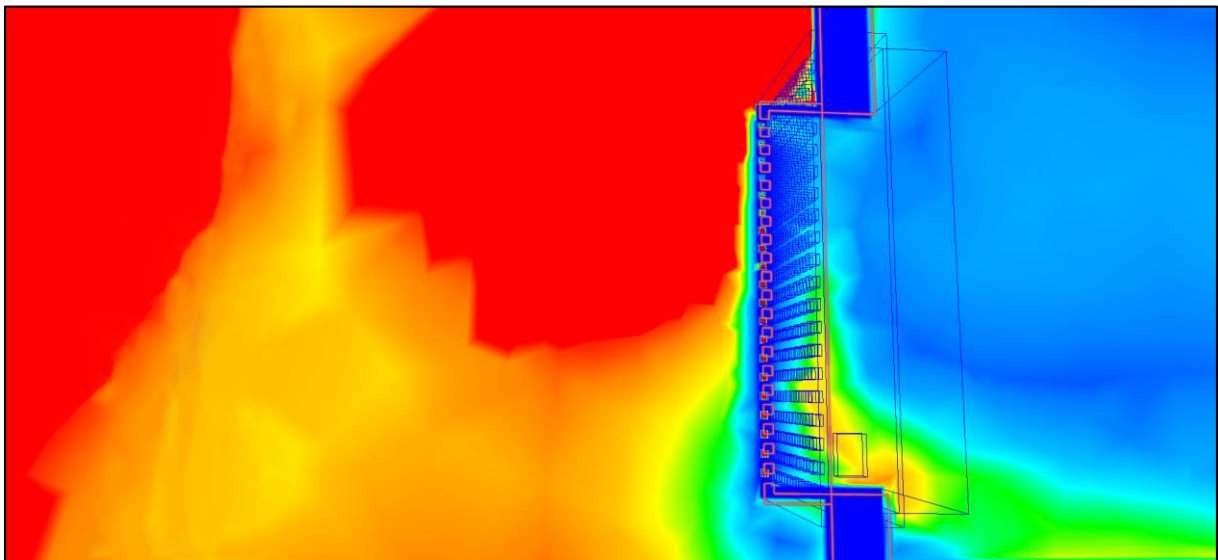


Technische Universität München  
Lehrstuhl für energieeffizientes und nachhaltiges Planen und Bauen  
Prof. Dr.-Ing. Werner Lang



**Dissertation**

**Potential of vernacular architecture for an integrated model  
for passive design in hot-arid climate**

**Wael Ahmad Yousuf Mousa**



TECHNISCHE UNIVERSITÄT MÜNCHEN

Fakultät Architektur

Lehrstuhl für energieeffizientes und nachhaltiges Planen und Bauen

Potential of vernacular architecture for an integrated model for  
passive design in hot-arid climate

Wael Ahmad Yousuf Mousa

Vollständiger Abdruck der von der Fakultät Architektur der Technischen Universität  
München zur Erlangung des akademischen Grades eines

Doktor-Ingenieurs

genehmigten Dissertation.

Vorsitzender: Univ.-Prof. Dr.-Ing. Rainer Barthel

Prüfer der Dissertation: 1. Univ.-Prof. Dr.-Ing. Werner Lang  
2. Univ.-Prof. Dipl.-Ing. Thomas Auer

Die Dissertation wurde am 24.05.2016 bei der Technischen Universität München  
eingereicht und durch die Fakultät Architektur am 04.07.2016 angenommen.



## Acknowledgments

In the beginning and at the end, all praises and thanks are due to God.

This dissertation is the yield of efforts of several parties. The doctoral study, as well as the thesis printing cost, were financed through a scholarship from the German Academic Exchange Service (DAAD). However, the research work would not have been possible without various support of numerous individuals.

First of all I would like to express my sincere gratitude to my academic supervisor Prof. Werner Lang for his continuous support which expanded even from the early stages of the research proposal until the time of writing these lines. I would like to thank him for his guidance, insight and patience to elaborate my knowledge and background into a meaningful scientific work. I am sincerely grateful as well to Prof. Thomas Auer, my second supervisor, for his enlightening and inspiring thoughts which caused a real paradigm shift and opened up a whole new range to this research.

I would like to thank all my colleagues in the Institute of Energy Efficient and Sustainable Design and Building (ENPB) at the *Technische Universität München* (TUM). I would like to thank John Anderson and all my fellow doctoral candidates for their support, feedback and stimulating discussions. In particular I sincerely thank Manuel Lindauer and Haythem Chelly for their outstanding contribution to the simulation work; the experiments in this research would not have been successfully done without your support.

Sincere thanks goes to Dr. Waleed Yousef for the deliberate work he has done in the regression analysis and the inference of the air change rate prediction rule which is a crucial milestone in this research. I also would like to thank the staff of the Egyptian Supreme Council of Antiquity for enabling the field measurements in the monuments in Cairo, in particular I thank Mrs. Hwayda Sobhy for her support.

Finally, I am really indebted to all my family members, especially my parents to whom I will always owe every success. I would like to express deepest gratitude to Susanne; thank you for being always there; inspiring, sincere and supportive wife. Thank you Aleyah and Amina; it is really great having such daughters.



## **Abstract**

In addition to the correspondence to cultural background and social customs, it is commonly acknowledged that traditional buildings embed many climatically responsive features which contribute to the achievement of indoor thermal comfort. Vernacular architecture was always adopting physical principles which were processed within the urban settings and the building as an integrated structure. This research examines the potentials of traditional building methods in hot-arid climate to assess the role of common features incorporated within. A principle passive design strategy is determined and different nominated features are examined through the empirical study within a holistic passive framework. Assessments focused on the impact of different features and building material, as well as the interoperability of those features within the integral passive system.

The experimental study employed different thermal simulation tools, i.e. TRNSYS 17 and computational fluid dynamics (CFD). Simulation models were validated against field measurements of indoor temperatures for selected cases. A comparative analysis applied to adopt a case which showed the validity to be introduced as an integrated model for passive design. The analysis verified the role of thermal mass and shading mechanisms in lowering the indoor temperature. Through pattern recognition an equation to predict the air change rates was subsequently inferred from the aggregated results obtained through the CFD modelling for the adopted case. The air flow analysis addressed the role of the courtyard and fenestration system in the natural ventilation process. Through thermal simulations and air-flow modelling the empirical work demonstrated the influence of the adopted features on lowering the indoor temperature and improving the indoor air quality. The study confirms the contribution of such methods to the enhancement of the indoor thermal comfort and energy efficiency.



# Table of Contents

<b>List of Figures</b>	<b>iii</b>
<b>List of Tables</b>	<b>vii</b>
<b>1 Introduction</b>	<b>1</b>
1.1 Research background.....	1
1.2 Scientific goal.....	2
1.3 The current state of the art.....	3
1.4 Research methodology.....	3
1.5 Research outline.....	4
<b>2 Climate, tradition, and the passive design strategy</b>	<b>7</b>
2.1 Introduction.....	7
2.2 Climate.....	8
2.3 Requirements of indoor thermal comfort.....	10
2.4 Solar geometry and building.....	12
2.5 The traditional house in context.....	16
2.5.1 The urban built form.....	16
2.5.2 Construction method and material.....	18
2.5.3 Components of the house and space design.....	20
2.5.4 Traditional house in response to climate.....	24
2.6 Relevant results in the existing literature.....	29
2.7 The passive design strategy.....	31
2.8 Conclusion.....	32
<b>3 Measurements and observations</b>	<b>33</b>
3.1 Introduction.....	33
3.2 Case study (CM).....	35
3.2.1 Measurements (CM).....	36
3.2.2 Observations (CM).....	36
3.3 Case study (CT1).....	39
3.3.1 Measurements (CT1).....	43
3.3.2 Observations (CT1).....	44
3.4 Case study (CT2).....	49
3.4.1 Measurements (CT2).....	51
3.4.2 Observations (CT2).....	52
3.5 Conclusion.....	57

<b>4 Experiments (1), thermal mass and shading mechanisms</b>	<b>59</b>
4.1 Introduction.....	59
4.2 Simulation package.....	60
4.2.1 Presumption of air change rate (ACH).....	61
4.2.2 Validation of the simulation model.....	61
4.3 Observations and analysis.....	69
4.3.1 Indoor temperature and heat storage capacity.....	72
4.3.2 Solar radiation.....	75
4.4 The role of shading mechanisms.....	81
4.5 Conclusion.....	85
<b>5 Experiments (2), air flow</b>	<b>87</b>
5.1 Introduction.....	87
5.2 Wind analysis and CFD simulations.....	88
5.2.1 Configuration of the CFD model and time-steps.....	89
5.2.2 Air flow analysis.....	92
5.2.3 Openings' directional flow-functionality (ODFF).....	98
5.2.4 Cross ventilation breakdown assessment .....	100
5.2.5 Air flow and indoor temperature.....	103
5.3 Pattern recognition design and assessment for ACH modeling.....	106
5.3.1 Pattern recognition framework.....	106
5.3.2 Classification and regression trees (CART) for ACH modeling.....	107
5.4 Validation of the simulation model upon predicted ACH.....	108
5.5 Conclusion.....	110
<b>6 Temperature, comfort and energy; conclusive analysis</b>	<b>111</b>
6.1 Introduction.....	111
6.2 Ventilation schedule.....	112
6.3 Indoor temperature.....	113
6.4 Thermal comfort.....	117
6.5 Energy efficiency.....	121
6.6 Conclusion.....	126
<b>Potentials for future building practices</b>	<b>127</b>
<b>References</b>	<b>131</b>
<b>List of abbreviations</b>	<b>137</b>
<b>Appendix A</b>	<b>139</b>
<b>Appendix B</b>	<b>153</b>
<b>Appendix C</b>	<b>155</b>

# List of Figures

1.1 Construction, climate, culture and function; the mutual influence.....	1
1.2 Step-process and work flow.....	4
2.1 World Climate Zones.....	8
2.2 Annual sum of irradiation, Africa.....	9
2.3 Precipitation chart for Cairo.....	9
2.4 Prevailing wind frequency Hrs. Cairo.....	9
2.5 Daily temperature chart for Cairo.....	9
2.6 Radiation chart for Cairo.....	9
2.7 Sunshine chart for Cairo.....	9
2.8 Psychometric chart, comfort zone for Cairo.....	10
2.9 Influential factors for thermal comfort.....	11
2.10 Thermal comfort sensation scale.....	12
2.11 Sun Path, Cairo.....	13
2.12 Sun angles.....	13
2.13 Shadowing angles.....	13
2.14 Climate influence on build form.....	14
2.15 Sun at winter solstice (21 December at 12:00 pm).....	15
2.16 Sun at summer solstice (21 December at 12:00 pm).....	15
2.17 Quarters, major and minor roads, old Cairo.....	16
2.18 Secondary street east-west orientation.....	16
2.19 Narrow street shading.....	17
2.20 Minimized visual contact.....	17
2.21 Staggered entrances of Houses.....	19
2.22 Superposed beam construction with stepped floor slab.....	19
2.23 Succession of spaces around the courtyard.....	20
2.24 Principle components of the house.....	20
2.25 View of the courtyard towards south.....	21
2.26 Influence of geometry of the courtyard in protecting from dust.....	21
2.27 Interior view in a hall, looking towards the northern façade.....	22
2.28 Looking up at the <i>Shokhshekha</i> (skylight).....	22
2.29 Cross section showing conceptual air-flow and cross ventilation.....	22
2.30 View from the <i>maq'ad</i> (balcony).....	23
2.31 <i>Mashrabiya</i> overlooking the courtyard in House of al-Suhaimy.....	23
2.32 Gradual perforation of balusters of the <i>mashrabiya</i> .....	23
2.33 Aspect ratio and building shading.....	24
2.34 Convective current in street canyon.....	24
2.35 The heat transfer at wall surface.....	24
2.36 The heat transfer at window glass.....	24
2.37 Heat transfer and heat gain/loss in the building.....	25
2.38 Incident radiation on a white surface.....	25
2.39 Means of heat gain in buildings.....	25

2.40 Means of heat loss in buildings.....	25
2.41 Convective current in the courtyard.....	26
2.42 Radiant cooling through the roof.....	27
2.43 Convective ventilation, stack effect.....	27
2.44 Creating a low pressure area inside of a built-up space.....	27
2.45 Day-time room temperature in July, with different air exchange rates.....	27
2.46 <i>Mashrabiya</i> of turned wood.....	28
2.47 Required cooling loads with different opening sizes.....	28
2.48 The effect of light falling on a cylinder.....	28
2.49 Passive cooling strategy in the traditional building.....	31
2.50 Proposed integrated model.....	32
3.1 Selected cases' locations.....	34
3.2 House of Zeinab Khatun (CT1), urban setting.....	34
3.3 House of Amna bint Salem (CT2), urban setting.....	34
3.4 Heliopolis apartment (CM), urban setting.....	34
3.5 CM, site.....	35
3.6 CM, general view.....	35
3.7 CM, floor plan showing measurement spots.....	35
3.8 CM, data loggers' installation.....	36
3.9 CM, measured temperatures 18-24 April.....	37
3.10 CM, measured outdoor temperature against real weather data.....	37
3.11 CM, measured temperature, Aug. 13 to Sep. 3.....	38
3.12 CM, average day temperature, Aug. 13 to Sep. 3.....	38
3.13 CT1, site layout.....	39
3.14 CT1, exterior view of the main façade, south-west.....	39
3.15 CT1, a. ground floor plan, b. first floor plan.....	39
3.16 CT1, view of the courtyard from the roof.....	40
3.17 CT1, cross section in the grand hall and the courtyard.....	40
3.18 CT1, grand hall, <i>mashrabiya</i> .....	41
3.19 CT1, grand hall, interior view.....	41
3.20 CT1, multiple openings of the secondary hall on the courtyard.....	42
3.21 CT1, interior view of the secondary hall.....	42
3.22 CT1, floor plan showing measurement spots.....	43
3.23 CT1, data loggers' installation.....	43
3.24 CT1-GH, measured temperatures in the grand hall and courtyard.....	45
3.25 CT1-GH, average day temperature.....	45
3.26 CT1-GH, measured Indoor temperature and relative humidity.....	46
3.27 CT1-GH, average day illumination in the grand hall.....	46
3.28 CT1-SH, comparison between indoor temperatures in the secondary hall.....	47
3.29 CT1-SH, measured Indoor temperature and relative humidity.....	47
3.30 CT1-SH, average day temperature.....	48
3.31 CT1-GH vs. SH, average day temperature.....	48
3.32 CT2, site layout.....	49
3.33 CT2, exterior view, south-west.....	49
3.34 CT2, view towards the mosque.....	49
3.35 CT2, a. ground floor plan, b. first floor plan.....	49
3.36 CT2, view from the courtyard towards the balcony, south-east.....	50
3.37 CT2, Interior view of the main hall.....	50
3.38 CT2, Floor plan showing measurement spots.....	51
3.39 CT1, data loggers' installation.....	51
3.40 CT2-MH, measured Temperatures in the main hall and courtyard.....	53

3.41 CT2-MH, average day temperature.....	53
3.42 CT2-MH, a two-day record of temperature on the wall and window screen.....	54
3.43 CT2-MH, an average day of temperature at level 2.5 m and 6 m.....	54
3.44 CT2-MH, measured Indoor temperature and relative humidity.....	55
3.45 CT2-MH, average day illumination in the grand hall.....	55
3.46 CT1-CT2-CM, measured ambient temperature in three cases.....	56
3.47 CT1-CT2-CM, Average day ambient temperature in three cases.....	57
4.1 Obtained dry bulb temperature compared to test reference data.....	60
4.2 CM, 3d model, TRNSYS 3D tool.....	62
4.3 CT1, 3D model, TRNSYS3d tool.....	62
4.4 CT2, 3D model, TRNSYS3d tool.....	62
4.5 CT1, window screen modeling.....	62
4.6 CM, simulation results for indoor temperature against measured data.....	64
4.7 CM, average day temperature, Simulation results against measured data.....	64
4.8 CT1-GH, average day temperature. Values of ACH 6, 8, and 10/h.....	65
4.9 CT1-GH, simulation results for indoor temperature, ACH 6/h.....	65
4.10 CT1-GH, average day temperature, ACH 6/h. conformity $\pm 0.3\text{ C}^\circ$ .....	66
4.11 CT1-SH, simulation results for indoor temperature, values of ACH 6/h.....	66
4.12 CT1-SH, average day temperature, ACH 6/h. conformity $\pm 0.3\text{ C}^\circ$ .....	67
4.13 CT2-MH, average day temperature, values of ACH 6, 8, and 10/h.....	67
4.14 CT2-MH, Simulation results for indoor temperature, ACH 6/h.....	68
4.15 CT2-MH, average day temperature, conformity $\pm 0.3\text{ C}^\circ$ .....	68
4.16 CM, CT2, and CT1-SH, no ventilation.....	70
4.17 CM, CT2, and CT1-SH, average day indoor temperature, no ventilation.....	70
4.18 CM, CT2, and CT1-SH, ACH 6/h, average day.....	71
4.19 CT1-GH, matrix-plot of outdoor and indoor temperatures.....	72
4.20 CM, matrix-plot of outdoor and indoor temperatures.....	72
4.21 CT1-GH, regression of indoor on outdoor temperature, 17-31 Aug.....	73
4.22 CT1-GH, regression of indoor on outdoor temperature, Jun.-Aug.....	73
4.23 CT1-GH, indoor on outdoor temperature and before 12 hours, Jun.-Aug.....	74
4.24 CM, average daily transmitted solar radiation.....	75
4.25 CM, shadow on the south west façade at 10 am 11 am. 4 pm and 6 pm.....	76
4.26 CM, average daily incident solar radiation, shaded and un-shaded walls.....	76
4.27 CM, north-west wall, average daily incident solar radiation.....	76
4.28 CM, monthly average solar gains.....	76
4.29 CT1, courtyard solar gain.....	77
4.30 CT1 total direct radiation.....	77
4.31 CT1 courtyard daytime shadowing, 23 <sup>rd</sup> August.....	77
4.32 Courtyard shadow range on different façade orientations.....	78
4.33 CT1, average daily incident solar radiation, roof GH and SH.....	79
4.34 CT1, average daily incident radiation on the courtyard walls north-west.....	79
4.35 CT1, average daily incident radiation on the courtyard walls south-west.....	79
4.36 CT1, monthly average direct solar gains, GH and SH.....	79
4.37 CM, CT1-SH, average day indoor temperature, scheduled ACH 6/h.....	80
4.38 CM, simulation results for indoor temperature, 18-24 April.....	81
4.39 CM, a building opposite to the south-west façade, as a shading device.....	82
4.40 CM, window screen incorporated on the south-west façade.....	82
4.41 CM, comparison between the three situations.....	83
4.42 CM, total solar radiation transmitted; with and without a shading.....	83
4.43 CM, predicted annual indoor temperature, base case vs modified models.....	84
4.44 Resulted shading in different cases.....	84

5.1	Cairo wind direction wind speed distribution respectively, June – August.....	89
5.2	Simulation time-steps.....	90
5.3	Building orientation and prevailing wind.....	90
5.4	Created geometry for the simulation model and urban setting.....	90
5.5	Simulation environment, sample scenario north wind.....	91
5.6	Mesh sizing for air volumes.....	91
5.7	Transient simulation, northern wind.....	92
5.8	Wind velocity range around the building and inside the courtyard.....	92
5.9	Observed velocity nodes.....	92
5.10	Cyclone behavior of wind inside the courtyard.....	92
5.11	Velocity magnitude at different nodes for all simulation scenarios.....	93
5.12	Openings variation of air inlet (+) and outlet (-).....	94
5.13	Distribution of air inlets (+) and outlets (-) for each wind direction.....	94
5.14	Matrix of opening directional flow functionality.....	98
5.15	Average Indoor velocity magnitude, GH, Jun.-Aug.....	99
5.16	Average ACH per direction and overall average for all scenarios.....	100
5.17	GH, air flow rate for different opening variations, 17 scenario, WNW.....	101
5.18	SH, air flow rate for different opening variations, 17 scenario, WNW.....	101
5.19	GH, ACH for different opening variations, 17 scenario, WNW.....	102
5.20	SH, ACH for different opening variations, 17 scenario, WNW.....	103
5.21	GH, correlation between air flow pattern and temperature gradient.....	104
5.22	SH, correlation between air flow pattern and temperature gradient.....	105
5.23	Indoor temperature gradient, different ventilation options for GH and SH.....	105
5.24	Predicted output from CART vs the simulated output of CFD.....	108
5.25	CT1-GH, simulation results for indoor temperature upon predicted ACH.....	109
5.26	CT1-SH, simulation results for indoor temperature upon predicted ACH.....	109
5.27	CT1-GH, average indoor temperature upon predicted ACH.....	109
5.28	CT1-SH, average indoor temperature upon predicted ACH.....	109
6.1	GH-SH, indoor temperatures, predicted ACH, natural ventilation, Jun-Aug.....	112
6.2	GH-SH, average summer day indoor temperatures, predicted ACH.....	113
6.3	GH, summer indoor temperature, base case vs no-screen model.....	114
6.4	SH, summer indoor temperature, base case vs no-screen model.....	114
6.5	GH, winter indoor temperature, base case vs no-screen model.....	114
6.6	SH, winter indoor temperature, base case vs no-screen model.....	114
6.7	GH, annual indoor temperature, base case vs brick-walls model.....	115
6.8	SH, annual indoor temperature, base case vs brick-walls model.....	115
6.9	GH, average summer indoor temperature, base case vs. modified models.....	116
6.10	Acceptable indoor operative temperature (acc. DIN EN 15251).....	118
6.11	GH-SH, summer indoor operative temperature, base case.....	119
6.12	GH-SH, summer indoor operative temperature, brick walls.....	119
6.13	GH-SH, summer indoor operative temperature, no-screen.....	120
6.14	GH-SH, winter indoor operative temperature, base case (acc. DIN EN 15251).....	121
6.15	GH-SH, winter indoor operative temperature, no-screen (acc. DIN EN 15251).....	121
6.16	GH, winter PMV, base case vs. modified model (no-screen) (acc. EN ISO 7730).....	121
6.17	SH, winter PMV, base case vs. modified model (no-screen) (acc. EN ISO 7730).....	121
6.18	GH-SH, monthly energy demand (kW) for cooling and heating.....	122
6.19	GH-SH, total annual energy demand (kw/h) for cooling and heating.....	123
6.20	GH-SH, modified model (no window-screens), monthly energy demand.....	124
6.21	GH-SH, modified model (brick walls), monthly energy demand.....	124
6.22	GH-SH, total annual energy demand, Base case vs. modified models.....	125

# List of Tables

2.1	Angles of declination and altitude at latitude 30° N, Cairo.....	15
3.1	CM, building description.....	35
3.2	CM, U-value of material.....	35
3.3	CT1, grand hall (GH) description.....	41
3.4	CT1, secondary hall (SH) description.....	42
3.5	CT1, sensors installation.....	43
3.6	CT2, main hall (MH) description.....	51
3.7	CT2, sensors installation.....	51
4.1	Smoke decay tests results for ACH and rooms description [2].....	61
4.2	CM, construction material and thermal properties.....	63
4.3	CT1-CT2, construction material and thermal properties.....	63
5.1	Cairo wind events, June – August 2014.....	88
5.2	Design-study scenarios.....	91
5.3	Visualization of air intake and output and percentages of occurrence (1).....	95
5.4	Visualization of air intake and output and percentages of occurrence (2).....	96
5.5	Visualization of air intake and output and percentages of occurrence (3).....	97
6.1	Average differences of indoor temperature, base case vs modified models.....	116
6.2	Assigned clothing factors and metabolic rates.....	118
6.3	Assigned clothing factors and metabolic rates.....	118
6.4	Energy saving of the base case compared to the modified models.....	125



# Chapter 1

## Introduction

### 1.1 Research background

The basic principle of regional vernacular architecture is to respond to the climatic pattern, geographic and topographic character and as well the cultural identity of a certain area. It reflects a high level of self-consciousness and respects the values derived from both spirits of place and time. Such values comprise cultural, social, and economic aspects which are directly influenced by regional climatic conditions, topography and natural building materials that substantially contribute to the formulation of a distinctive design criteria. The spirit of place stands for the architect's response to the distinctive climatic and geographic considerations in a certain place. It results in the regional architectural identity, which implies that there is something special about the architecture of a particular region, something that occurs nowhere else. The spirit of time however, stands for the response to the contemporary methods of construction, innovations, techniques and available design tools. It embodies the prevailing theories of the time. Hence, a value-centred architecture is that one which contextualizes the aspects of regional and cultural identity within the design process where functionality will be directly influenced by these aspects (fig. 1.1).

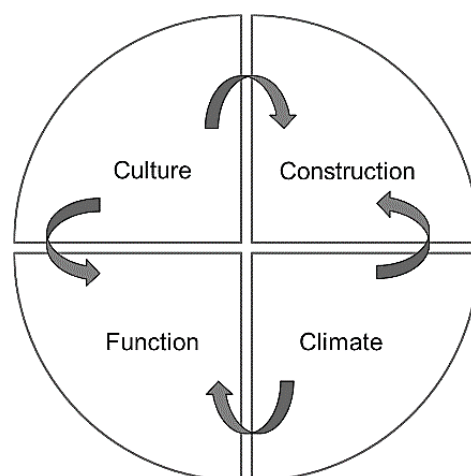


**Figure 1.1:** Construction, climate, culture and function; the mutual influence

With regards to the increased energy consumption worldwide and the ascending threat of the oil reserve being close to depletion, the construction sector consumes an average of 40% of the global energy consumption. The extensive adoption of active climate control methods in buildings and the complete reliance on air conditioning systems, especially in hot and arid climate zones such as Egypt, became more questionable in terms of energy efficiency as well as the rates of greenhouse gas emissions, and hence should be replaced by more energy-aware methods. The built environment hence should play a role in striking balance in the process and the adoption of more environmentally-aware and responsive passive systems is therefore a possible resolution in this context. The revitalisation of passive strategies for new architecture that count on the building as self-sufficient climate modifier arises as key elements in this respect.

The building as an entity closely resembles the human body with its skeleton, feeding and drainage system. The healthy building hence should breathe efficiently. In such a complicated system, the building envelope and elements of ventilation and shading work together as an integrated respiratory system. This system should be enhanced and maintained to the limit that securely suffice the building's inhabitants and restrain the acquisition of artificial respiration to the minimum limits. Such artificial inspiratory devices are exclusively represented in the active climate control methods and HVAC devices. Hence, a tendency towards dealing with the building as an inherited passive modifier should take place within the early design stages. In regions with hot and arid climate such as the Egyptian capital Cairo, where air temperature exceeds 40° C in the summer, the annual consumption of air-conditioning devices is enormous due to the relative long-term operation and capacity needed to reach the comfort zone of temperature in hot summer days. However, operation time of active climate control devices can be diminished through the development of passive building design and enhancement of the inherited climatic responsive capabilities of the building.

## 1.2 Scientific goal

The main research question is: "To what extent can traditional building solutions be efficient to establish a passive design model for hot climate?" The evaluation is based on indoor temperature, achieved levels of comfort and energy efficiency of the adopted model.

The study therefore aims to introduce an assessment of the effectiveness of the features adopted in traditional buildings in their entirety and interoperability. Further studies, based hence upon plausible quantification, can be conducted in the future to the adopted model to produce a more holistic and integrated strategy. The anticipated role of the proposed model is to mediate the need for active climate control intervention to the minimum limits, whether in terms of seasonal or diurnal operational time span or capacity. The anticipated results of the project can be concluded in the following:

1. Introduce an assessment of the contribution of traditional building techniques in lowering the indoor temperature in hot climate.
2. Optimization of energy efficiency of a selected building model.
3. Diminishment of the intervention of active systems for air cooling.
4. Improvement of indoor levels of comfort.

### 1.3 The current state of the art

A literature study was carried out for the following purposes:

1. Gain an overview of the subject (passive sustainable architecture).
2. Categorize existing information in support of the research work.
3. Draw conclusions as to which literature is of greatest relevance regarding the contribution to the overall body of knowledge of the topic.
4. Place own work in context of existing literature and determine how it departs from previous researches.

Through the literature review it was concluded that an abandon of research work is dedicated to investigate the performance of buildings that depend mainly on the passive solution for air cooling. These researches could be categorized into two majors:

1. General qualitative studies vary mainly between general surveys on vernacular and passive architecture, and social and stylistic authenticity.
2. Precise quantitative studies conducted to individual features.

However, an attempt to produce an integrated and inclusive passive system is rare to be found. The results and findings of the second group of researchers are of great significance to this project since they act as point of departure to the proposed evolutionary study. Results of the current literature and previous research work are discussed within the context of the first part of study. This research attempts to reinvestigate the aspects of the existing studies by correlation to the local parameters and deliberately integrate verified results within a holistic passive framework.

### 1.4 Research methodology

The study comprises two major parts, theoretical and empirical. The theoretical part starts with a study of the full climatic condition of Cairo in relation to the accumulative experience of vernacular architecture in Egypt and related features used for passive cooling. The study sheds light upon the cultural background and the readiness to absorb principles of sustainability. The procession of basic physical principles in the traditional building is then discussed within this section in order to draw better understanding of the particular roles of different features of the traditional building. Upon this understanding a primal passive design strategy is identified, which defines the most decisive factors and the manner of their operability.

The empirical part then comprises examining a number of selected buildings, through an analytical study and experimental research work. Field measurements for indoor temperatures took place in the selected cases. Simulations applied using selected tools and accordingly a comparative study was conducted to verify the adopted integrated model. Further simulation-based experiments conducted to the adopted model in order to obtain a plausible assessment of the role of analyzed features in lowering indoor temperature, achieving higher levels of thermal comfort and reduction in energy consumption. Figure 1.2 illustrates the work flow in this research.

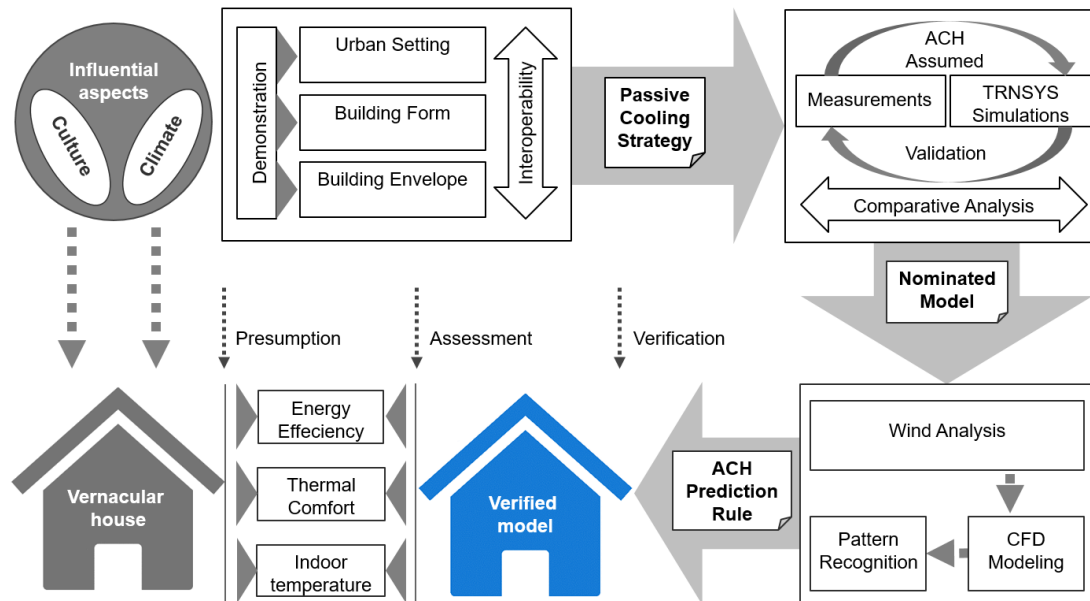


**Figure 1.2:** Step-process and work-flow

## 1.5 Research outline

The work through the step-process illustrated above is distributed over six chapters. This chapter, chapter 1, explains the background of the research, scientific goals, the structure and the work flow within the next chapters.

Chapter 2 comprises the theoretical part of the study which aims to draw a better understanding of the direct influence of climatic conditions and cultural aspects on vernacular architecture in Cairo. The objectives of this part are to demonstrate how the traditional building responded to cultural needs and climatic conditions. This chapter includes the following aspects:

1. An overview of climatic conditions and requirements of thermal comfort.
2. Traditional house and its components in response to cultural needs and climatic conditions.
3. Heat transfer and the procession of physical phenomenon within the traditional building's components.
4. Concluding the principle passive design strategy of traditional buildings and most decisive features.

The empirical work of the research then is encompassed within the next chapters which aim to examine the features concluded within the theoretical part. The main objective is to obtain quantifications and clear assessments of the impact of those features and the interrelation between them in response to the climatic conditions and solar geometry. The experiments embody field measurements in different cases, vernacular and contemporary cases.

Simulation models of the selected cases are created and validated against real measurements. Accordingly thermal and air flow simulations are consecutively conducted to obtain plausible assessments for the examined aspects. Subsequently the impacts of these features on both the levels of thermal comfort and energy efficiency are concluded.

The work in chapter 3 comprises field measurements for selected traditional houses of medieval time and a contemporary multifamily residential building. The field measurements took place in summer for indoor temperature in the three cases. The work in this chapter includes:

1. Comprehensive information about the selected cases in terms of building description, material and construction methods, and urban setting.
2. Upon the obtained data some basic observations and primal analysis were concluded for the three cases prior to conducting the thermal modeling and simulations.

In Chapter 4 investigations of thermal performance of the selected cases took place through applying a series of consecutive simulations. The simulations investigate the performance of each corresponding building component in order to verify the capability of the suggested model to introduce an integrated passive building system. The work in this chapter comprises the following:

1. Validation of the simulation model for each case against measured data
2. Analysis of the thermal performance of each case in response to solar radiation
3. Comparative analysis of the efficacy of the thermal mass.
4. Analysis of the role of shading mechanisms

Upon the results concluded in this chapter one of the cases is adopted as a potential model to which further experiments are conducted within the next chapters. The major simulation tool used in this section is TRNSYS 17 in addition to Ecotect 11 for solar radiation analysis.

The analysis in chapter 4 does not comprehensively embed the wind factor and actual air flow rates. In other words, a constant value of air change rate was assumed in the simulation model according to the existing literature. In chapter 5 however, wind analysis took place and aggregated results for air flow and air change rates (ACH) were then obtained through numerous computational fluid dynamics simulation runs (CFD) for the adopted model. This chapter achieves a couple of goals:

1. Draw better understanding of the wind behavior, inside and outside the building, and the manner of the wind-driven ventilation whether through single-side or cross ventilation.
2. Understand the role of the courtyard and fenestration system in the natural ventilation process.
3. Extract plausible results for air change rates upon which a precise prediction rule is inferred through pattern recognition.

The prediction rule was then processed as an equation for a function of air change rate in TRNSYS. Accordingly the simulation was reinitialized to get real values of indoor temperature and hence the levels of thermal comfort.

Finally, Chapter 6 comprises conclusive remarks on thermal comfort and energy efficiency. The chapter includes a comparative analysis between the base case and two modified options of the simulation model. The analysis addresses the base case contributions in achieving higher level of indoor thermal comfort and energy savings through a couple of features; the heat storage capacity of the wall material wall material and shading through the window screens.



## Chapter 2

# Climate, tradition, and the passive design strategy

### 2.1 Introduction

The term vernacular architecture describes structures built by people whose design decisions are influenced by their traditions and cultural backgrounds [75]. Along with climatic conditions the most decisive factor in producing a typical regional architectural product is Socio-religious, especially for a society in which beliefs and religious backgrounds are constituent elements in people's life. Among layers of influence Islam is counted as the most influential in the Egyptian history and the most efficacious and exuberant among all inherited factors. Islamic beliefs and related customs play a crucial role in forming the pattern of people's way of life, their perspective towards relationships, and interpretation of incidents [1]. Although Islam does not dictate a certain manner for urban planning and building typology, many practices has a legitimate dimension derived from the Islamic law, which influences the entire way of life.

The Egyptian capital Cairo is located on 30.05° N, 31.22° E in the north east side of the African continent. Cairo is characterized by a hot and arid climate that receives an average annual sum of 3000 hours of sunshine (the possible maximum is 4000 hours). In summer, the operative temperature varies from 37 to 46 °C and from 13 to 21 °C for maximum and minimum respectively, while it varies in winter between 25 and 28 °C and between 6 and 9 °C for maximum and minimum temperatures respectively [37]. The climate in general is characterized by large diurnal temperature differences. These characteristics impose special considerations on building design and the urbanization process in general, especially with regards to the solar geometry and the building as responsive structure. Vernacular architecture hence responds to solar geometry and physical principles which can be applied to urban settings and the building as an integrated structure. The results of heat transmission can be concluded then in radiation, heat absorption, heat conduction and heat transmission by the resulted convection.

Components and features employed in the traditional building reflect both cultural authenticity of the region and response to climatic variables. A particular passive design strategy therefore is followed in the traditional building, which is mainly characterized by the duality of function of each corresponding building component. This chapter reviews the full climatic condition of Cairo and requirements of thermal comfort. It also sheds light upon the influence of solar geometry on the building design in general as a threshold to review how the traditional house responded to climate. In order to find out the magnitude of traditional architecture, this part of the study analyzes the existing architectural components with regards to their duality of function, which responds to both cultural needs and climatic conditions.

## 2.2 Climate

According to the dictionary of Oxford, climate is defined as "... certain conditions of temperature, dryness, wind, light, etc." However, climate could be defined scientifically as the integration in time of the physical states of the atmospheric environment and characteristics of a certain geographic location. The accumulative analysis of regional architecture suggests that building design is crucially influenced by the climatic conditions in terms of building components, materials, internal circulation, roofing systems and building orientation. As a case study for hot and arid climate zones, the Egyptian capital is an example on how the building design is influenced by the regional climatic conditions. Hot-Arid climate zones are found in the sub-tropical regions of Africa, central and western Asia, north western and southern America, and in central and Western Australia (fig. 2.1). In all of these cases the climatic conditions are caused by the trade winds, blowing southwest and northwest towards the equator, losing most of their water vapor. Due to the pressure and down-flow in these regions the air becomes hot and dry [28].

The direct solar radiation intensity in North Africa generally is up to 814-930 W/m<sup>2</sup> on the horizontal surfaces (fig. 2.2). As for Cairo, solar radiation is direct and strong during the day, but the absence of clouds permits easy release to the heat stored during the daytime, in the form of long-wave radiation towards the sky during night-time. The annual and seasonal rates of precipitation is very low. Cairo receives less than 250 mm of water annually (fig. 2.3), which is a sum total of rain, fog and dew when precipitation starts sometimes at higher altitude and water evaporates before reaching the ground. The air temperature exceeds 40° C in the summer. The prevailing wind direction is north and north-east (fig. 2.4) and the wind speed is quite low in the morning and reaches its maximum in the afternoon. Average humidity is between 50-70 %. The climate in general is characterized by large diurnal temperature differences range between 15-25 degrees, which allow intense solar radiation during the day and quick cooling down at night (fig.2.5).

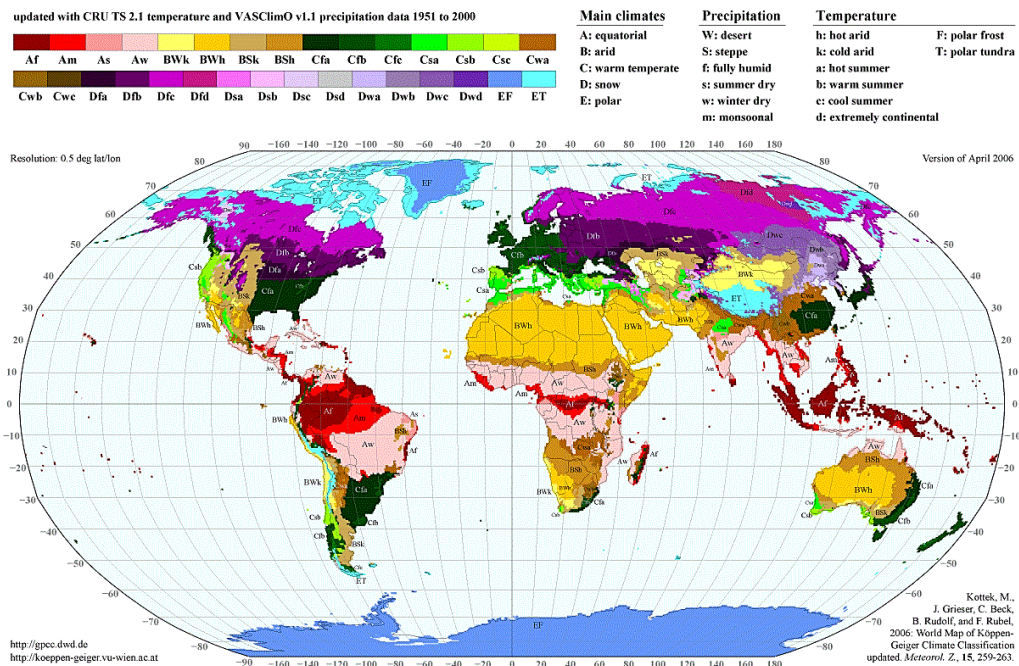
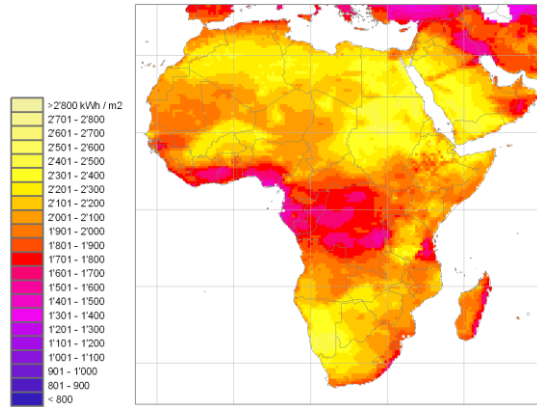
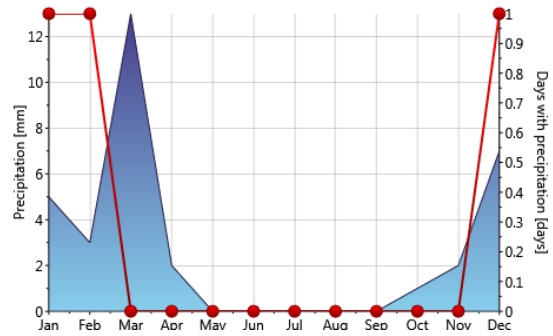


Figure 2.1: World Climate Zones (source: koeppen-geiger.vu-wien.ac.at/)



**Figure 2.2:** Annual sum of irradiation, Africa [51]



**Figure 2.3:** Precipitation chart for Cairo (source: Meteonom 7)

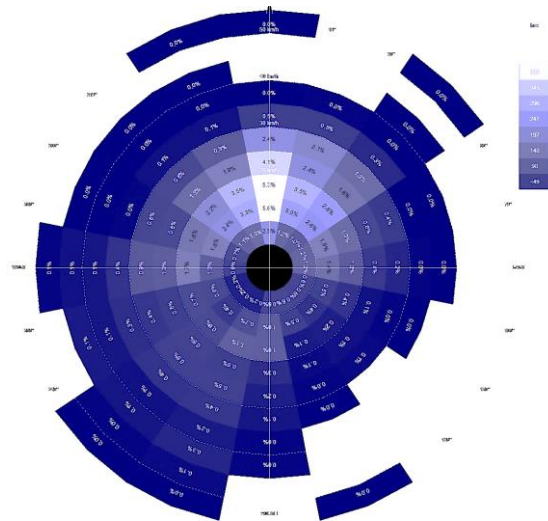


**Figure 2.4:** Prevailing wind frequency Hrs. Cairo, (source: Autodesk weather data)

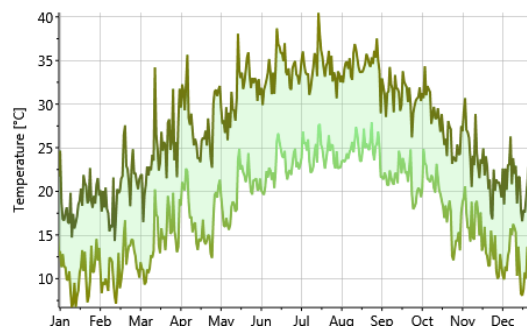


**Figure 2.5:** Daily temperature chart for Cairo (source: Meteonom 7)

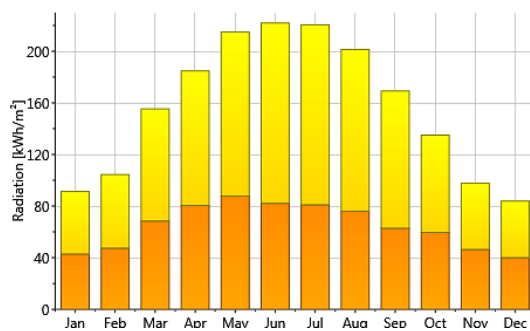


**Figure 2.6:** Radiation chart for Cairo (source: Meteonom 7)

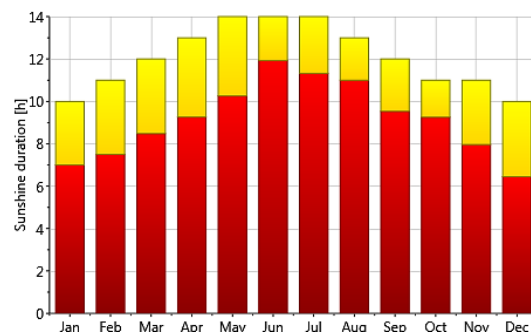


**Figure 2.7:** Sunshine chart for Cairo (source: Meteonom 7)

Egypt receives an average between 5.4 and 7.1 kWh/m<sup>2</sup> of annual daily direct solar radiation, from north to south. The solar radiation on horizontal surfaces reaches the highest range in June; 7.45 kWh/m<sup>2</sup>/day in Cairo. The annual direct normal solar irradiance ranges between 2,000 kWh/m<sup>2</sup> and 3,200 kWh/m<sup>2</sup>, rising from north to south, with a relatively steady daily profile and only small variations in resource (fig. 2.6). 9 to 11 hours of sunlight per day (fig. 2.7) are provided, with few cloudy days throughout the year. Diffuse solar radiation has no fixed direction at any instant and scattered in all directions. A portion of this radiation reaches the surface of the earth [63]. Monthly mean values of the hourly global solar radiation and diffuse components were measured at the urban area of Cairo during the non-urbanized period (1969-1973). The results showed that these values have remarkably exceeded those measured during the urbanization period (1990-2003) for all months of the year. The annual mean values of the hourly global solar radiation are found to be 21.65 and 18.06 MJ m<sup>2</sup> during the non-urbanized and urbanized periods, respectively, with a mean relative reduction in value of 17.63%. This reveals that urbanization and industrialization processes are the main reasons for the reduction of the global solar radiation values at the urban area of Cairo. The maximum values of both the hourly global solar radiation and diffuse components were recorded around noon in Cairo city, while the minimum values were observed at early mornings and late afternoons, and the corresponding values of the diffuse fraction of global radiation show the opposite behavior to the hourly global solar radiation and diffuse components patterns. However, maximum values of the hourly global solar radiation and diffuse components are found in summer and minimum values in winter [62].

### 2.3 Requirements of indoor thermal comfort

Desirable thermal comfort is not determined merely by temperature and is generally identified within buildings by air temperature, temperature of surrounding surfaces, air humidity, rate of air movement, level of radiation, and rate of heat production by the bodies of people in the building. An index used in the United States, and which with one limitation appears to provide an adequate measure of environmental warmth, is effective temperature. This takes into account temperature, humidity, and airspeed, but not radiation. Introduced by Houghton and Yaglou, this measure of heat sensation is defined as the temperature of saturated motionless air that would produce the same sensation of heat or cold as the combination of temperature, humidity, and air motion considered.

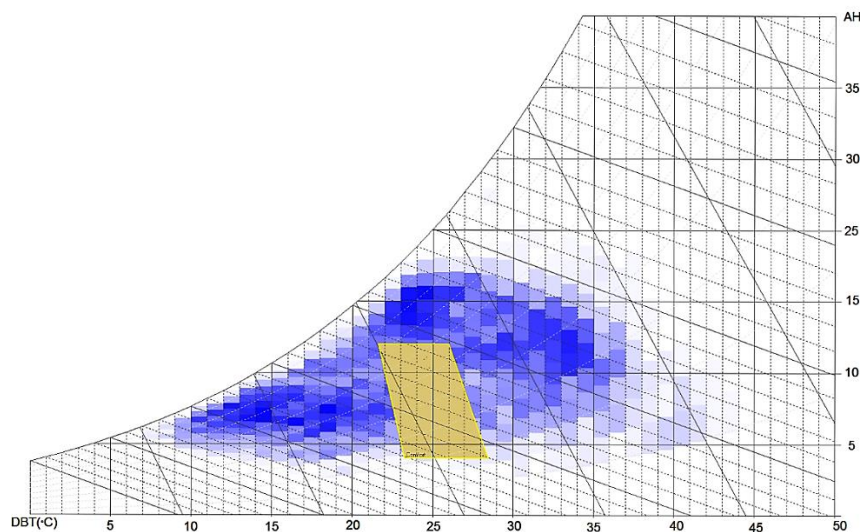


**Figure 2.8:** Psychrometric chart, comfort zone for Cairo

An improvement on this measurement by Vernon and Warner uses the temperature given by the globe thermometer instead of the dry-bulb air temperature (DBT) and thus includes an approximation of the radiation component. This standard is known as the corrected effective temperature and is the most useful scale of thermal sensation now available for the Tropics. A bioclimatic chart created by Olgay defines the comfort zone in terms of DBT and relative humidity (RH) [57]. Psychometric charts are used to describe thermal comfort zones considering variables of air temperature and humidity. The comfort zone for the city of Cairo however, in terms of DBT and absolute humidity (AH) is shown in the psychometric chart in figure 2.8.

Many physical and physiological factors affect the maintenance of the indoor thermal comfort (fig. 2.9) Throughout the day time, the heat is transmitted to the interior of the building through various ways; radiation heating of roofs; heat gain by ventilation; conduction through walls; in addition to heating by the inhabitants. In this respect the conductivity of building materials, roofing system, and cross ventilation play a crucial role in the heat gain-loss process. The rates of thermal conduction depend on the thermal resistance and transmission of building material and the area exposed to the solar radiation. The direct and reflected solar radiation, absorbed and re-emitted heat and heat gain are differently responsible for heat gain. About 3% of incident energy is transformed into heating the structure. Shading can be used to prevent solar radiation from directly falling on building surfaces. The building's envelope and roof shapes, geometry, color and construction materials' thermal properties can effectively provide passive indoor thermal comfort [23]. The role of construction material, shading devices, fenestration system, and various climatic responsive building components will be discussed subsequently in detail. Climatically responsive buildings therefore are anticipated to provide higher levels of thermal comfort. Overheating leads to lethargy and requires more effort for actions and can also be stressful because of the overstimulation it causes. The glaring sunlight, especially if accompanied by inescapable dry wind, can exhaust the nerves. In such overheating conditions man needs an opposite antidote [38]. Only 20% of the heat produced by the biochemical process of the human body is utilized and remaining heat must be dissipated to the environment.

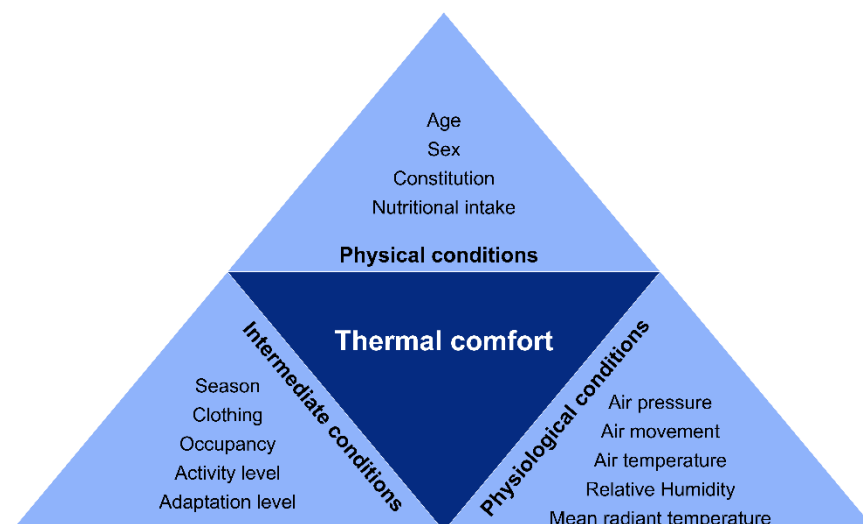


**Figure 2.9:** Influential factors for thermal comfort

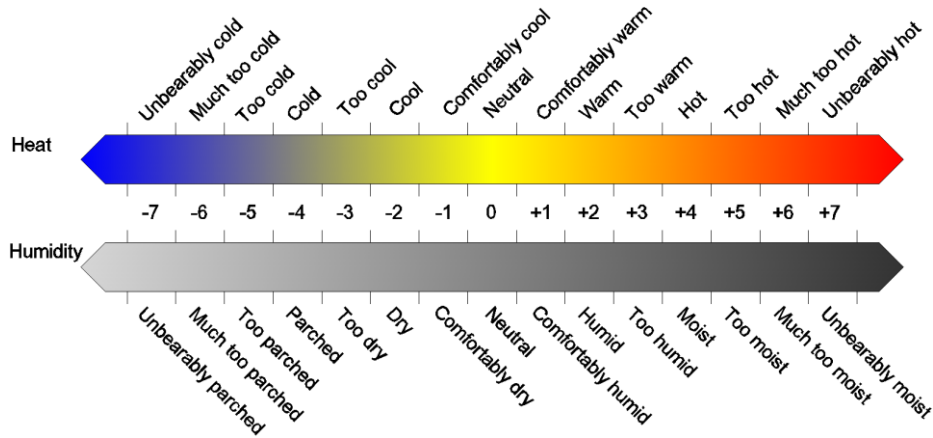


**Figure 2.10:** Thermal comfort sensation scale

To keep the temperature of the human body balanced around  $37.5^{\circ}$  all surplus heat gained by solar radiation or hot air must as well be dissipated to the surrounding environment. This heat gain-loss process occurs through various ways to maintain the body's thermal balance [47]. Heat dissipation occurs then in several ways; convection and conductivity; heat radiation; evaporation; exhalation; and excretion [39]. In addition to the various physical and intermediate conditions mentioned in figure 2.9, the thermal comfort sensation depends on four main climatic variables; temperature, solar radiation, humidity and air movement. Figure 2.10 shows a thermal comfort sensation scale for a couple of variables; temperature and humidity. According to the British department of Scientific and Industrial Research, the ideal temperature with slight air movement ( $0.25 \text{ m/s}$  or less) is  $18.9^{\circ}\text{C}$  in summer and  $16.7^{\circ}\text{C}$  in winter. This gives the ideal indoor air temperature as  $18.1^{\circ}\text{C}$ , and defined the comfort zone ranges as being from  $14$  to  $22.5^{\circ}\text{C}$ . Others suggested that the standard is  $20.8^{\circ}\text{C}$  with  $50\%$  relative humidity. Temperature range from  $21$  to  $24.5^{\circ}\text{C}$  with relative humidity varying from  $40$  to  $70\%$ . C. E. P. Brooks shows that the British comfort zone lies between  $14.5$  and  $21^{\circ}\text{C}$ ; the comfort zone in the USA lies between  $20.5$  and  $26^{\circ}\text{C}$ . In the tropics it is between  $23$  and  $28^{\circ}\text{C}$  with relative humidity between  $30$  and  $70\%$  [57]. Many standards were established to assess the thermal comfort in buildings according to the model established by P. O. Fanger for predicted mean vote (PMV) and percentage of people dissatisfied (PPD). However adaptive thermal comfort standards are provided for naturally ventilated buildings, such as Ashrae Standard 55 [7] and EN 15251 [16] which is adopted in this study as described in chapter 6.

## 2.4 Solar geometry and building

In passive design methods the building makes use of the solar energy by the advantages of its orientation, geometry and building components [64]. Determination of the daily and annual sun path is essential to calculate the solar intensity of radiation that hits the building (fig. 2.11) It also helps to predict the resulted shadows and hence the placement of shading devices. The sun position in the sky is determined by the rotation of the earth about its axis and its elliptical path around the sun. To define the sun's position at any given time, angles of altitude and azimuth are required, as shown in figure 2.12, and can be calculated by the following equation:

$$\sin A_s = \sin \delta \sin \phi + \cos \delta \cos \phi \cos h \quad (2.1)$$

where  $\delta$  is solar declination,  $\phi$  is geographical latitude, and  $h$  is hour angle ( $15^{\circ}$ , at  $12:00 \text{ h} = 0 \text{ deg.}$ ).

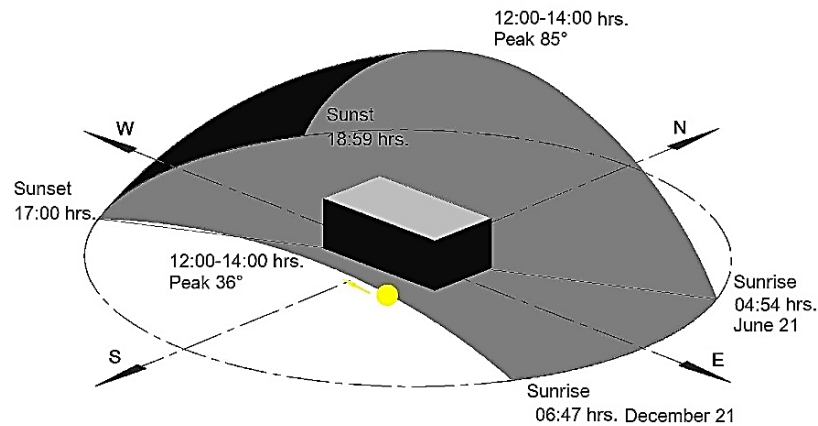


**Figure 2.11:** Sun Path, Cairo

Building orientation is of great significance when considering the thermal behavior in summer. It determines the azimuth and altitude angles of the sun to the façade and hence the intensity of the solar irradiance [33]. According to orientation, each façade will receive direct sunlight for a particular period during the day. In summer the northern façade receives direct sunlight around the summer solstice and the penetration of solar radiation is limited unless for the diffused sunlight. However, providing adequate shading without reduction of daylight entry and view to the outside is difficult on eastern façade due to the large amount of solar radiation that enters at a shallow angle. However, shading devices such as projecting louvers and window screens can be more efficient on western facades which receive light at a steep angle with less intensity of solar radiation. The length of shadow on a wall surface can be determined, in relation to solar geometry, by horizontal and vertical shadow angles, as shown in figure 2.13.

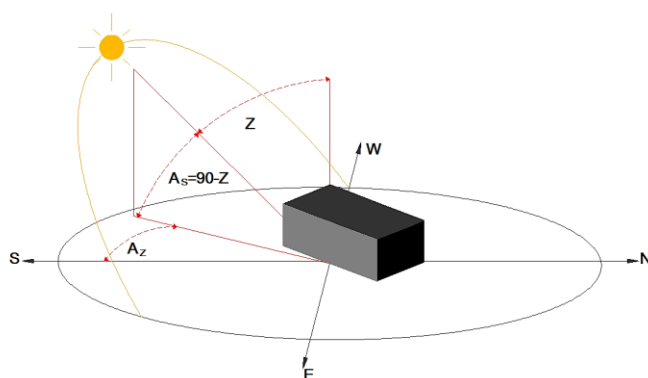


**Figure 2.12:** Sun angles

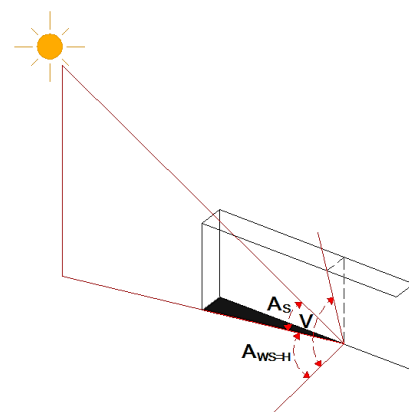


**Figure 2.13:** Shadowing angles

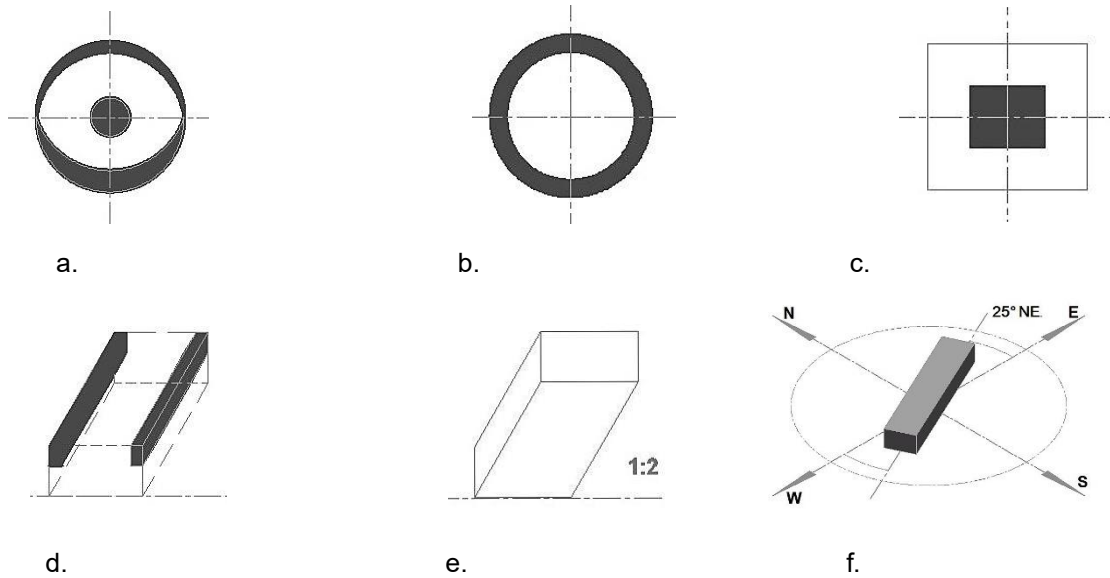


**Figure 2.14 a-f:** Climate influence on build form [39]

- a. Placement of transitional spaces (e.g. hallways, stairs and lobbies)
- b. Placement of shading devices
- c. Use of atria, center of building for cool shading
- d. Placement of cores (vertical chases, stair cases)
- e. Length/Width ratio
- f. Building orientation

The western façade is the most unfavorable side of the building during the summer due to the large amount of solar energy enters with decreased possibilities to incorporate shading devices and maintain visual accessibility. External fixed horizontal louvers hence are effective not only for reducing cooling loads in summer but the overall annual primary energy loads of the building. However, care must be taken while choosing the shading devices according to façade location [20] Figures 2.14 a-f show influence of climate and solar geometry on building form and components.

The winter-summer solstice is of great importance when considering shading devices. Being a bit far from the equator resulted in bigger differences of sun angles between winter and summer. Therefore, winter sun penetrates south-oriented rooms more deeply, when warmth is more needed (fig. 2.15 a- b). Summer sun also gives shaded porches and never reaches south-side façade of the courtyard (fig. 2.16 a-b). However, winter sun (low angle) penetrates north-side living quarters when it is preferable in cold winter. Studies have proven that incorporating overhangs depending on the different mean azimuth angles for summer and winter direct sunshine decreases the thermal gain through the building. For vertical glazing shaded by horizontal overhangs facing south, the rate of heat transfer into the building was ca.  $75 \text{ W/m}^2$  lower than unshaded windows, for June 21 [8]. Table 2.1 for the angles of declination and altitude for Cairo indicates that the optimum orientation of the building block with regard to the sun factor is east-west. At the summer solstice, the north façade is exposed to sun rays from 05:00 AM at an angle of altitude  $0^\circ$  to 09:00 AM at an angle of altitude  $49^\circ 30'$  and an angle of declination  $88^\circ 13'$  and the sun rays hit the façade at angle of only  $1^\circ 03'$ . However, the angle of altitude on the south façade is  $83^\circ 36'$  at noon. Therefore, solar radiation does not penetrate the openings on the south façade and properly placed shading devices could be efficient. The solar control mechanisms in the traditional building are discussed in detail within the experiments in chapter 4.

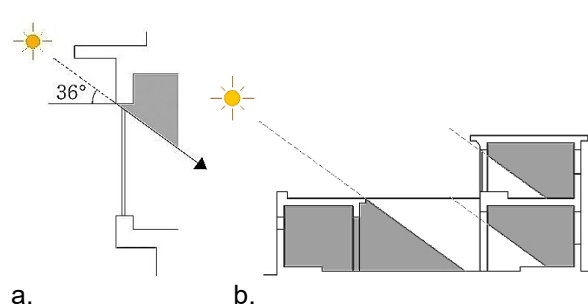


**Figure 2.15 a-b:** Sun at winter solstice (21 December at 12:00 pm)

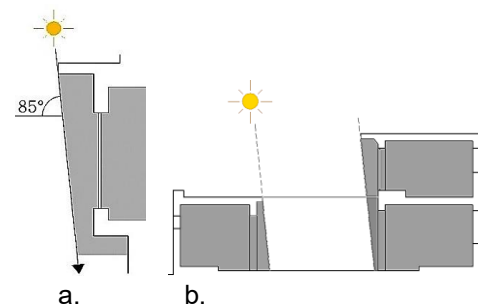


**Figure 2.16 a-b:** Sun at summer solstice (21 June at 12:00 pm)

**Table 2.1:** Angles of declination and altitude at latitude 30° N, Cairo [25]

Time of Day	21 June Summer Solstice		21 March or 21 September Equinoxes		21 December Winter Solstice	
	Angle of Declination to the North	Angle of Altitude	Angle of Declination to the North	Angle of Altitude	Angle of Declination to the North	Angle of Altitude
5:00	62°40'	Sunrise-zero	...	...	...	...
6:00	69°24'	11°27'	90°00'	Sunrise-zero	...	...
7:00	75°42'	23°51'	97°24'	12°57'	117°20'	Sunrise-zero
8:00	81°48'	36°35'	106°53'	25°40'	125°50'	11°27'
9:00	88°13'	49°30'	116°27'	37°45'	135°24'	21°18'
10:00	96°34'	62°28'	130°00'	48°36'	148°36'	29°18'
11:00	112°34'	75°05'	151°11'	56°43'	163°15'	34°40'
12:00	180°00'	83°26'	180°00'	60°00'	180°00'	36°34'
13:00	247°56'	75°05'	208°49'	56°43'	196°45'	34°40'
14:00	263°56'	62°28'	230°00'	48°36'	211°24'	29°18'
15:00	271°77'	49°30'	243°33'	37°45'	224°06'	21°18'
16:00	278°12'	36°25'	253°07'	25°40'	234°10'	11°27'
17:00	284°18'	23°51'	262°36'	12°57'	242°40'	Sunset at 16:57
18:00	290°66'	11°27'	270°00'	Sunset-zero		
18:58	279°20'	Sunset-zero				



The old city of Cairo can be easily identified by a main north-south axis and relatively wide parallel artery (fig. 2.17). Climatically it is the optimum orientation as it determines the path for wind coming from the north. The structure of the city is a homogeneous integration of little principle neighbourhood units (quarters). In addition to houses and residential units, each quarter comprises numerous public buildings, baths and bazars. Here the streets become narrower and the sense of privacy, isolation and tranquility can be more evident. Here buildings are earth-bounded and horizontal in conception. Height is much less than the building length.

This horizontal effect emphasizes the perpendicular minarets and domes of the mosques, which form the skyline of the city [55]. The congregational mosque was the heart of the city, however, the city pattern developed outwards from the residential unit. Streets were designed mainly for pedestrians with minimum width of 7 cubits (ca. 3.5 m.) Basim Hakim mentioned that the minimum vertical height of a public through street is also 7 cubits which correspond to a maximum vertical height of a fully loaded camel [31]. The organic compact planning dominated streets' layout with narrow winding paths and cul-de sacs which were usually 4 cubits or narrower where the distances between buildings on both side of the street become remarkably narrower due to the projection of windows on the upper floor (fig. 2.18). Within this setting the streets remain hence shaded (fig. 2.19).

Solutions that took place to deal with both social customs and climatic conditions were initiated from the surrounding built environment, which eventually complemented by the architecture of distinct buildings. The traditional Arab town in general is a result of dense grouping of courtyard houses. This dense fabric eliminated wasted spaces between buildings and reduced the external heat gain-loss process. This formation had shades as well on the social dimension as it maintained a high level of privacy and avoidance of disputes between neighbours [59]. The town grows hence in organic form derivatively from small growing units added to each other. Streets branches out from a central square and end up in narrow alleys or subsidiary streets. Main streets have north-south orientation and side streets accordingly are east-west oriented.

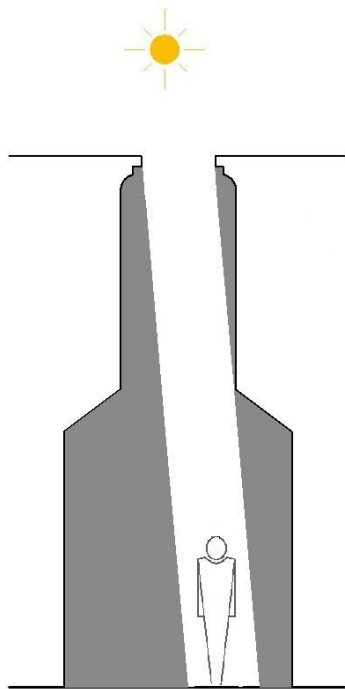


**Figure 2.19:** Narrow-street shading

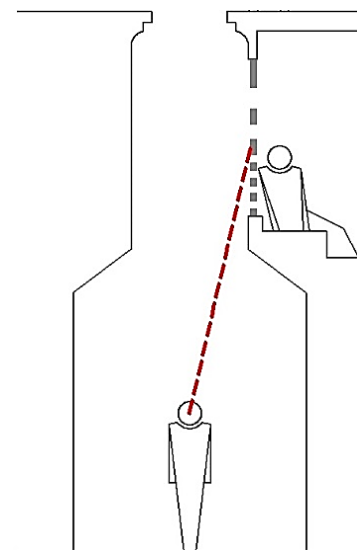


**Figure 2.20:** Minimized visual contact

The emphasis on privacy as a basic need is tangible not only in the traditional house as an individual structure but also within more comprehensive perspective of the urban setting. However, privacy in this respect could be classified to various levels; from the seclusion of the territory as a whole from the region to the integrated housing units encompassed within each individual quarter [52]. Each quarter/neighborhood is physically separated from the other even in terms of social activities as the population of each had almost the same profession. Then subdivisions could be found inside each quarter when the subsidiary streets become narrower and hence shaded become more shaded and tranquil as previously discussed. Finally comes the highest level of privacy, that of the family. This was achieved through the house design. The segregation between the men and women is quite evident through grouping the spaces designated for men and visitors on the ground floor while the upper floor/s were reserved for women as well as bed rooms. Thanks to the window screens, rooms on upper floor were designed to enable overlooking the courtyards without being visually violated from the visitors in the ground floor. Even staircase connecting floor levels are enclosed to allow visually secured vertical circulation.

To limit the visual contact with street to the minimum, the staggered or bent entrance is found in almost all traditional houses (fig. 2.21). The main courtyard is approached by a vestibule from the main entrance which provides indirect access to the interior and eliminates the probability of visual violence to the interior of the house even in the case of the door being open. M. Abd-el-Aziz Nour in his study of Traditional Arab Domestic Architecture argues that if a stranger entered the main door way while the courtyard is occupied by the ladies of the house the length of the entrance corridor will take him at least the same period of time as they to reach the nearest staircase [55]. In most cases no openings are found to the street on ground floor level on external facades which are almost solid except for projected screens in upper floor. The street is quite narrow and the space between buildings on both sides in the level of the first floor becomes even narrower. This setting limits the visual accessibility from the passerby into the house. However, the inhabitants of the house have the visual access to the street through the screens (fig. 2.20).

## 2.5.2 Construction method and material

Most walls were built as load bearing elements with average massive thickness between 40 and 120 cm. The walls embedded functions other than delineating internal spaces; its mass provides high levels of security and privacy and acts as acoustical barriers [31]. The thickness of the wall depends on its height, this ratio rarely exceeds 1:6 in traditional construction. To increase stability interior partitions are closely spaced and buttresses are frequently incorporated. In many cases the walls are tapered gradually towards the top which conveys solidity [59]. The thickness of the walls allows the incorporation of elements of storage and cupboard as well as space to place water containers and jars in front of the windows to benefit by the cool air. Marble and stone columns are used mainly as support for arcades in courtyards and in the upper floor *maq'ad* (balcony). In addition to their aesthetic value, arches are perfect substitute for beams due to the inherited strength, durability and resistance to deflection as well as the capabilities of increasing the height of construction in relation to spans. Various arch types are employed; however the pointed arch which migrated along history from its origins in Mesopotamia is the most common in vernacular Cairene houses.

The roof is rested upon the bearing walls and supported by timber beams. The spans of the beams are limited to 3.5 meters due to the available quality of timber (fig. 2.22). The beams are exposed in the ceiling as decorative elements and are frequently painted or gilded. The distances between these primary beams are bridged by another layer of secondary beams (joists). A third layer parallel to the primary beams in the form of reed matting or brushwood exists upon which the slab is placed. Slabs then had relative great weight, ca. 500 kg/m<sup>2</sup> for a 25 cm thickness floor slab [59]. The timber beams are also used as lintels for openings. The structural elements in general are highly celebrated and the use of structure as ornament is remarkable. The floor slabs have flat topping and hardened and dust-proofed by special screed compositions to serve as flooring. Supporting beams have an average depth of 10 cm; usually the walls were stepped back at the beam level as they become thinner on the upper floor.

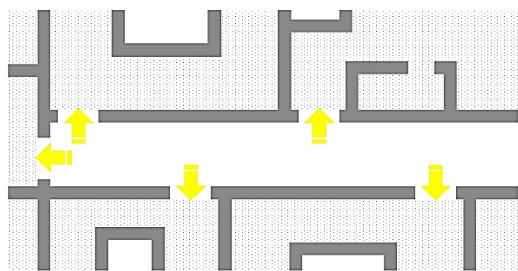


**Figure 2.21:** Staggered entrances of Houses

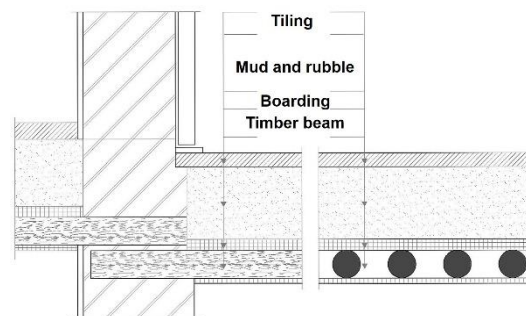


**Figure 2.22:** Superposed beam construction with stepped floor slab

Due to the introversion of house to the inside the main functions, even visually, are concentrated inside the house around the internal courtyard as the heart of the entire structure. The form of the external facades therefore is governed by the capacity of functions behind them. These facades are mainly solid except for the overhanging projecting *mashrabiya*s in the upper stories, which play a significant role also as shading devices in narrow streets and limit the direct visual contact from the passersby. On the contrary the internal facades demonstrate more luxurious treatments and more variant solid-void ratio due to various components deployed around the courtyard.

Normally stone was the most preferable construction material in Cairo. In addition to the durability factor, this can be attributed to the sheer amount of limestone provided by the adjacent Muqattam hills in southeastern part of the city. However, upon load distribution purposes it was very common to construct the walls of the ground floor with limestone of variable thickness; between 40 and 120 cm while brick walls are widely found on upper stories. It is quite understood that limestone in great thicknesses would need longer time to pass the heat received during daytime. However, in upper floors which accommodated sleeping rooms, the light walls on upper floors would cool down immediately after sunset and benefit from the coolness at night. A direct relationship hence is evident between the thermal characteristics of the structure material and spaces.

### 2.5.3 Components of the house and space design

The traditional Arab house in general demonstrated various possibilities for space arrangement and growth around the courtyard (fig. 2.23). These possibilities could be concluded in the following: (1) Extended growth at the back of the house; (2) Circumferential growth along all sides of the courtyard; and (3) Vertical growth through the addition of upper floors (this was not extensively applied within medieval practices due to technical limitations) the question of combination here arises with advancements of concrete and steel construction. The succession of spaces around the courtyard reflects the level to which the space benefits by fresh air and light and to what extent the space is private. However the traditional Cairene house had almost a basic components and space arrangement around a central courtyard (fig. 2.24).

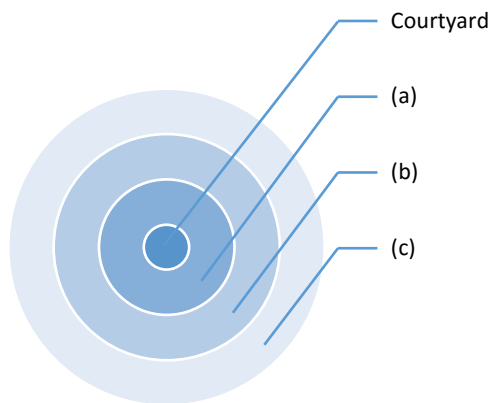


**Figure 2.23:** Succession of spaces around the courtyard,

- a. More accessible, more exposed to light and air.
- b. Less accessible, less exposed to light and air.
- c. Additional space to be added around subsidiary courtyards

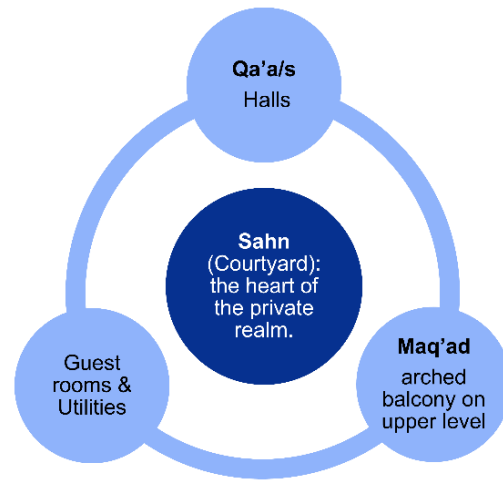


**Figure 2.24:** Principle components of the house

1. The courtyard.

The basic principle behind the centralization of plan around an internal courtyard (fig. 2.25) is to avoid external openings. Light and air are provided from the courtyard. The house is designed as a succession of spaces from the inside out with an understanding of the hierarchy of volumes. In such a climate characterized by large diurnal temperature differences it serves as a reservoir for cool air as well as the heart of the private realm. Some recent studies demonstrated that the courtyard configuration showed better response through the calculated environmental variables (surface to volume ratio, shadow density and daylight distribution) than the pavilion types [61]. Abandon of literature stated as well that the courtyard geometry contributes to the protection of the house against dust and undesirable high wind velocity [48] (fig. 2.26 a-d).

The courtyard hence acts as the main reference space through which various paces are accessible. In addition to the existence of the courtyard as the heart of the private realm and the medium of connecting the inhabitants with a relative private exterior, many factors contribute to make the courtyard a decisive factor in controlling climate extremes and achieving comfort to the inhabitants. Among these factors are the geometry of the courtyard and the relation between its footprint and height and the quality of the courtyard envelope in terms of solid-void ratio. The proportions of the courtyard in traditional Arab buildings generally vary between 1:1, 1:2 and 3:4 in plan and 1:2 in elevation of the narrower side. With respect to the courtyard envelope it is quite evident that the rigidity of the inner surfaces around the courtyard is remarkably reduced by opening voids or recesses and windows. The iron grills of rooms surrounding the courtyard on ground floor, the *mashrabiya*s projecting out from different levels on upper floors and the open arches of the balcony in the first floor play crucial role in this context and optimize the functional capacity of the courtyard in terms of cross ventilation.



**Figure 2.25:** View of the courtyard towards south facing the *maq'ad*,

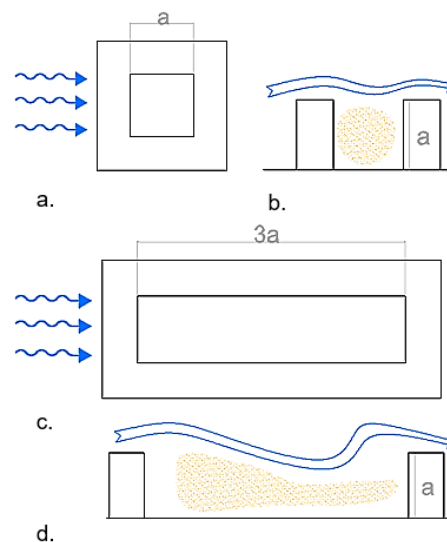


**Figure 2.26 a-d:** Influence of geometry of the courtyard in protecting from windblown dust

## 2. The main hall (*qa'a*)

With a relatively tall clear height, it is a central space (fig. 2.27) that has a ventilation element integrated to the roof (fig. 2.28). The hall is usually flanked on two sides by two *iwans* (a barrel vaulted space opened at one end) on a step higher level. It could be supplied by fresh air by a wind catcher as the hot air exhausted by the roof device. The *ivan* principally faces the north side to avoid direct sunshine. Some incorporated features were used for cross ventilation such as the wind catcher (*malqaf*) and the wind-escape (*shokhshekha*). Wind catchers can be widely found in many lands of the Arab region with various interpretations according to the climatic conditions and wind direction. While in the Gulf the whole parapet all around the roof is turned into wind-escape, in Cairo a large wind-catcher is incorporated to ventilate the principle living room. Parallel with the roof pop-up (wind-escape) it plays a crucial role in creating convection current and hence enhancing the cross ventilation process of a certain space (fig. 2.29).



**Figure 2.27:** Interior view in a hall, looking towards the screen on the northern façade. Thanks to the width of fenestration, the distribution of light at the warm colors of the interior creates an overall inviting atmosphere. Thick walls allowed the inclusion of niches and built-in cupboards and shelves.



**Figure 2.28:** Looking up at the *Shokhshekha* (wind-escape)

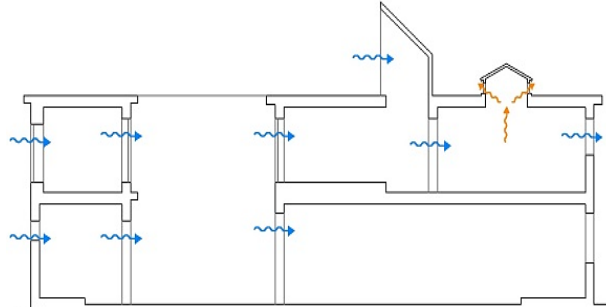


**Figure 2.29:** Cross section showing conceptual air-flow and cross ventilation within traditional house components

### 3. The balcony (*Maq'ad*)

The *Maq'ad* is an arched balcony on upper level (fig. 2.30) oriented towards the courtyard on the southern side to face the northern wind. It might have fenestration to the street on the southern side. In most cases it has access to the courtyard through a stair case and direct access, through a doorway, to the main hall in the first floor.



**Figure 2.30:** View from the *maq'ad* (balcony) in the 1<sup>st</sup> floor looking north to the courtyard

#### 4. Fenestration system

It is quite difficult to provide privacy and allow the passage of air and light at the same time. The basic design principle of incorporated window-screen composition (*mashrabiya*) (fig. 2.31) hence depends mainly on the fulfillment of a dual-function that responds to both climatic and social/cultural conditions. The window screens protect against direct solar heat gain and the resulting increase in room temperature. In addition, the gradual arrangement of perforation works on the control of air-flow and visual contact. On the eye level, the lower section of the *mashrabiya* has balusters in close mesh. This arrangement allows the inhabitants to overlook the street without being seen from the passersby. However, the upper section is composed of a comparatively wide mesh grill to provide sufficient air movement (fig. 2.32). To overcome the dimming effect of the screen, in many cases a floor to ceiling screens where applied, which increased the illumination as well as the air feeding for the interior. Screens were also incorporated on the interior facades facing the courtyard; however the opening ratio is remarkably greater. This can be attributed to the fact that these openings are facing a private open space so visual violence is not counted, unlike the screens overlooking the street, which has relatively narrow openings.



**Figure 2.31:** *Mashrabiya* overlooking the courtyard in House of al-Suhaimy

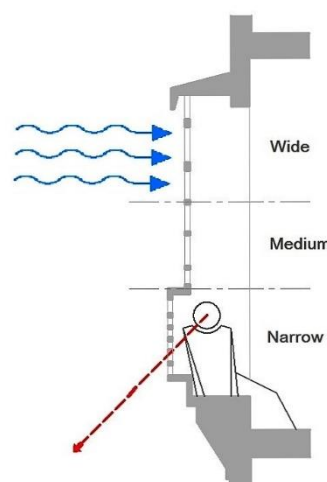


**Figure 2.32:** Gradual perforation of balusters of the *mashrabiya*

### 2.5.4 Traditional house in response to climate

The orientation of main roads in the old town is north-south; however the secondary streets of the residential quarters are east-west oriented. The buildings as a cluster therefore are shading each other. The amount of shading depends mainly on the morphology of the street canyon which results in decrease of the canyon's temperature and hence the façade temperature and subsequently the amount of heat transferred to the indoor space through the walls. The old town is characterized by narrow urban canyons with aspect ratio  $H/W = 2$ , (fig. 2.33). As the street width is proportional to the building height, the percentage of overshadowing, of one building by the other, obstruction angle ( $\theta$ ), remains constant for different building heights [11]. When the sun hits the façade of the building, convective current results as the air density changes. The hot air moves to the upper level and be replaced with cooler air which has greater density (fig. 2.34). The exposure of gap to the night sky enhances the night time cooling since the heat radiates up to the sky. The street is cooled down during night and daytime unless the sun is coming on a vertical angle. The phenomena of heat transfer occurs through the building components simultaneously by the three mechanisms; conduction; convection; and radiation. A convective heat transfer can be resulted from surface to air and vice versa, according to both temperatures [39]. Figures 2.35-6 describe the modes of heat transfer at wall surface and window. The building can gain heat in different ways; the principle source of which in hot climates is the solar radiation. Figure 2.37 illustrates the heat transfer mechanisms and heat gain/loss process in the building. Opposite to a black body which absorbs all of the incident radiation hits its surface and reflect none, a white painted surface absorbs ca. 30% of the incident radiation and reflects ca. 70% (fig. 2.38). The rest of the incoming energy is emitted to the surrounding and can be transferred to the interior by the generated convective current. The heat gain can be significantly increased when the solar radiation is allowed to penetrate the interior through openings. Here the U value of glass in windows is also a decisive factor, and the restriction of sizes of the openings is of great importance (fig. 2.39).

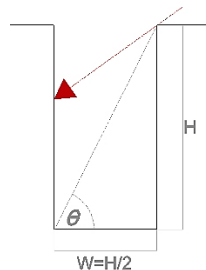


**Figure 2.33:** Aspect ratio and building shading

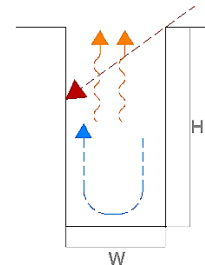


**Figure 2.34:** Convective current in street canyon

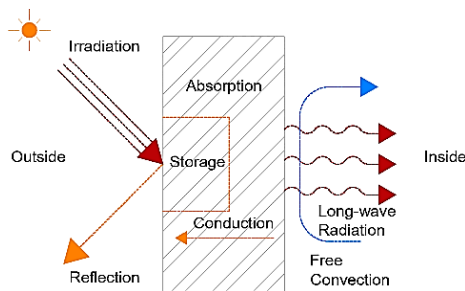


**Figure 2.35:** The heat transfer at wall surface

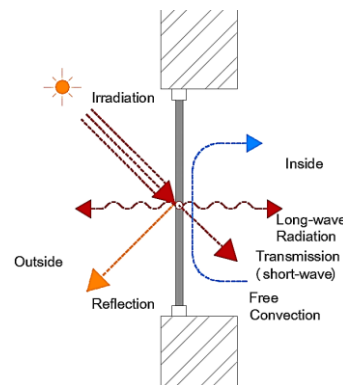


**Figure 2.36:** The heat transfer at window glass

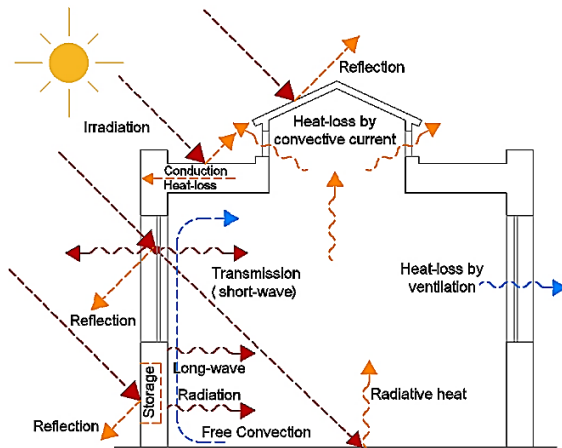


**Figure 2.37:** Heat transfer and heat gain/loss in the building

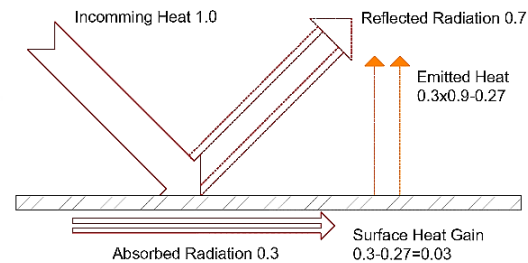


**Figure 2.38:** Incident radiation on a white surface

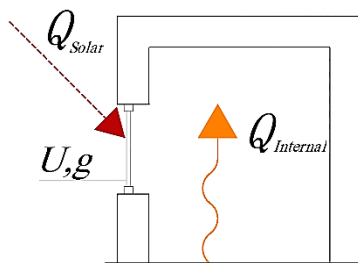


**Figure 2.39:** Means of heat gain in buildings.  $Q_{Internal}$  (electrical devices, inhabitants...etc.)

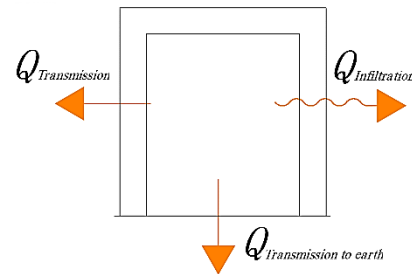


**Figure 2.40:** Means of heat loss in buildings

Typically by the way the heat is gained through the wall by solar radiation; it can be lost by conduction or convective current (see figure 2.37). However the building can lose heat mainly through three major ways; transmission (through walls, ceiling, windows...etc.); infiltration; and transmission to earth (fig. 2.40). Infiltration occurs due to leakage in the building construction and opening and closing of doors and windows which leads to shifting the air inside the building. The value of air exchange rate is dependent on various factors such as wind speed, difference between inside and outside temperature. The overall heat loss from a building hence is the sum of heat loss due transmission and infiltration in addition to the heat loss caused by ventilation. In low rise buildings the airflow through openings in summer is wind driven [45]. Heat loss through ventilation (convective heat loss) is in proportion to the air change rate, difference in temperature between the inside and the outside, and the capacity of air [11]. This study is concerned with convection in buildings through air movement. A decisive factor in this process is the ventilation rate  $V$ , which is described as:  $V = nV_R$  ( $m^3/h$ ), where  $n$  is the air exchange rate per hour ( $h^{-1}$ ), and  $V_R$  is the volume of room air ( $m^3$ ). The heat transfer between interior space and the ambient air ventilating the space can be calculated as:

$$\phi = V \cdot (c \cdot p)_{air} \cdot (\vartheta_i + \vartheta_a) \quad (2.2)$$

where  $\phi$  is the heat flux (W),  $V$  is the ventilation rate ( $m^3/h$ ),  $(c \cdot p)_{air}$  is the thermal capacity (Wh/ $m^3K$ ), and  $\vartheta$  is the air temperature ( $^{\circ}C$ ).

In the summer season a continuous air change rate of  $n = 1-2 h^{-1}$  is necessary. Moreover, night ventilation is necessary to cool down the building, which requires high ventilation air flow rates, typically air change rates of  $4-6 h^{-1}$  [36]. Convective heat transfer coefficient depends hence on the air flow velocity, surface and air temperature, roughness of the surface and the position of building component.

Wind driven ventilation can be enhanced through the courtyard. The airflow pattern will determine the potential of natural ventilation, which depends on changeable driving forces [60]. The courtyard works as an air well that collects cool air at night, and as surrounding rooms are protected from direct sunlight, they stay cool at daytime. At daytime, once the sun reaches the court, the air heats up and rises. When the courtyard air temperature raises the air within the courtyard will be less dense than that of the surrounding narrow streets. A convective current is then resulted and the hot air will be replaced by a denser, cooler, air moving from the street through the house (fig. 2.41) In this case the narrow streets will act as a store for cool air. In the same way the courtyard will replace the hotter air of the surrounding rooms. Thus, a cooling system between the street, the courtyard, and the rooms surrounding the courtyard will take place as the air temperature rises to any of them. To show the effect of the courtyard on air temperature a comparison were carried out between the roof and the courtyard of the house of al- Suhaimy in Cairo. Measurements recorded for the period between July 15 and September 15 show that the courtyard air temperature is lower than the air temperature on the roof during a period of 10 to 12 hours a day. It was apparent that the courtyard is cooler than the roof by a maximum of 4 °C to 7 °C. This peak usually lasts about four hours (from 12:00 to 16:00) [55].

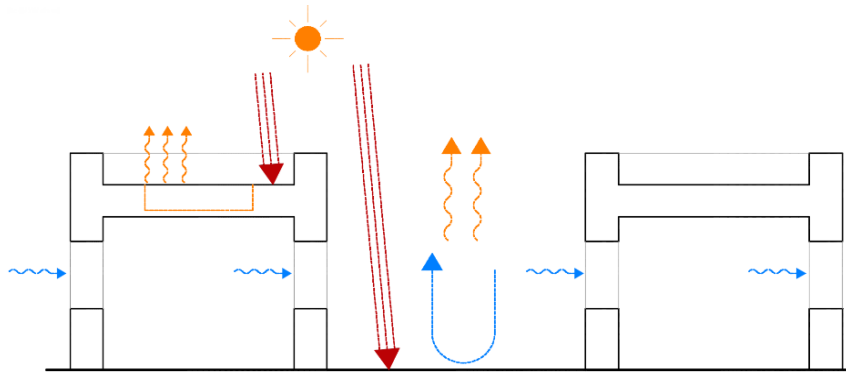


**Figure 2.41:** Convective current in the courtyard as a secondary effect of solar radiation.

The radiative cooling can be most efficient in desert climates [17]. Since it receives the greatest amount of solar radiation during daytime, the roof is considered one of the most critical components of the structure. The traditional designers relied on two major aspects to resolve this problem. First is the shading and planting of the most available parts of the roof in the form of plantations and pergolas. The second resolution is the materials of the roof itself. It was common to construct the roof as follows: most parts of the roof were of palm trunks covered by 5-8 cm mortar layer, limestone gravel and sand, followed by a layer of mud, 8-10 cm and finally paved by stone tiles. Stone paving with its light color reflects a great part of the solar radiation and the mud layer delays the heat penetration through the roof (fig. 2.42).

The greater the difference between inside and outside temperatures the greater the resulted convective current which allows the hot air to be released and replaced by cooler ambient air through the cross ventilation process as previously discussed (fig. 2.43). The ventilation rate,  $V$  ( $m^3/s$ ), is as well a direct proportion of the height of the shaft, the vertical distance between inlet and outlet of air. It can be calculated as:

$$V = 0.117 \cdot A[h(\vartheta_i - \vartheta_a)]^{\frac{1}{2}} \quad (2.3)$$

where  $A$  is the area of fair inlet ( $m^2$ ),  $h$  is the shaft height (m),  $\vartheta_i$  is the inside air temperature ( $^{\circ}C$ ), and  $\vartheta_a$  is the ambient air temperature ( $^{\circ}C$ ).

In traditional houses, a wind escape device is usually incorporated in the roof. It is heated up by the sun affect creating a temperature difference between supplies and exhaust air, and effectively ventilates the interior space by thermodynamic forces. Integrating an efficient wind scape optimally enhance the cross ventilation process. The role of the wind-escape device is examined within the CFD simulations in chapter 5.

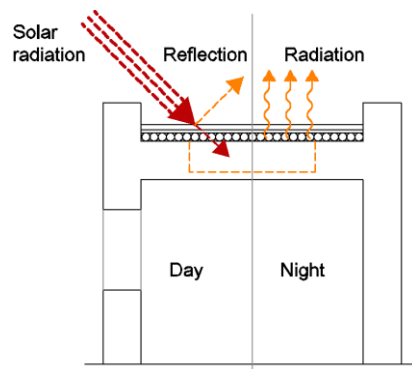


**Figure 2.42:** Radiant cooling through the roof

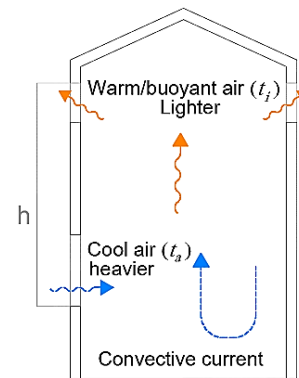


**Figure 2.43:** Convective ventilation

The differential opening ratio between the screens on the external facades, which in many cases face the prevailing wind direction, and those on the interior facades can result in enhancement of the cross ventilation of a distinct space. The scarcity of openings to the outside in such hot and arid climate has various advantages other than the fulfillment of privacy purposes. Facing the open side of the building downwind restricts the penetration of dust. The density differences caused by warm air inside the building creates pressure differences between the interior and the exterior, which drives the flow through the building by the stack effect [44]. The narrow perforation, especially on facades on the north and north-east sides can paradoxically increase the air flow through the rooms since it creates a low pressure area inside the building, which allows sucking the air in (fig. 2.44). The cross ventilation can work more efficiently along with having wide openings to the courtyard. In hot and arid climate with significant diurnal temperature swing, the storage capacity can be improved by night time ventilation (fig. 2.45).

Walls with sufficient amount of thermal mass, with low surface absorptivity, are recommended to be used in places where there is considerable diurnal temperature variation around design indoor condition [5]. The rate of heat transfer and the effectiveness of thermal mass are determined by various parameters; material thermal properties; location and distribution of the thermal mass in the building; insulation portion; the occupancy pattern and ventilation [10]. In addition to enhancement of the indoor air quality and providing cooling to the inhabitants, ventilation can be used for cooling the thermal mass of the building [58]. To allow the cooling effect of the thermal mass, the air temperature at night should be at least 6 K below the desired day-time room temperature [39].

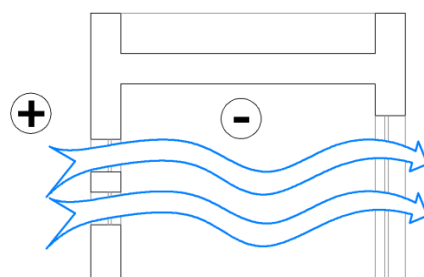


**Figure 2.44:** Creating a low pressure area inside of a built-up space by narrow openings facing the wind direction and resulting air flow and cross ventilation

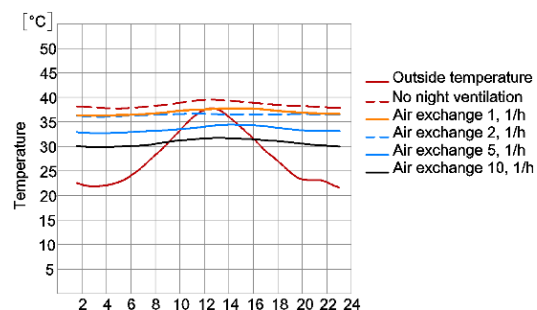


**Figure 2.45:** Day-time room temperature in July, with different air exchange rates at night-time ventilation, Cairo. [39]

In addition to the direction of the façade on which the screen is applied as previously discussed, the depth of the screen and the perforation ratio is a decisive factor in determination of the amount of solar radiation that penetrates the room. The *mashrabiya* (window screen) acts as a baffle zone between the interior and the exterior, so the glare of sunlight is broken up by the lattice that provides a dark area. The cylindered form of the basic unit of the *mashrabiya* design subdue the dazzling effect of dark-light contrast which occurs when looking from the inside toward the light outside.

The careful arrangement of the wooden grating elements (fig. 2.46), their density, and pattern are of functional great importance. Lattices with small interstices are required to intercept the direct solar radiation. The round balusters graduate the light reaching their surface and hence soften the contrast between darkness of the opaque balusters and the brightness of the glare entering through the interstices (figs. 2.48 a-b) The lattice shape with its lines interrupted by the protruding sections of the balusters produces a silhouette which carries the eye from one baluster to the next across the interstices, vertically and horizontally [25].

The pattern of the screens does not vary only between the lower and upper level of the same window, but the window size decreases as the façade is more exposed to sunlight according to the sun movement during the day. The ratio between solid and void of the east and west facades is far less than that on north and south. In other words, the increased opening ratio on west, east, and south oriented facades leads to the increase in cooling loads (fig. 2.47). The role of window screens and shading devices are analyzed through modeling and simulations within the next part of this study.

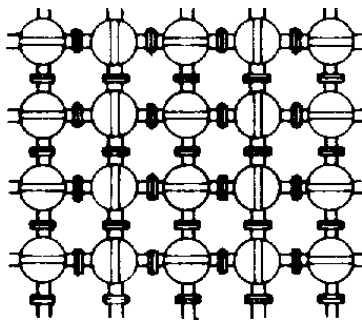


Figure 2.46: *Mashrabiya* of turned wood

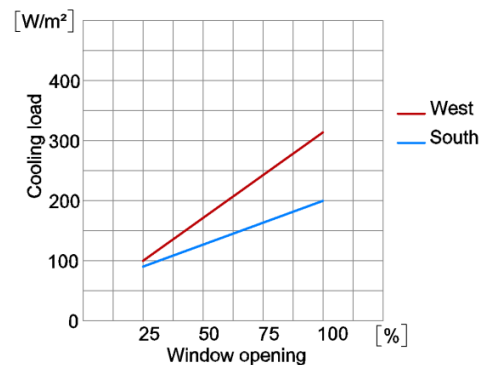


Figure 2.47: Required cooling loads with different opening sizes on west and south facades in hot and arid climate. Air change rate 2.5 ac/h, room volume 60 m<sup>2</sup>, internal cooling loads 46 W/m<sup>2</sup> [39]

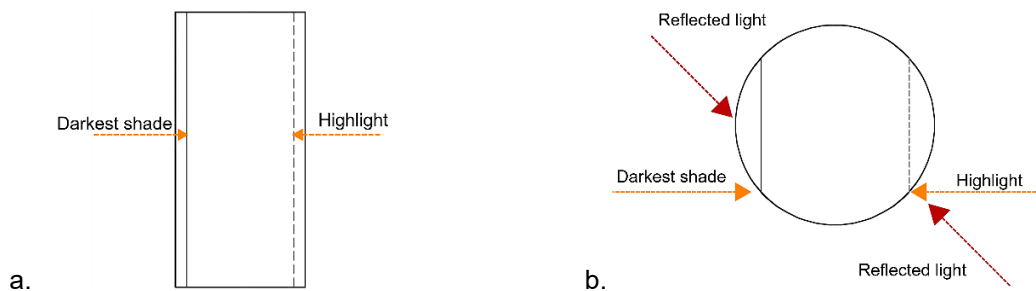


Figure 2.48 a-b: The effect of light falling on a cylinder. The graduated light and shade of the cylinder subdue the dazzling effect of dark-light contrast, which occurs when looking from the inside toward the light outside [25]

## 2.6 Relevant results in the existing literature

Comparative studies showed that suggested features achieved better performance in terms of air temperature on three levels; urban setting; building form; and building envelope.

### 1. Urban setting

Recent studies focused on the influence of cross shading, orientation, and proportions of the street canyon on temperature differences. The air temperature in the narrow urban canyon ( $H/W = 2$ ) decreases by  $4\text{ }^{\circ}\text{C}$  compared with the wide urban canyon ( $H/W = 0.5$ ) because of the lower solar gain in summer [13]. Ambient temperature above the canyon is found to be higher than the temperature inside the street with maximum of  $5\text{ }^{\circ}\text{C}$  [26]. The more open and exposed urban canyon the more increase in daytime temperature within the canyon. This effect can be reduced by the sky view factor and maximization of cross shading. It was proven that the increase in temperature in summer is more pronounced in east-west than north-south oriented canyons between 3-5 k. [13].

The duration of solar radiation incident on both the east and west facades simultaneously was less than 3 hours in a narrow canyons. The NS street orientation for  $H/W = 1.5:1$  and higher results in street shading between 40 to 80% of street area, whilst diagonal street orientations NW–SE (S2, S3) and NE–SW (S5, S6) only manage street shading between 30 to 50% of street area. A latitude of  $33^{\circ}\text{N}$ , EW street orientation achieves shading of 30% for an 8-month period, provided that a 2:1 or higher  $H/W$  ratios is used. The ratio 0.5:1 is least effective even with NS street orientation (less than 35% street shading). This means that under low latitude conditions deviation of the street from EW orientation may often be a desirable criterion in urban design [14].

### 2. Building form (the courtyard house)

Some researchers presented a study about the most appropriate depth ratio for a courtyard using a developed CFD numeral model. The numerical code took into account pre-computed solar radiation in the walls of the courtyard and predominant wind [12]. Some studies have examined the influence of courtyard geometry on the air-flow pattern and the thermal comfort in the surrounding rooms. CFD and thermal comfort simulations were employed. CFD simulations were validated by comparing them with 2D wind tunnel experiments in terms of air-flow and inside various cavity ratios. The low air speed values in single sided ventilated rooms does not contribute to the improvement of thermal comfort (this should be related to the performance of screens in the context of cross ventilation) Rooms facing one courtyard and having single-side natural ventilation had very low indoor quality and the existence of other courtyards provided better cross ventilation. The best cases in terms of thermal comfort were those facing the narrowest courtyards (with dimension ratio of 1x1 and 2x1) Rooms in ground floor achieved the best cooling performance, especially when protected from direct solar radiation [68].

Measurements recorded between July 15 and September 15 in house of al Suhaimy in Cairo show that the courtyard air temperature is lower than the air temperature on the roof during a period of 10 to 12 hours a day. It is also apparent that

the courtyard is cooler than the roof by a maximum of 4-7 °C [55]. Simulations were carried out to compare the mean shadow density of a courtyard and pavilion types considering the solar data for Morocco as a case study for hot-arid climate. The courtyard recorded an average of 11 hours of shadow on the ground on 21 June when the two pavilions recorded 9.8 and 6.1 hours [61].

### 3. Building envelope

It was proved that the maximum temperature of a low mass building was about 2° C above the outdoor maxima, while that of a high mass one was about 2° C below. Also mass was found to be more effective in reducing the rise of indoor temperature caused by heat gain through the external walls than that caused by penetrating solar radiation. The shading of the window has reduced the indoor average temperature by about 1 °C [27]. Measurements showed that in a hot and arid climate it is possible to achieve a reduction of 3-6 °C in a heavy constructed building without operating an air conditioning unit. The anticipated reduction depends on the amount of thermal mass, the rate of night ventilation, and day and night temperature swing [56].

Hypothetical modules of different types of Australian residential constructions were numerically analyzed. The analysis showed that the heavier mass constructions were found to be the most effective walling systems which offer the least energy consumption and indoor temperature fluctuations, especially when protected within the insulation portion [30]. A different study has developed a simple model coupling thermal mass and natural ventilation. The experiments showed that the internal thermal mass affects the time lag of indoor air temperature. By comparing six different external walls it is found that the use of heavy wall with external insulation is predicted to have the lowest amplitude of indoor air temperature and hence the heavy walls with external insulation are suitable for naturally ventilation [76].

In cold climates, however, a study investigated the effect of thermal mass on annual heat load of buildings. The results indicated that increased thermal mass is not effective for decreasing annual heat demand in typical residential buildings [67]. As a result of optimizing thermal mass, different study concluded that the maximum savings in yearly transmission loads are about 17% for cooling and 35% for heating [4].

In different study the sensitivity of air change rates in a naturally ventilated atrium space was analyzed. The study concluded that the number of vents included in the model was found to have a significant effect on the ACH. External wind speeds from 25 to 250% of the mean site wind speed (5.7 m/s) were found to result in an almost linear increase in the ACH rate. For a single wind speed, the relationship between wind direction and the ACH rate was also found to be approximately linear for wind directions between 0° and 90 ° to the wall vent openings, but non-linear for other wind directions (90–135°) [40].

It has been proven that the use of window screens in hot climates reduces the cooling loads and the perforation ratio of the screens influences the indoor temperature. Simulations were applied to screens on west, south, east and north facades and an ultimate ratios were proved as achieving the highest rate of energy saving. Proposed ratio between the width and depth was 1:1 with an 80% perforation in the west and north orientation and 90% in east and south. In comparison with non-shading windows, the energy savings resulted from the use of these screens reached 30%, 30%, 25% and 7% for the west, south, east, and north orientations [65].

## 2.7 The passive design strategy

In hot and arid climate regions, the main purpose of passive design is to achieve comfort inside the building through reducing the thermal loads. The first factor encountered in this process is the solar intensity and how to reduce the heat transferred to the building by the solar radiation. Solar geometry plays a major role that should be considered in terms of orientation and building form. Apart from thermal loads resulted from the inhabitants and appliances, the thermal load in general resulted from direct solar penetration, heat transfer by conduction through building components and infiltration. A passive cooling strategy hence has two main pivots; minimization of heat transferred into the building and disposal of heat. As this study is concerned with traditional house components in which the physical principles, mainly the heat transfer mechanisms, are processed, figure 2.49 illustrates the procession of physical principles within the passive cooling strategy. In traditional buildings in hot climate i.e. Cairo, cooling effect is an outcome of processing physical phenomena/s through the incorporated elements and devices.

The traditional designers understood the thermal behavior of the structure and the modes of heat transfer through building components. Procession of physical phenomenon occurs on three major levels which are influenced by the resulted effects; urban setting; building form; and building envelope. Each of these levels of influence comprises various components through which physical phenomenon take place. It is a quite complicated process since each of the proposed building components and urban parameters adopt one or more method or mechanism by which the heat is transferred. A convective current for instance could be a secondary effect for radiation and conduction when processed within the building materials responding to the solar geometry. Previous analysis showed that the basic principle in designing the traditional house was to accomplish a couple of goals; fulfill privacy; and achieve comfort. These proposes were fulfilled through the proposed components within urban setting, building form, and building envelope. The analysis identified some key components and other subsidiary elements. The main aspect is the duality of nature of these key elements through which both thermal comfort and privacy were achieved. Accordingly, the key elements discussed above are demonstrated in the model in figure 2.50, upon which the base case study is selected in the next chapter.

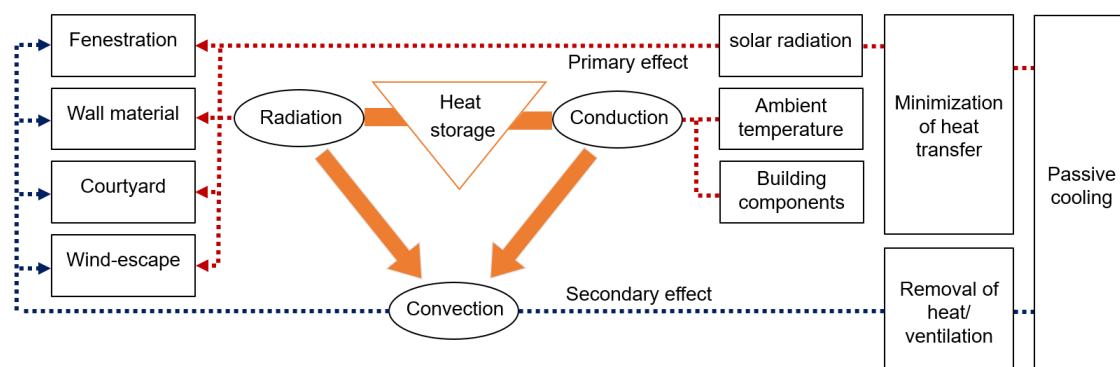


**Figure 2.49:** Passive cooling strategy in the traditional building

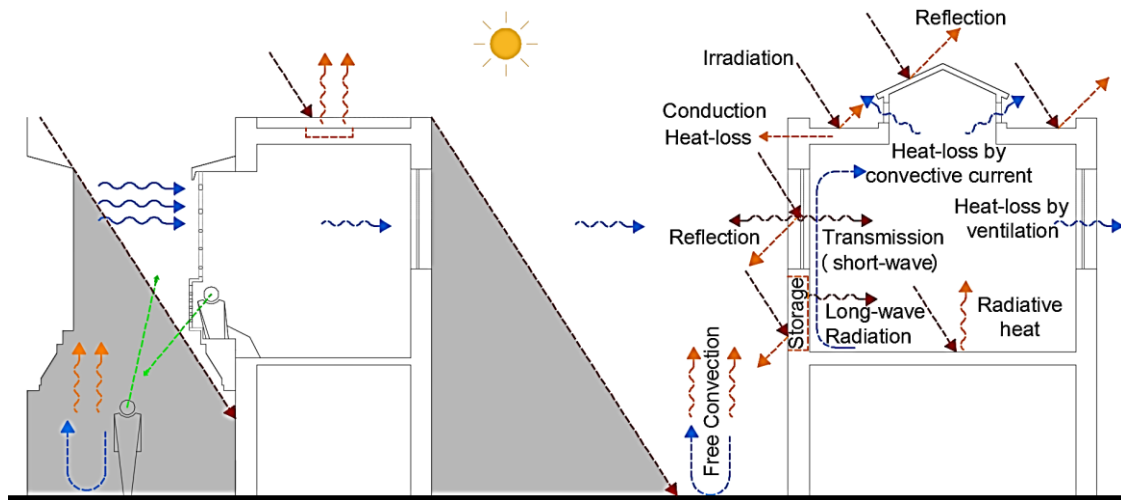


**Figure 2.50:** Proposed integrated model

## 2.8 Conclusion

1. Cairo is located in the hot-arid climate zone of northeast Africa, and hence receives an average annual sum of 3000 hours of sunshine, ca. 9 hrs. /day and direct solar intensity up to  $900 \text{ W/m}^2$ . The Prevailing wind is north and northeast. Air temperature exceeds  $40 \text{ }^\circ\text{C}$  in summer with large diurnal temperature differences,  $15\text{-}25 \text{ }^\circ\text{C}$ . The annual direct normal solar irradiance ranges between  $2,000 \text{ kWh/m}^2$  from north to south. Thermal comfort zone for Cairo lies between  $20\text{-}26 \text{ }^\circ\text{C}$  with relative humidity 50%. Solar geometry is a decisive factor for optimal building orientation northeast. Winter sun penetrates south oriented rooms deeply, solar altitude ca.  $36^\circ$ , however, summer sun, altitude ca.  $85^\circ$  gives shaded porches and does not penetrate rooms oriented south. Shading devices could be efficient on south oriented façade in summer time. Studies proved that horizontal overhangs facing south reduces heat transfer into the building with ca.  $75 \text{ Wm}^2$  during June.
2. Culture and religious beliefs have significantly influenced the urban built form and the house design on different levels. Due to centralization of houses around courtyard to fulfill the need for privacy, the city was a dense grouping of courtyard houses. In the old city the main road is north-south oriented and subsidiary streets are east-west oriented thus remain shaded during daytime, especially when considering the aspect ratio of the street which is relatively narrow. External façades were almost solid which allowed the benefit of the high storage capacity of the stone walls. The house is perceived as a succession of spaces around an internal courtyard which provides cool air to the surrounding spaces. Fenestration system has a dual function; it maintains privacy to the inhabitants without sacrificing overlooking the outside, and protects against direct solar heat gain and control natural ventilation through the gradual arrangement of perforation.
3. Thermal comfort is a result of processing physical principles within building components and urban surroundings. Traditional house demonstrates awareness of heat transfer mechanisms and ways of heat gain/loss in the building. Heat gain is significantly decreased due to the quality of building envelope; i.e. thermal conductivity of materials and paucity of openings. Traditional building demonstrates a passive cooling strategy comprises minimization of heat transferred into the building and disposal of heat. The most decisive components in the proposed passive strategy are courtyard form, openings, and street aspect ratio, in addition to construction materials.

## Chapter 3

# Measurements and observations

### 3.1 Introduction

This part of the study is concerned with the empirical work which aims to the investigation of the potentials of the traditional building as a self-climate modifier. The empirical work comprises field measurements for selected cases. The subsequent simulations aim to comparative analysis to determine a case study to be adopted as a valid model for passive design. This chapter comprises explanation of the field measurements took place for three selected cases and primal analysis for indoor temperatures of each. Three cases are selected to undertake field measurements in, two of which represent the typology of medieval traditional Cairene houses. The other case however, is a contemporary multi-story residential building following the modern typology and construction methods prevailing in today's Cairo. The field measurements took place during August and September 2014. The weather data for Cairo was obtained for the measurement period on daily basis according to the records of the weather station installed in Cairo International Airport.

The first traditional case (CT1) which is the main case-study is an integral representation of traditional residential buildings of medieval Islamic Cairo, which comprises most of the so considered climatic responsive building features. The second case (CT2) is similar, however, it lacks the roof wind-escape which plays a significant role in controlling the air flow inside the space, as it will be illustrated. As for the contemporary case; will be referred to as (CM), it was intended to compromise the major opposites to suggested traditional characteristics, especially shading options. The ultimate target of this stage is to make a statement of consideration for various parameters through which the best thermal performance took place. The first traditional case (CT1) is found to be the most representative for traditional buildings not merely because of the passive features embodied within its design, but also in terms of the dense setting of the surrounding urban fabric, as it is shown in the satellite images in figures 3.1-4.



**Figure 3.1:** Selected cases' locations (source: Google Earth 2014)



**Figure 3.2:** House of Zeinab Khatun (CT1), urban setting (source: Google Earth 2014)



**Figure 3.3:** House of Amna bint Salem (CT2), urban setting (source: Google Earth 2014)



**Figure 3.4:** Heliopolis apartment (CM), urban setting (source: Google Earth 2014)

### 3.2 Case study (CM)

The selected building is located on the eastern borders of Cairo. Figure 3.5 is a satellite image of the site. The monitored case exists in the first floor of the nine-story residential building on a ground floor area of 310 m<sup>2</sup>. Each floor consists of two identical apartments with an area of 135 m<sup>2</sup>. The main façade is south-west oriented on a main street with a width of 75 m and a central green area, shown in figure 3.6. The building is a concrete structure and its walls are of hollow red bricks with density of 1790 kg/m<sup>3</sup>, thermal conductivity 2.1 kJ/hmk, and specific heat 840 J/kg.C, according to the Egyptian code. Tables 3.1-2 include the building description and the U-values of the building materials respectively. Windows are 6 mm single clear glass with aluminum frames and all doors are made of wood. Parquet timber flooring is applied to the monitored case. The monitored room, shaded in the floor plan (fig. 3.7) is the main living area of the western apartment in the first floor. The room is overlooking the main street through a wide window, 6 m<sup>2</sup>, about 54% of the wall with no shading device. The case lacks any cross shadings from opposite buildings except for the building facing the north east façade.



**Figure 3.5:** CM, site  
(source: Google Earth 2014)



**Figure 3.6:** CM, general view

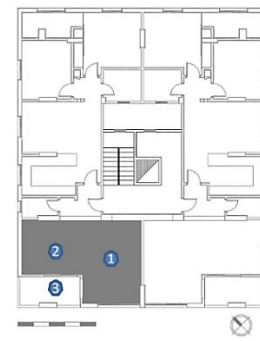


**Figure 3.7:** CM, floor plan showing measurement spots

**Table 3.1:** CM, building description

Item	Description
Location	Eastern borders of Cairo
Building type	Residential
Floor area	310 m <sup>2</sup>
Wall material	Hollow red bricks
Skeleton	Concrete
Wall thickness	10-20 cm
Slab thickness	12-18 cm
Windows	6 mm single clear glass with aluminum frames

**Table 3.2:** CM, U-value of material

Material	W/m <sup>2</sup> K
External wall (solid red brick 20 cm and 2 cm plaster)	1.82
Internal wall (solid red brick 10 cm and 2 cm plaster)	2.65
Internal floor (concrete slab 18 cm and massive wood floor)	0.71
Roof (concrete slab 12 cm with stereo-pore insulation and tiles)	0.45
Glazing (6 m single glass)	5.6

### 3.2.1 Measurements (CM)

Field measurements took place for indoor air temperature of the selected room on two stages, the first of which spanned from April 18 to 25. The second stage spanned from August 13 to September 3. Data loggers were hanged from the ceiling on a height of 1.7 m. Two data loggers were installed in the room, one facing the window directly overlooking the street and the other facing the balcony as shown in figures 3.8 a-c. One logger was as well placed in the balcony to get real ambient temperature records. The data loggers used are HOBO U12-012. According to the manufacturer, the measurement range of the loggers are  $-20^{\circ}$  to  $70^{\circ}$  C and 5% to 95% RH. The accuracy of the loggers is  $\pm 0.35^{\circ}$  C from  $0^{\circ}$  to  $50^{\circ}$  and  $\pm 2.5\%$  from 10% to 90% RH. The loggers were set to continuously take readings each 10 minutes. The apartment was vacant and closed during the measurement period and no mechanical cooling was operated. Results of the field measurements are shown in figure 3.9. The first stage of measurements in April is not the most representative of the hot climate of the region, however it is quite adequate for validation of the simulation model. Moreover, a comparatively high temperatures, reached a maximum of  $38^{\circ}$  C were recorded, which closely matches the hottest summer days. The weather data for Cairo was obtained on daily basis during the measurements period and a week before from the NOAA (National Oceanic and Atmospheric Administration) [53]. The obtained data included hourly records which were subsequently used to create a weather data file that was given to TRNSYS to run the simulations.

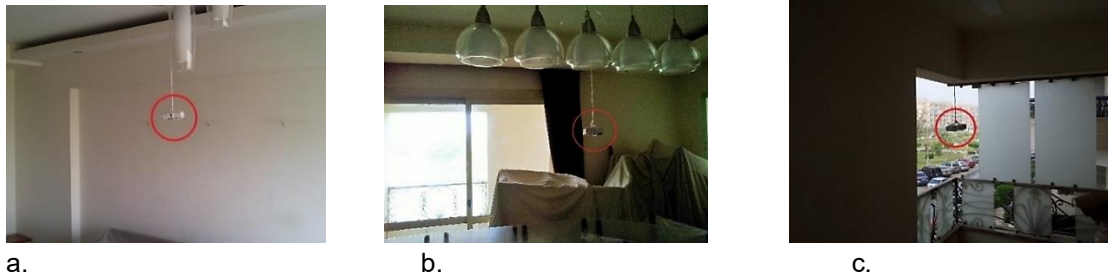
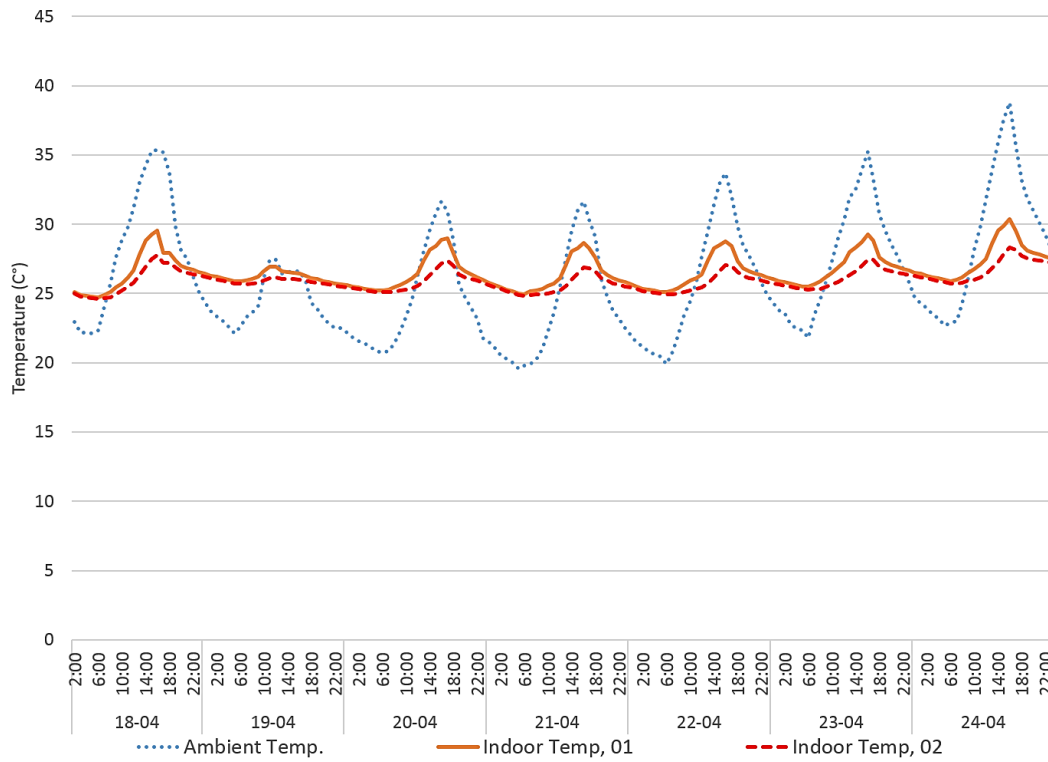


Figure 3.8 a-c: CM, data loggers' installation

### 3.2.2 Observations (CM)

Some differences were traced between the values of the measured ambient temperature, especially for the minimum values, and those of the obtained weather data which found to be  $4^{\circ}$  C lower in average as shown in Figure 3.10. This could be attributed to the differences between both sites of measurements as the weather data is obtained from the weather station installed in Cairo airport in a totally open and un-urbanized area. This is quite different from the site in which the readings were recorded; within comparatively dense urban fabric in which the measured temperature should be influenced by the heat island effect and the heat released from the buildings during night-time. Measurements for indoor and outdoor temperature and relative humidity were obtained as well coincidentally with the other cases from August 13 until September 3 (fig. 3.11). The air flow factor was neglected, except for an infiltration rate of 0.4/h considered in the simulation model, as the windows were closed along the measurement period. The diurnal temperature differences were likely limited as the heat transfer occurs merely through transmission through the walls and closed windows; hence the interior space did not widely respond to the ambient temperature. The indoor maximum temperature recorded on August 26 at 5 pm was  $34.02^{\circ}$  C with an average  $33.4^{\circ}$  C, while the minimum was  $30.54^{\circ}$  C on September 3 at 7 am with an average of  $31.23^{\circ}$  C (fig. 3.12). Due to the clear windows area which is approximately as the double as that in the traditional cases, the levels of illuminance were quite higher.



**Figure 3.9:** CM, measured temperatures 18-24 April

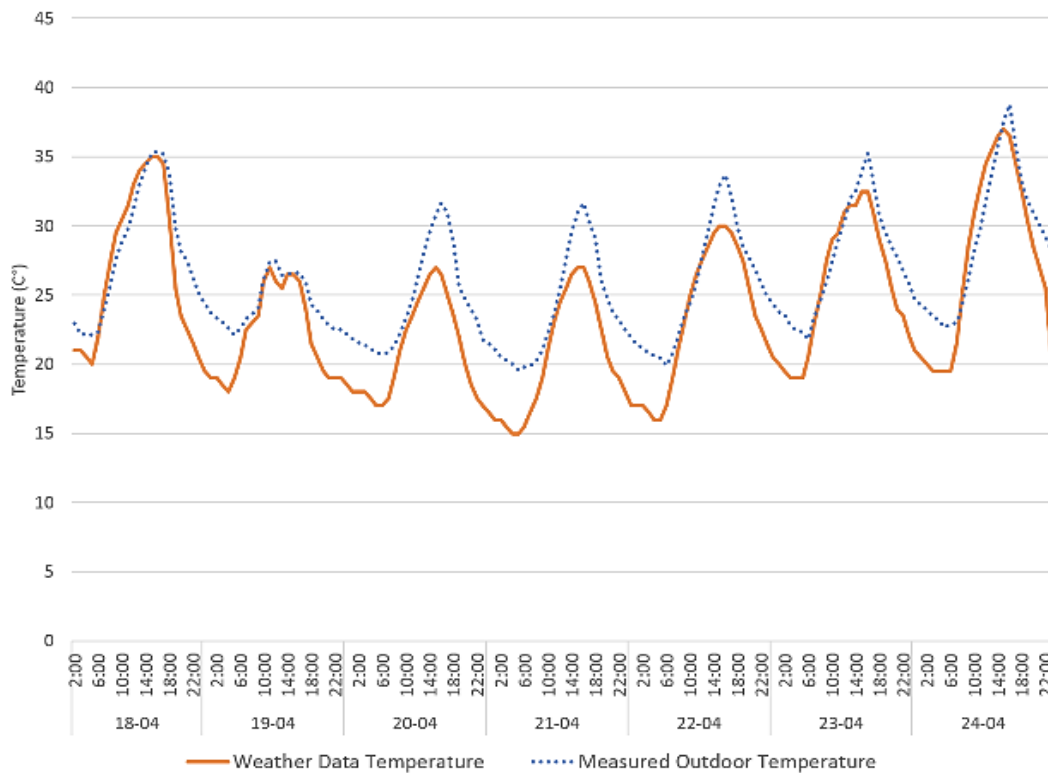


**Figure 3.10:** CM, measured outdoor temperature against real weather data

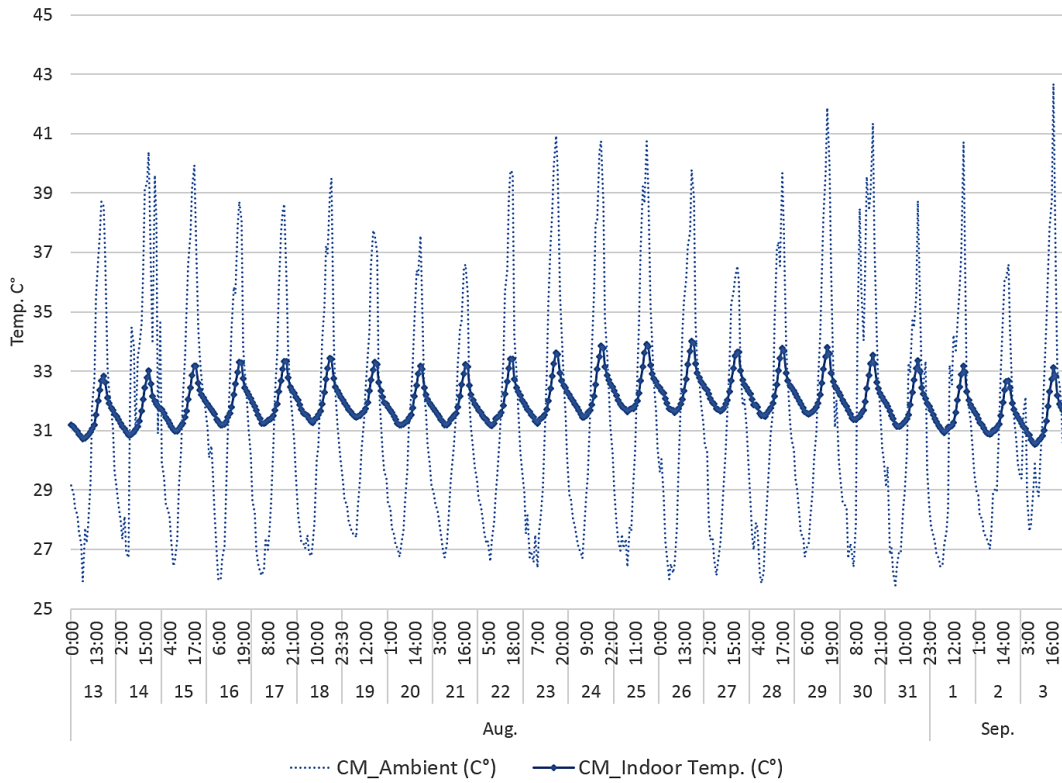


Figure 3.11: CM, measured temperature, Aug. 13 to Sep. 3

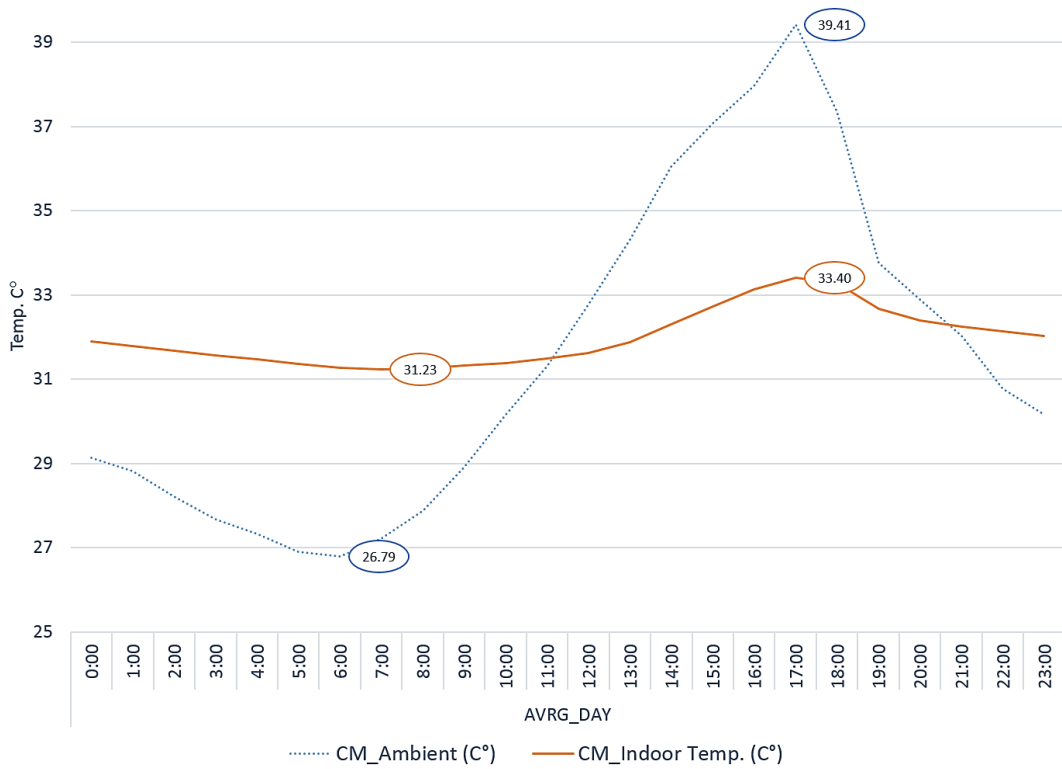
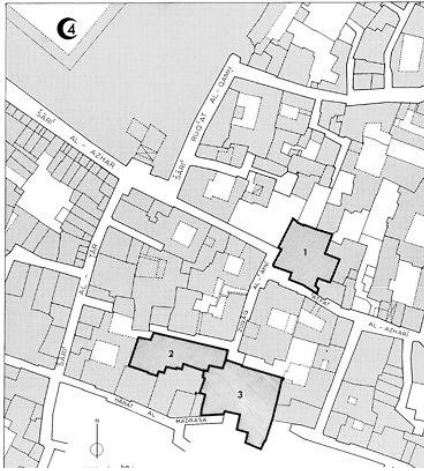


Figure 3.12: CM, average day temperature, Aug. 13 to Sep. 3

### 3.3 Case study (CT1)

The house House of Zeinab Khatun is situated in the district of Darb al Ahmar in the heart of the old city of Cairo on the narrow alleys right behind the south eastern wall of mosque of al Azhar. It is a quite famous residential area of the time where two other famous houses can be found; Bait El-Harrawi and Bait Sitt Wasila as shown in the site layout (fig. 3.13). The house was built in 1468 AD during the reign of Sultan al Ashraf Qaytbay and renovated in 1713. It is considered one of the representative examples of the middle class residential buildings during the Mamluk period. Figure 3.14 is an exterior view of the main façade, south-west.



**Figure 3.13:** House of Zaynab Khatun (CT1), site Layout: 1. House of Zaynab Khatūn, 2. House of Sitt Wasīla, 3. House of al-Harrawi, 4. Mosque of al-Azhar [50]



**Figure 3.14:** CT1, exterior view of the main façade, south-west

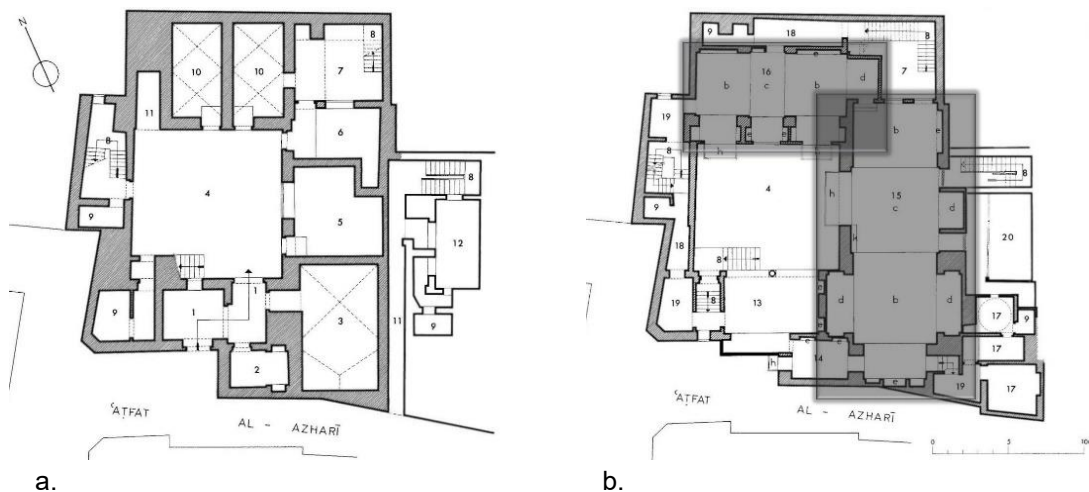


**Figure 3.15 a-b:** CT1, a. ground floor plan, b. first floor plan, monitored halls are shaded [50]: 1. Entrance, 2. chamber, 3. *qa'a* (meeting room for men), 4. courtyard, 5. *qa'a* (reception room for men), 6. chamber, 7. small yard, 8. stairway, 9. latrines, 10. storage, 11. corridor, 12. common area, 13. balcony (Maq'ad), (e) wardrobe, 14. antechamber, (e) wardrobe, (h) *mashrabiya*, 15. grand hall (GH), (d) niche, (e) wardrobe, (h) *mashrabiya*, (k) sideboard, 16. secondary hall (SH), (b) *iwān*, (c) *durqa'a*, (d) niche, (e) wardrobe, (h) *mashrabiya*, 17. hammām (bath), 18. Corridor, 19. open space, 20. former *riwāq*

Figures 3.15 a-b are ground floor and first floor plans respectively. The first floor is which the two major halls, shaded in plan, examined in this study occupy. The house is surrounded by buildings of similar height, ca. 15 m. The building occupies an area of ca. 450 m<sup>2</sup> over a square plan and oriented ca. 30° north-east. As most of the houses of Islamic Cairo in mediaeval times the house plan is centralized around an internal courtyard ca. 9 x 9 m (fig. 3.16). The main façade, south-west, and the north-west façade meets the intersection of three short alleys. However the other two facades were adjacent to neighbor buildings which currently do not exist with their original height.



**Figure 3.16:** CT1, view of the courtyard from the roof

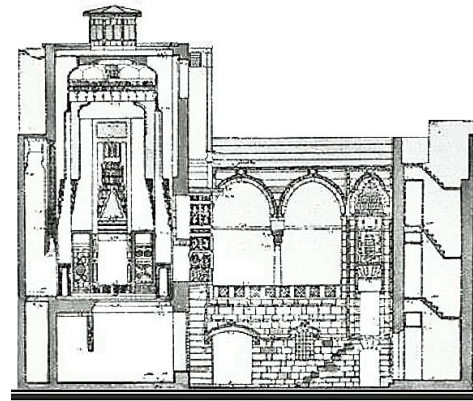


**Figure 3.17:** CT1, cross section in the grand hall and the courtyard looking towards the balcony, south-west [50]

The main building material is limestone, the roofs are made of wood, and the windows varies between wooden lattice work and iron grills. The exterior facades are made of clear cut simple limestones and lacks any distinguished ornaments of extensive lattice work on the windows. However the interior façade overlooking the courtyard presents more lavish lattice work in the *Mashrabiyas*. A large terrace (*maq'ad*) occupies the area right above the entrance on the south western wing, facing the north east summer wind and overlooks the courtyard through a couple of pointed arches (fig. 3.17). The balcony is directly connected with a staircase to the courtyard. The fourth wing of the house however comprises a stairway and other services and utility spaces. The house embeds two main principle spaces overlooking the courtyard in the first floor level, which are the main measurement and simulation interest of this research. The first space is the main grand hall which mostly occupies the south eastern wing of the house and generally attributed as the summer hall. The second is a secondary hall, also on the first floor but located on the north eastern wing over the courtyard. Both halls can be described in details as the following:

1. Grand hall (GH).

With an overall height of ca. 11.6 m, and a space volume of ca. 1090 m<sup>3</sup> this hall is highly protected against solar radiation and high temperature with a percentage of openings of ca. 20 % of the exposed surface. It has a mere large opening only to the courtyard, which is 50% shaded by an extensive lattice work *mashrabiya* on a single glass pane (fig. 3.18). Table 3.3 concludes the room description. The hall has a clear rectangular plan consists of two large *iwans* flanking a central squared space called *durqa'a* which is a step lower.

Figure 3.19 is an interior view towards the south-west *ivan*. The entire roof is made of carved wood and interrupted in the center with a sky-light which works as a wind-escape device that plays a significant role in the ventilation process as well as in the space illumination. The wind-escape has an octagonal plan and height of 1.5 m. Each of the eight sides has an axial revolving glass window; only four were opened during the measurement period. A couple of large windows are placed on the north eastern wall, which overlook a small backyard. Another pair of small windows with iron grills exist on the upper part of the wall facing the courtyard however, they remained closed all the time. The lower indoor temperature recorded in this room is also attributed to its high thermal mass as it will be discussed. The wall stones varies in section, however an average of 60 cm thickness is considered in the simulation model. The interior walls are covered with marble to a height of 1.5 m.

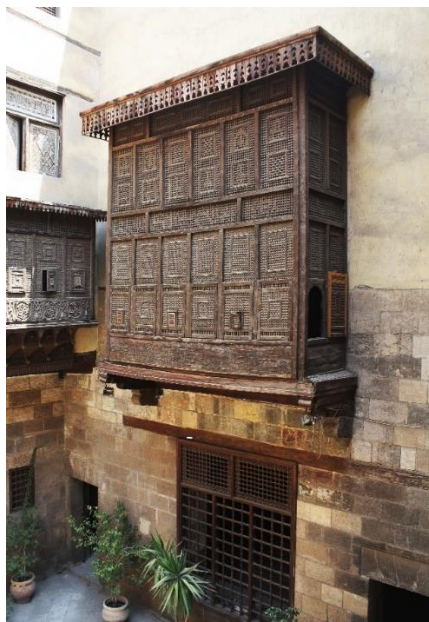


**Figure 3.18:** CT1, grand hall, *mashrabiya*    **Figure 3.19:** CT1, grand hall, interior view

**Table 3.3:** CT1, grand hall (GH) description

<b>CT1 Grand Hall (GH)</b>	
Floor	1st
Height	11.6 m
Area	95 m <sup>2</sup>
Volume	1090 m <sup>3</sup>
Exterior surface area of courtyard facade	164 m <sup>2</sup>
Percent window area	20 %, 50 % shaded
Window orientation	North-west
Measurement period	13 Aug.-8 Sep. 2014
Measurement output	Indoor temperature Relative humidity
Ventilation	Windows always opened

## 2. Secondary hall (SH)

This hall which is located on the north-east wing of the house is proportionally smaller than the grand hall. It has a height of 9.3 m and area of 54 m<sup>2</sup>. In plan it is similar to the grand hall, however it has a greater opening ratio to the courtyard through several windows (fig. 3.20). Three openings on the lower level of the hall has the extensive lattice work of the *mashrabiya* while the upper parts has more opening ratio through the iron window grill. The overall opening ratio is ca. 22% of the exposed surface. Moreover, two windows are placed on a higher level on the south eastern wall overlooking the outside, one of which remained opened during the measurements. Figure 3.21 is an interior view looking towards south-east wall. The hall has a roof wind-escape similar to that in the grand hall. Table 3.4 includes a brief description of the hall.



**Figure 3.20:** CT1, multiple openings of the secondary hall on the courtyard



**Figure 3.21:** CT1, interior view of the secondary hall

**Table 3.4:** CT1, secondary hall (SH) description

CT1 Secondary Hall (SH)	
Floor	1st
Height	9.3 m
Area	54 m <sup>2</sup>
Volume	490 m <sup>3</sup>
Exterior surface area of courtyard facade	82 m <sup>2</sup>
Percent window area	22 %
Window orientation	South-west
Measurement period	13 Aug.-8 Sep. 2014
Measurement output	Indoor temperature
	Relative humidity
Ventilation	Windows always opened

### 3.3.1 Measurements (CT1)

The building is registered as a monument and opened to visitors year round. The field measurements took place along four weeks between August 13 and September 8, 2014. Although the building is relatively preserved, many windows are in bad condition and remain opened with no consistent opening schedule. After the official visiting hours the building remains closed until next morning. It was important then to ensure that all windows on the greater heights remains closed and keep lower windows opened along the measurement period through regular visits through coordination with the monument administration. A total of six data loggers and sensors were used in this house, which measure temperature, relative humidity and light intensity. Six sensors were installed in the halls while one logger were installed in the courtyard. The data loggers' specifications are as the same as in (CM).

In the grand hall two data loggers were installed with three sensors. One logger was installed at the very top of the hall, hanged from the sky-light at height of 9 m from the finish floor level. A thermal cable was connected to the logger to hang down ending with a sensor at the level of 2.5 m. The main purpose of this installation was to get a record for air temperature in the middle of the room compared to temperature at the level of the roof were the warmer air escapes from the roof device. The third sensor was mounted on the window screen at 2.5 m. One sensor was hanged from the ceiling in the middle of the secondary hall at 2.5 m from the finish floor level, in addition to a window mounted logger on a height of 4 m. To get a record for the outdoor temperature of the courtyard a data logger was hanged from the window screen of the grand hall and remained shaded underneath the protrusion of the *mashrabiya*. Figures 3.22-3 and table 3.5 describe the installation order of all sensors. Although measurements expanded along 4 weeks from August 13 to September 8, measurements in the secondary hall took place one week later, from August 21. This time span is which considered to compare both halls.



**Figure 3.22:** CT1, floor plan showing measurement spots.

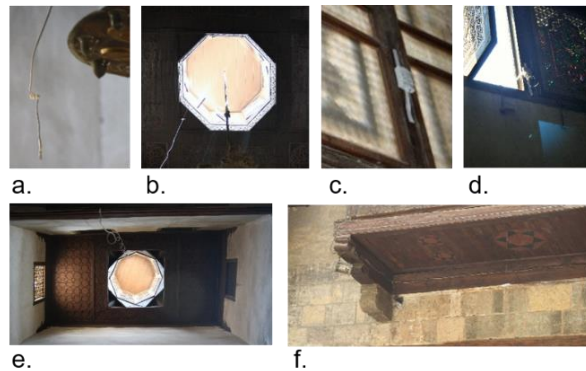


**Figure 3.23 a-f:** CT1, data loggers' installation GH1-3, SH1, 2 & CRT respectively

**Table 3.5:** CT1, sensors installation

Space	Sensor	Position
Grand hall	GH1	Ceiling-hanged at 2.5 m from F.F.L.
	GH2	ceiling-hanged at 9 m from F.F.L.
	GH3	Mounted on window screen at 2.5 m from F.F.L
Secondary hall	SH1	Ceiling-hanged at 2.5 m from F.F.L
	SH2	Mounted on window screen at 4 m
Courtyard	CRT	Hanged at 4 m from G.F.L

### 3.3.2 Observations (CT1)

The maximum recorded courtyard temperature is found to be 37.75 °C in August 26 at 3 pm where the average maximum of the entire measurement period is found to be 35.79 °C. The minimum courtyard temperature however was 27.06 °C in September 1 at 6 am and the average minimum was 27.8 °C. The lowest indoor temperatures in the house were recorded in the grand hall, especially in the middle of the room at the level of 2.5 m, however the highest records were recorded by the window-mounted loggers. The average maximum indoor temperature of the grand hall is found to be lower than that of the courtyard with an average of 2.23 °C however, the minimum courtyard temperature is found to be lower with an average of 0.81 °C. The highest maximum indoor temperature of the grand hall was recorded by the logger GH3 at the window screen at level 2.5 m in Aug 24 at 4 pm while the lowest maximum temperature recorded by logger GH1 in the middle of the space at level 2.5.m was 28.52 °C, which had also recorded the lowest minimum temperature in the hall, 27.25 °C. The highest maximum temperature recorded in the middle of the room at level 2.5 m (GH1) was 35.15 °C while the average maximum was 33.56 °C. The lowest minimum temperature of the same spot however was 27.25 °C and the average was 28.6 °C. It is quite relevant then that temperature in the middle of the hall at level 2.5 m (GH1) is found to be consistently lower than that at level 9 m (GH2). The average difference was 1.01 °C and 1.93 °C for maximum and minimum temperatures respectively (figs. 3.24-5).

The inverse relationship between indoor temperature and relative humidity is apparent along the measurement time span (fig. 3.26). The maximum record of relative humidity was 61.5 % with indoor temperature 28.96 °C, while the lowest RH was 26.79% with temperature of 34.2 °C. Similar correspondence between relative humidity and indoor temperature can be found in the secondary hall as well.

Although the light intensity is not a major concern of this research, it is important to shed light upon illuminance levels in this case study to assure livability levels especially with the adoption of shading devices as dense as the window screens. Illumination during daytime is what to be referred to in this respect. The highest illumination level (Lux) is found to be 526.8 Lumen/m<sup>2</sup> and the minimum level was 27.6 Lumen/m<sup>2</sup>. The average maximum level is 280.61 Lumen/m<sup>2</sup> which is normally recorded right before and after the midday where the solar radiation can penetrate the space whether through the skylight or the window screens. The average minimum however is 61.47 Lumen/m<sup>2</sup> which is generally recorded right after and before sun rise and sunset respectively (fig. 3.27). The average illumination in general is 194 Lumen/m<sup>2</sup> which is quite acceptable for naturally illuminated indoor residential spaces.

As for the secondary hall, similar observations exist with slight differences. Figures 3.28-30 show the measurements' output for the secondary hall. The maximum temperature was lower than that of the courtyard with only 0.96 °C while the average minimum in the courtyard is found to be 1.79 °C lower than in the hall. Generally the grand hall (GH) showed a slight better performance than secondary one (SH) with average difference of 1.12 °C and 0.97 °C for maximum and minimum temperature respectively (fig. 3.31). The comparison between both halls took place for a time span between August 21 and September 8 as measurement took place in the secondary hall a week later. Taking into account that both rooms has the same conditions in terms of design and construction material, the wind direction and hence air flow inside the space remain subject to question as key factors for resulting in that temperature differences.

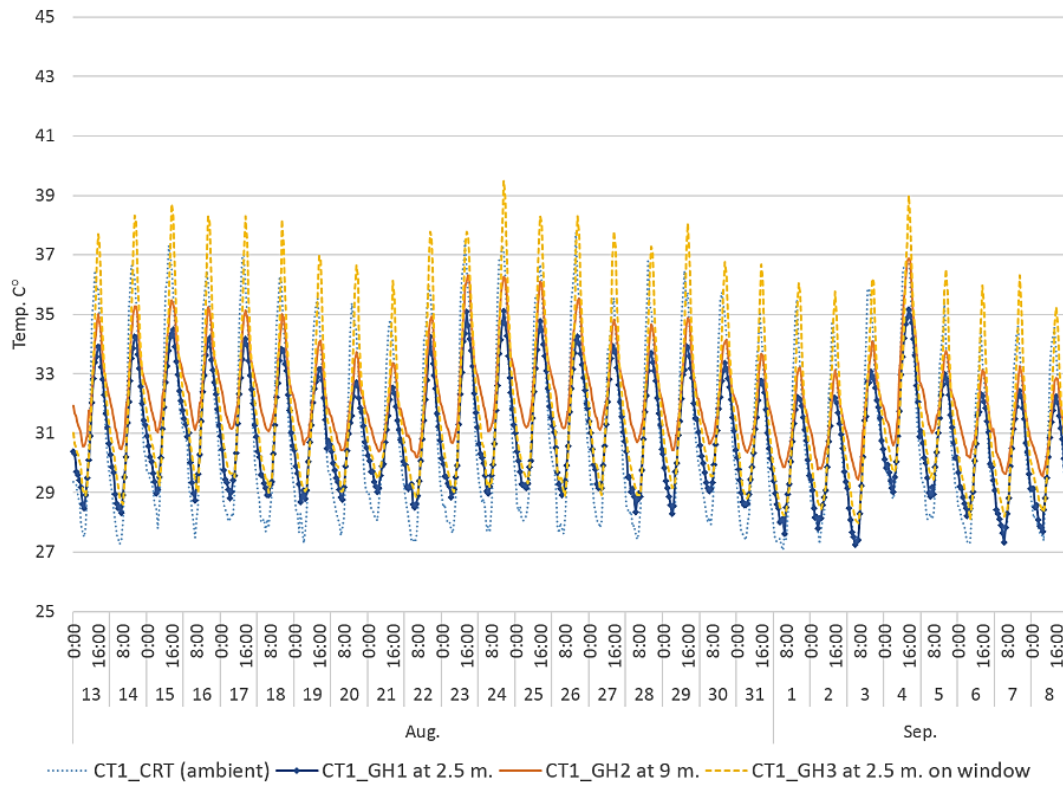


**Figure 3.24:** CT1-GH, measured temperatures in the grand hall and courtyard

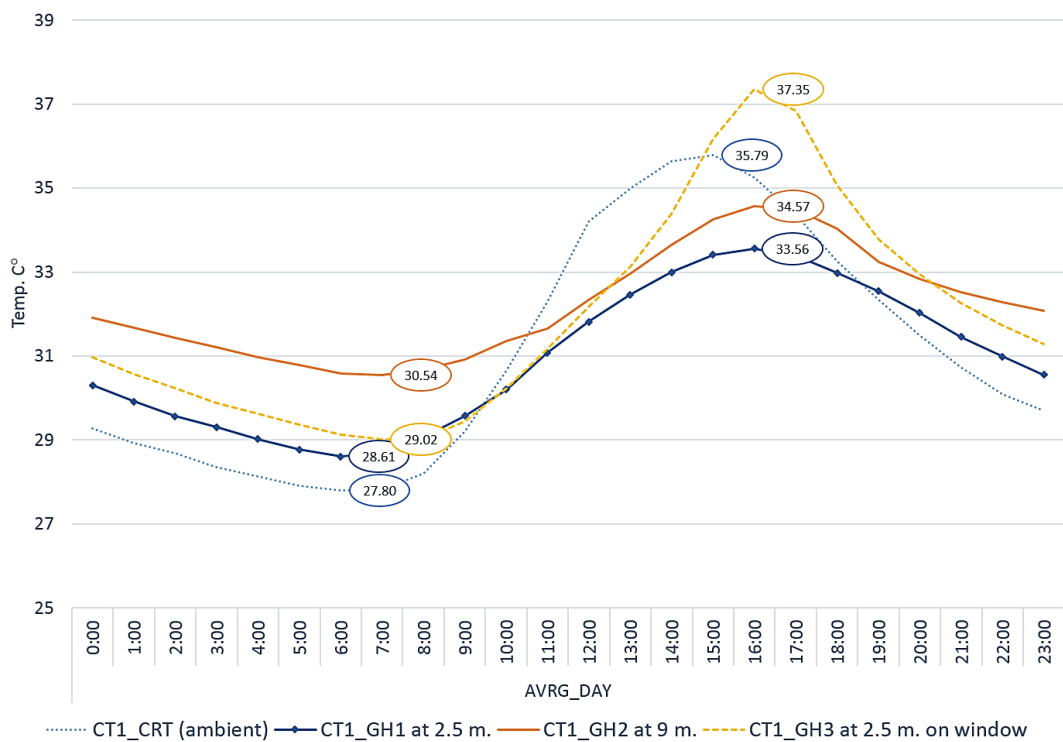


**Figure 3.25:** CT1-GH, average day temperature

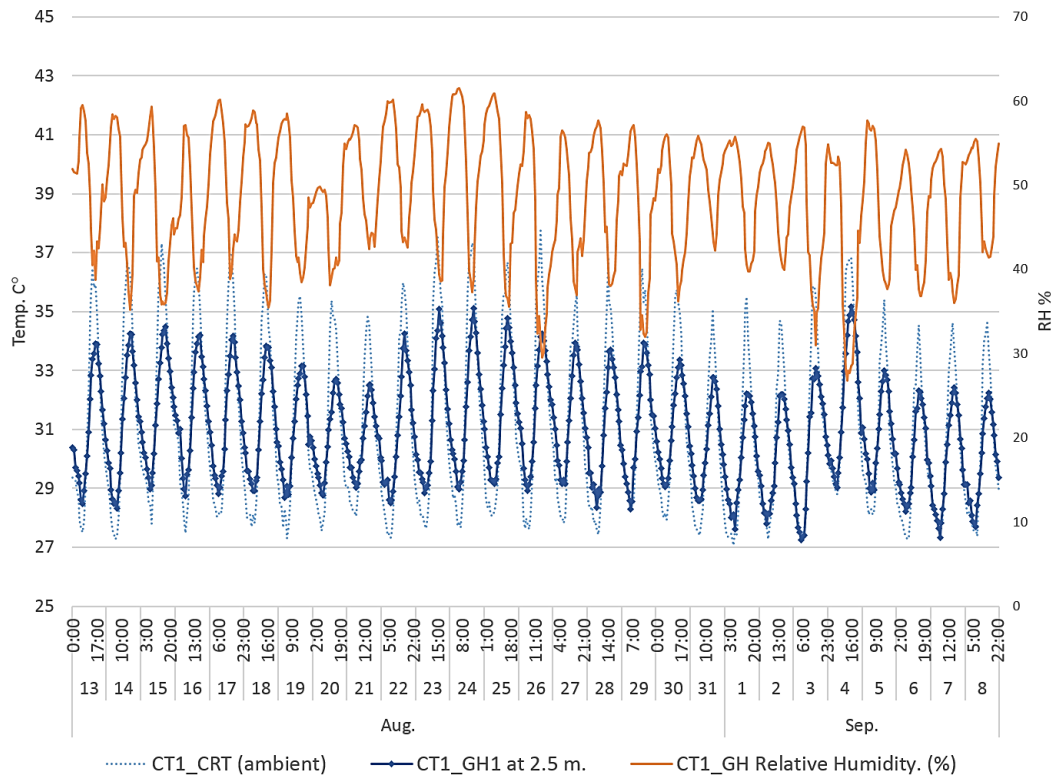


**Figure 3.26:** CT1-GH, measured Indoor temperature and relative humidity

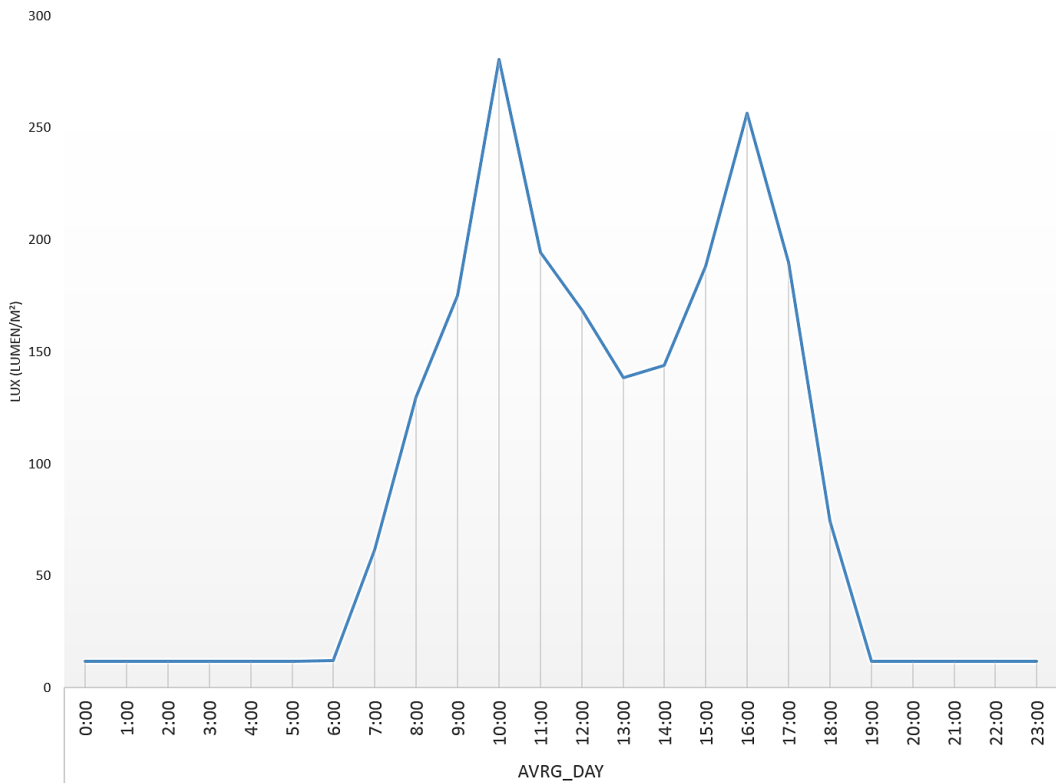


**Figure 3.27:** CT1-GH, average day illumination in the grand hall

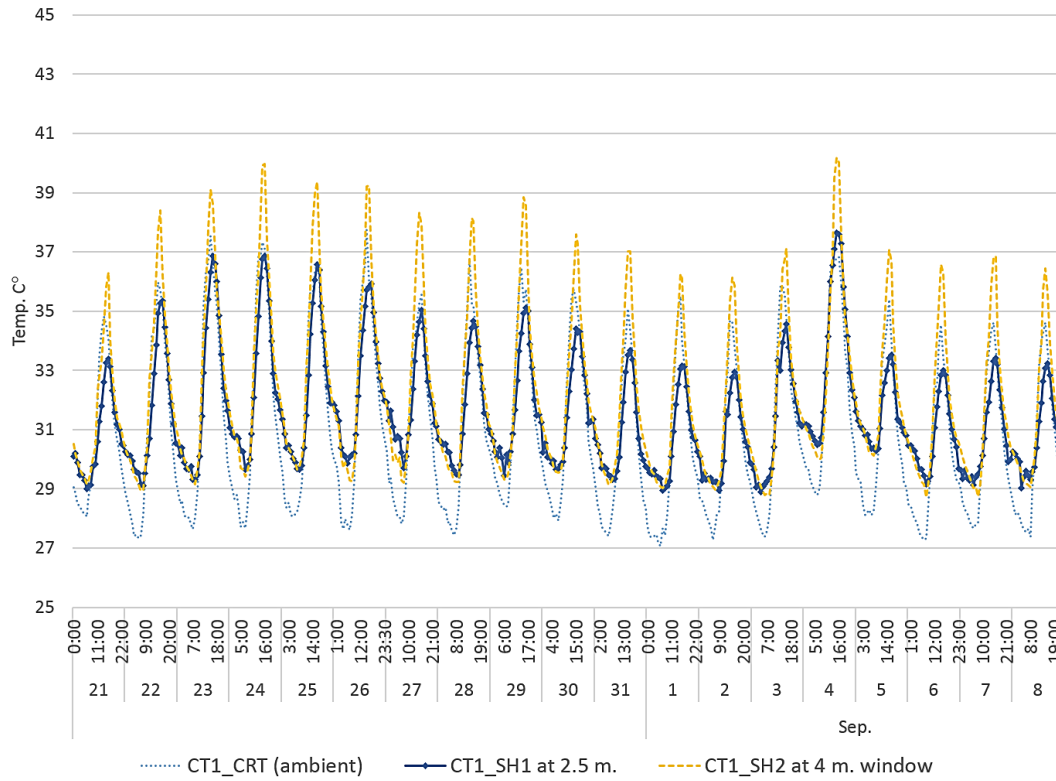


**Figure 3.28:** CT1-SH, comparison between indoor temperatures in the secondary hall, in the middle of the space at 2.5 m (sH1) and on window at 4 m (SH2)

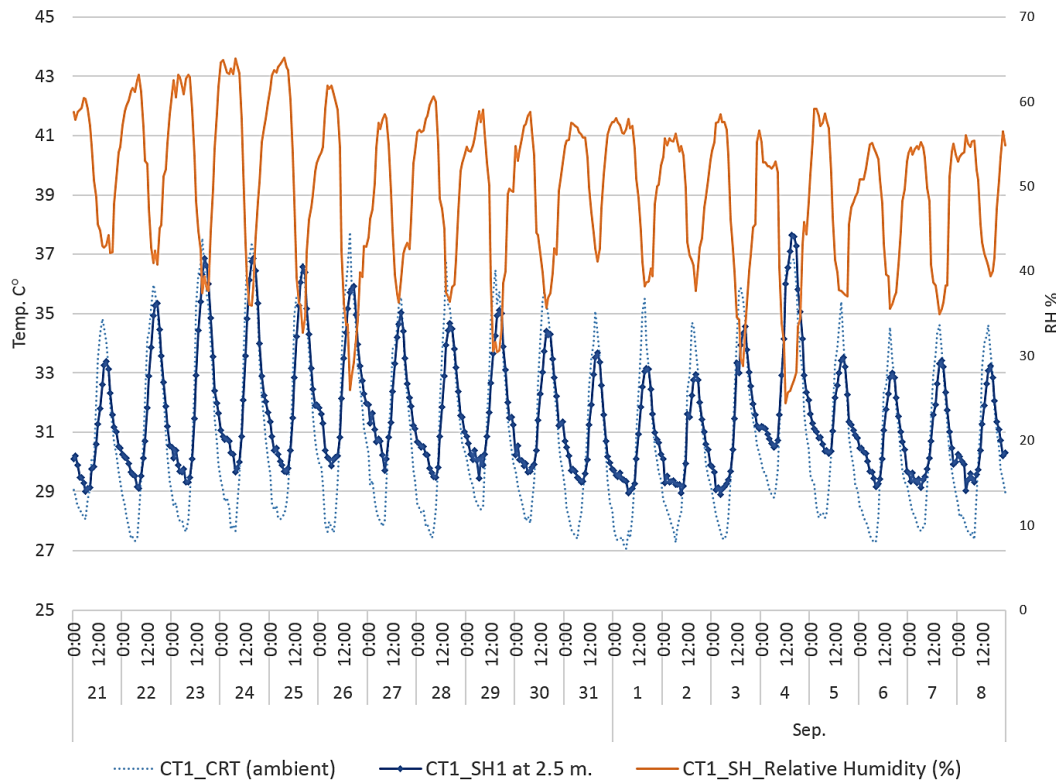


**Figure 3.29:** CT1-SH, measured Indoor temperature and relative humidity

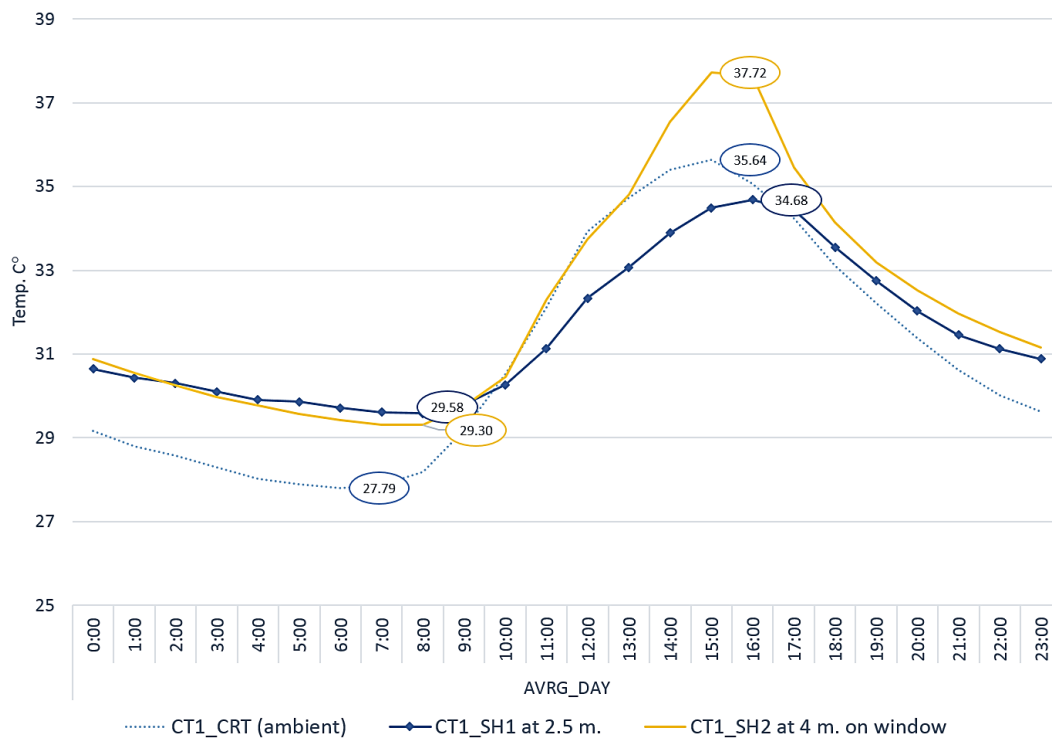


Figure 3.30: CT1-SH, average day temperature

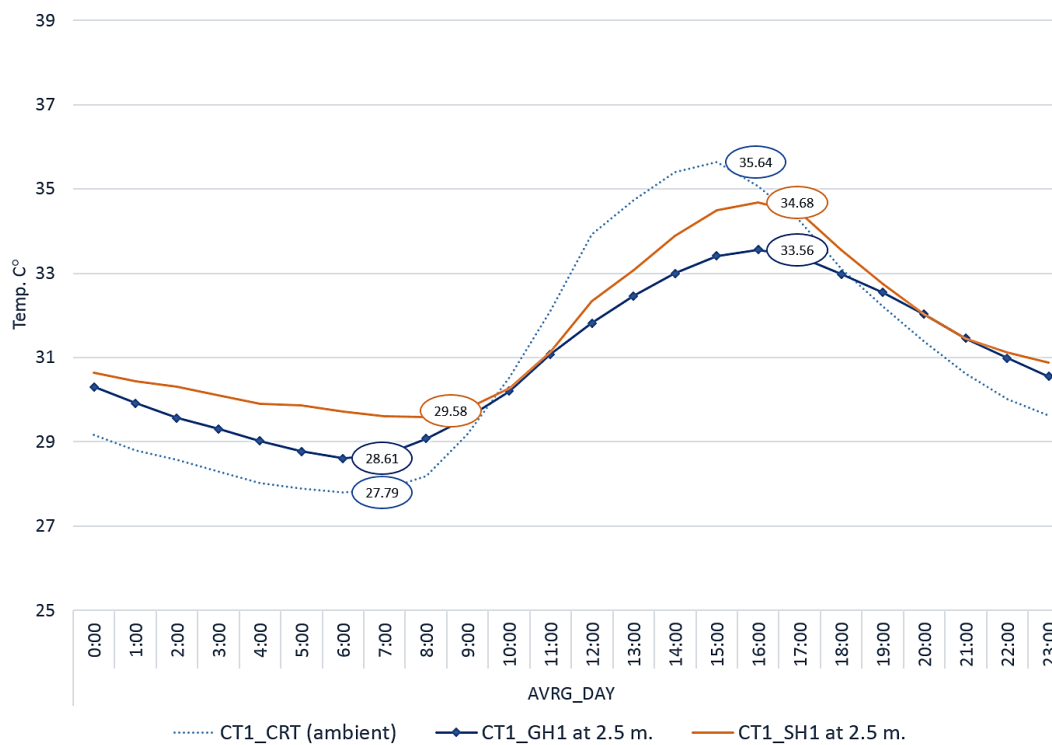
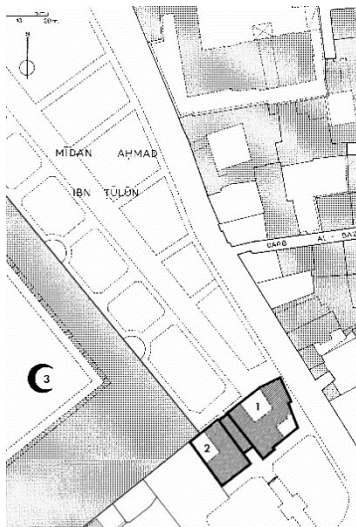


Figure 3.31: CT1-GH vs. SH, average day temperature

### 3.4 Case study (CT2)

At the very end of the south eastern part of the mosque of Ibn Tulun in the district of Alsayeda Zeinab in old Cairo the House of Amna bint Salem is located as part of a today's museum. The museum comprises both this house, built in 1540 AD, and another larger structure called al Kretliya. Since the house is adjacent to the walls of the largest mosque of mediaeval Cairo, which occupies a spacious land plot (fig. 3.32), it is surrounded with an open space, when compared to CT1.



**Figure 3.32:** CT2, House of Amna bint Salem, site layout: 1.al Kretliya, 2.House of Amna bint Salem, 3.Mosque of Ibn Tulun [50]



**Figure 3.33:** CT2, exterior view, south-west



**Figure 3.34:** CT2, view towards the mosque surrounding enclosure

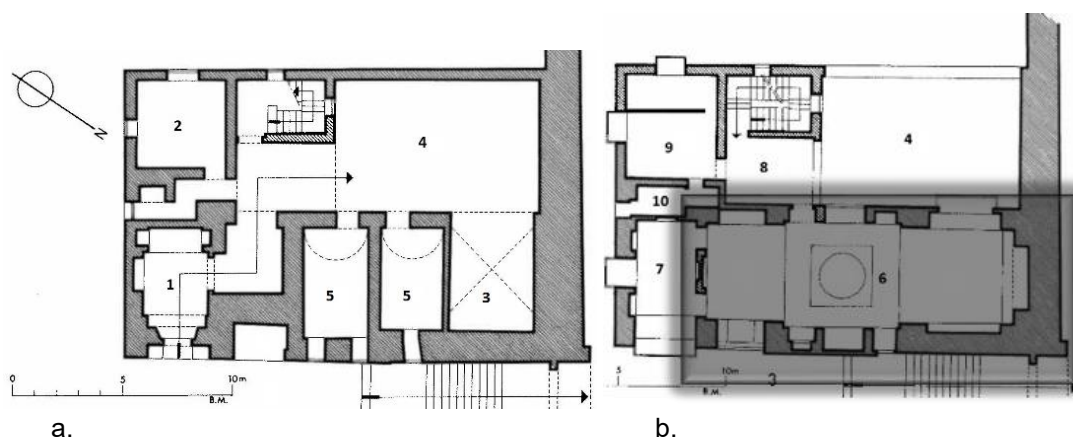


**Figure 3.35 a-b:** CT2, a. ground floor plan, b. first floor plan, monitored hall is shaded [50]: 1. Entrance, 2. Chamber, 3. vaulted porch, 4. Courtyard, 5. storage, 6. main hall (MH), 7. Chamber, 8. balcony (*Maq'ad*), 9. Chamber, 10. Toilet

The building scale is smaller than CT1, ca. 300 m<sup>2</sup> ground floor area, and consists of three floors (fig. 3.33). A 3 meter wide corridor separates the main façade, north-east from the neighbor house (al Keretliya) while the north western façade is adjacent to the walls of the mosque (fig. 3.34). The ground floor comprises the entrance lobby, and a small reception chamber. In addition to a vaulted porch, a couple of storage rooms are opened directly to the courtyard that occupies the north western part of the house. The main construction material is limestone. Figures 3.35 a-b are ground and first floor plans respectively. The first floor however comprises the main hall (MH) in which the measurements took place in this building. With an area of 72 m<sup>2</sup> the hall occupies the most of the north eastern side of both the first and the second floors with a height of 9 m. It has the traditional elongated rectangular plan comprising two large *iwans* flanking a central squared space in which a water fountain is placed. The ceiling is made of carved wood and lacks the sky-light device found in CT1. The floor is covered with inlaid marble patterns. Figure 3.36 is a view from the courtyard towards the balcony on south-east, where the windows of the main hall appear on the left hand side. Figure 3.37 is an interior view of the hall towards north-west. Table 3.6 includes a brief description of the hall.

The hall overlooks the courtyard from its south-west wall through four large openings covered with lattice wooden screens; two of which are on the upper part of the wall. The window openings occupies 20% of the exposed façade area and are 50% shaded by the wooden screens. Since the building is turned into a museum that contains valuable master pieces of furniture and antiques, it is well preserved and complies with strict visiting hours. It was assured with the administrative staff that windows remain opened during regular working hours. This condition applies only to the couple of windows on the lower level of the wall, while the upper couple remained permanently closed. The windows opening schedule spanned hence between 8 am to 4 pm, which is subsequently considered within the simulation model.



**Figure 3.36:** CT2, view from the courtyard towards the balcony, south-east



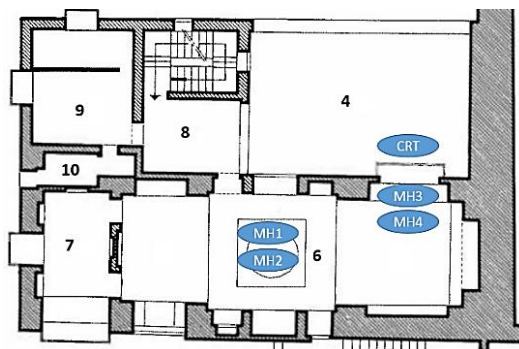
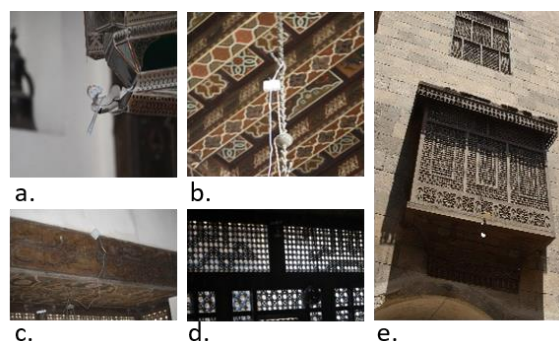
**Figure 3.37:** CT2, interior view of the main hall

**Table 3.6:** CT2, main hall (MH) description

CT2 Main hall (MH)	
Floor	1st
Height	9 m
Area	72 m <sup>2</sup>
Volume	580 m <sup>3</sup>
Exterior surface area of courtyard facade	120 m <sup>2</sup>
Percent window area	20 %, 50 % shaded
Window orientation	South-west
Measurement period	13 Aug.-8 Sep. 2014
Measurement output	Indoor temperature Relative humidity
Ventilation	Opening schedule: 8 am – 4 pm

### 3.4.1 Measurements (CT2)

Following the same method in the previous case, the measurements took place along the same time span between August 13 and September 8. One logger was hanged from the chandelier at 6 m high from finish floor level and connected with thermal cable ending with a sensor at the level of 2.5 m. in order to get a record for temperature differences at different heights. Unlike the previous case, the hot air that would rise would not have a chance to escape due to the lack of opening in the roof. The second logger was mounted on the wall right above a window screen on the wall on the courtyard side at level 3 m. A thermal cable extended with sensor to be affixed at the window screen at the level of 2.5 m. This installment aimed to observation of the temperature at the heavy stone and that at the wooden screen which found to be obviously different. Moreover, one data logger was hanged on the outside underneath the window screen to get the ambient temperature in the courtyard. Figures 3.38-9 and table 3.7 show the installation of data logger in this house.

**Figure 3.38:** CT2, floor plan showing measurement spots.**Figure 3.39 a-e:** CT1, data loggers' installation MH1-4 & CRT respectively**Table 3.7:** CT2, sensors installation

Space	Sensor	Position
Main hall	MH1	Ceiling-hanged at 2.5 m from F.F.L
	MH2	ceiling-hanged at 6 m from F.F.L
	MH3	Wall mounted at 3 m from F.F.L
	MH4	Mounted on window screen at 2.5 m from F.F.L
Courtyard	CRT	Hanged at 4 m from G.F.L

### 3.4.2 Observations (CT2)

The courtyard in this case recorded higher maximum temperature than that in the courtyard of the previous case, which reached 39.23 °C in August 23 at 3 pm where the average maximum of the entire measurement period is found to be 37.84 °C. The minimum courtyard temperature however was 26.99 °C in September 1 at 6 am and the average minimum was 27.88 °C. The lowest maximum indoor temperature was recorded in the main hall, MH1 and MH3, in the middle of the space at the level of 2.5 m and on the wall at level 3 m, however the highest records were recorded by the window-mounted logger.

The highest maximum temperature recorded in the middle of the room at level 2.5 m (MH1) was 34.65 °C while average maximum was 33.48 °C. The lowest minimum temperature of the same spot however was 30.84 °C and the average was 31.52 °C. The temperature in the middle of the hall at level 2.5 m (GMH1) is found to be consistently lower than that at the level 6 m (GH2). Nevertheless the differences are not as significant as in case CT1. This could be attributed to the lack of roof wind-escape through which the warm air should be released out. The average differences were 0.51 °C and 1.13 °C for maximum and minimum temperatures respectively. The average maximum indoor temperature in the middle of the space was 33.47 °C, 4.37 °C lower than ambient. However the ambient average minimum was 3.3 °C lower than the lowest indoor average which recorded at the window screen where the highest maximum was also recorded, 34.7 °C, since it is would be the closest temperature to the courtyard. Figure 3.40-1 show the temperature records, averages, and comparison between records of different data loggers.

Despite the position proximity between MH3 and MH4, the temperature differences recorded by both loggers reveal significant disparity, especially for values of maximum temperatures. Maximum and minimum temperature recorded by MH4 on the window screen are 36.17 °C and 30.49 °C respectively, which correspond constantly to the ambient temperature as previously referred to. This is due to the adjacency of the window which directly overlooks the courtyard and the comparative low heat storage capacity of the wood so the heat is directly transferred by conduction to the sensor and hence to the interior space.

On the contrary the highest maximum on the wall was 34.28 °C on August 24 at 9 pm which reveals the delay in heat transfer caused by higher thermal mass of the stone. The thick stones of the wall stores the heat transferred to the wall by radiation and store it for longer time and releases it to the outside when the outdoor temperature is lower than the indoor. Some of this heat might be released to the indoor space if it was well protected during the daytime against overheating, where ventilation plays a significant role in the night time cooling process. The lowest minimum temperature of the wall however, 32.04 °C, was recorded in September 3 at 9 am as the stones take longer time to release the heat during nighttime (fig. 3.42).

Since the windows remained closed during nighttime, daily from 4 pm until next morning, the indoor temperatures, especially in the middle of the space, were comparatively high since the hot air is not allowed to be released out. At 7:30 am the temperature drops significantly as the cool air comes in when the windows open and then starts to rise along the next few hours when the hot air flows in during daytime (fig. 3.43). The real measurements' conditions are considered in the next chapter within the simulation package, however an expedient operating schedule is maintained after the model validation within the discussion of air flow and ventilation process.

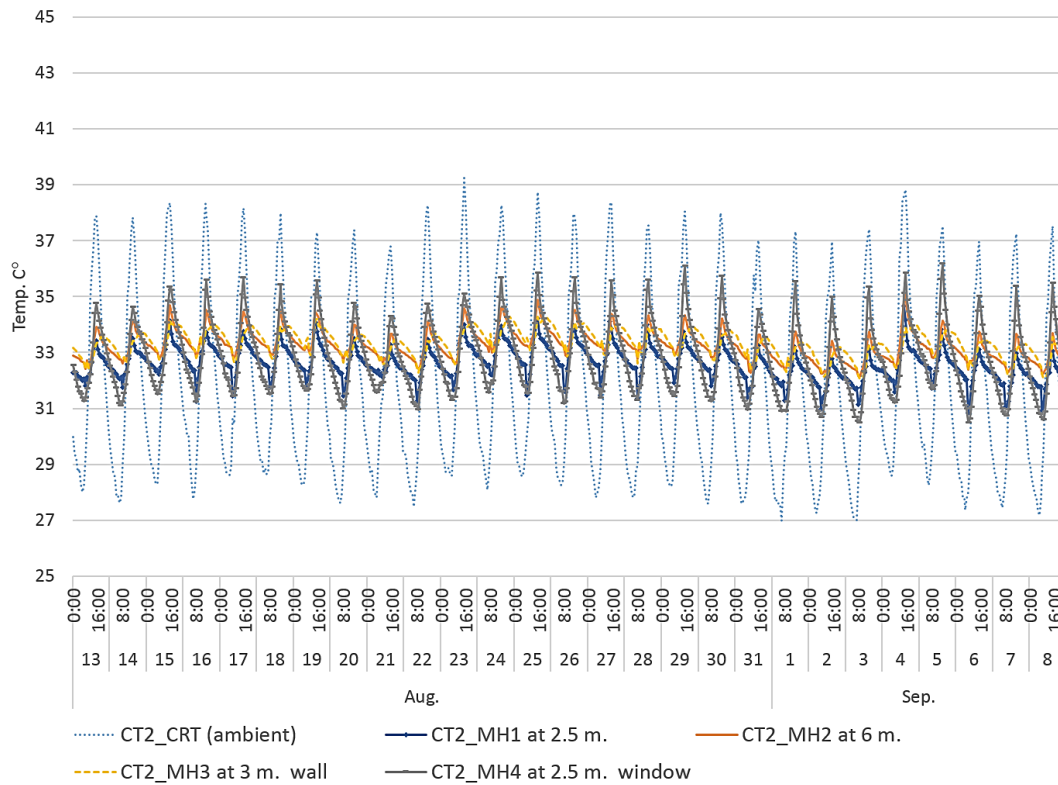


Figure 3.40: CT2-MH, measured Temperatures in the main hall and courtyard

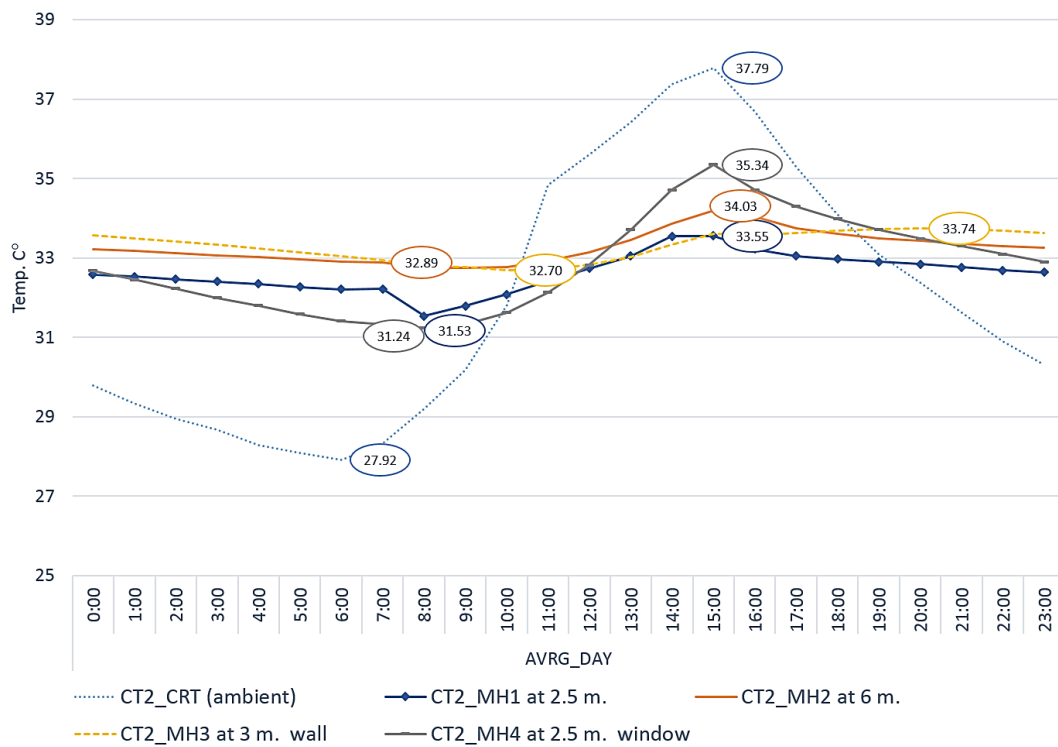
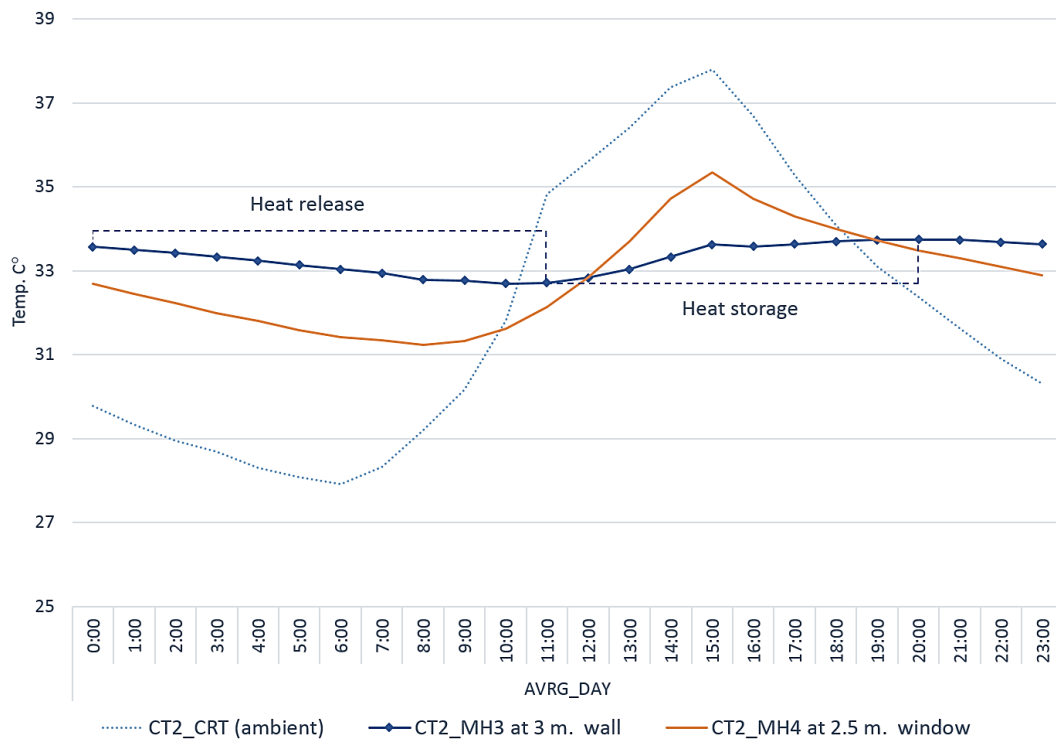
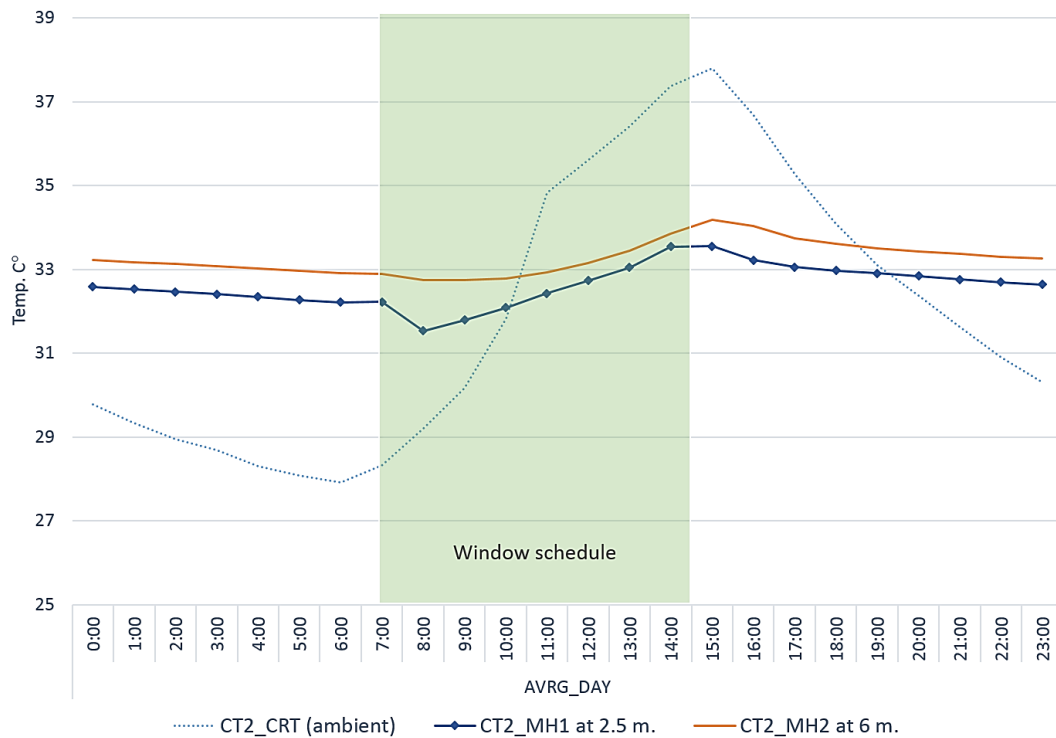


Figure 3.41: CT2-MH, average day temperature



**Figure 3.42:** CT2-MH, a two-day record of temperature on the wall (MH3) and window screen (MH4).



**Figure 3.43:** CT2-MH, an average day of temperature at level 2.5 m (MH1) and 6 m (MH4).

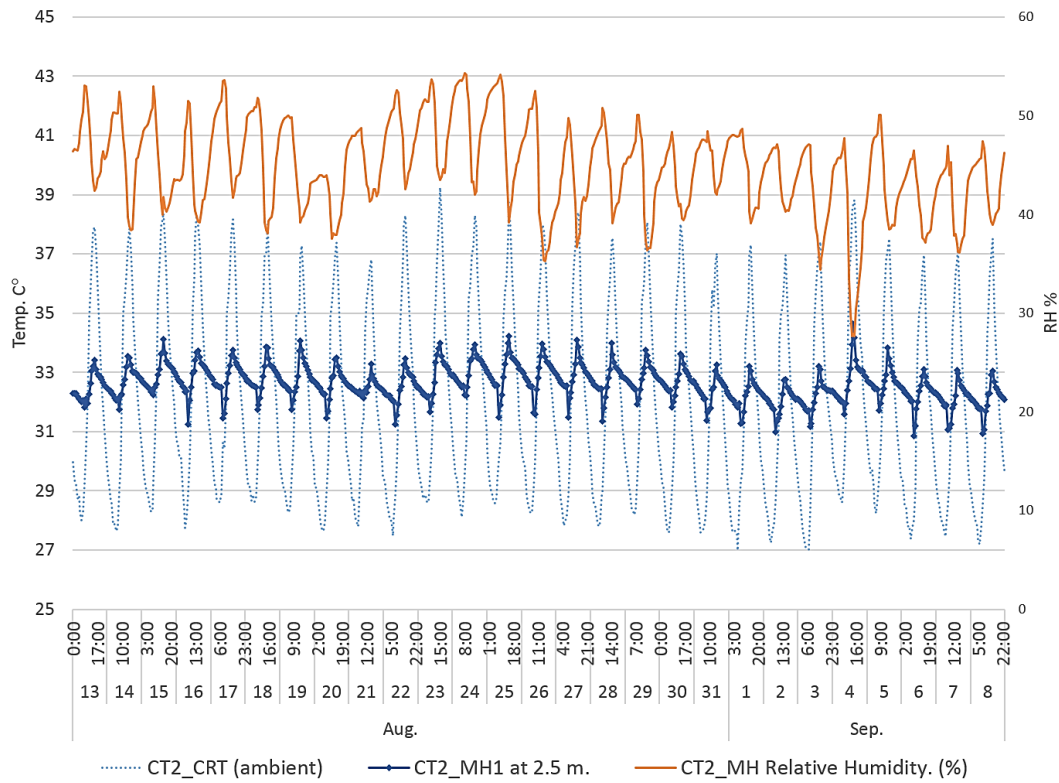


**Figure 3.44:** CT2-MH, measured Indoor temperature and relative humidity

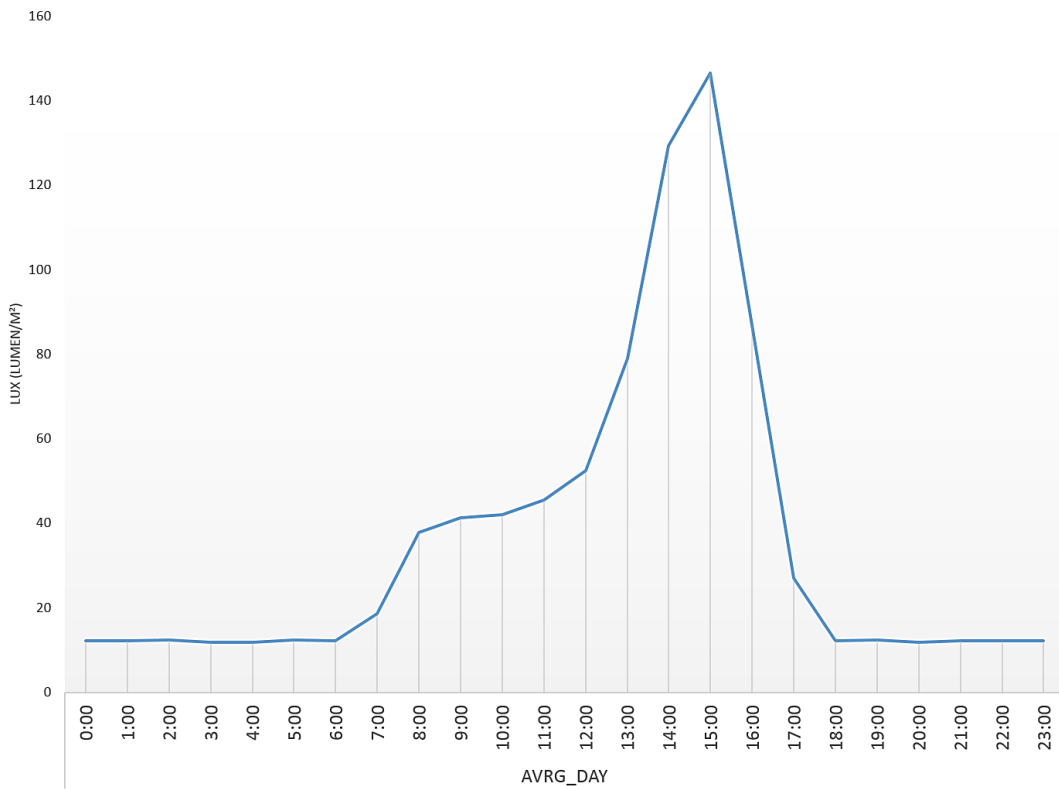


**Figure 3.45:** CT2-MH, average day illumination in the grand hall

The relative humidity was inversely variable against indoor temperature (fig. 3.44). Nevertheless, as the indoor space never got the chance to be cooled down during nighttime, the indoor temperature did not go below 30.84 °C where humidity was 46.44 %, maximum record was 54.26 %, unlike the case CT1 where maximum humidity reached 61.5 % at .96 %. The minimum record of relative humidity inside the hall was then 27.63 % at when indoor temperature was 34.17 °C.

Although the space is supposedly being well illuminated with four large openings to the courtyard, the light intensity recorded in this hall was quite lower than in the case CT1 (fig. 3.45). This could be attributed to the lack of the sky-light/wind-escape device which allows the light to penetrate the space from the roof, especially before and afternoon. The average maximum illuminance level was 131.56 Lumen/m<sup>2</sup>, ca. 53 % lower than in the grand hall in the previous case.

Finally, it is quite evident that the courtyard in both traditional cases recorded lower maximum temperature than the balcony in the modern case where the maximum temperature reached 42.86 °C at 5 pm on September 3. The average maximum in (CM) was 39.41 °C where it is found to be 3.62 °C lower in CT1, 35.79 °C, and 1.57 °C lower in CT2, 37.84 °C. However, the average minimum ambient in CM, 26.97 °C was slightly lower than both traditional cases CT1 and CT2, 27.77 °C and 27.95 °C respectively (figs. 3.46-7). This could be simply attributed to the fact that CM is located in a less dense urban fabric than both other cases, where a less heat island effect exists. The density of buildings hinders the thermal radiation to the cold sky and lowers the convective heat losses by blocking the wind which increase the chances for the urban heat island effect [3]. The heat released by the surrounding buildings in the case of CM has the chance to be dispersed by the faster wind velocity through the more open space. However the same process might take longer time in the traditional case due to density of buildings and the enclosure of the courtyard environment.

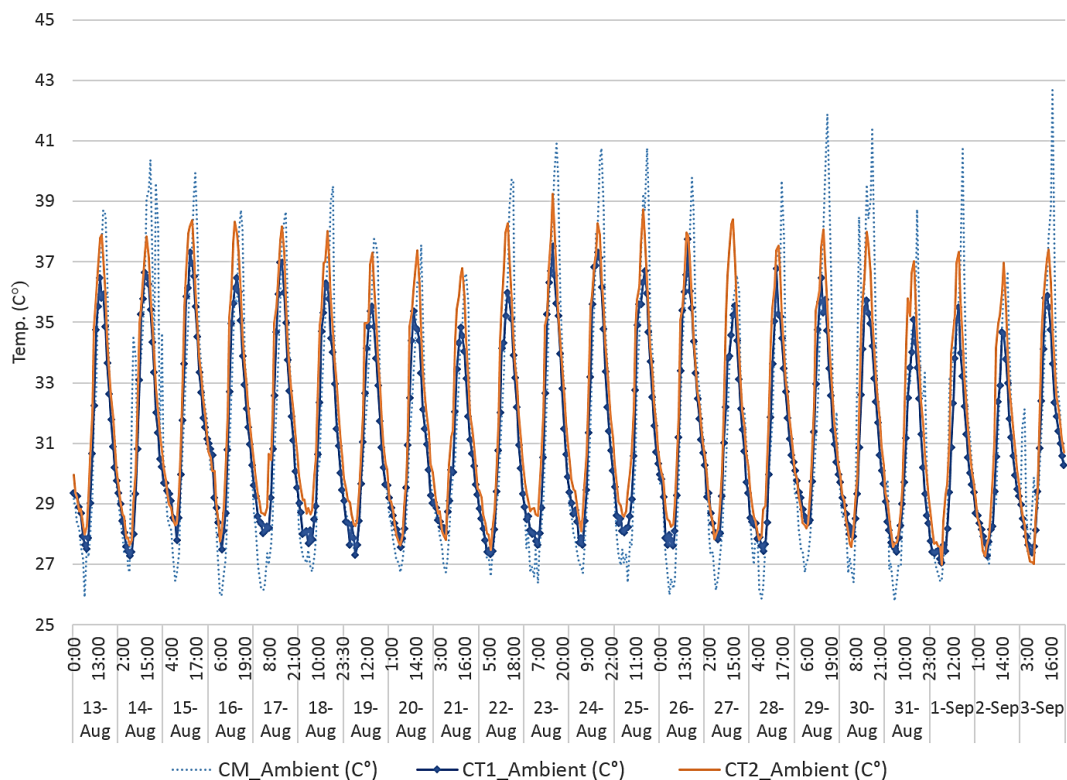


**Figure 3.46:** CT1-CT2-CM, measured ambient temperature in three cases, Aug. 13 to Sep. 3.

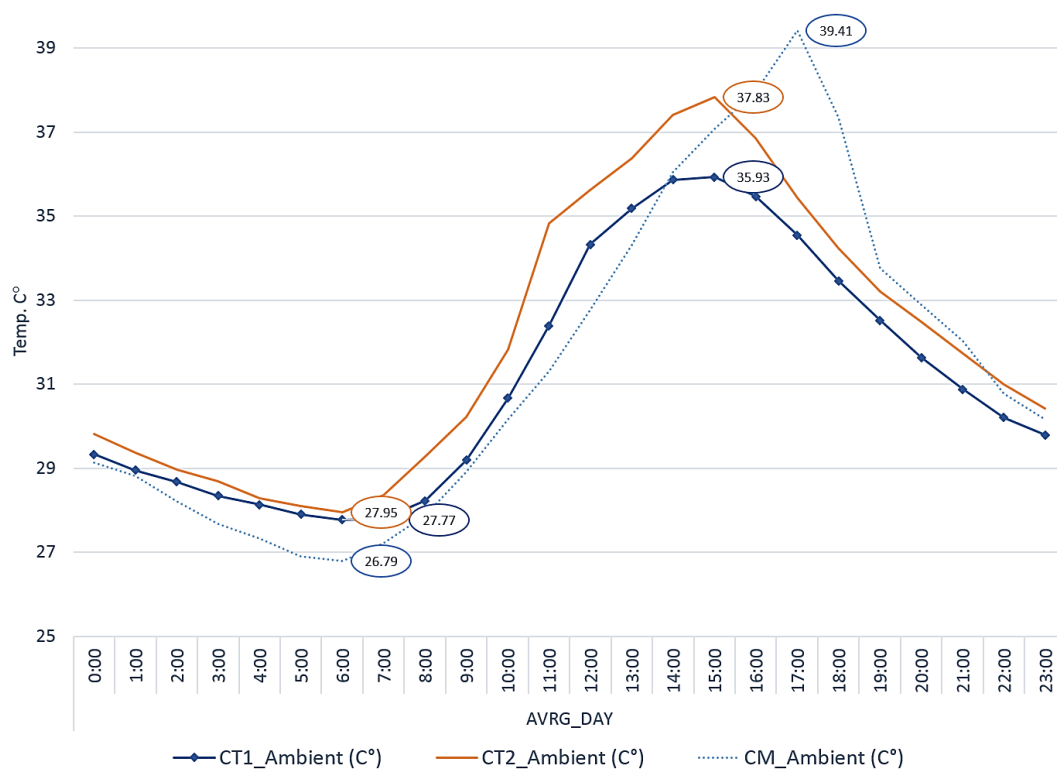


**Figure 3.47:** CT1-CT2-CM, Average day ambient temperature in three cases

### 3.5 Conclusion

1. 3 cases were selected, in which field measurements took place during summer of 2014. The first is a contemporary residential building (CM). The second is traditional house (CT1), and is the main case-study in his research, which comprises all suggested features. The third case (CT2) is similar to the former, however lacks the wind-escape device and has less dense surrounding urban fabric.
2. The wind-escape is found to be quite effective where, In CT1, the average maximum and minimum temperatures in the middle of the grand hall where lower corresponding average at the top of the space with 1.01 °C and 1.93 °C respectively.
3. The indoor temperature in CT1 is found to be lower than the ambient in the courtyard with 2.23 °C in average. However, due to the fact that no deliberate window schedule was adopted the indoor minimum was higher than the ambient.
4. The higher thermal mass of the stone structure has the ability to store heat for longer time and protect the indoor space from overheating.
5. The ventilation plays a significant role in lowering indoor temperature within night time cooling. In CT2 indoor temperature remained comparatively high, alike CT1 where windows remained opened during nighttime.
6. Both traditional houses are relatively well naturally illuminated despite of the extensive use of window screens.
7. The courtyard micro climate is comparatively better than that of the modern case in terms of maximum temperature, more than 3 °C lower.



## Chapter 4

# Experiments (1), thermal mass and shading mechanisms

### 4.1 Introduction

In the previous chapter measurements for indoor temperature were obtained for three cases. However measurements took place in the three cases within different conditions in terms of window operating schedules and hence the air change rate resulted in each space. A plausible comparison hence between the cases would not be possible unless all boundary conditions being stabilized. Moreover, the ultimate assessment of a building performance would not be feasible with the absence of appropriate response to the climate. In other words, the windows opening and hence the allowed ventilation did not take place within the measurement period, in all cases, according to a climate responsive manner, which would not be the case when the building is practically inhabited. These buildings therefore might show better thermal performance if more climatic responsive behavior maintained.

This chapter comprises the second part of the empirical work of the study, which includes a validation of the simulation models, for all cases, and determination of the potentiality of suggested features for passive design. The work in this stage is to examine the effect of the suggested traditional features. Discussed features are the resulted cross shading in narrow street canyon and window screens as well as the building material and thermal mass. Models created in the TRNSYS 17 environment are tested for indoor temperature and validated by comparing results to measured data. The air change rate is consistently assumed for all cases in this stage of simulation. The shading mechanisms were introduced as shading groups to the model within consecutive simulation runs. The traditional building (CT1) demonstrated the best performance in terms of indoor temperatures and hence undergoes further experiments for air flow analysis within the next chapter.

## 4.2 Simulation package

Simulation strategy tended basically to the integration of a couple of simulation tools and getting profit of both advantages. The first is TRNSYS 17, a complete simulation environment for systems transient simulations. Normally the basic multi-zone building model in TRNSYS does not simulate the airflow unless through TRNFlow, a modified version which integrates the COMIS engine for airflow simulation. However, the modular nature of TRNSYS facilitates the addition of new mathematical models to the program [18]. Equations for various functions can then be incorporated. The statement of equations allows variables to be defined as algebraic functions of constants and outputs from TRNSYS components. Upon this advantage the second simulation method was determined, the computational fluid dynamic modeling (CFD), which is explained within the next chapter. The method followed in these experiments is to apply CFD modeling for the principle case study which would be selected upon the analysis applied on the three cases.

Models of the selected cases have been created and all related data is given to TRNSYS 17. Weather data was collected on daily basis from the NOAA (National Oceanic and Atmospheric Administration). The recorded data is normally obtained from the weather station installed in Cairo international airport and includes hourly records for air temperature, dew point, relative humidity, wind velocity, and air pressure. For the three cases the data collected for a time spanned from August 7 2014, one week before measurements, until September 8. The weather data file used in TRNSYS is the type TM2 which includes more extensive details i.e. direct and diffuse radiation, and precipitation, which are adopted from the test reference file. However, data for ambient air temperature were replaced by records obtained in site for each case; courtyard temperature in traditional cases and ambient temperature in the balcony for the modern one. A separate weather data file hence was created to each case. Daily temperatures obtained for the measurement period were compared to the test reference annual temperature, obtained from Meteororm 7. The comparison showed tangible proximity that authorizes obtained data for the year 2014 to be a climate representative data for Cairo (fig. 4.1).

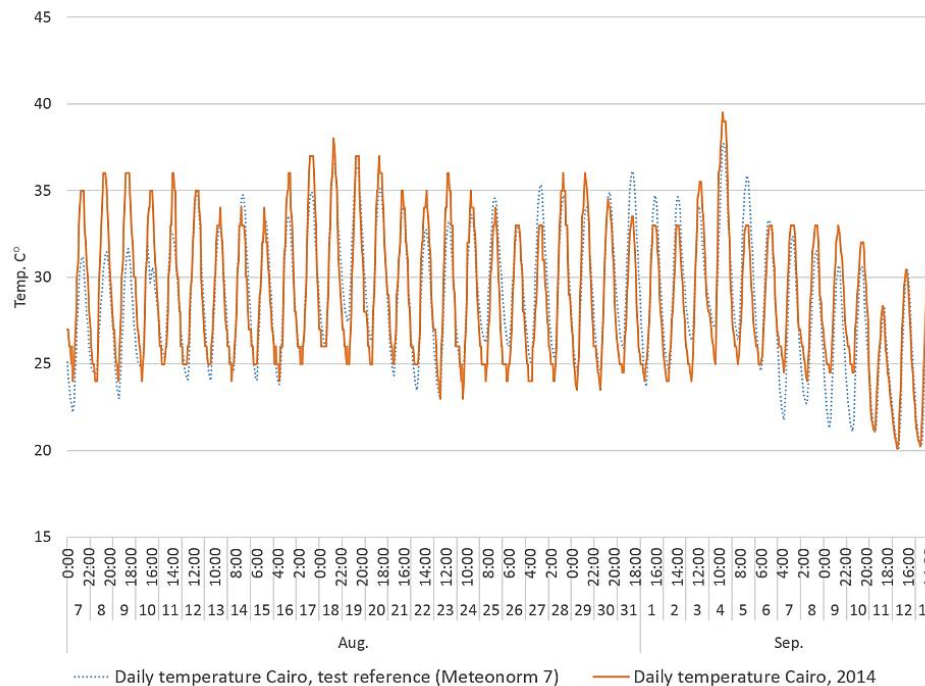


**Figure 4.1:** Obtained dry bulb temperature from August 7 to September 13 2014 compared to test reference data for the same period

### 4.2.1 Presumption of air change rate (ACH)

The analysis of the wind factor and air flow rates remains limited within the simulations applied with TRNSYS in this chapter and quantifications for air change rates (ACH) were presumed and further investigated within the next part through the CFD modeling, which includes wind analysis and results for flow rates. However, plausible values of air change rate were assumed within the TRNSYS simulation package. A study analyzed the sensitivity of air change rates in a naturally ventilated atrium space concluded that the wind direction and number of vents included in the model have significant influence on the ACH. However wind speed was found to have an almost linear relationship with ACH rate for all wind directions regardless of the number of side vents [40]. Finite values of ACH upon which rates can be presumed is rare to be found. However, in a study that took place in 2006, applied on the same house adopted in this research CT1, a model for thermal simulation of courtyard microclimate was created. The author intended to assume 6 values of air change rates for upper and lower nodes in the courtyard, with 70% and 30 % respectively. The best fit was found with an ACH rate equal to 35 with error of 1.5% for summer and 3.5% for winter. An hourly schedule was then applied to a DOE-2 input file which considered ACH rates range varying between 1 and 40 around the day that produced the best calibration [9]. A study from 1997 for natural ventilation in courtyard houses in Saudi Arabia, a rather different climatic conditions, adopted 9 of cases on which smoke decay tests were applied to obtain values for ventilation rates. The author concluded values of air change rates for each tested room. For the most two relevant cases, records of ACH varied between 0.72 and 12/h. Velocity in each case varied between 0.5 and 2.0 m/s. The measurements took place in traditional mud-brick double story houses, however records were obtained from rooms overlooking the courtyard in the ground floor [2]. Table 4.1 concludes results of ACH.

**Table 4.1:** Smoke decay tests results for ACH and rooms description [2]

Case	Space	Volume (m <sup>3</sup> )	ACH	Velocity m/s	Wind direction	Opening area m <sup>2</sup>
01	01	190	3.48	0.5	N	22.6
	02	112	3.43	0.5	N	1.21
	03	142	3.55	2.0	NW	0.27
	04	194	4.63	2.0	NW	0.4
	05	138	5.59	0.2	NW	0.73
02	01	172	12.08	0.7	SW	2.95
	02	175	0.72	0.7	SW	0.44
	03	125	0.97	0.7	SW	0.48

### 4.2.2 Validation of the simulation model

3D models for the three cases CM, CT1 and CT2 were created by TRNSYS3d tool, as shown in figures 4.2-4. All models were created upon real dimensions and construction material. Material thermal properties, as shown in tables 4.2-3 for contemporary and modern cases respectively were entered in TRNBuild. Surrounding buildings were modeled as shading groups. Window screens were designed with modular sections of 5x5 cm. with ratio between the width and the depth 1:1 and 50% perforation, as shown in figure 4.5, and modeled as shading groups in TRNSYS3d. The large window in the grand hall (GH) and windows on the lower level of the secondary hall (SH) as well as the sky-light were set into the condition, no window, corresponding to the condition of being opened along the measurement period.

In this stage of simulations hence 3 values for air change rates were defined to the simulation model for both cases, CT1 and CT2, 6, 8, and 10/h. For Ct1 the windows scheduled to be opened consistently, however for CT2 a ventilation schedule between 7 am and 4 pm was set up. As for the case CM an infiltration rate of 0.4/h was defined to correspond only to the leakage since windows were totally closed along the measurement time span. Initial values for indoor temperature was set to 21° C and relative humidity to 50%. The solar beam radiation distribution mode was set into a detailed model. Weather data was obtained through the simulation studio from separate TM2 file for each case upon the ambient temperature measured on its site. Simulation ran for annual round and results for the measurement periods were extracted. Results for Indoor temperature in all cases in general showed a high level of conformity in all spaces. High proximity as well was found between results upon all presumed values of air change rates. However, it is found that ACH 6/h achieved the highest level of conformity with measured indoor temperature for all spaces. The mean absolute deviance (ADE) between simulation results and measured data is found to be  $\pm 0.3$  °C for all indoor temperatures. Figures 4.6-15 demonstrate the validation of the simulation results against measured data and average indoor temperatures for the three cases. The mean absolute difference/deviance between simulated and measured indoor temperatures is defined as:

$$ADE = \frac{1}{n} \sum_{i=1}^n |ts_i - tm_i| \quad (4.1)$$

where,  $ts_i$  and  $tm_i$  are the simulated and experimentally measured temperatures respectively at a time step  $i$ .



**Figure 4.2:** CM, 3d model, TRNSYS 3D tool

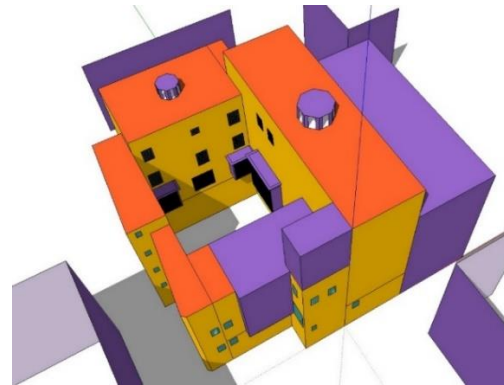


**Figure 4.3:** CT1, 3D model, TRNSYS3d tool

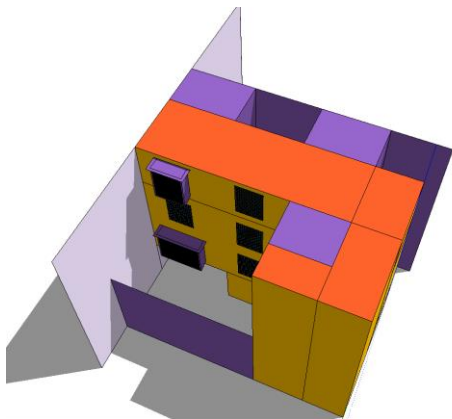


**Figure 4.4:** CT2, 3D model, TRNSYS3d tool

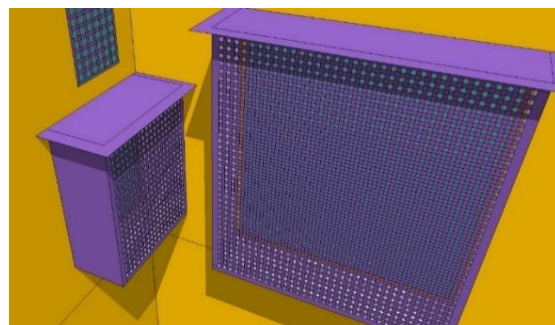


**Figure 4.5:** CT1, window screen modeling TRNSYS3d tool

**Table 4.2:** CM, construction material and thermal properties

Component		Thermal conductivity (kJ/hmK)	Capacity (kJ/kg K)	Density (kg/m <sup>3</sup> )	Total thickness (m)	U-value (W/m <sup>2</sup> K)
External walls	Hollow red brick	2.10	0.84	1790	0.25	1.82
	Cement mortar	5.04	1.0	2000		
Internal walls	Hollow red brick	2.10	0.84	1790	0.15	2.65
	Cement mortar	5.04	1.0	2000		
Ground floor	Concrete slab	4.07	1.0	1400	0.38	1.75
	Tiles	3.6	1.0	2000		
	Sand	2.52	1.0	1800		
Flat roof	Concrete slab	4.07	1.0	1400	0.36	0.45
	Tiles	3.6	1.0	2000		
	Sand	2.52	1.0	1800		
	Bitumen	0.61	1.0	1100		
	Polystyrene	0.09	1.25	15		
Internal floor	Concrete slab	4.07	1.0	1400	0.33	0.71
	Wooden floor	0.50	1.2	650		
Windows	Glass	3.60	0.75	2400	0.11	5.8
	Frames	Aluminum frames				

**Table 4.3:** CT1-CT2, construction material and thermal properties

Component		Thermal conductivity (kJ/hmK)	Capacity (kJ/kg K)	Density (kg/m <sup>3</sup> )	Total thickness (m)	U-value (W/m <sup>2</sup> K)
External walls	Limestone	4.68	1.0	2200	0.85	1.19
	Lime mortar	3.13	1.0	1800		
Internal walls	Limestone	4.68	1.0	2200	0.65	1.45
	Lime mortar	3.13	1.0	1800		
Ground floor	Limestone	4.68	1.0	2200	0.3	2.47
Flat roof	Limestone	4.68	1.0	2200	0.35	1.25
	Sand	2.52	1.0	1800		
	Wood	0.72	2	800		
Internal floor	Limestone	4.68	1.0	2200	0.35	1.25
	Sand	2.52	1.0	1800		
	Wood	0.72	2	800		
Windows	Glass	3.6	0.75	2400	0.11	5.8
	Frames	Wooden screen lattice work added as shading group in simulation model				

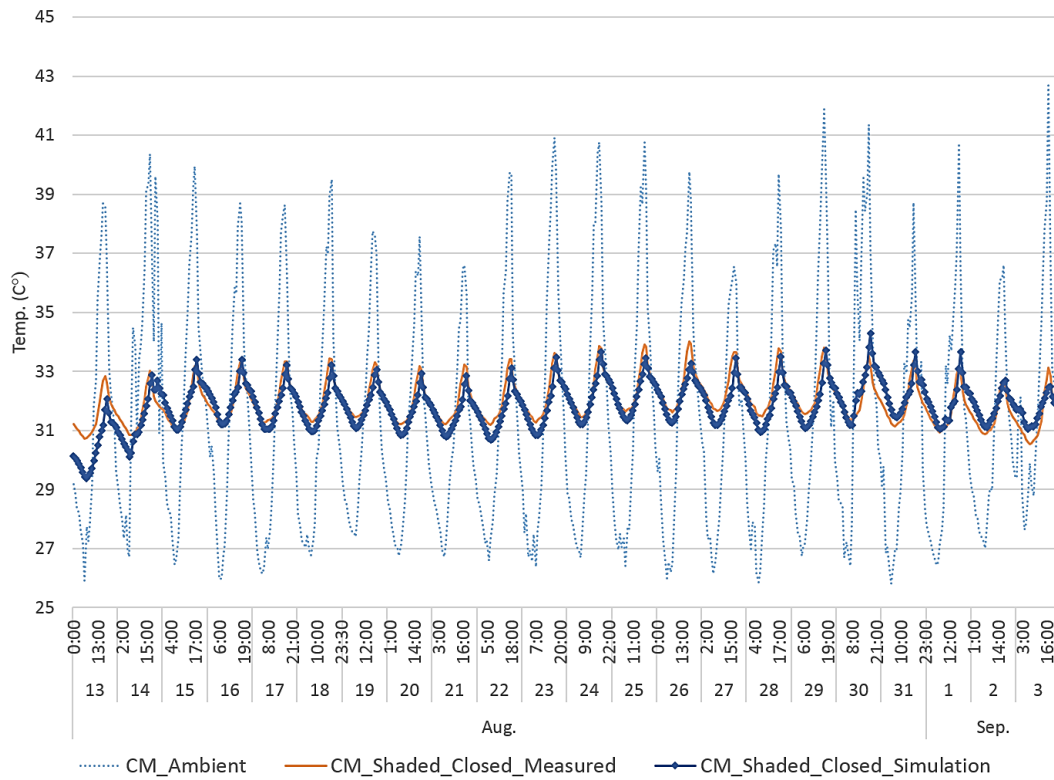


**Figure 4.6:** CM, simulation results for indoor temperature against measured data

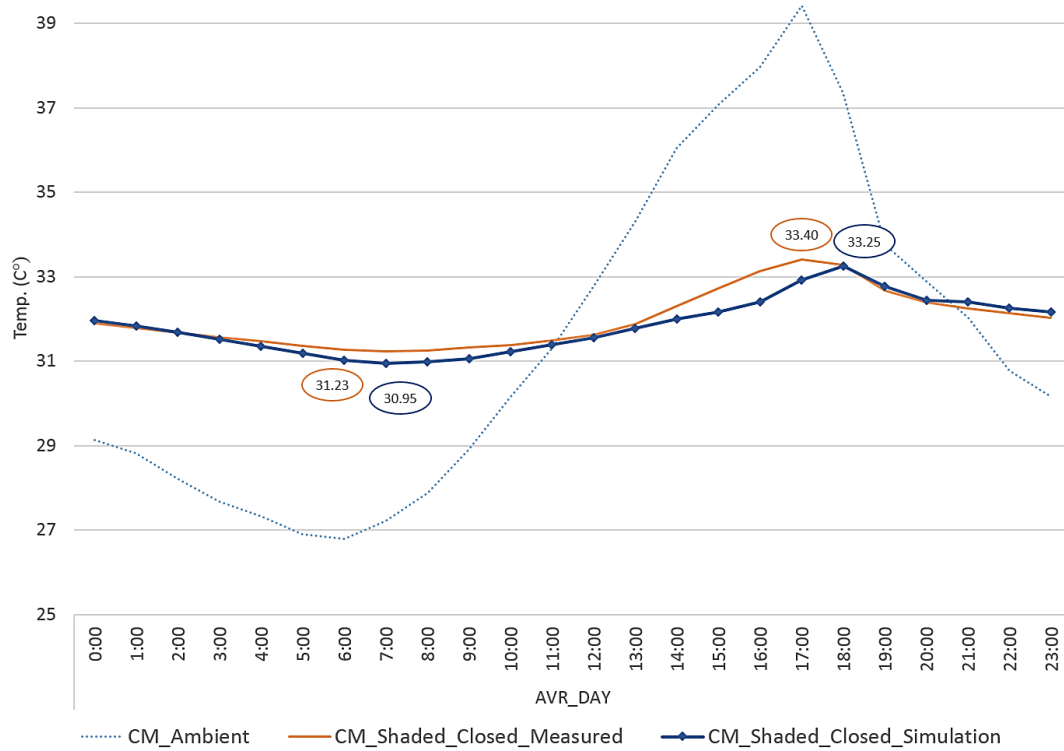


**Figure 4.7:** CM, average day temperature, Simulation results against measured data. ADE  $\pm$  0.2 °C

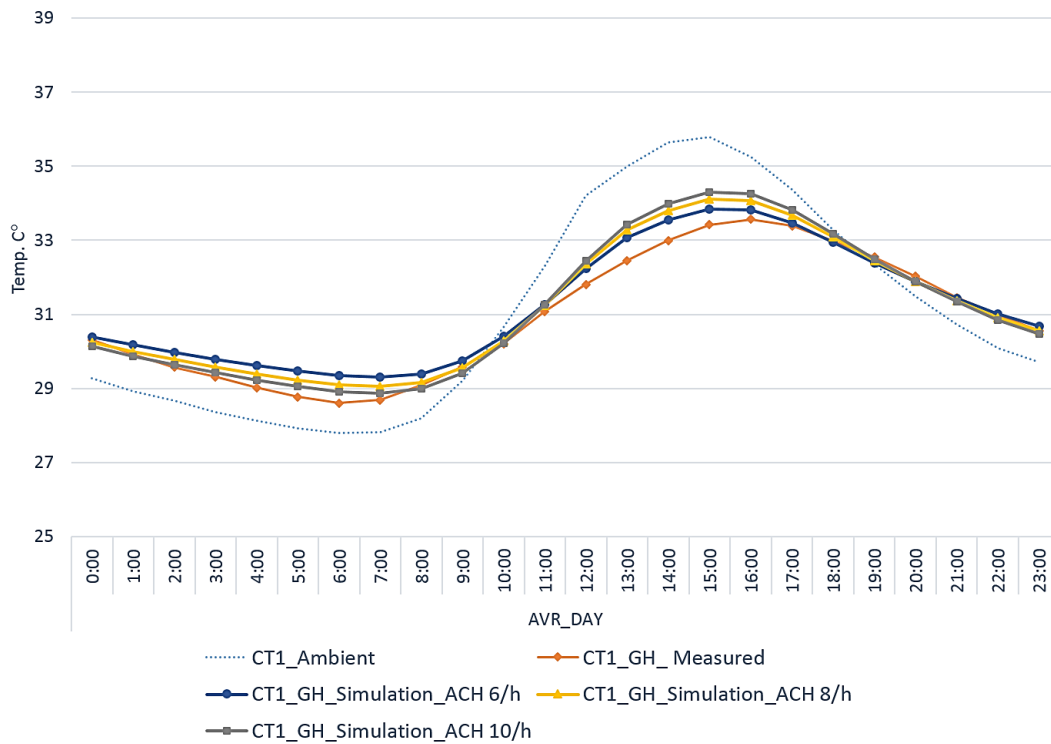


**Figure 4.8:** CT1-GH, average day temperature, simulation results against measured data. Presumed values of ACH 6, 8, and 10/h

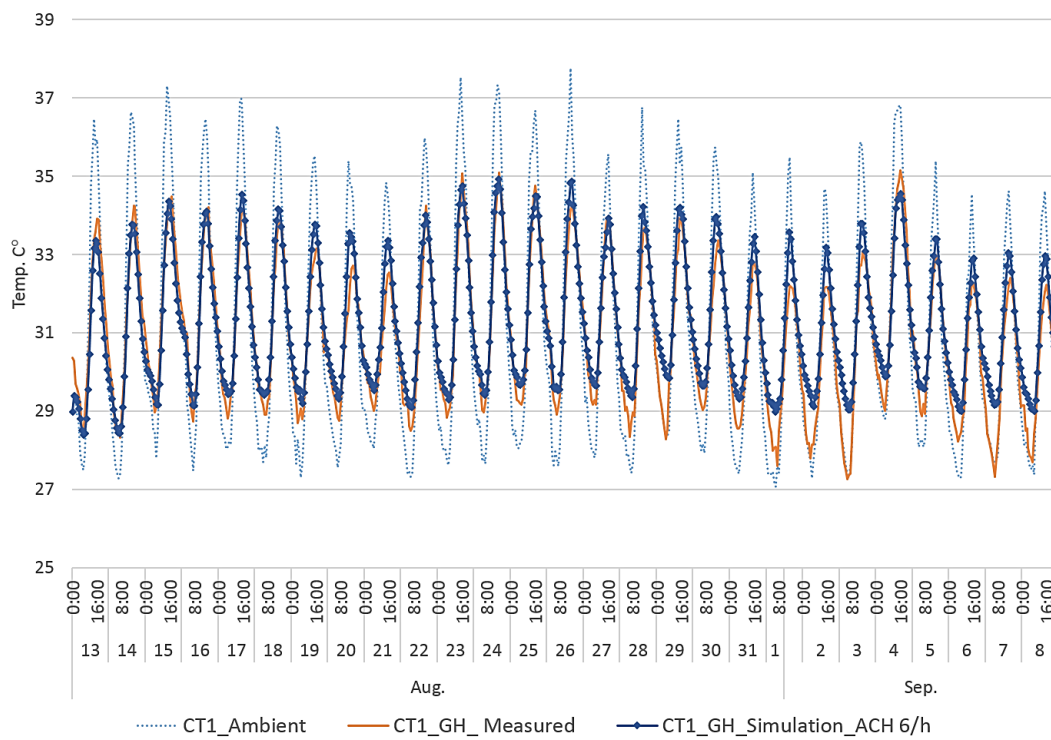


**Figure 4.9:** CT1-GH, simulation results for indoor temperature against measured data. Presumed values of ACH 6/h

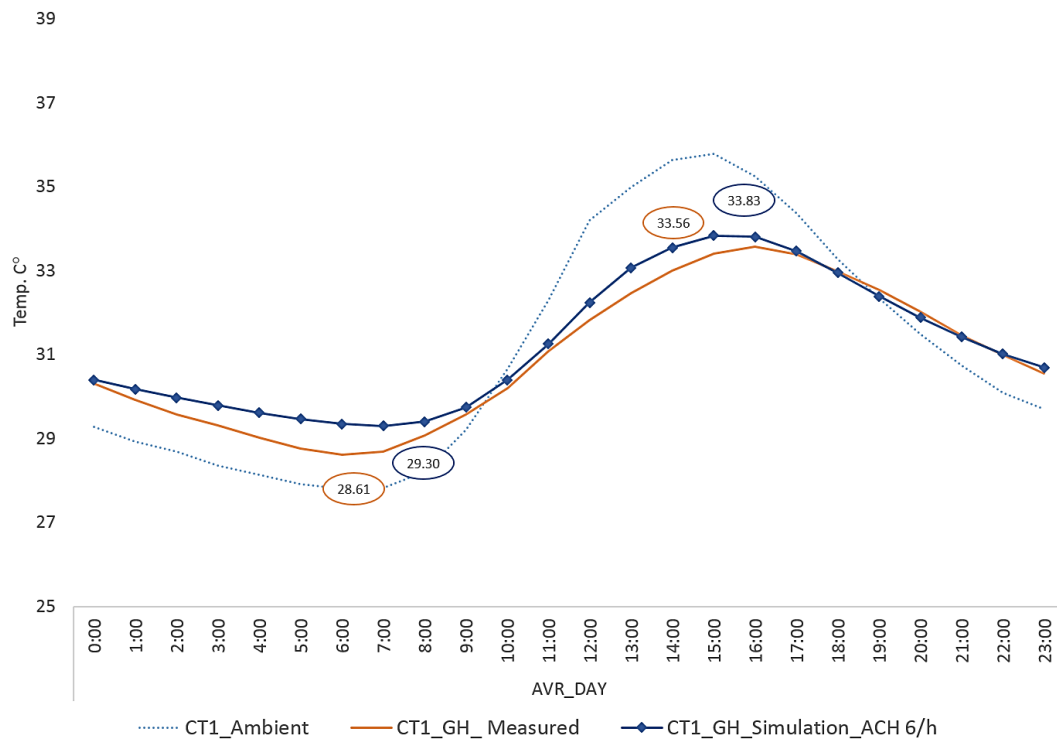


**Figure 4.10:** CT1-GH, average day temperature, Simulation results against measured data. Presumed values of ACH 6/h. ADE  $\pm 0.3$  °C

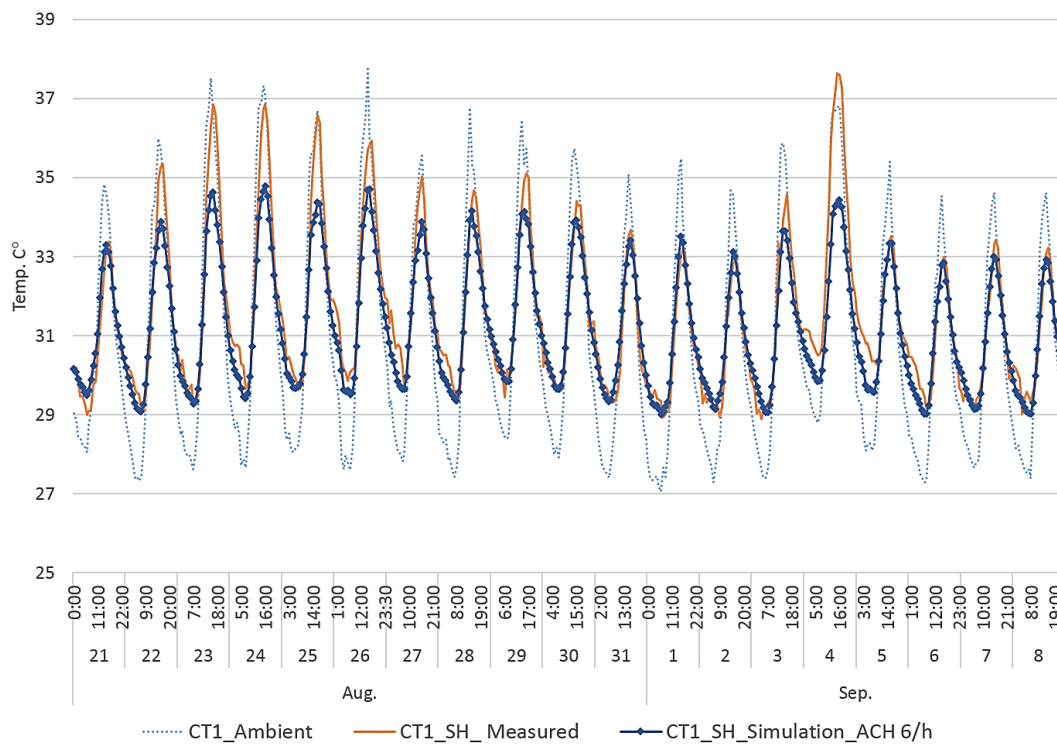


**Figure 4.11:** CT1-SH, simulation results for indoor temperature against measured data. Presumed values of ACH 6/h

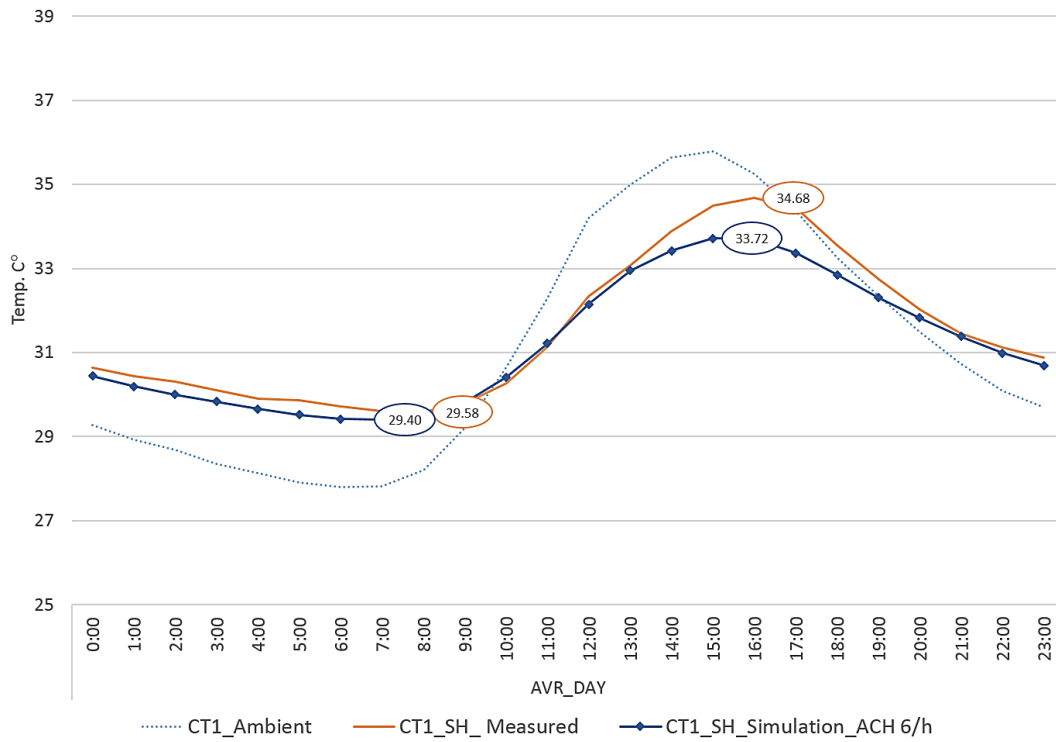


**Figure 4.12:** CT1-SH, average day temperature, simulation results against measured data. Presumed values of ACH 6/h. ADE  $\pm 0.3$  °C

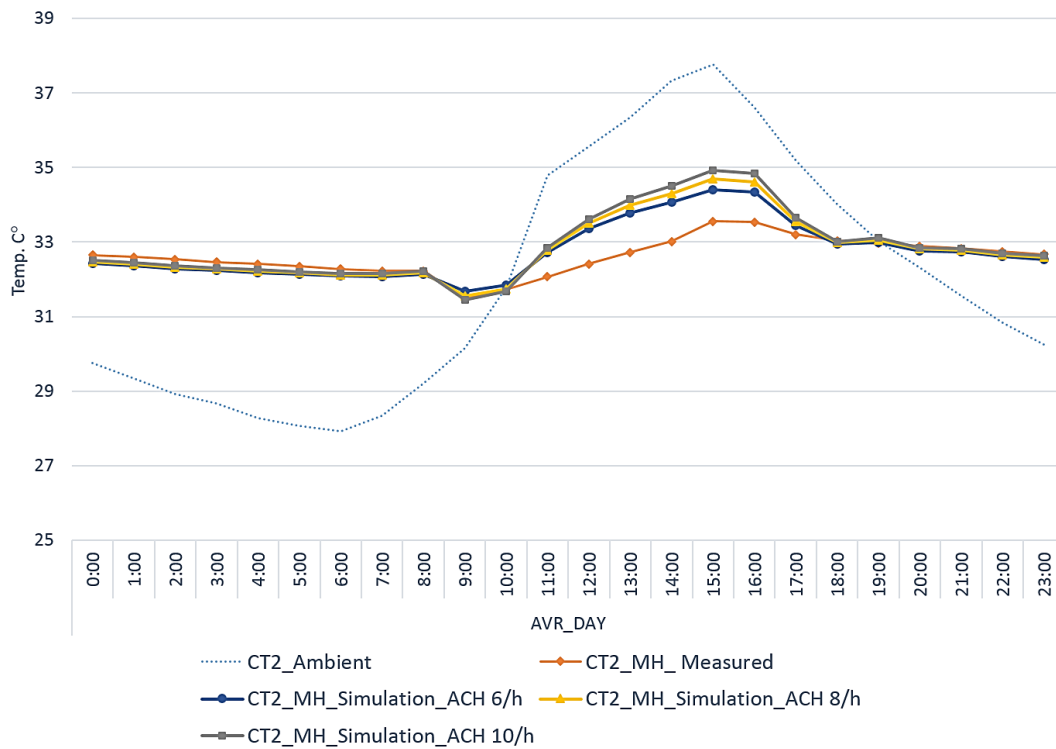


**Figure 4.13:** CT2-MH, average day temperature, simulation results against measured data. Presumed values of ACH 6, 8, and 10/h

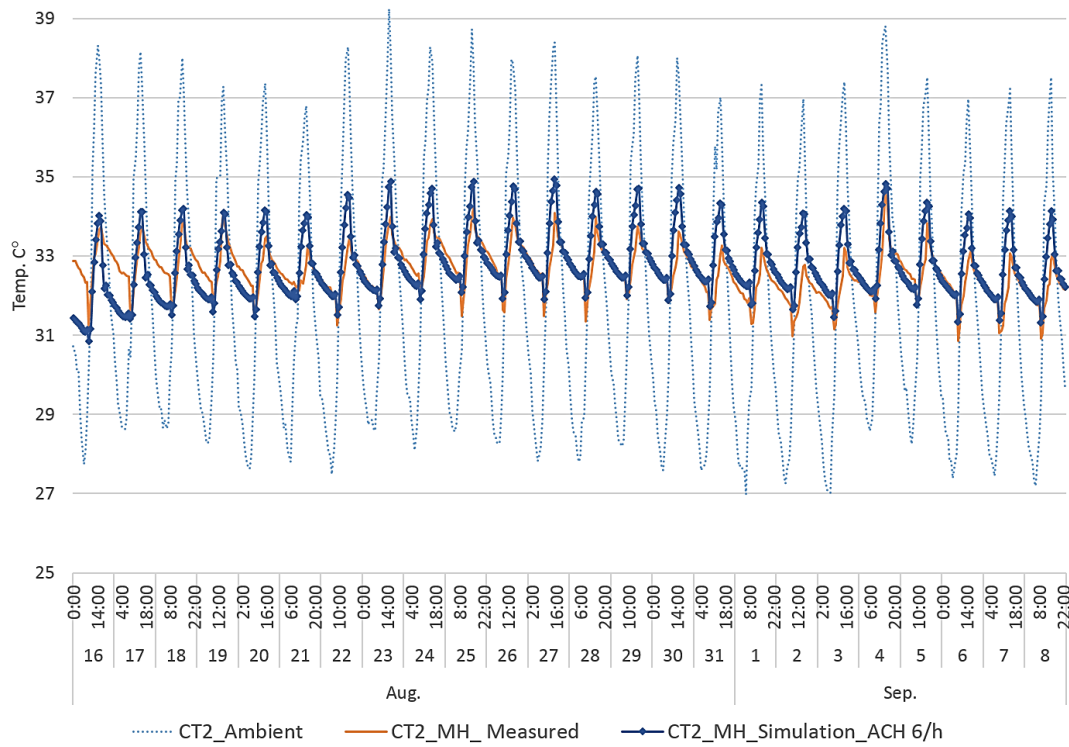


**Figure 4.14:** CT2-MH, simulation results for indoor temperature against measured data. Presumed values of ACH 6/h

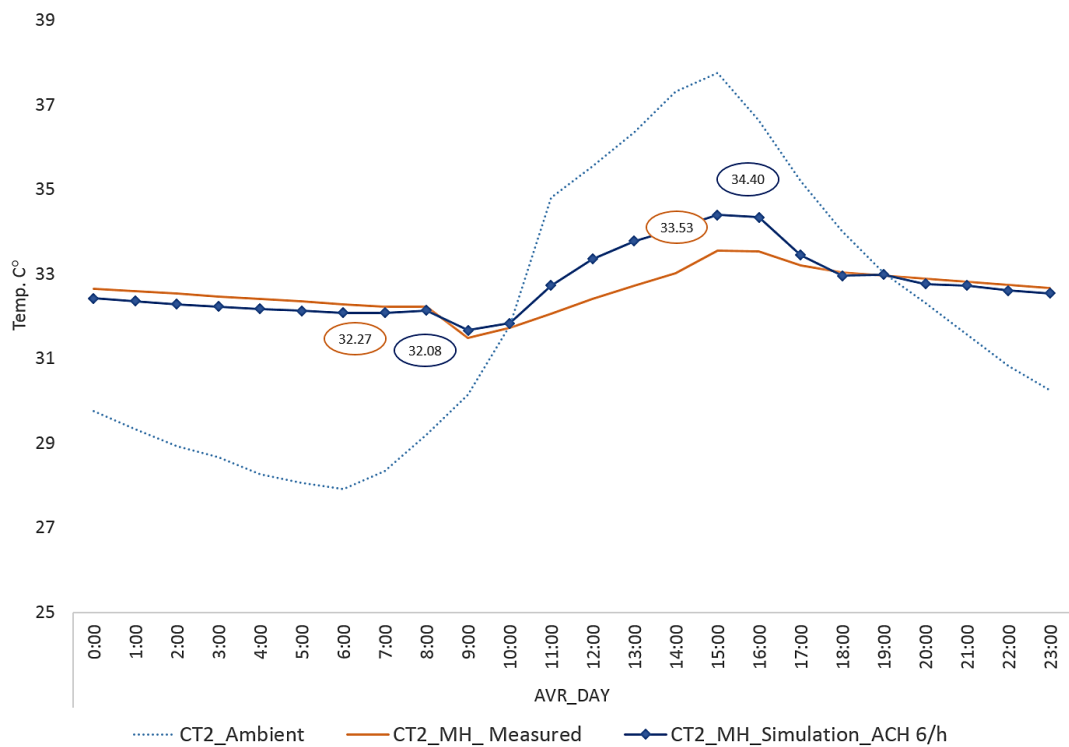


**Figure 4.15:** CT2-MH, average day temperature, simulation results against measured data. Presumed values of ACH 6/h. ADE  $\pm 0.3$  °C

As for the modern case (CM) indoor temperature was measured during August only in the space adjacent to the balcony, where the façade and hence the window were always shaded. Infiltration rate was defined as 0.4/h, only for the leakage as the windows were closed along the measurements. Simulation applied for this period and results were quite close to the real measurement. The absolute deviance error (ADE) between simulated and measured temperatures was  $\pm 0.2$  °C. Indoor temperature in the un-shaded part of this room however, should be relatively higher. As the simulation model has been validated against measured data, for both nodes in April and for the shaded node in August, a plausible results for the un-shaded node could be then obtained from the simulation model. This was manipulated in TRNSYS through adding a virtual adjacent wall as a dummy section (massless layer) that nearly has no heat resistance. Through this virtual wall the heat, as well as the air, could flow freely between both spaces. The indoor temperature for the un-shaded node is found to be significantly higher than the shaded node due to the higher amount of solar radiation transmitted through the un-shaded window, as discussed within the following analysis.

### 4.3 Observations and Analysis

As the simulation models have been validated for all cases, it is valid then to make a comparison between their thermal performances upon unified boundary conditions. The comparison here is to select the case which could undergo further experimental analysis. Further analysis aim to investigate the validity of the selected case to be adopted as an integrated model for passive design. Both the traditional case (CT2) and the modern case (CM) are south-west oriented, however traditional case (CT1) has two halls; the grand hall which is oriented north-west; and the secondary hall which is south-west oriented as the same as the other cases, and therefore is adopted within the comparison, though it recorded higher temperatures than the other hall. In order to understand the performance of the three cases, different ventilation conditions were applied to each; closed and opened windows.

For the open window condition it is applied for both daylong schedule and for more weather responsive schedule between 8 pm and 12 pm so the interior space could be protected against overheating through the hot air during daytime. As for the closed window condition, both traditional cases, CT1 and CT2, showed better performance than the modern one, especially when compared to the unshaded node (fig. 4.16). For the shaded node, the average maximum temperature in case CT1 and CT2 was lower than in case CM with 1.34 °C and 0.42 °C respectively, while no significant differences found for minimum temperature, it was in CM even 1.01 °C lower than in CT2. However, maximum and minimum temperatures were in both CT1 and CT2 significantly lower than in CM in the case of the un-shaded node. In CT1 and CT2 average maximum temperatures were lower than those in the exposed node of CM with 5.23 °C and 4.31 °C respectively, where average minimums were 2.4 °C and 1.54 °C. The average difference between maximum and minimum temperature in the case CT1 did not exceed 0.84 °C while in the case CM it reached 2.33 °C and 3.67 °C in shaded and un-shaded spaces respectively (fig. 4.17)

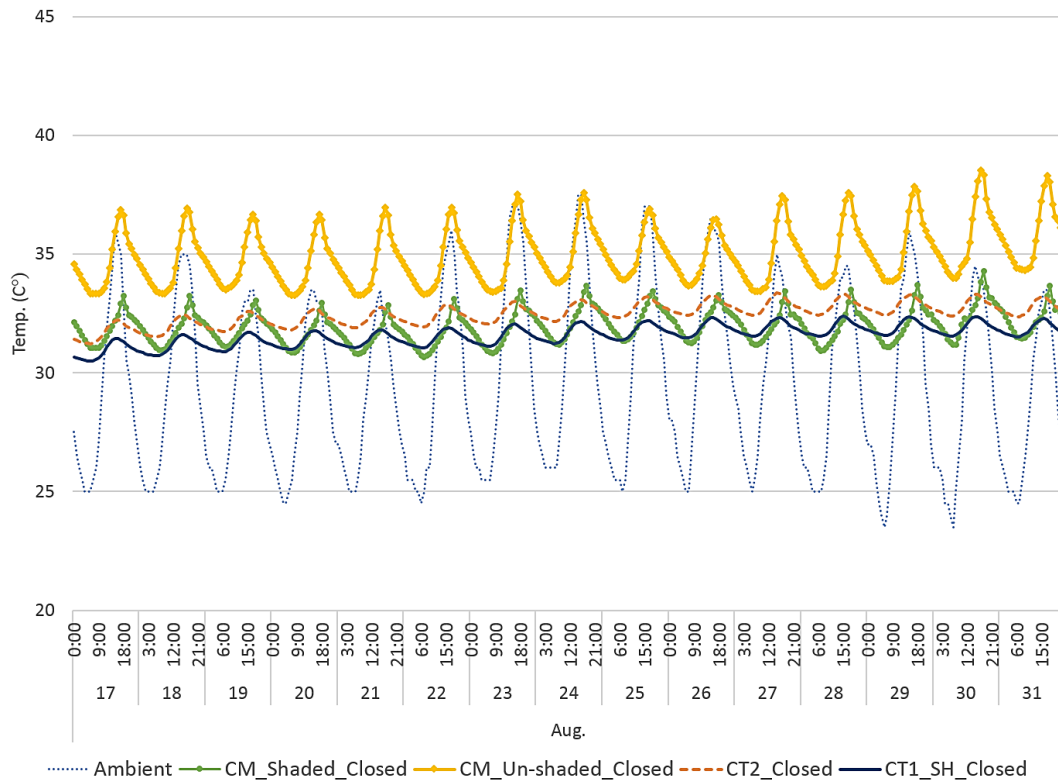


**Figure 4.16:** CM (shaded and un-shaded nodes), CT2, and CT1-SH, comparison between simulations results for indoor temperature, no ventilation

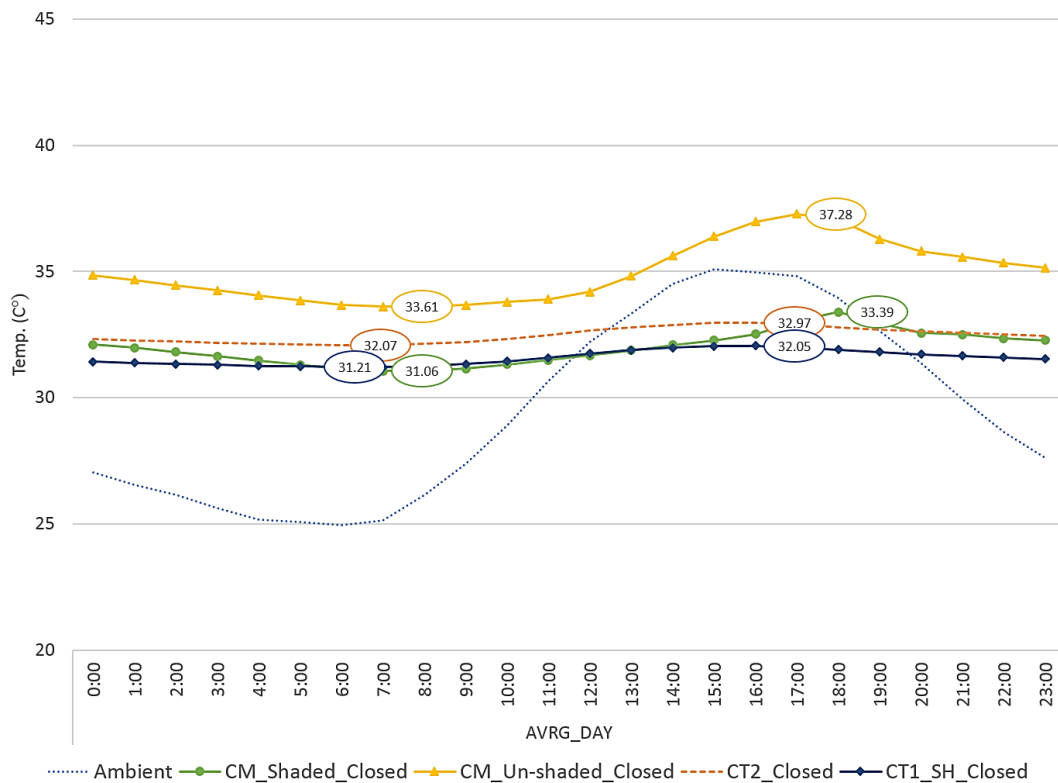


**Figure 4.17:** CM (shaded and un-shaded nodes), CT2, and CT1-SH, average day indoor temperature, no ventilation

However the average diurnal differences in all cases significantly vary when ventilation is active along the day where higher correlation between indoor and ambient temperature takes place. As previously discussed in chapter 2, the heat loss through ventilation (convective heat loss) is in proportion to the air exchange rate, difference in temperature between the inside and the outside, and the capacity of air. When an air change rate value is defined in the simulation models, the above observed values dramatically change as the heat flux increases according to the equation:

$$Q_V = C_p \cdot \rho \cdot q_v (\vartheta_i - \vartheta_a) \quad (4.2)$$

where  $C_p$  is the heat capacity of air (1006 J/kgK),  $\rho$  is density of air (1.2 kg/m<sup>3</sup> for dry air),  $q_v$  is air volume flow (m<sup>3</sup>/s),  $\vartheta_i$  is the inside air temperature (°C), and  $\vartheta_a$  is the ambient air temperature (°C).

A higher correlation with ambient temperature occurred in all cases with significant temperature fluctuation between day and night temperatures. The temperature differences between all cases were comparatively diminished, especially for minimum temperatures which remained much higher above ambient in all cases and did not drop below 29.46 °C in CT1, 4.53 °C above ambient temperature. The average maximum indoor temperature in CT1 however reached 33.96 °C, 1.14 °C below ambient and 1.24 °C and 3.14 °C below CM shaded and un-shaded nodes respectively (fig. 4.18).

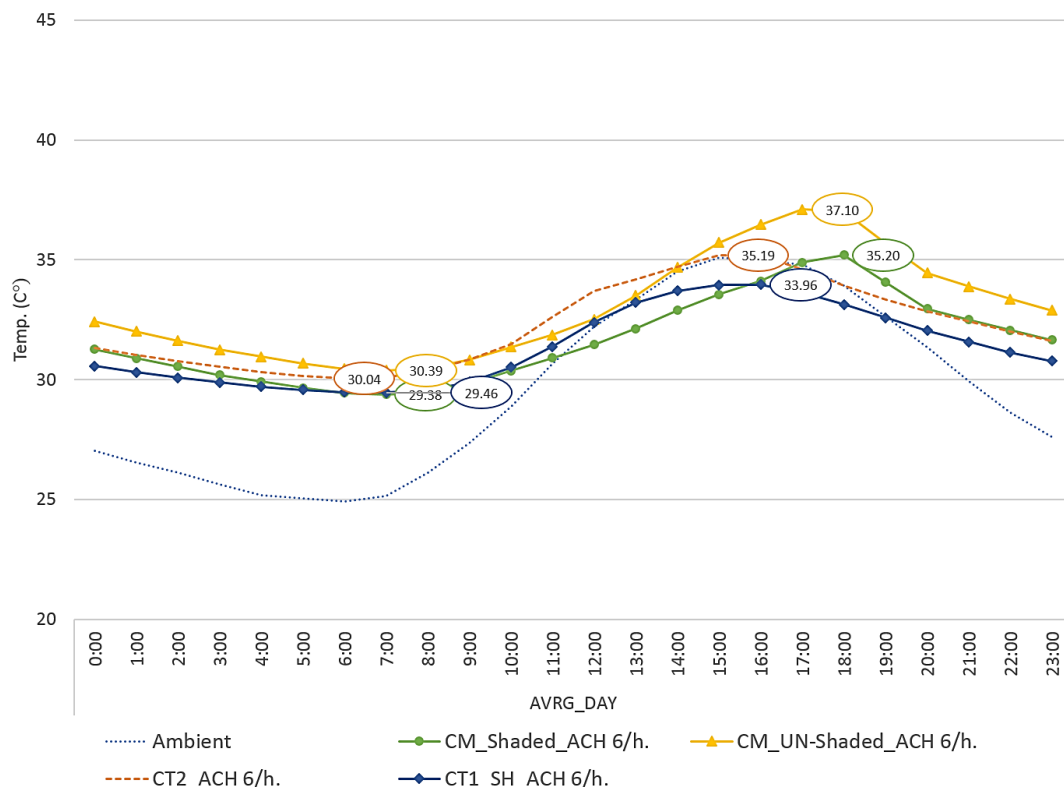


**Figure 4.18:** CM (shaded and un-shaded nodes), CT2, and CT1-SH, comparison between simulation results for indoor temperature, ACH 6/h, average day

### 4.3.1 Indoor temperature and heat storage capacity

The use of thermal mass can be more effective with a significant diurnal variation of ambient temperature and/or diurnal variation in solar radiation intensity [73]. The lower heat storage capacity of the brick in the case CM results in more indoor temperature fluctuation especially when the wall is more exposed to solar radiation. Considering the relatively low density of the hollow red bricks in the case CM, the role of the stone higher thermal mass is hence evident through its ability to store the absorbed heat, which results in less temperature fluctuation along the day. The energy intake required to heat up 1 m<sup>2</sup> of both walls 1°C can be calculated by the following equation:

$$Q = c \cdot \rho \cdot V \cdot \Delta T \quad (4.3)$$

where  $c$  is the specific heat Wh/kgK,  $\rho$  is density kg/m<sup>3</sup>,  $V$  is volume, and  $\Delta T$  is the change in temperature. For the brick wall of CM:  $= 0.23 \times 1790 \times 1 \times 1 = 411.7 \text{ J/}^\circ\text{C}$ . However, for cases CT1 and CT2 it would be:  $0.28 \times 2200 \times 1 \times 1 = 616 \text{ J/}^\circ\text{C}$ .

For further demonstration of the relationship between indoor and outdoor temperatures, a regression analysis is carried out. A fast data visualization for indoor and outdoor temperatures for the data acquired during the last two weeks of Aug, which fall into the measurement period, can illustrate the relationship between indoor and outdoor temperatures in both cases, CT1-GH and CM. As for the case CM1-GH, figure 4.19 is a matrix-plot of three variables; outdoor temperature ( $T_{out}$ ); simulated indoor temperature with no ventilation ( $T_{in}$ ), and simulated indoor temperature with ventilation and air change rate ACH of 6/hour ( $T_{in-v}$ ). The three subplots on the diagonal, from top left to bottom right, are histograms of the three variables  $T_{out}$ ,  $T_{in}$  and  $T_{in-v}$  respectively. The pair-wise plot of each of the three variables results in the six subplots located off diagonal of the figure. For example, the subplot on the first column and second row is a plot of  $T_{in}$ , vs.  $T_{out}$ ; while  $T_{out}$  vs.  $T_{in}$  is located on second column and first row.

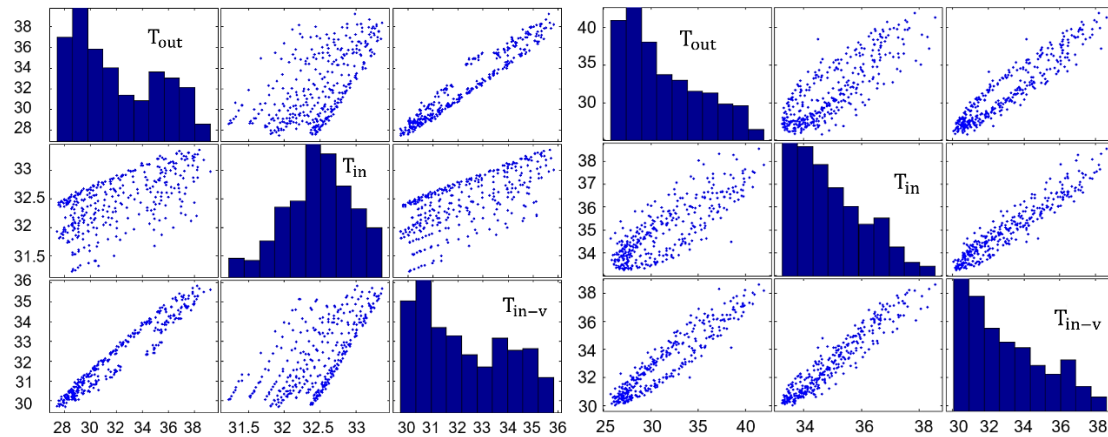


**Figure 4.19:** CT1-GH, matrix-plot of outdoor and indoor temperatures

**Figure 4.20:** CM, matrix-plot of outdoor and indoor temperatures

From the histograms it is clear that  $T_{in-v}$  and  $T_{out}$  have very similar distributions, a direct consequence of the air flow and exposure to the ambient temperature. In contrast, the distributions of  $T_{in}$ , indoor temperature with no ventilation, and  $T_{out}$  are dissimilar in two aspects. First, the temperature range (31-33.5) vs. (29-40); this conveys the effect of building design in stabilizing the temperature inside. Second, and very interestingly, the shape of the distribution, where  $T_{out}$  has a bi-modal shape (at temperatures 29, 37) and  $T_{in}$  has a uni-modal shape (at temperature 32.5). In the vernacular, this means that even when the ambient temperature frequently occurs at 29 and 37 (with variation), the indoor temperature frequently occurs only at 32.5 (with variation). This is another stabilizing effect of the building design.

However applying the same visualization for the modern case (fig. 4.20) a similarity between the distribution of  $T_{out}$  and both  $T_{in}$  and  $T_{in-v}$  is evident, reflecting a higher correlation between indoor and outdoor temperatures. This could be basically attributed to the lower storage capacity of the brick walls which take shorter time to release the heat inside the room. Undoubtedly other parameters also govern the thermal responsiveness of the building, especially when two different typologies are compared. However, given the anticipated capacitance of the stone thermal mass, the observations above can be interpreted as a delay of heat transfer in the case CT1. The heat storage capacity can hence be counted as the most decisive factor for indoor temperature stabilization as it will be demonstrated through the following regression analysis. The data visualization above, for the case CT1, conveys the relationship between outdoor and indoor temperatures qualitatively. A quantitative description however can be provided using regression analysis to estimate the linear relationship that appears in the figures. A straight forward first order regression analysis gives:

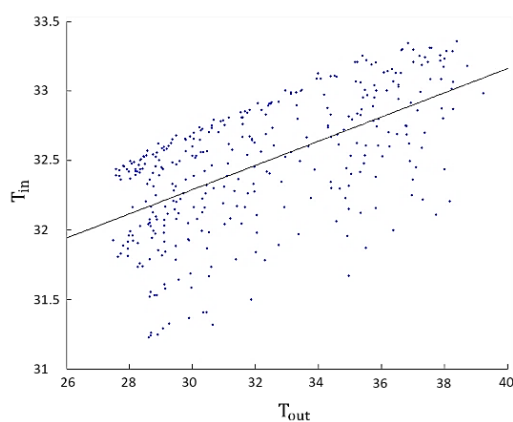
$$\text{Mean of } T_{in} = 29.7 + 0.087 T_{out} \quad (4.4)$$

Figure 4.21 is a plot of this regression line equation (in black), where the blue points are the actual readings appearing on the matrix plot discussed above. The regression line comes in-between the data points to show the average trend of the relationship between these two variables. The root-mean-square-error (RMSE) of this line is 0.37 degree, which shows accurate regression.

The quantitative interpretation of this regression equation says that an increase of 1 degree in the ambient temperature results in an increase of only 0.087 degree inside. Said differently, the inside temperature will increase by 1 degree only if the outside temperature increases by  $(1/0.087 = 11.5)$  degree. This emphasizes quantitatively the stabilizing effect of building design that is observed above from reading the histograms in the data visualization step. When the regression above is repeated on the whole period of summer time (June--August); it gives the following equation:

$$\text{Mean of } T_{in} = 23.5813 + 0.2096 T_{out} \quad (4.5)$$

Figure 4.22 is an analogue for figure 4.21. The RMSE of this equation is 1.3 degree, obviously larger than the RMSE obtained for regression during only the last two weeks of Aug. This is foreseeable since more explanatory variables (than merely  $T_{out}$ ) will be needed to model the relationship when the period extends and hence more factors interact.



**Figure 4.21:** CT1-GH, regression of indoor temperature on outdoor temperature, 17-31 Aug.

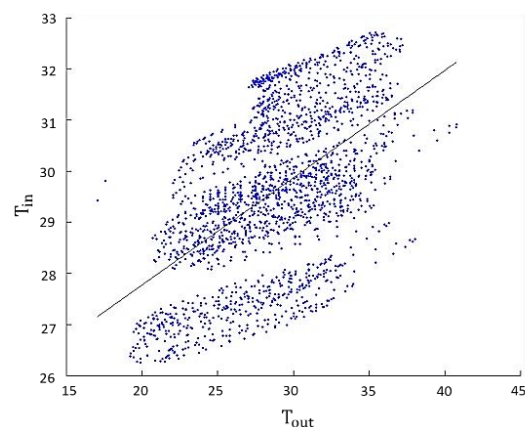


**Figure 4.22:** CT1-GH, regression of indoor temperature on outdoor temperature, Jun.-Aug.

In the equation above, the variable  $T_{out}$  is called "predictor" and the variable  $T_{in}$  is called "response"; this terminology is borrowed from the literature of statistics. From the physics of the current problem it can be anticipated that  $T_{in}$  depends, in parallel to  $T_{out}$ , on the temperature outside the building hours ago, a direct result of the capacitance effect of building material (Limestone). Accordingly, a table of 13 columns is formulated; the first column includes the outdoor temperature at a moment and the other 12 columns are the temperature each preceding hour. The correlation coefficient was calculated and the smallest correlation was with the temperature outside 12 hours ago ( $T_{out-12}$ ). Then  $T_{in}$  is regressed on  $T_{out}$  and  $T_{out-12}$ , and obtained the equation:

$$T_{in} = 15.1313 + 0.2979 T_{out} + 0.2056 T_{out-12} \quad (4.6)$$

Figure 4.23 is the 3D analogue to figures 4.21-2. The RMSE of this equation is 1.05 degree, a 19% reduction when compared to the 1.3 mentioned above. Obviously, when  $T_{out-12}$  is replaced by any other temperature that is more correlated with  $T_{out}$ , i.e.  $T_{out-10}$ , a higher regression error will be obtained. The interpretation of this regression equation is of interest. The coefficients of both  $T_{out}$  and  $T_{out-12}$  are close to each other, which means that the temperature outside now and 12 hours ago are almost equally important in predicting the temperature inside, which can be attributed to the heat storage capacity of the walls' material. However, the reduction in error is not very significant; only 19% as indicated above. More elaborate regression methods can be employed to reduce the error and to better formalize  $T_{in}$  in terms of outdoor temperature. For example, slicing the data, as it appears from figures 4.22-3 then building a regression model for each slice will build a more accurate equation. However this regression analysis is carried out to demonstrate the efficacy of the thermal mass of the building material, since the prediction of indoor temperature is already carried out in TRNSYS. It should be noted that employing the two-explanatory variable ( $T_{out}$  and  $T_{out-12}$ ) for the data of the last two weeks of August does not help in reducing the RMSE below the 0.37 degree mentioned upfront. Moreover the coefficient of  $T_{out-12}$  for this data is almost zero, producing a very similar equation to equation (4.6).

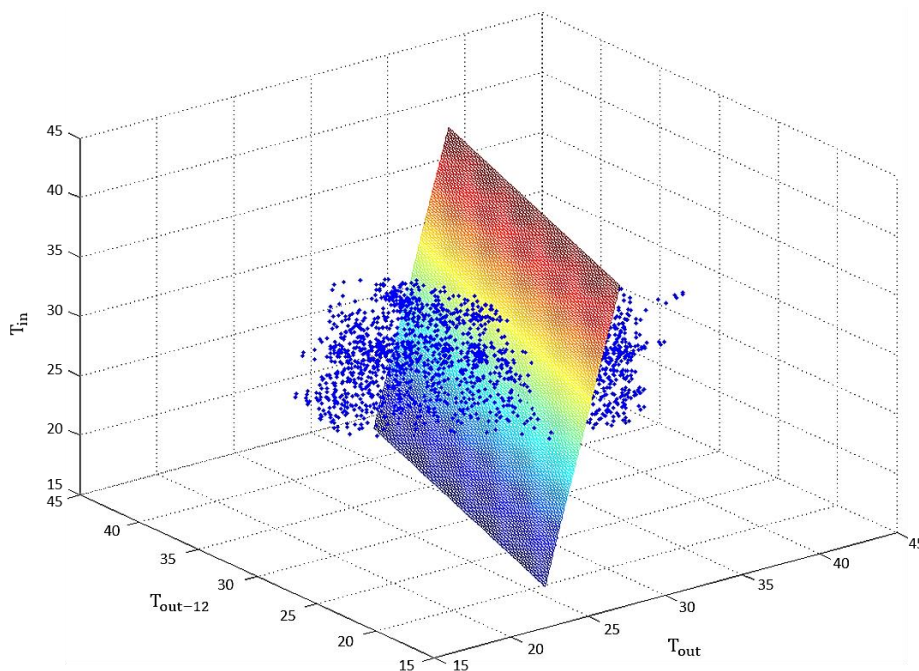


**Figure 4.23:** CT1-GH, regression of indoor temperature on simultaneous outdoor temperature and before 12 hours, Jun.-Aug.

### 4.3.2 Solar radiation

The significant amount of shading obtained by the shaded node in the case CM is a major factor in lowering the indoor temperature. The amount of solar radiation transmitted through the glass is dramatically reduced when the window is shaded by the balcony. As shown in figure 4.24 solar transmittance starts to increase gradually from 7 am as the sun shines, however in the middle of the day it starts to jump to maximum level in the case of unshaded window. However this rapid increment is delayed until 4 pm in case of the shaded window. Both values drop then by the sunset after 6 pm. This means that the space adjacent to the balcony remains protected against direct solar radiation daylong except for less than two hours when the sun is too low in the sky.

Figures 4.25 a-d trace the shadowing range between 10 am and 6 pm. The shaded wall receives less than  $100 \text{ W/m}^2$  during summer days, while the maximum incident solar radiation is found during winter time in February;  $200 \text{ W/m}^2$ , where the sun is low enough to penetrate the balcony and hit the shaded wall. However the incident solar radiation on the un-shaded wall which is totally exposed is more than  $400 \text{ W/m}^2$  during summer and reaches  $600 \text{ W/m}^2$  in winter months. Generally, the south oriented walls are preferred for optimal solar gains in winter [71]. Figures 4.26-8 illustrate the average daily incident solar radiation on the walls of this case and the monthly average solar gains. The role of cross shading in this case is discussed within subsequent experiments in this chapter.

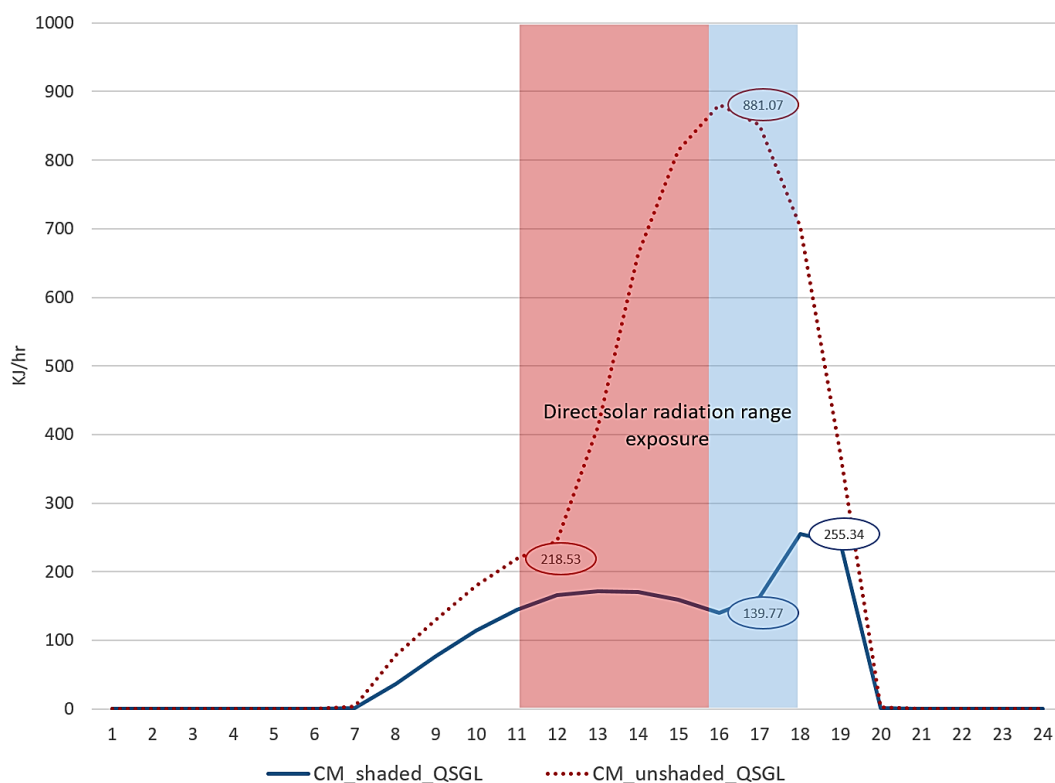


**Figure 4.24:** CM (shaded and un-shaded nodes), average daily transmitted solar radiation

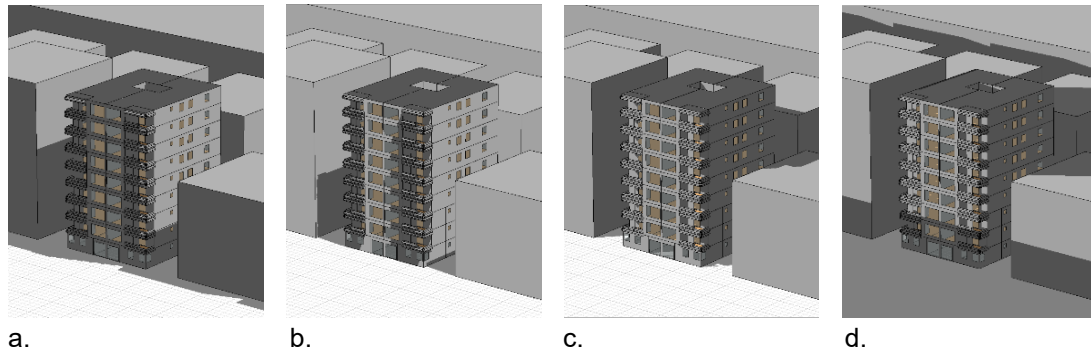


**Figure 4.25 a-d:** CM, shading on the south-west façade at 10 am, 11 am 4 pm and 6 pm

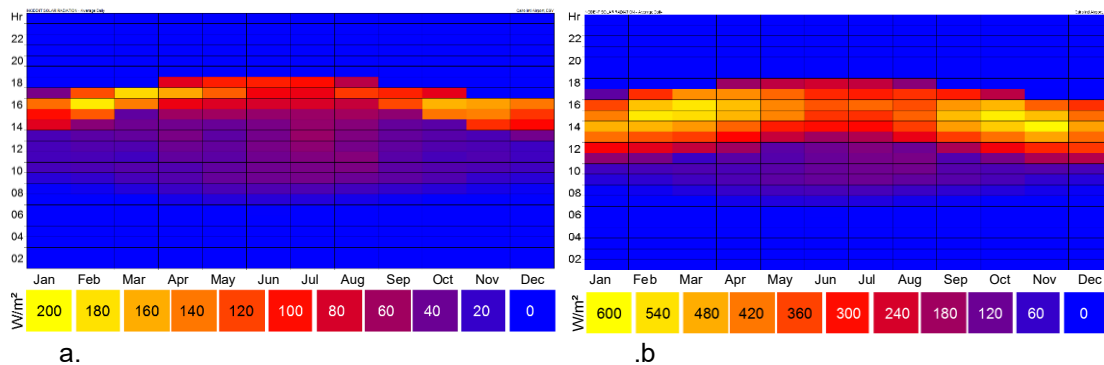


**Figure 4.26 a-b:** CM, average daily incident solar radiation, shaded and un-shaded walls

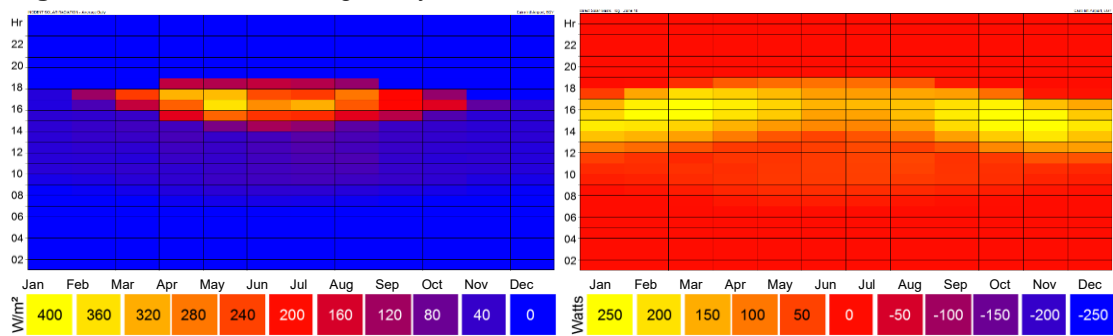


**Figure 4.27:** CM, north-west wall, average daily incident solar radiation

**Figure 4.28:** CM, monthly average solar gains

As for the case CT1, it is obvious through modeling the solar radiation that the courtyard receives lower amounts of solar gains as being shaded for longer spans along the day (fig. 4.29). The courtyard enclosure plays a significant role here in the distribution of the shadowing range. The facades facing the courtyard receive a large amount of shading along the day, especially on the ground floor level. The south-west façade of the secondary hall remains shaded until 11 am and then be exposed to solar radiation until 4 pm while the north-west façade of the grand hall receives greater amount of shading as being exposed to solar radiation only between 1 pm and 3 pm. The amount of shading over the courtyard facades results in a relative reduction of the incident solar radiation on these facades when compared to the overly exposed façade surface of the modern case CM. Figures 4.31 a-h trace the shadowing range in August 23 between 11 am and 6 pm. In a courtyard building oriented north-south the courtyard facades can be shaded on all sides by the building itself [34]. Figures 4.32 a-d illustrate proximity of the shadow distribution over different facades of an assumed north oriented courtyard.

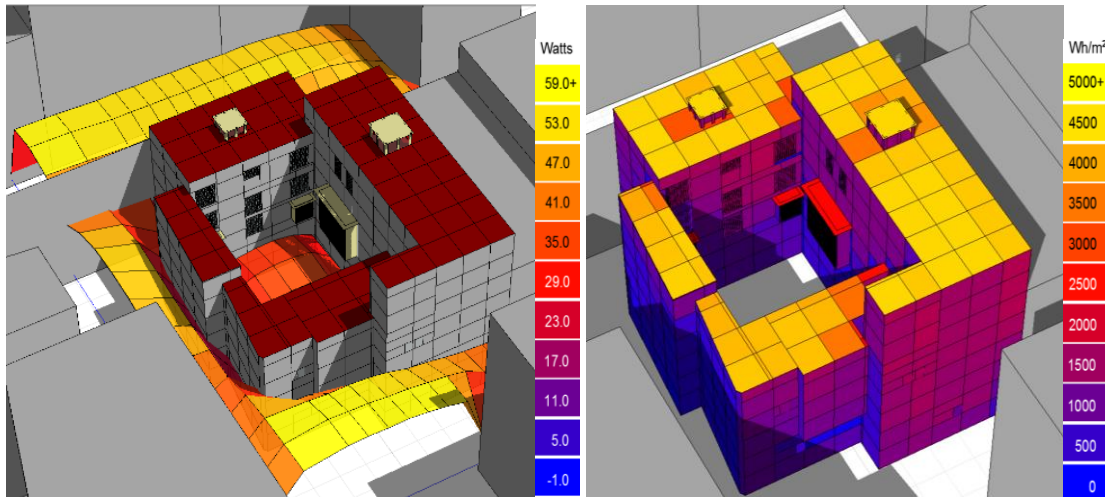


**Figure 4.29:** CT1, courtyard solar gain

**Figure 4.30:** CT1 Total direct radiation

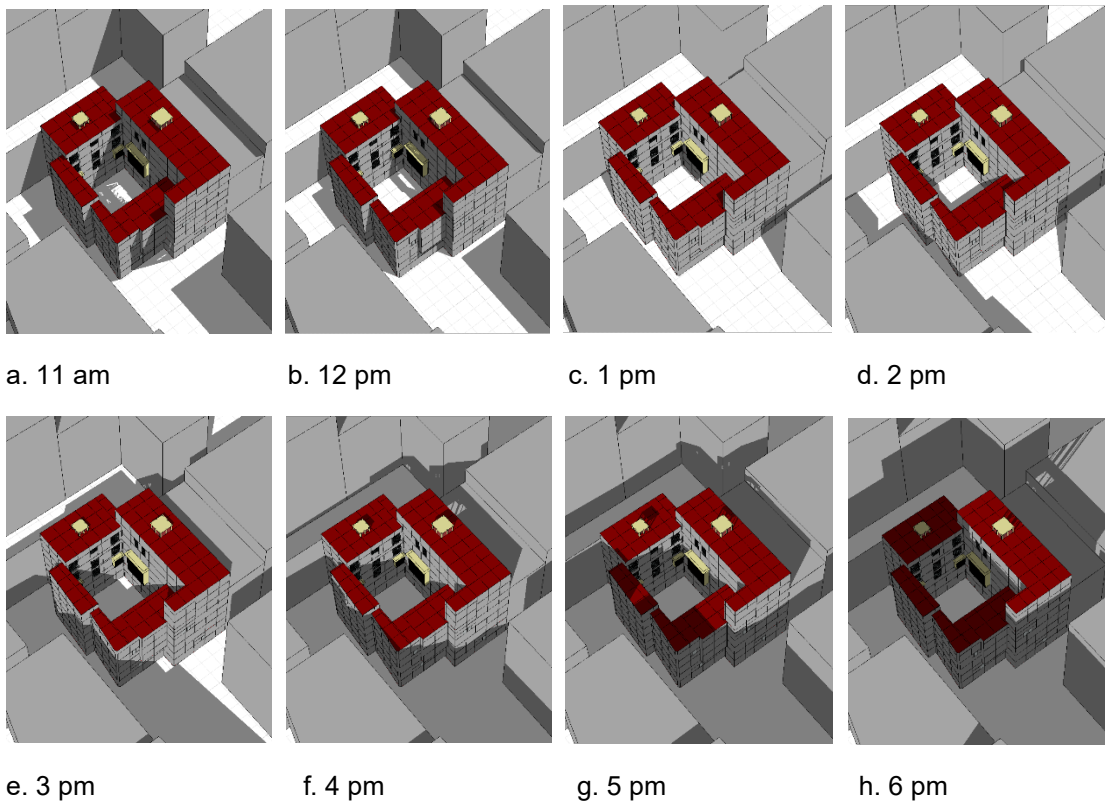


**Figure 4.31 a-h:** CT1 courtyard daytime shadowing, 23<sup>rd</sup> August

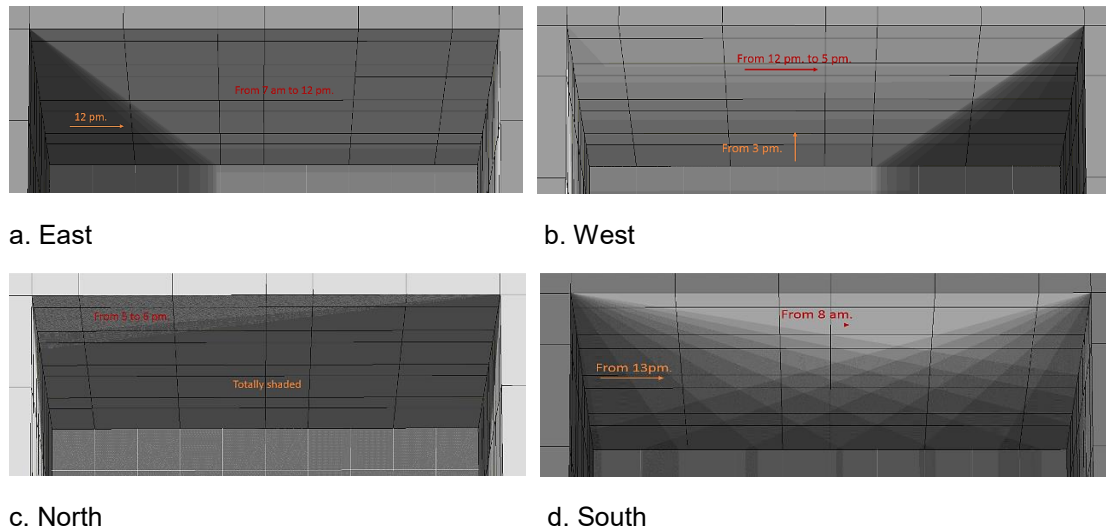
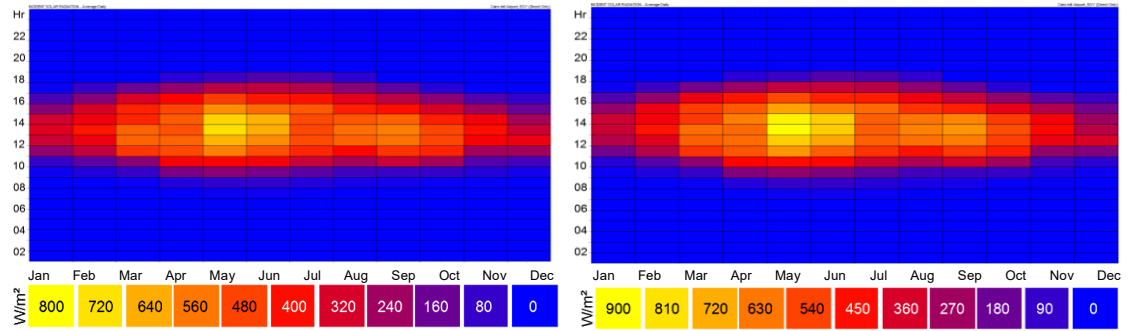


**Figure 4.32 a-d:** Courtyard shading range on different façades orientations between 9 am and 6 pm

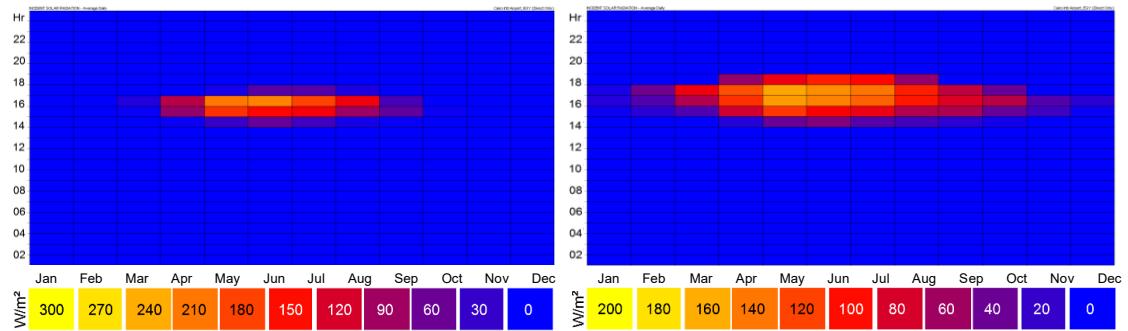
However, emphasis here should be placed upon the amount of incident solar radiation hits the roofs and walls of each hall (fig. 4.30). Unlike the other cases, the roof here, in both halls of the house, is totally exposed to solar radiation. Modeling the solar radiation in this case is hence useful to understand the amount of heat gains. The average daily incident solar radiation on the roof of the grand hall reaches its maximum limits of  $900 \text{ W/m}^2$  in May and varies during the summer season to  $540 \text{ W/m}^2$  in August. These values slightly decrease for the secondary hall to reach  $480 \text{ W/m}^2$  in August and a maximum of  $800 \text{ W/m}^2$  during middays of May. Figures 4.33-5 illustrate the average daily incident solar radiation for all roofs and walls of both grand and secondary halls.

As for the ground floor level of the north-west façade of the courtyard, it receives a maximum of  $160 \text{ W/m}^2$  in the afternoon in June, as the sun starts to hit the façade after 2 pm. Nevertheless the value at the same time during August is less than  $100 \text{ W/m}^2$  and almost no values of solar radiation can be counted otherwise along the year. The façade on the first floor level however receives higher amounts, however remains comparatively low;  $240 \text{ W/m}^2$  in May and  $150 \text{ W/m}^2$  during August for the same daytimes. On the contrary the incident solar radiation on the south-west façade reaches its minimum limits during summer;  $80\text{-}120 \text{ W/m}^2$  and  $120\text{-}200 \text{ W/m}^2$  in July and August for the ground floor and first floor levels respectively; and  $320\text{-}400 \text{ W/m}^2$  in March and October for both levels. This is quite reasonable due to the summer sun solstice, ca.  $84^\circ$ , which does not reach the façade that remains almost shaded by the other wing of the courtyard (south-east). However in winter the sun becomes much lower in the sky and can penetrate the courtyard to hit the south-west façade, and hence the values of the incident radiation increase during winter time.

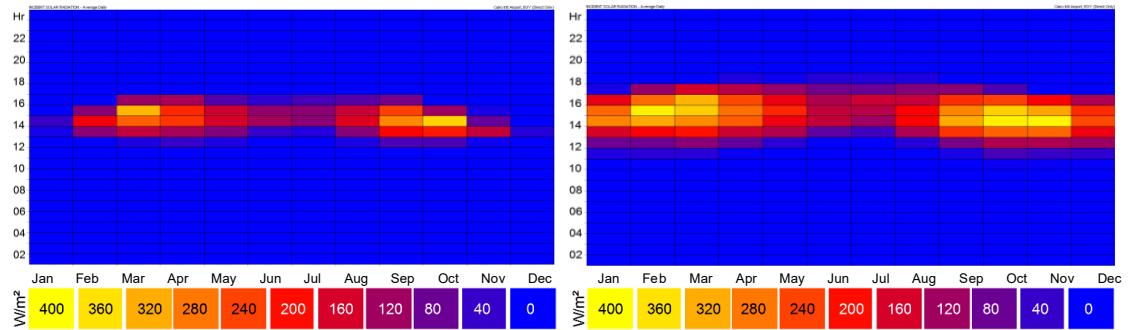
The manner of solar radiation distribution over the courtyard's south-west façade has accordingly its impact over the amount of solar gains which reaches its minimum during summer time. The overall amounts of direct solar gains for all spaces can then be clearly understood in accordance with the previous analysis. In the grand hall (GH) the highest amount of solar gains is found during summer, June to August, in the afternoon until 5 pm (figs. 4.36 a-b). This is the time-span where the roof receives the greatest amount of incident solar radiation, an average daily of ca.  $800 \text{ W/m}^2$  in the afternoon during summer. However the case CM has the same pattern of direct solar gains as the secondary hall (SH) with regards to the seasonal distribution, regardless of the amount which is dramatically higher in CT1 due to the significantly larger exposed surfaces.



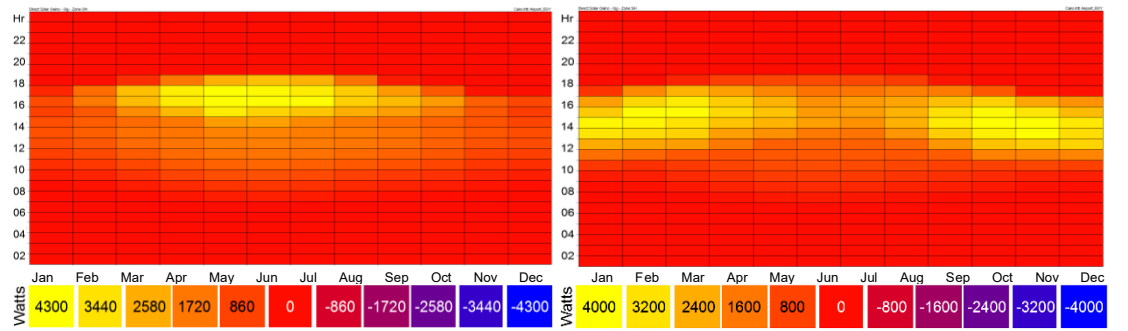
a. **Figure 4.33 a-b:** CT1, average daily incident solar radiation, roof GH and SH respectively



a. **Figure 4.34 a-b:** CT1, average daily incident solar radiation on the courtyard walls north-west, ground and 1<sup>st</sup> floor levels respectively



a. **Figure 4.35 a-b:** CT1, average daily incident solar radiation on the courtyard walls south-west, ground and 1<sup>st</sup> floor levels respectively



a. **Figure 4.36 a-b:** CT1, monthly average direct solar gains, GH and SH respectively

Despite the exposure of its roof to solar radiation, the hall SH in case CT1 showed better thermal performance than the hall MH in case CT2. The indoor temperature in SH is found to be consistently lower than MH with average difference of 0.81 °C. Realistically this could be attributed to a couple of factors; the first of which is the absence of surrounding buildings around the case CT2 which results in lower amounts of cross shading and hence affects the microclimate. The second factor is the role the wind-escape plays in the ventilation process and the release of hot air from the roof side. However, it would not be realistic to count on this element within this simulations. The simulation runs in TRNSYS defined a consistent air change rate though a ventilation schedule regardless of the air flow pattern inside the space or the inlets and outlets of air and with no determination of the finite role of each opening. The role of the wind-escape hence is not examined and will therefore be subsequently investigated through the CFD modeling. However, protecting the roof of the hall SH against direct solar radiation by adding an upper floor for instance, as it would be the case for a three-story courtyard building, can result in lower indoor temperatures (fig. 4.37) due to the decrees of the amounts of direct solar gains. Although having the same material thermal properties, design, and close volume, the case CT1 showed a relative consistent and stabilized performance than CT2 with an average temperature difference of 0.9 °C. In reality this could be attributed to the influence of the roof wind-escape device, which plays a significant role in releasing the hot air outside of the space.

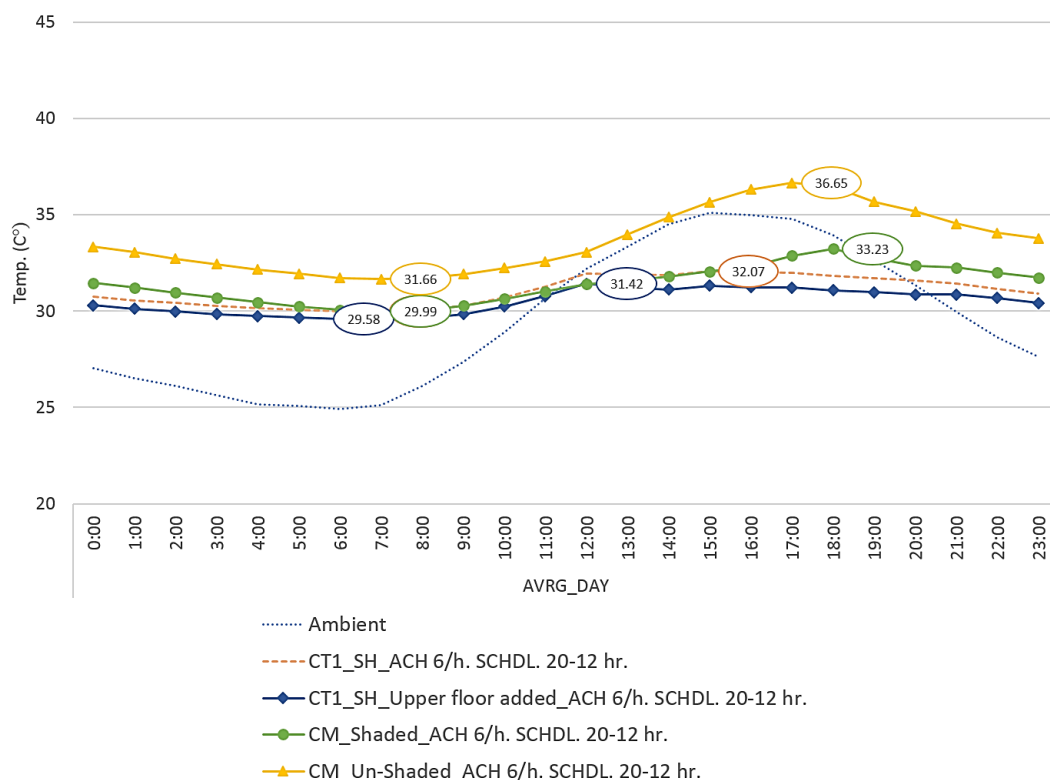


**Figure 4.37:** CM (shaded and un-shaded nodes), CT1-SH (real case and with upper floor), average day indoor temperature, ACH 6/h. schedule 8 pm-12 pm

#### 4.4 The role of shading mechanisms

The traditional house demonstrates awareness of solar geometry and heat transfer mechanisms as basic physical principles which govern the heat gain/loss process within the building. The following experiments are confined to examining the effect of traditional solar controls and shading mechanisms as basic features of passive climate design of traditional architecture. Discussed features are the resulted cross shading in narrow street canyon and window screens. Conceptually, the following experiments aim to test the indoor air temperature of an existing contemporary building that compromises the major opposites to the suggested features which would be introduced as shading devices to the simulation model of the case (CM) to compare results with those of the base case and hence determine the extent to which those features can influence the indoor temperature. The experiments took place upon a short time-span; 18-24 April, a period during which field measurements for indoor temperature were obtained and the simulation model was also validated against (fig. 4.38). The model was modified by introducing suggested features which found to be comparatively effective in lowering the indoor temperature. The primal objective of these experiments is to determine the potentiality of the suggested features for solar control when applied to modern buildings. Two major experiments then took place which to be described within the following pages.

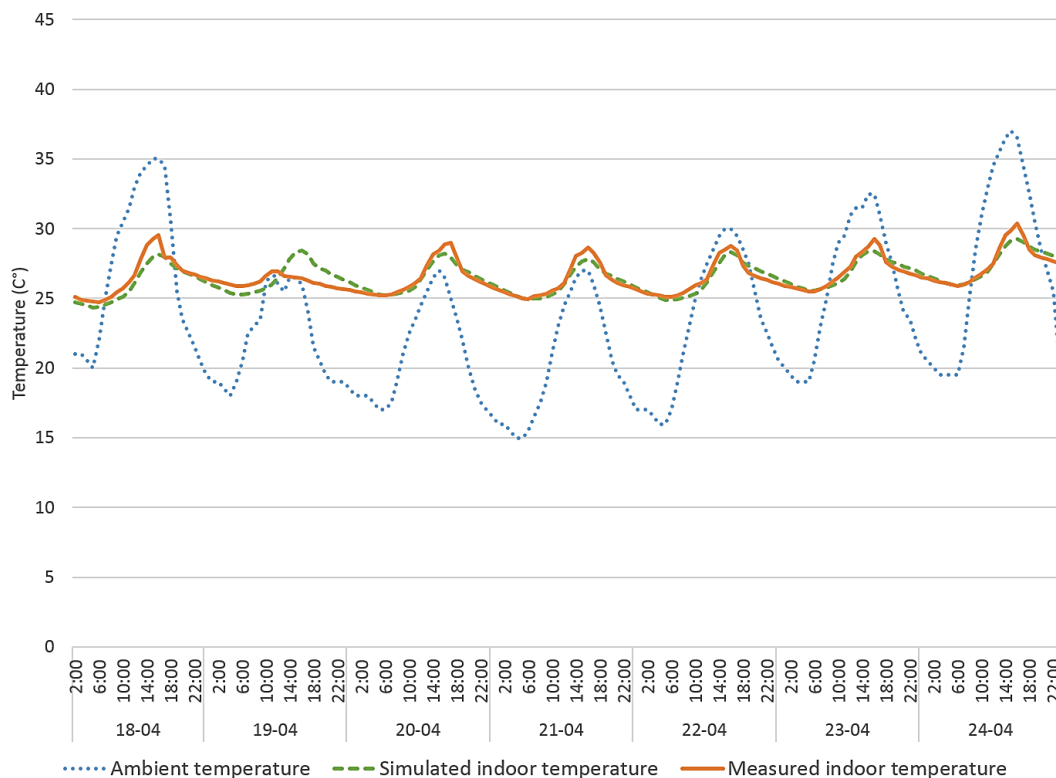


**Figure 4.38:** CM, simulation results for indoor temperature against measured data, 18-24 April

The traditional city was always characterized by dense urban fabric and narrow streets that generally form deep narrow canyons with average width of 3.5 meters. This formation resulted in subsidiary streets which are almost east-west oriented being shaded along the day. The case study represents an extreme opposite to this situation with a street width of 75 m, which supposedly played a significant role in the relative high indoor temperature. According to the west-south orientation of the main façade, it would be then exposed to the direct solar radiation especially from the middle of the day on. This experimental step proposed a building opposite to the main façade and as the same height as the monitored building, leaving a street width of 6 m, which creates a relatively deep narrow street canyon with aspect ratio much over 2. The increase of the aspect ratio results in decrease of temperature, however the mean radiant temperature is a more decisive factor [71]. Although the case of adding a building in front of another is unlikely to happen within existing urban settlement, this experiment takes place to demonstrate the effect of narrow street canyon cross shading if being considered within urban development that takes place in the future. The opposite building is added as a shading group in TRNSYS 3D model, as shown in figure 4.39. An updated shading matrix was then generated in TRNSYS Build and the simulation applied as the same as for the base case in terms of period, material properties and other parameters. The results showed a significant decrease in indoor temperature that averages 4° C when compared to the values taken from simulation results for the base case (fig 4.41).

The second experiment demonstrates the effect of window screens which is incorporated as a shading group, similar to the screen modeling in the traditional cases. The screen was incorporated to the window on the south-west façade. The window occupies an area of 6 m<sup>2</sup>, about 54% of its wall. The screen was designed with modular sections of 5x5 cm. with proposed ratio between the width and the depth 1:1 and 50% perforation, as shown in figure 4.40. The resulted exposed glazing surface was then 19%. The simulation applied with new shading matrix generated and without the opposite building. The results showed also decrease in maximum indoor air temperature with an average of 2.5 °C, as shown in figure 4.41.

It is quite relevant that the first case in which an opposite building exists is found to result in lower indoor temperature, as shown in figure 4.41. As Thermal radiation and natural convection are, in roughly equal measures, responsible for the heat transfer in buildings [54], this could be attributed to a couple of factors. The first is that the entire façade is shaded by the opposite building not only the shaded proportion of the window. Hence the transmitted solar radiation into the space is significantly reduced, as shown in Figure 4.42. The second factor is the role of resulted reduced outdoor temperature of the street and hence the façade temperature. In this case when the sun hits the surface of the building in a street canyon, convective current results as the air density changes. The hot air moves to the upper level and be replaced with cooler air which has greater density. The exposure of gap to the night sky enhances the night time cooling as the heat radiates up to the sky. The street is cooled down during night and daytime unless the sun is coming on a vertical angle.

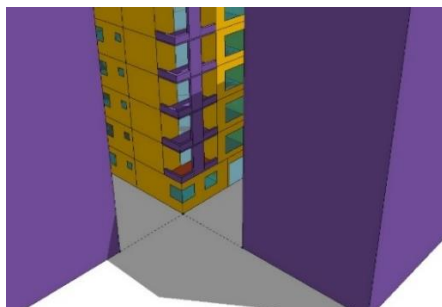


**Figure 4.39:** CM, a building opposite to the south-west façade, added as a shading device

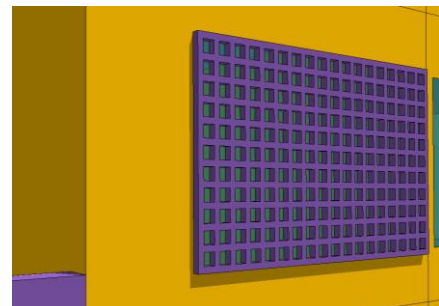


**Figure 4.40:** CM, window screen incorporated on the south-west façade

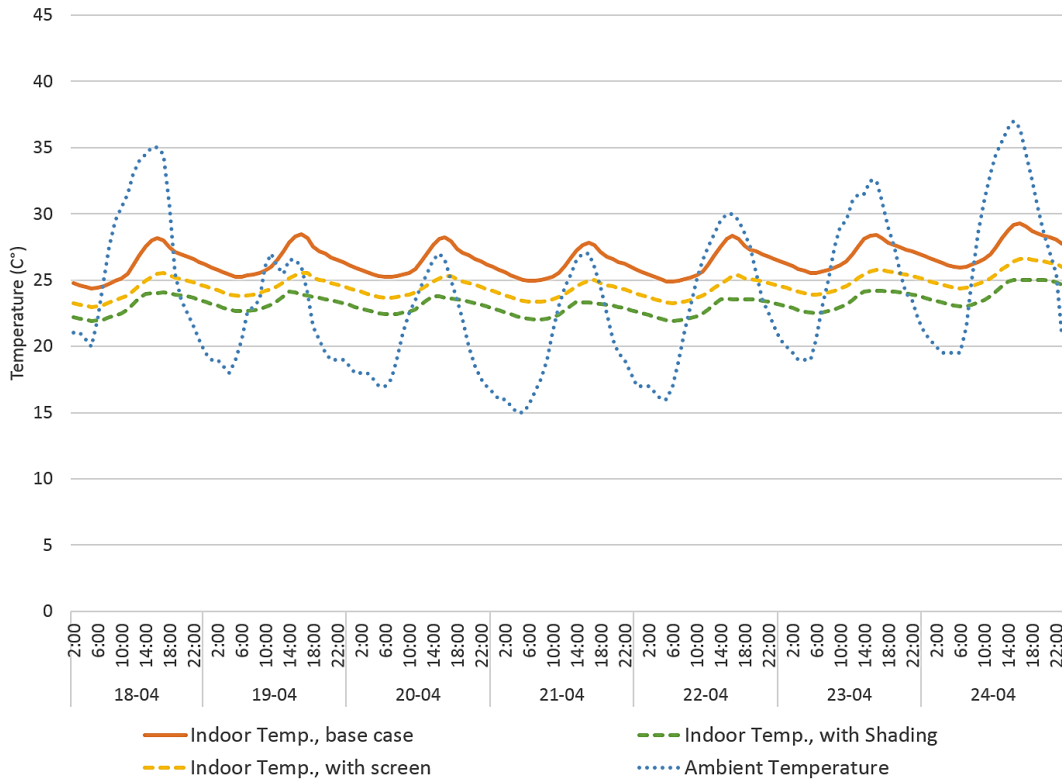


Figure 4.41: CM, comparison between the three situations

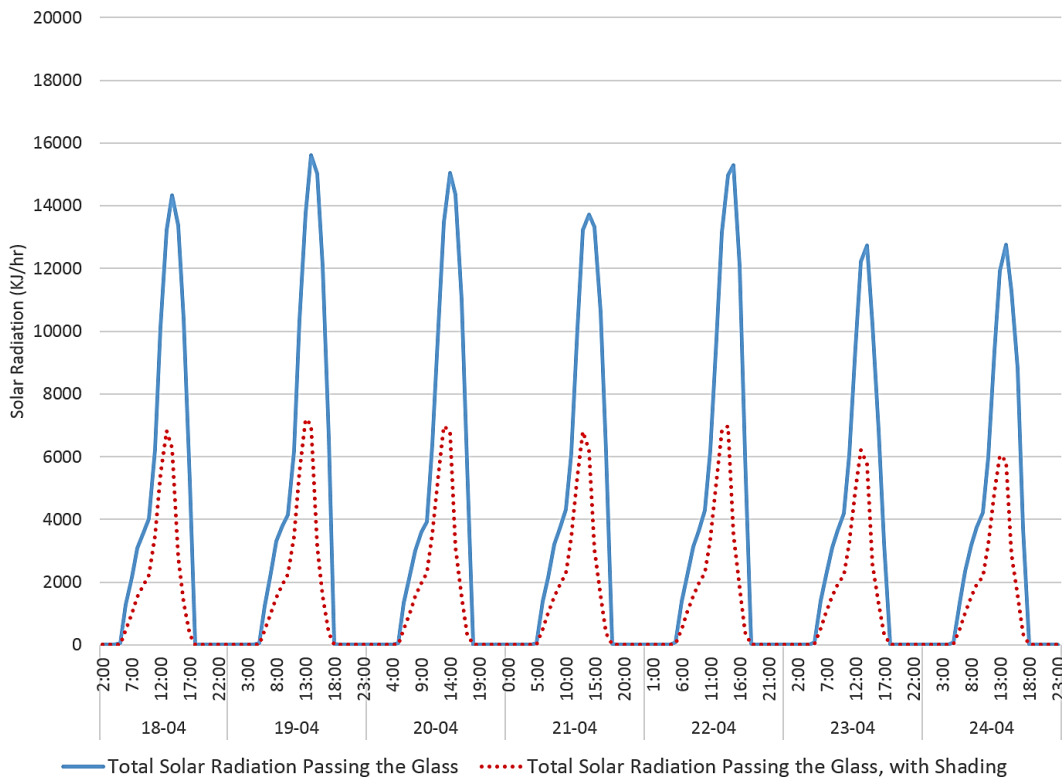
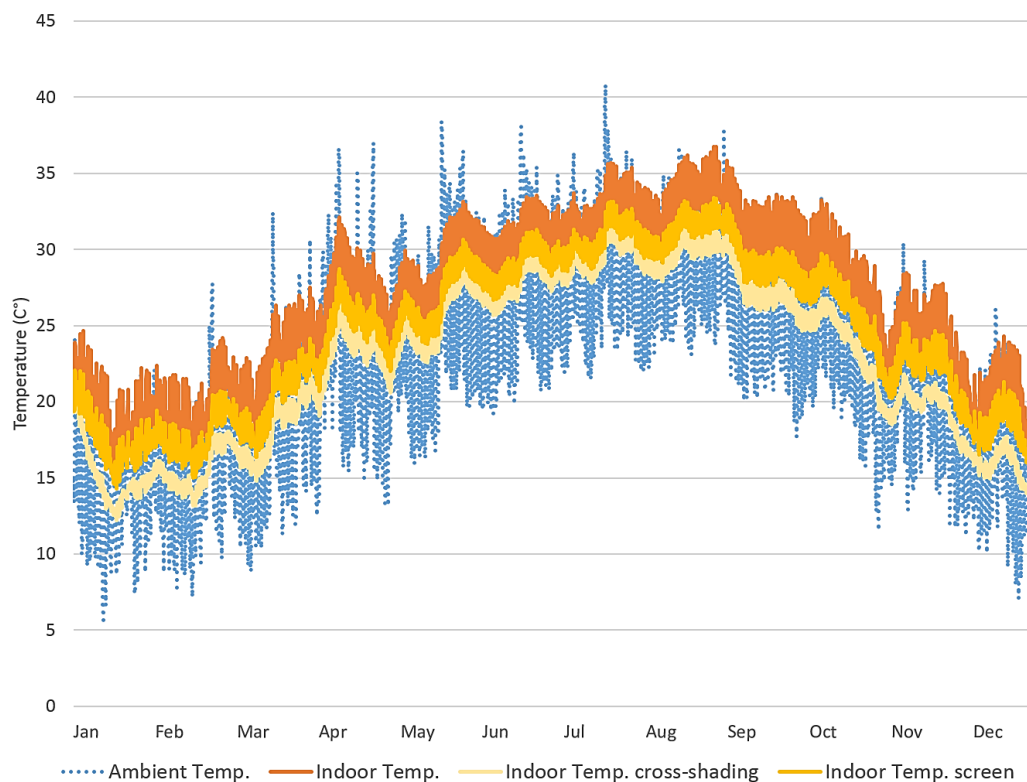
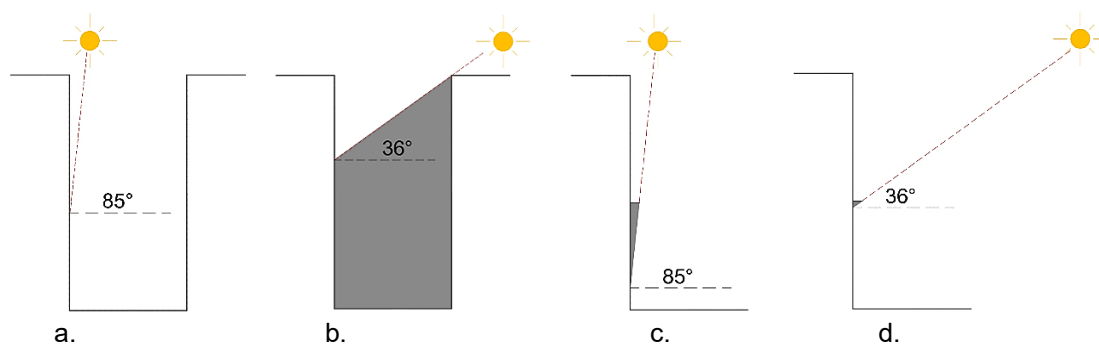


Figure 4.42: CM, total solar radiation transmitted through the glass; with and without a shading

To predict the performance of the suggested features during the hottest summer days, simulations applied for the base case to a year time span, (fig. 4.43). The same experiments were applied upon yearly weather data and a relative differences were found for maximum temperature in both cases within summer days in July and August. In winter days however, the case of cross shading condition showed comparatively dramatic decreases in indoor temperature. As the length of shadow on a wall surface can be determined by horizontal and vertical shadow angles, the decrease of indoor temperature could then be attributed to the position of the sun being too low in the sky and the opposing building that would almost block the radiation that would not reach the lower floors which remain shaded all the time. However the window screens would be less effective in winter due to the limited shading resulted by the angle of the sun beam (figs. 4.44 a-d). This can be more desirable in cold winter, as discussed in chapter 6.



**Figure 4.43:** CM, predicted annual indoor temperature, comparing base case with modified models



**Figure 4.44 a-d:** resulted shading in different cases, a. summer sun with cross shading, b. winter sun with cross shading, c. summer sun with window screens, d. winter sun with window screens

## 4.5 Conclusion

1. Simulation models were validated against real measured data for indoor temperatures for the three selected cases CM, CT1, and CT2 with absolute deviance error  $\pm 0.3$  °C.
2. A constant value of 6/h was assumed for air change rate (ACH) which is predicted in the next chapter through the CFD modeling
3. The traditional case CT1 showed better thermal performance in terms of indoor temperatures and hence will be adopted as a valid model for passive design
4. Average indoor temperature is significantly correlated to diurnal difference in ambient temperature with higher ACH through ventilation
5. A regression of indoor temperature on simultaneous outdoor temperature and before 12 hours, for the case CT1, shows a relative stability of the indoor temperature. This is a direct result of the heat storage capacity of the walls' material
6. Shading has significant impact on both the amount of solar transmittance and to delay the occurrence of direct solar transmittance for ca. 4 hours during summer
7. The courtyard enclosure plays a significant role in the distribution of shading range. The facades facing the courtyard receive a large amount of shading along the day, especially on the ground floor level.
8. The courtyards' north-west façade receives greater amount of shading than south-west façade as being exposed to solar radiation only between 1 pm and 3 pm.
9. The amount of shading over the courtyard facades results in a relative reduction of the incident solar radiation on these facades when compared to the overly exposed façade surface of the modern case
10. The summer sun does not reach the north-west façade that remains almost shaded by the other wing of the courtyard (south-east).
11. In winter the sun altitude is much lower and hence the solar beams can penetrate the courtyard to hit the south-west façade, and hence the incident radiation increases during winter time which is more desirable
12. Solar control was achieved within the old city on both levels of urban density and the building envelope.
13. The amount of shading depends mainly on the morphology of the street canyon which results in decrease in the canyon temperature and hence the façade temperature and subsequently the amount of heat transferred by conduction through the walls.
14. The incorporation of window screens also contributes to lower the indoor air temperature in hot and arid climate.
15. The screen acts as a baffle zone between the interior and the exterior, so the glare of sunlight is broken up by the lattice that provides a dark area.
16. By introducing both techniques to a contemporary building by running simulations using TRNSYS it is found to be relatively effective in reducing maximum indoor temperature in hot weather.
17. The adopted shading mechanisms can be more efficient with the consideration of convective current resulted in narrow street canyons and the role of cross ventilation in night-time cooling.



# Chapter 5

## Experiments (2), air flow

### 5.1 Introduction

In the previous chapter the traditional case CT1 was introduced as a potential integrated model. However, further thorough investigations take place within this chapter through analysis of the wind behavior and aggregated results for air flow. A major limitation of natural ventilation techniques is the unpredictability of the driving forces. Wind data used in the design process is usually based on averaged data for a particular area [46]. In natural ventilation the influential factors are wind and thermal effects, which are time-dependent. The air change rates will hence vary and the use of constant values will lead to implausible results [49]. The flow rate is not constant, firstly since it is affected by the human behavior and secondly, since it depends on changing wind and thermal forces [72]. Physical experimental methods i.e. tracer gas method and pressure method such as pressure coefficient method can express the ventilation process close to reality. However, these methods remain subject to high cost and time consumption in addition to involving high errors especially in naturally ventilated buildings [24]. On the contrary, computational fluid dynamics (CFD) is a powerful technique which is used to predict airflow rate, velocity and temperature, and airflow patterns inside and around buildings [6]. CFD can simulate the fluid numerically based on fundamental equations of fluid motion and can predict the indoor and outdoor air flow and can provide detailed information of the air motion when direct measurements are difficult to acquire [66]. Recent CFD simulations have shown good agreement between prediction and measurement of natural ventilation in small buildings and have become a reliable method for evaluation of the indoor air quality [70].

This chapter therefore has a couple of objectives. The first is to understand the wind behavior inside and outside the building and the manner of the wind-driven ventilation through conducting CFD modeling and simulations for the selected building. Autodesk simulation CFD 2015 is used to apply several simulation runs for different time-steps and different climatic variables to get aggregated results for air flow along the monitoring period. The results were then analyzed and air change rates values were extracted for the summer season. Accordingly the roles of various components which are involved in the natural ventilation process were identified through determination of the air flow pattern. These components are the courtyard, openings, and the roof wind-escape device. The second goal is to extract aggregated results for flow rates. Hence, an equation to predict the ACH was inferred through classification and regression trees (CART). A prediction rule was subsequently processed as an equation for the function of air change rate where variables were defined as algebraic functions of constants and outputs from TRNSYS components. Simulation was afterwards reinitialized to obtain real values of indoor temperatures.

## 5.2 Wind Analysis and CFD simulations

As previously demonstrated the monitoring period spanned along four weeks during August and September. However the thermal behavior of the building should be investigated for a wider range of summer, between June and August. Given a stability of wind velocity, the most influential is the change of the wind's approaching angle to the building [43]. For the case of Egypt as the air normally moves from the relatively cold Mediterranean to the warm desert, northern wind is the most prevailing with an average daily maximum of 5 m/s. However, detailed records were obtained according to the recorded weather data and descriptive charts for wind velocity and directions were created for the respective period. Considering hourly time steps, a time span of three months includes over 2160 time step. Therefore, a sensitivity analysis of wind is done to confine the selection to the most climatically representative time steps.

Figure 5.1a illustrates the distribution of wind direction during summer, June to August. It is clear that the wind events occurs mostly from the eight northern cardinals along the summer with a sum of 1999 events. The southern winds however are too rare to occur as only 50 events recorded from a sum of 2049, in addition to 59 events of calm wind (0 m/s). As shown in figure 5.1b for distribution of wind speed, velocity varies between 1 and 7 m/s with predominance of speeds between 1 and 5 m/s. The most prevailing of all winds however are found to come from north, and north west (junction of two cardinals; NW and NNW) with percentage of 26.35% and 40.95% respectively. The predominant speeds for all directions as mentioned above vary between 1 and 5 m/s with total occurrence percentage of 70.92%. Records of the wind events for period from June to August 2014 are described in detail in table 5.1. Generally no conditional probabilities were observed between wind direction and velocity in relation with nor time of the day neither ambient temperature. Figure 5.3 shows the building orientation with regards to the prevailing wind directions. Theoretically the windows, for both spaces GH and SH, overlooking the courtyard would not receive any direct flow, unless of western wind, and hence might act as air outlet all the time. Nevertheless, in light of the flow pattern inside the courtyard this is not the situation, as demonstrated through results of the CFD modeling.

**Table 5.1:** Cairo wind events, June – August 2014

Direction	Wind Speed m/s								Number of Events	Event (%)	AVRG. Speed M/s
	0 <= WS < 1	1 <= WS < 2	2 <= WS < 3	3 <= WS < 4	4 <= WS < 5	5 <= WS < 6	6 <= WS < 7	WS >= 7			
N	64	89	128	141	75	25	15	3	540	26.35	3.1
NNE	10	34	33	38	24	12	9	7	167	8.15	3.6
NE	3	24	45	32	16	3	3	3	129	6.30	3.3
ENE	2	13	14	8	10	2	3	7	59	2.88	3.9
E	1	5	0	4	2	1	1	3	17	0.83	4.1
ESE	1	0	0	0	0	0	0	3	4	0.20	6.3
SE	0	1	0	1	1	0	0	0	3	0.15	3.7
SSE	0	0	0	0	0	0	0	0	0	0.00	0
S	0	1	0	0	0	0	1	4	6	0.29	7.4
SSW	0	0	0	0	0	0	0	3	3	0.15	8.2
SW	0	0	1	2	0	0	0	0	3	0.15	3.4
WSW	1	2	7	4	0	0	0	0	14	0.68	2.8
W	4	16	37	22	11	3	0	0	93	4.54	3.1
WNW	6	17	61	55	29	2	2	0	172	8.39	3.4
NW	9	57	109	103	56	4	5	2	345	16.84	3.3
NNW	18	64	121	134	129	14	14	0	494	24.11	3.6
Number of Events	119	323	556	544	353	66	53	35	2049	Calm wind 59 event	
Event (%)	5.81	15.76	27.14	26.55	17.23	3.22	2.59	1.71			

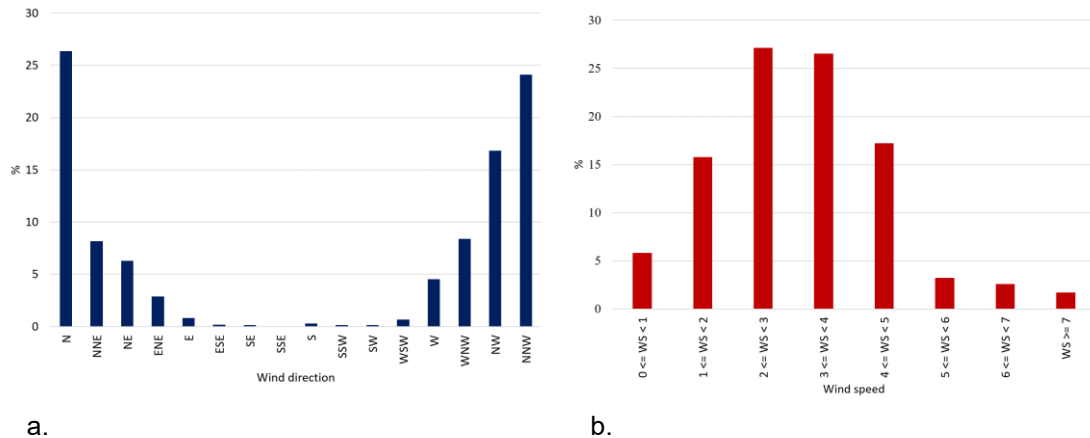


**Figure 5.1 a-b:** Cairo wind direction wind speed distribution respectively, June – August

### 5.2.1 Configuration of the CFD model and time-steps

In addition to the possible results for the airflow when running a transient CFD simulation, the solar load can be a more realistic representation of the diurnal cycle. However, in transient simulation individual values of wind direction and velocity are required. A study used a coupled analysis of Boundary Layer Wind Tunnel (BLWT) and CFD provided accurate predictions cross ventilation flow rates. However, in steady states the prediction was accurate only when no changes in flow direction existed [42]. However, Velocity and wind direction are normally defined within the simulation model by assigning their data as boundary conditions to the sides of the fluid surrounding environment created around the building. It could be hence quite impossible to run a transient simulation for a wide time span, such as 3 months. The wind direction changes frequently over eight directions unless creating at least an octagonal domain representing all possible directions on its faces. Even though, this can result in possible change in the flow direction. The surrounding domain would as well be quite larger, therefore the velocity might drop off through the central section as it is allowed to travel around the outside of the buildings where the domain is wider. Furthermore, very small time-steps are needed to accurately capture the changing flow domain, which would take an extremely long time even with a super computer machine. Therefore an adequate number of investigative steady state simulation runs would be necessary.

A simple sensitivity analysis is followed to configure the simulation time-steps. The method intended to cover all possible wind events, considering possible influential boundary conditions (solar radiation and air temperature), within the minimum number of simulation runs. In addition to the wind direction and velocity, different boundary conditions are counted in the CFD modeling, i.e. solar radiation and air temperature. Along an average day summer records, no wide fluctuation of temperature is found from a time-step/hour to the next. In other words temperature gradually ascends or descends from an hour to the next along the 24 hours. As the time of the day corresponds to the solar radiation, there is a daily possible 24 time-steps. Assuming that two successive hours has the same wind direction and velocity, one time-step would be then representative for both. Each selected time-step hence has a tripartite correspondence, to its hour and to both preceding and succeeding hours, only when considering having the same wind direction and velocity as illustrated in figure 5.2. If for example the record of wind in August 11 at 5 pm was 1.6 m/s NW as the same as in June 4 pm or July 6 pm, only one time-step will correspond to the three. Here the daily sun path is considered the same along those three summer months. However, if for example the record of wind at the same time-step, August 11 at 5 pm, was 1.6 m/s NW and the record in the same day but one hour before was 1.6 m/s NNE, both time-steps are considered.

31 May < Day < 1 Sep.																								
Hr.	0:00	1:00	2:00	3:00	4:00	5:00	6:00	7:00	8:00	9:00	10:00	11:00	12:00	13:00	14:00	15:00	16:00	17:00	18:00	19:00	20:00	21:00	22:00	23:00
Avg. Temp. (C°)	29.4	28.9	28.6	28.3	28.1	27.9	27.9	27.9	28.3	29.3	30.7	32.5	34.4	35.2	35.8	35.9	35.5	34.6	33.6	32.6	31.7	30.8	30.1	29.7
Time-step																								
	Hour-temperature dependent for each recurrent wind event																							

**Figure 5.2:** Simulation time-steps

A sum of 180 time-steps were hence selected, which covered all possible events of conditional combinations. As mentioned above, boundary conditions should be assigned in the CFD model to the side, of the external air environment, which represents the wind direction according to the building orientation inside the domain. Therefore, a design study for each direction was created (8 cases; N, NNE, NE, ENE, W, WNW, NW, NNW). 15 possible wind velocities; between 0.3 and 7.7 m/s, and temperature variations between 22 to 38 °C were assigned according to weather records.

As the air flow is momentum driven through large openings, it is necessary to simulate both indoor and outdoor domains to investigate the cross ventilation [66]. A CAD model of the building was created (fig. 5.4). The model included the surrounding urban settlement existing within a radius of 50 m around the building. The model was then rotated around 8 axes corresponding to possible wind directions inside the surrounding environment. Hence, 8 design-studies/files were then exported to the CFD tool as various simulation scenarios were then created to each. Table 5.2 lists possible simulation configurations for design-studies' scenarios. The simulation environment in a sample scenario of north wind is shown in figure 5.5. Several simulations however took place afterwards to compare various conditions of ventilations, in addition to a transient simulation for a selected day with constant wind direction to relate indoor temperature variation to air flow.

As previously described the grand hall (GH) has a large opening overlooking the courtyard, ca. 3.6 x 3.6 m, which is divided into screen panels of lavish lattice work, 50% shading (not all panels remained opened along the measurement period, the sum of opened area was accordingly calculated). With regards to the meshing size required to air volumes a mesh refinement that produces at least 4-5 elements through each gap/opening was applied. Figures 5.6 a-d show the refined mesh sizes.

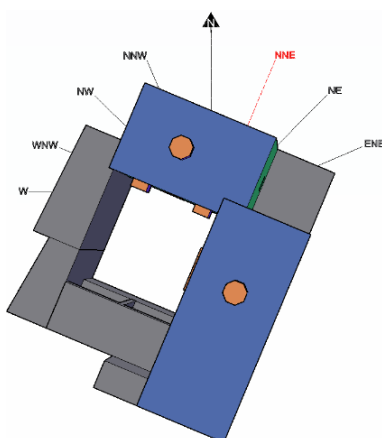


**Figure 5.3:** Building orientation and prevailing wind.

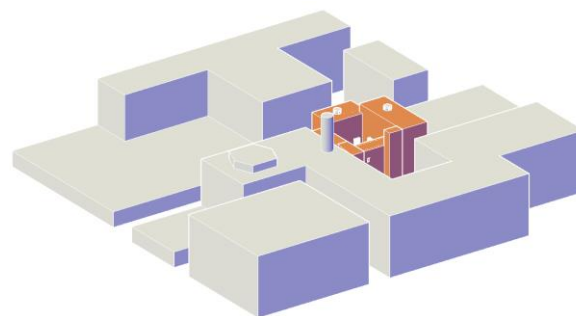


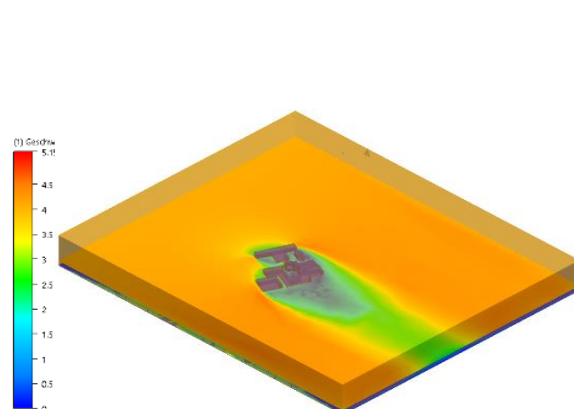
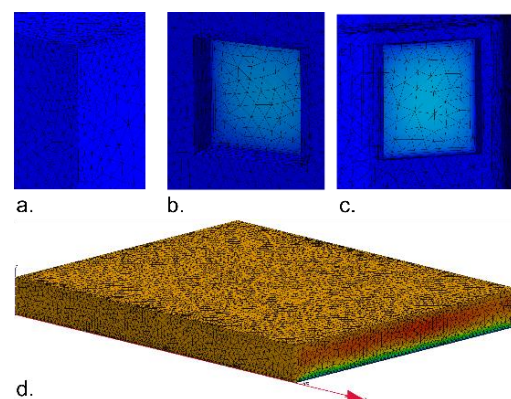
**Figure 5.4:** Created geometry for the simulation model and surrounding urban setting

According to the basic equation of calculating the air flow of a volume:  $Q = V \cdot A$ , where  $Q$  is the volumetric flow rate calculated in  $\text{m}^3/\text{s}$ ,  $V$  is the wind velocity  $\text{m/s}$ , and  $A$  is the area through which the air flow in one second. Given that depth and cross section of each of the tiny gaps/perforations of the screen is identical, the sum of flow rate through the entire screen would be the summation of flow rate at each section which is calculated as:  $\sum Q = \sum_i^n V_i \cdot A_i$

Accordingly the detailed large opening of the grand hall was extruded into one large window that measured  $2 \times 2 \text{ m}$ , considering the opened panels during the measurements. The same method is applied to all opened side windows of both halls and the secondary hall's courtyard windows which was compiled into a single window measured  $1.2 \times 1.2 \text{ m}$ . However the wind-escape device on the roof of each hall was modeled with the same dimensions as it has clear windows that were totally opened. Since the simulations applied for natural ventilation, all window openings were modeled as clear holes in the outer volume of each space with no material assignments or boundary conditions as the air flows in and out of the building according to wind and buoyancy. All spaces that were subject to analysis; GH, SH, and rooms on the ground floor level, were modeled with double volume as the building material (limestone) was assigned to the outer and the inner one was assigned as air volume. All other surrounding volume, surrounding buildings, were assigned as solids. A static gage pressure = 0 is assigned to the opposite side to which velocity is assigned. Radiation model was turned on in all scenarios according to the hour of the day.

**Table 5.2:** Design-study scenarios

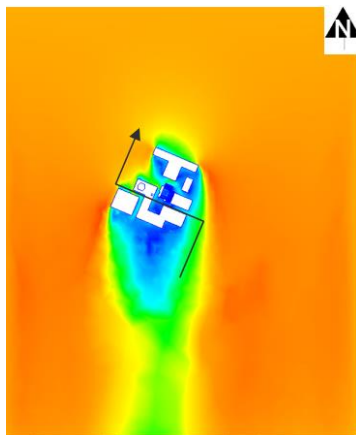
Time variation	Velocity	Temperature	Design-study	
24 hours	$0.3 \leq \text{m/s} \leq 7.7$ (15 probability)	$22 \leq 22^\circ\text{C} \leq 38$ (17 probability)	study/ Direction	Number of scenarios
			01-N	34
			02-NNE	21
			03-NE	17
			04-ENE	11
			13-W	10
			14-WNW	17
			15-NW	35
			16-NNW	35
Total number of simulation runs				180


**Figure 5.5:** Simulation environment, sample scenario for design-study for north wind (01-N)

**Figure 5.6 a-d:** Mesh sizing for air volumes, windows, wind-escape, and external environment respectively

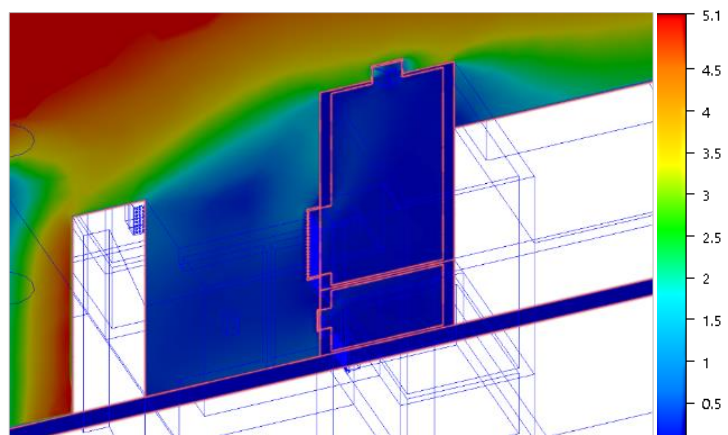
## 5.2.2 Air flow analysis

Some remarks should be initially stated about the wind behavior in the narrow street canyons around the building as well as inside the courtyard. Normally the wind speed is found to be reduced within the urban density of the subject area (fig. 5.7). However, a wind acceleration is then be created by air having to be squeezed through the narrow street canyons, but still comparatively corresponding to the initial velocity. However the wind speed dramatically reduced inside the courtyard, especially on lower levels (fig. 5.8). Despite the evident reduction of velocity inside the courtyard the air starts to move in cyclone manner as it falls on the courtyard facades (fig. 5.10) According to this cyclone movement of wind the air is allowed to penetrate the surrounding spaces through the openings or flow out of the courtyard in the wind direction. This behavior is almost observed in all scenarios with different wind directions and velocities.

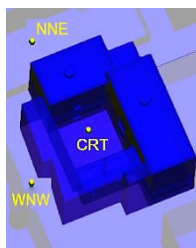
To clearly understand the courtyard's influence on air flow, three nodes were selected to compare the velocity magnitude of each. The first node is selected in the middle of the courtyard on a height of 7 m., approximately facing the middle of the openings of both halls. The second two nodes were selected outside of the building on NNE and WNW sides to represent the velocity magnitude in the street canyons around the building on the same level of 7m. Positioning of the nodes are shown in figure 5.9. In spite of the dramatic decrees of velocity inside the courtyard, two remarks were quite of interest. The first is a relative consistency of velocity rates inside the courtyard, which remained below 1 m/s regardless of the rates outside. However, velocity magnitudes at the other nodes were much corresponding and exceeded the initial rates in many scenarios (fig. 5.11). Second observation is the relatively magnified flow rates at the openings overlooking the courtyard due to the lower pressure at the openings.



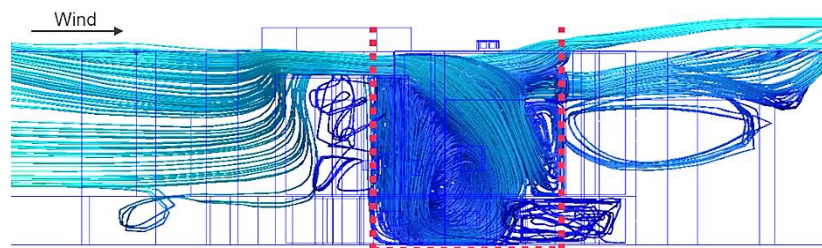
**Figure 5.7:** Transient simulation, northern wind (N)



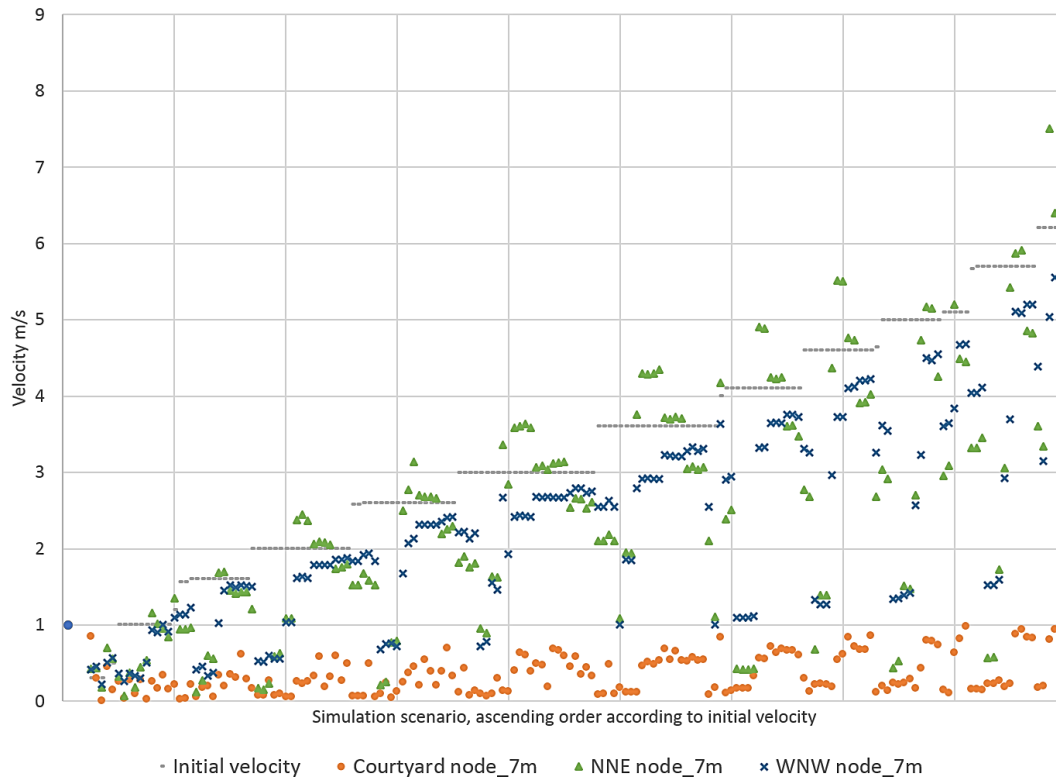
**Figure 5.8:** Wind velocity range around the building and inside the courtyard



**Figure 5.9:** Observed velocity nodes



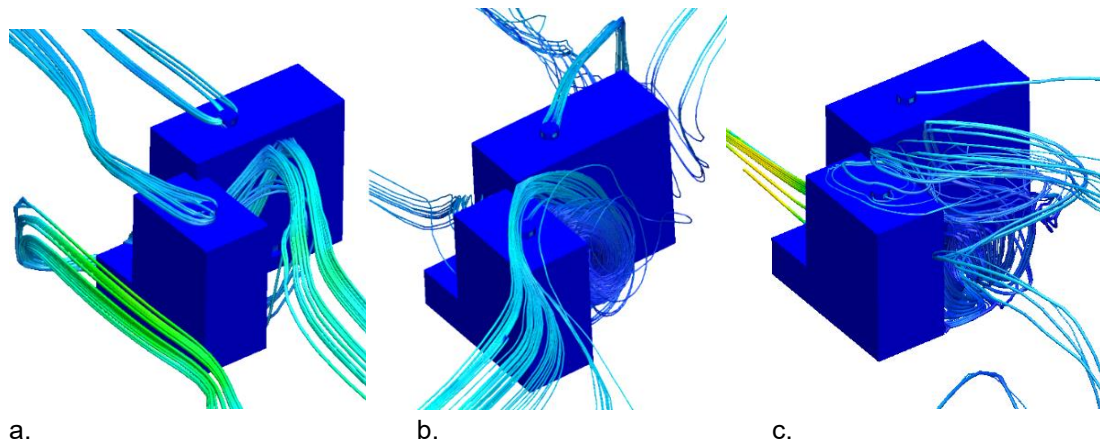
**Figure 5.10:** Cyclone behavior of wind inside the courtyard



**Figure 5.11:** Velocity magnitude at different nodes for all simulation scenarios

The observed velocity magnitudes' records demonstrate that the courtyard enclosure protects the building against higher undesirable wind speeds. Moreover, the cyclone air movement inside the courtyard results in the redirection of air flow which supposedly would not otherwise be facing any of the windows, with regards to the given wind direction. Through the observation of the air flow according to this cyclone movement the manner of which the air flows into both halls overlooking the courtyard is found to be varying in terms of air intakes and outlets. In other words, the distribution of inlets and outlets is not consistent (for wall openings) and in many cases has no conditional relationship with velocity, which is quite understood in the light of ununiformed air movement results inside the courtyard (figs. 5.12 a-c). Nevertheless, inlet and outlet distribution can be related to wind direction and some basic remarks could be stated. As for the grand hall (GH) it is found that the window overlooking the courtyard usually acts as air inlet regardless of the wind direction and velocity, except for the ENE wind, as the air comes entirely from the backside of the hall.

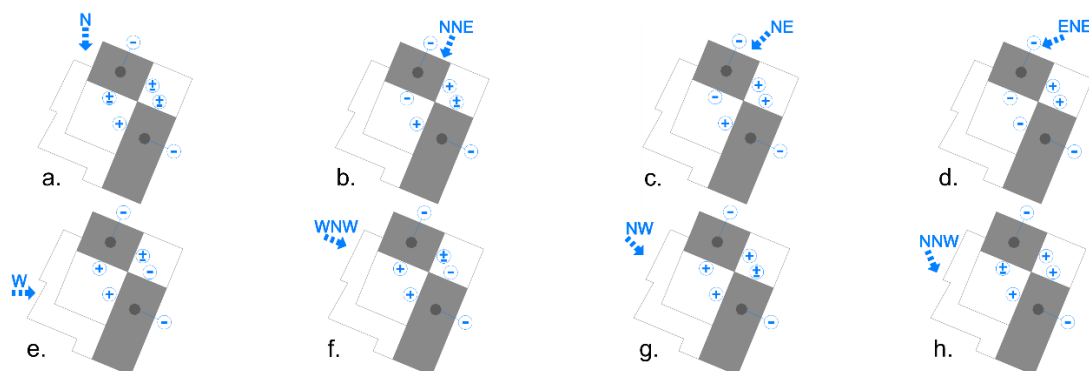
As a result of warmed air above the ground of the courtyard due to the absorbed solar radiation along the day, a free convection occurs and the hot air starts to rise to higher levels. An area of high pressure hence is created and as the air starts to recirculate inside the courtyard it moves from this high pressure region to the lower pressure at the openings and therefore has the chance to penetrate the interior space. This interpretation is supported by the fact that the side window of the hall does not act the same way when the wind is coming from its opposite side; W and WNW. The pressure outside this window is not be as high as in the previous case and the air hence flows out from the space through this side window. Figures 5.13 a-h show air inlets and outlets for each wind direction.



**Figure 5.12 a-c:** Openings variation of air inlet (+) and outlet (-), a. CRT (+), Side (+) from scenario (14WNW\_01Aug\_S02), b. CRT (+), Side (-) from scenario (01N\_01Aug\_S03), c. CRT (-), Side (+) from scenario (04ENE\_02Jun\_Aug\_S01), refer to appendix (A) for detailed results

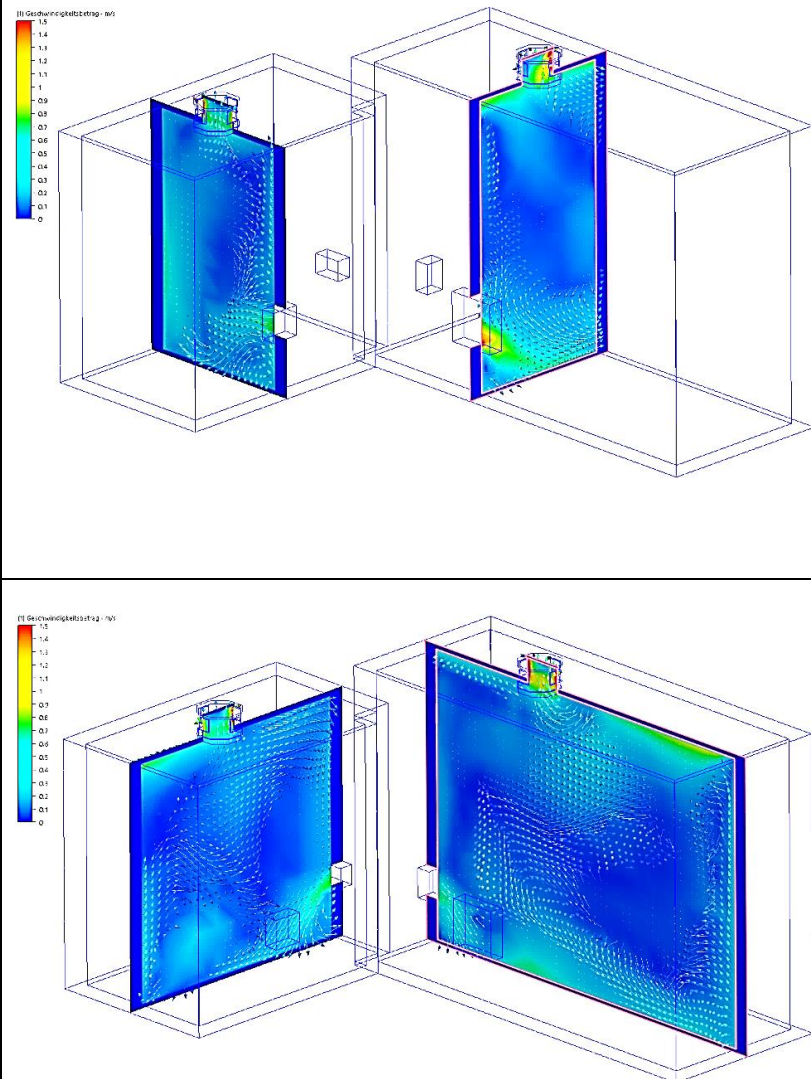
Similarly is the distribution of air inlets and outlets according to wind direction for the secondary hall (SH) with basic differences attributed to the room orientation. Since the wind comes almost from the backside of this hall (ENE to N) the courtyard openings act as outlets in these cases. The air intake occurs then with low amount of flow rates in response to N and NNW winds. However these openings act entirely as air inlets with W, WNW and NW winds. For these cases the velocity magnitudes and hence the flow rates at these openings are found to be relatively high. Contrarily acts the side window which directly faces the ENE wind and hence acts as a direct air inlet to the first wind quarter, opposite to the courtyard opening. The flow rates at the side windows in the course of ENE winds are found to be comparatively high, especially for the SH hall where the side window is directly facing the wind. Tables 5.3-5 show visualization of all possibilities for air intake and outlets and percentage of occurrence.

The consistent role of the wind-escape device at the roof of both halls as an air outlet, regardless of wind direction and velocity, is crucially significant. The free convection occurs inside of the space results in the movement of the low dense hot air to rise to the lower pressure region of the roof and therefore escapes from the roof device. The wind-escape plays a significant role in the equalization of air flow inside the space according to the equation,  $Q_{in} + Q_{out} = 0$ , where  $Q_{in}$  and  $Q_{out}$  are the inlet and outlet volumetric flow rates respectively. Detailed values of flow rates and air change rates for all scenarios are listed in appendix (A). The velocity magnitudes inside both rooms were almost maintained between 0.02 and 0.61 m/s with an average of 0.27 in GH (fig. 5.15).



**Figure 5.13 a-h:** Distribution of air inlets (+) and outlets (-) for each wind direction

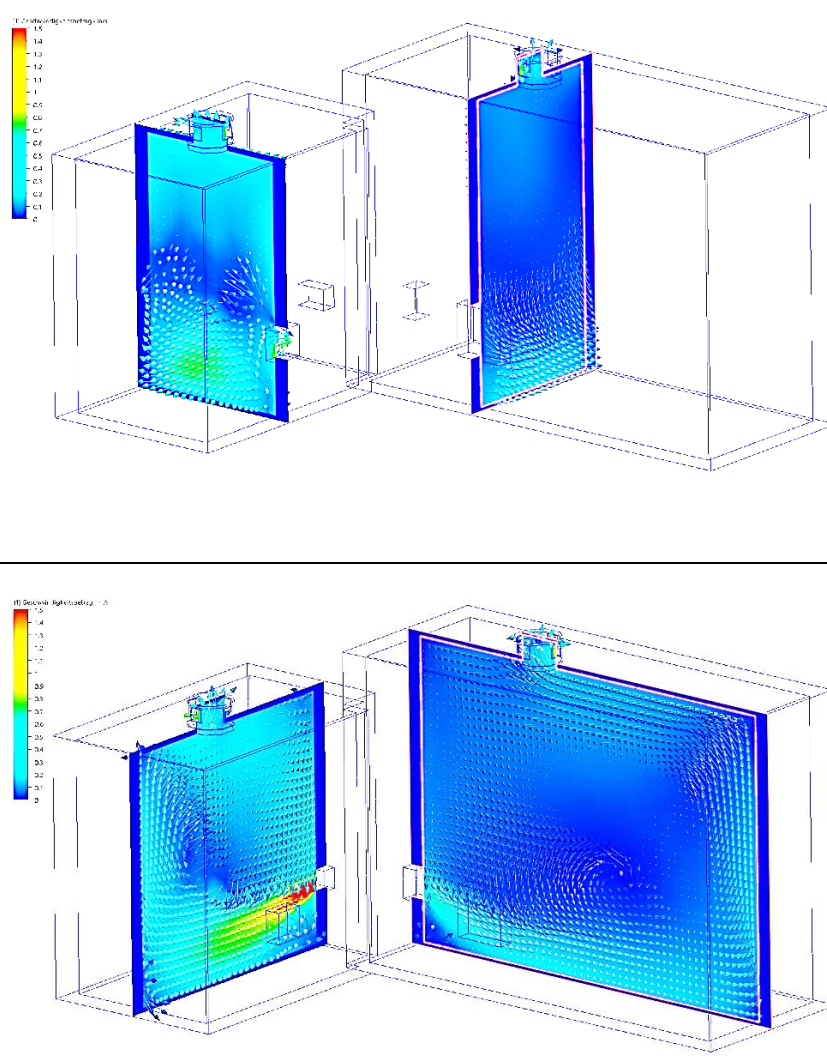
**Table 5.3:** Visualization of air intake and output and percentages of occurrence upon all simulation scenarios. All windows are air inlets while roof wind-escape devices are consistently acting as air outlet (visualization taken from scenario 14WNW\_01Aug\_S02, refer to appendix (A) for detailed air-flow readings).

Opening	Function	Occurrence % (aggregated)		Air flow visualization
		SH	GH	
CRT	Inlet (+)	71	95	
Roof	Outlet (-)	100	100	
Side	Inlet (+)	74	60	

**Table 5.4:** Visualization of air intake and output and percentages of occurrence upon all simulation scenarios. Courtyard windows are air inlets and side windows are air outlets. The roof wind-escape devices are consistently acting as air outlet (visualization taken from scenario 01N\_01Aug\_S03, refer to appendix (A) for detailed air-flow readings).

Opening	Function	Occurrence % (aggregated)		Air flow visualization
		SH	GH	
CRT	Inlet (+)	71	95	
Roof	Outlet (-)	100	100	
Side	Outlet (-)	26	40	

**Table 5.5:** Visualization of air intake and output and percentages of occurrence upon all simulation scenarios. Side windows are air inlets while courtyard windows are air outlets. The roof wind-escape devices are consistently acting as air outlet (visualization taken from scenario 04ENE\_01Aug\_S01, refer to appendix (A) for detailed air-flow readings.

Opening	Function	Occurrence % (aggregated)		Air flow visualization
		SH	GH	
CRT	Outlet (-)	29	5	
Roof	Outlet (-)	100	100	
Side	Inlet (+)	74	60	

### 5.2.3. Openings' directional flow-functionality (ODFF)

In terms of airflow distribution, the location of outlets plays a significant role [43]. In accordance with the above observations and the aggregated flow rates listed in appendix (A) a matrix of openings directional flow functionality (ODFF) is created (fig. 5.14). The matrix is a compilation of wind directions and percentage of occurrence of air flow in each opening according to its assumed inlet/outlet functionality. Positive and negative references stand for the opening as air inlet or outlet respectively. All windows are assumed to be air inlets, however the wind escape (roof) are expected to act as an outlet. The cells encircled with the dashed line indicate the cases in which the opening, according to its reference, was generally responsive to wind (directionally), whether in all or some scenarios for a distinct direction. However the grey scale indicates the percentage of this responsiveness in all scenarios of the same direction, which counted as well on other boundary conditions, i.e. velocity and radiation.

For example, the segment of SH-CRT, stands for the opening of the secondary hall on the courtyard. This opening acted mostly as an air inlet (+), supposedly functional, in response to only five wind directions, W, WNW, NW, NNW, and N. However it did not receive any air when the wind was coming from the other three directions, which is previously described. This means that this opening is 83 % responsive to wind direction (generally), considering the percentage of events for each direction. Nevertheless, the opening acted as an air inlet in 100% of the scenarios for directions W, WNW and NW and in only 83% and 82% of the scenarios for directions NNW and N respectively. The finite ODFF for this opening hence is 80%. Likewise, GH-CRT, large window opening of the grand hall, is 97% functional in terms of orientation as it receives air from all directions except ENE. Nevertheless, the aggregation of responsiveness occurrence was as high as 95 % since the opening was functional in the entire scenarios for 7 directions. As shown in the matrix the ODFF of the roof wind-escape for both halls is 100% as it acts as air outlet in all scenarios for all directions, which is previously discussed. The sum of ODFF for all openings, in terms of orientation and response to prevailing wind, is accumulated as 93 %.

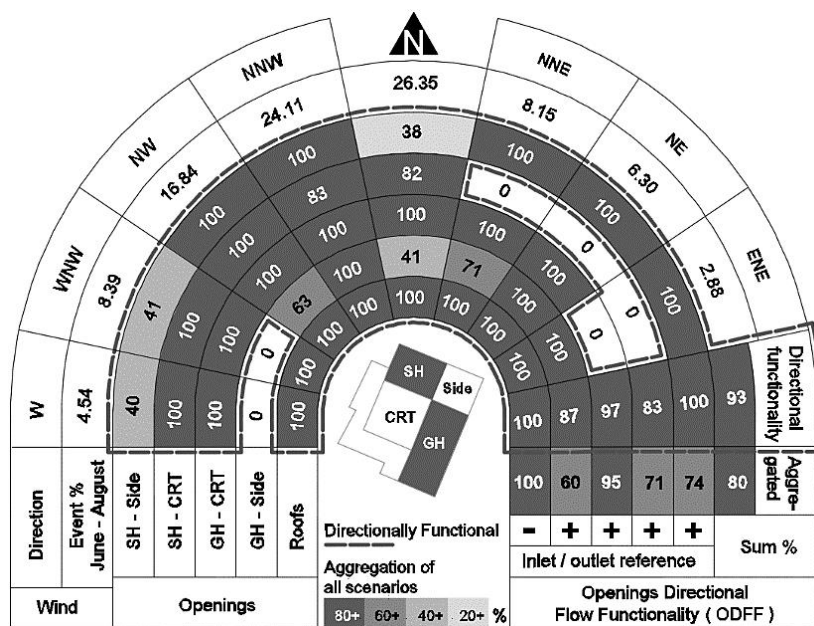
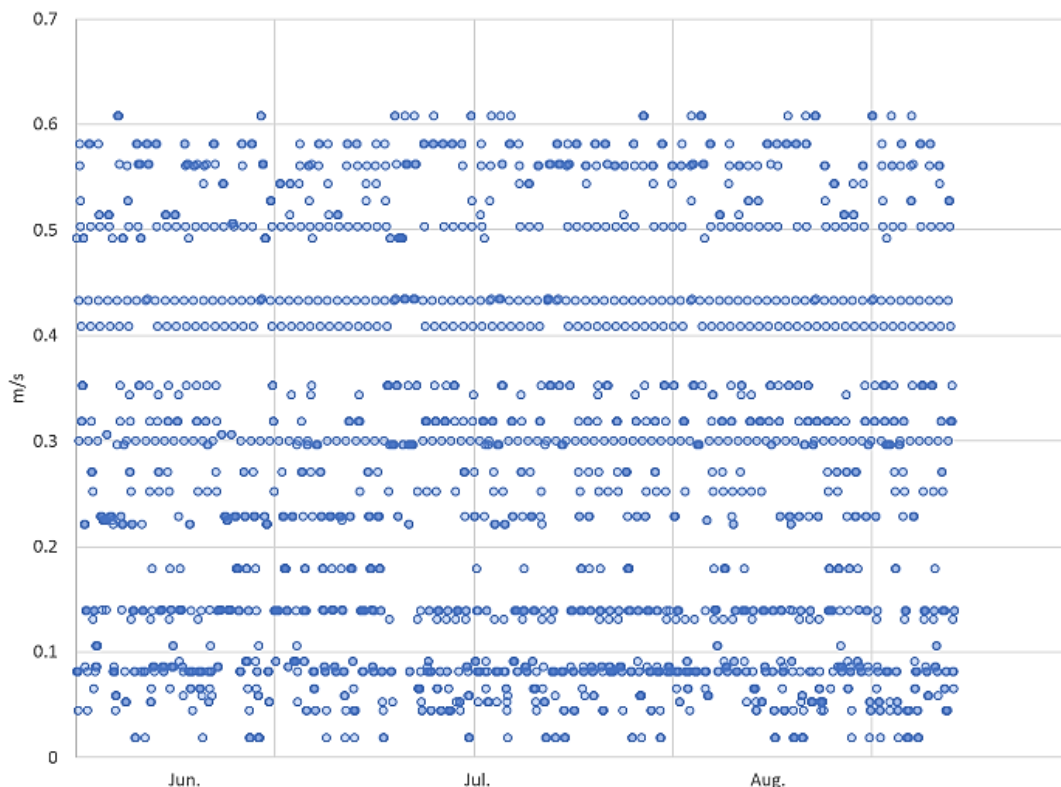


Figure 5.14: Matrix of opening directional flow functionality

From the matrix of direction functionality and tables 5.3-5 showing the visualization of different scenarios, some further remarks can be stated. Basically the building design, with regard to orientation and distribution of openings, evidently reveals high levels of awareness of local wind distribution and positively responds to the prevailing winds. As described above, the courtyard windows for instance act mainly as air inlets, especially in the grand hall, where the opening is north-west oriented. This orientation allows the courtyard window to air intake for all wind directions except the ENE wind. As shown through the air flow visualization in table 5.5 the amount of air output at this window in the ENE wind is too low,  $0.01 \text{ m}^3/\text{s}$  for this scenario and very close values were observed as well for all scenarios of that direction study (refer to appendix A). In those cases however the side window receives instead relatively higher amounts of air flow to equalize the difference. As for the cases in which the side windows do not intake air and act as air outlet, 40 % and 26 % of all scenarios for GH and SH respectively (table 5.4), it is found that the air flow rates at the courtyard windows however are relatively high. It can be then alleged that the opening design generally aims to maintain a consistency of air flow rates in the space, which correspond to the variability of boundary conditions.

The extent to which the openings' design and distribution are efficient can be hence determined by the sum of the output of the volumetric flow rate and therefore the air change rate (ACH) for each scenario. As previously mentioned  $\sum Q$  (sum of in and out volumetric flow rate) should be equal to 0. The air change rate per hour then can be calculated from the equation:  $ACH = 3600 Q / V$ , where  $ACH$  is air change rate per hour (1/h),  $Q$  is volumetric flow rate through the room ( $\text{m}^3/\text{s}$ ) and  $V$  is the volume of the room  $\text{m}^3$ . Accordingly values of ACH for all scenarios were obtained by applying this equation to the readings of the flow rates listed in the tables in appendix (A). The highest ACH expectedly occurred with the North-west winds and lowest rates however were with the north eastern winds (fig. 5.16). The average ACH upon all wind directions however was 4.5 /h, which is quite acceptable according to presumptions in the previous chapter.



**Figure 5.15:** Average Indoor velocity magnitude, GH, Jun.-Aug.

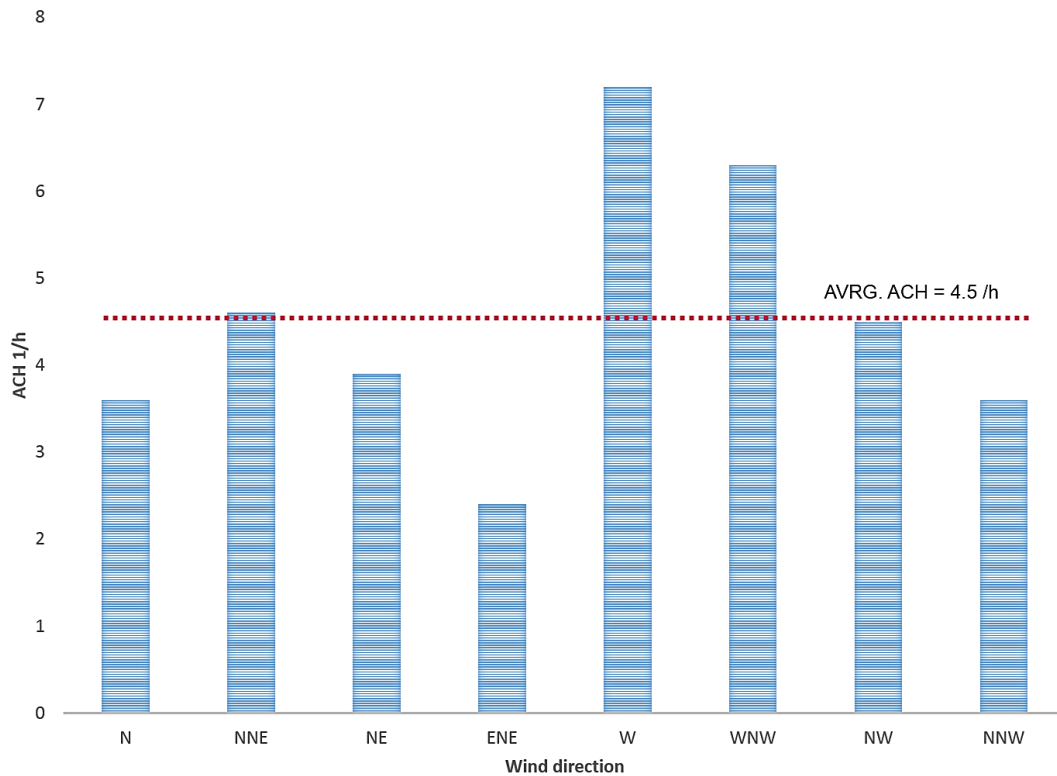


**Figure 5.16:** Average air change rate per direction and overall average for all simulation scenarios

#### 5.2.4. Cross ventilation breakdown assessment

In order to obtain an assessment of the role each opening plays in the natural ventilation process further simulation scenarios were applied. Modified geometries of the building, in terms of opening variations, were then simulated. The highest values of ACH were achieved in response to WNW winds, therefore the design-study corresponding to this direction was considered for such simulations. The simulations applied on 17 scenarios for WNW wind in which the wind velocity varied between 2 and 6.2 m/s along different hours of the day. Two different designs for opening variations were simulated to be subsequently compared against the base case. The first design excluded the side window, the ventilation process would be then taking place through the courtyard opening and roof wind-escape. The second design however excluded the roof wind-escape as ventilation would be occurring through courtyard and side openings.

Both halls GH and SH showed similar air flow behavior (figs. 5.17-8). As for the base case, the side windows varied in function, air inlet/outlet according to boundaries in different scenarios. In the design variation where the roof wind-escape devices were excluded, these windows were expectedly acting as air outlets in all scenarios, with no great differences of air flow rates when compared to the base case outlet's rates at the same openings. However the air flow rates at the courtyard windows are found to be significantly decreased, especially for the grand hall (GH), where the courtyard window is facing the wind. This could be attributed to the fact that in the base case, as previously explained, a low pressure area is created at the region of the wind-escape on the roof. As a result of the free convection occurs inside the room, the warm air is accelerated to rise up and equalize the pressure different. This interpretation is emphasized through the presence of the wind-escape in the second variation.

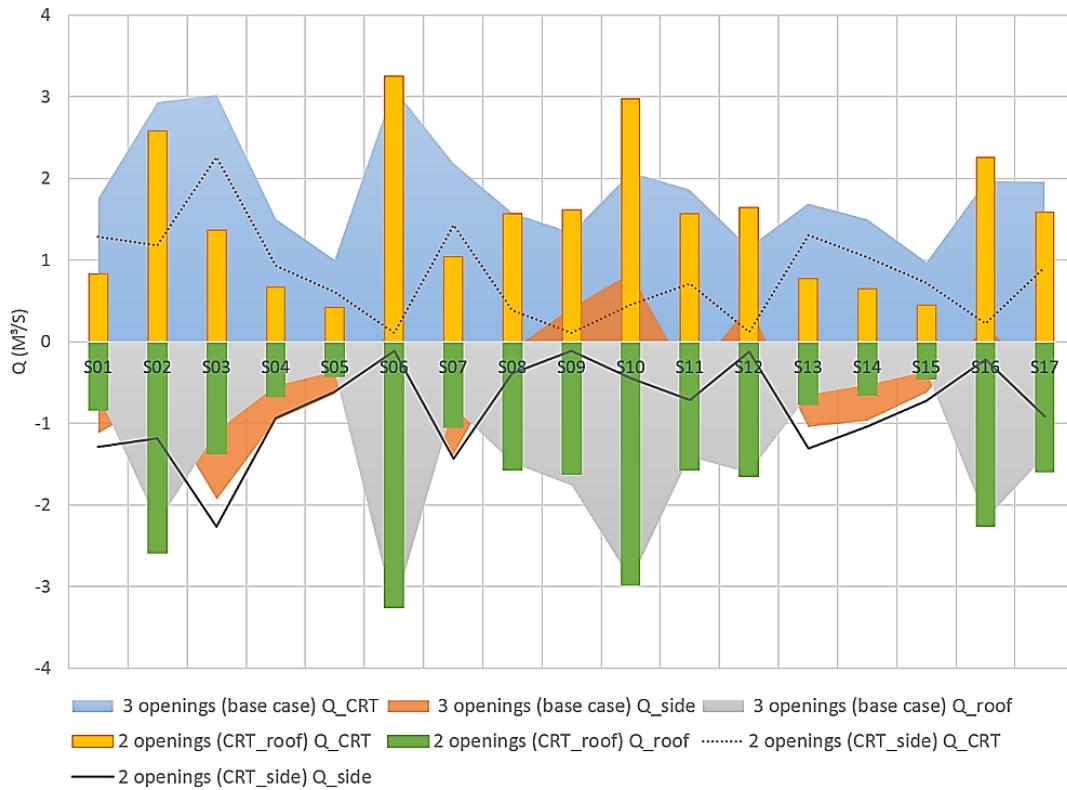


**Figure 5.17:** GH, air flow rate (Q) for different opening variations over 17 scenario for WNW wind

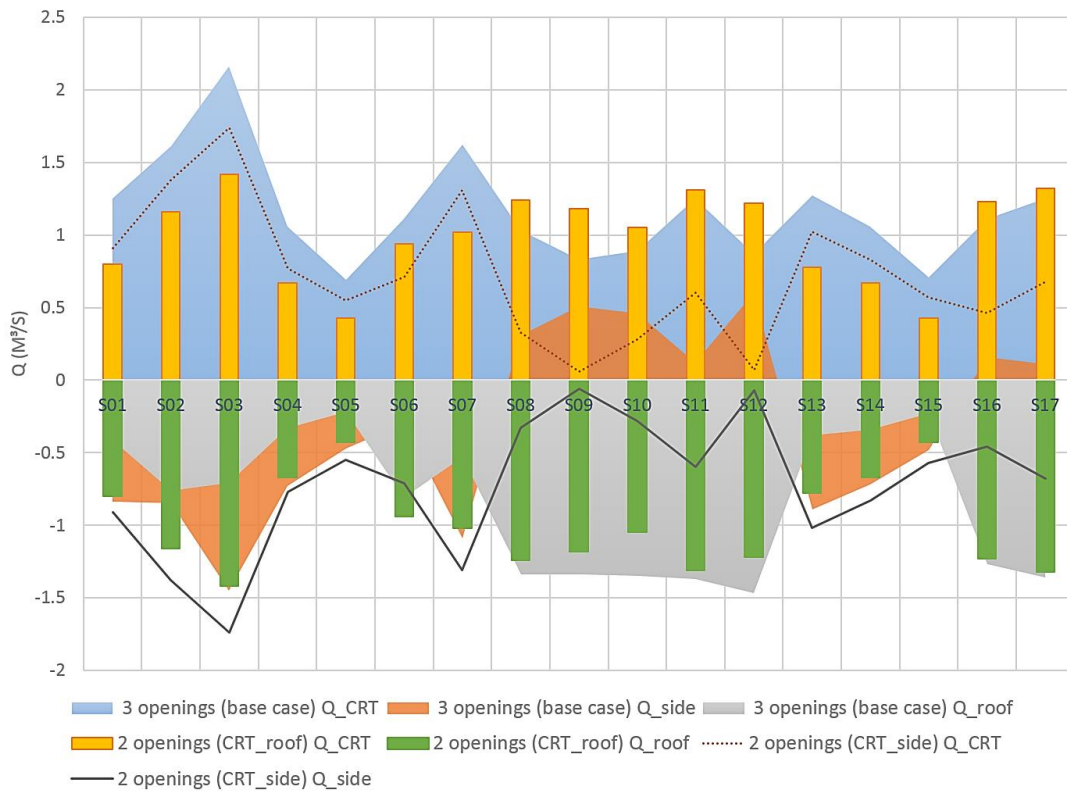


**Figure 5.18:** SH, air flow rate for different opening variations over 17 scenario for WNW wind

As for the second alternative where the side windows were absent and ventilation occurred through the courtyard and the roof openings, air flow rates were rather more responsive. The flow rates at the courtyard openings, in both halls, remained close to and even exceeded those in the base case. Moreover, the output flow rates at the wind escape significantly increased in scenarios where the intake rates were reduced at the courtyard openings. This behavior could be understood in light of the previous interpretation regarding rising of the warm air up to the roof. It should be however stated that the drop in air flow rates at the courtyard openings of SH were not as significant as in GH. However differences were more evident for the other openings, side and roof. The courtyard opening in SH is not facing the WNW wind as in the case of GH. The ventilation process then is more dependent on the air output to pull the air inside the space, and hence the flow rates increase at both the side and the roof openings.

In accordance with the observations above, it could be then concluded that the higher air change rates were accumulated within the base case scenarios (figs. 5.19-20), especially for SH. This reflects the significance of opening distribution over three sides including the roof, especially when the direct air inlet is not facing the wind, as in SH. The ACH in the case of SH drops from an average of 8.08 /h for the base case to 3.18 /h when having openings only on two sides, courtyard and roof. However it reaches the minimum limit of an average of 2.31 /h with the absence of the wind-escape and having the side opening instead. Nevertheless, as the ventilation process is more direct inlet-dependent, the drop of ACH between the three cases is found to be slightly more gradual; 6.35; 4.76; and 2.6 /h for the same order respectively. It could be concluded then that the distribution of opening significantly influences the air flow and thus the air change rates, especially when the wind is not facing the courtyard openings.

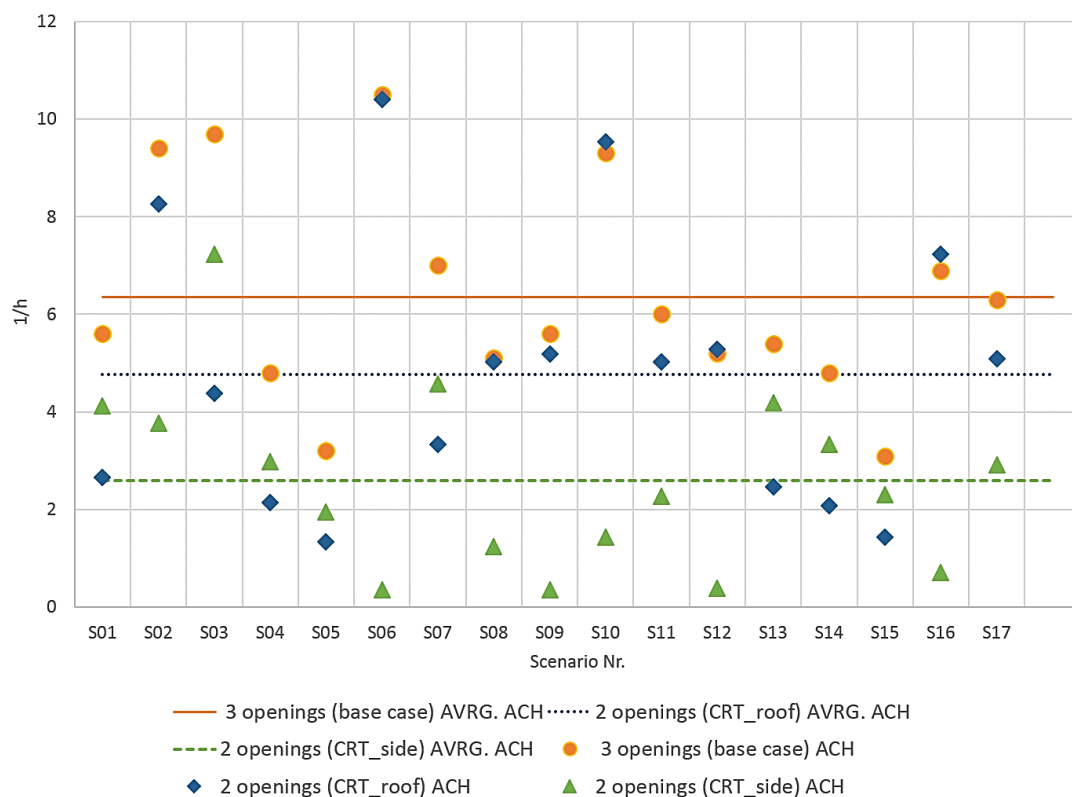


**Figure 5.19:** GH, air change rate (ACH) for different opening variations over 17 scenario for WNW wind. The wind escape increases the ACH 25% more than the 2 side case in which the ACH was increased with 45 % more than the single-side

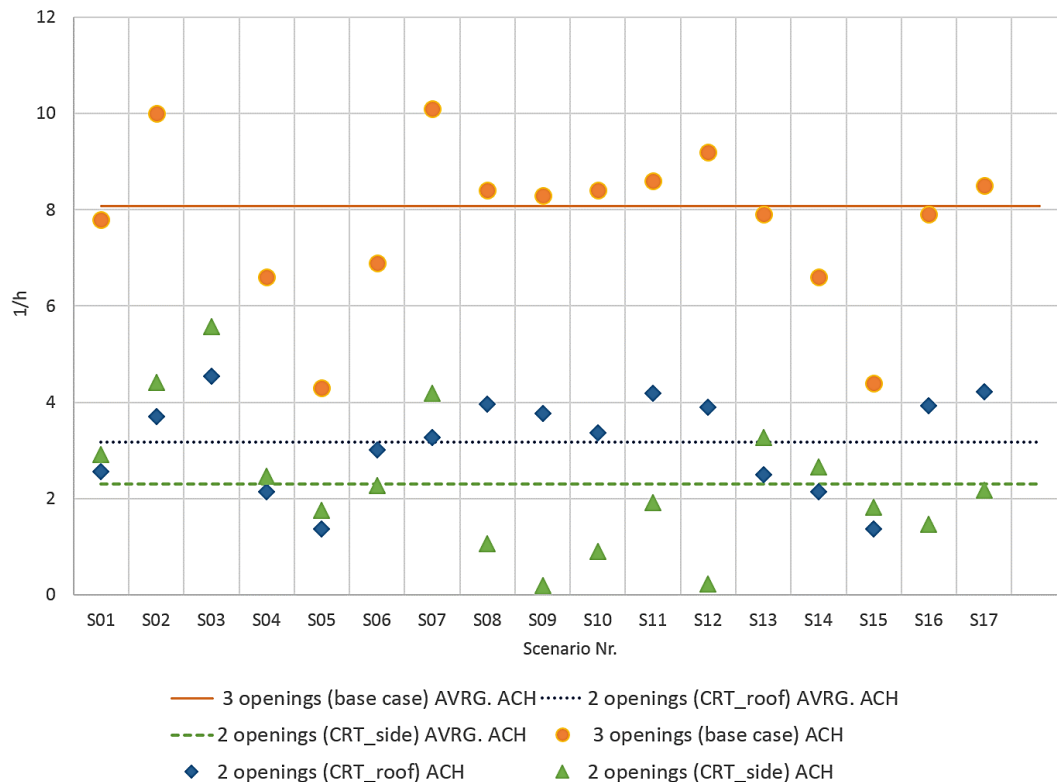


**Figure 5.20:** SH, air change rate (ACH) for different opening variations over 17 scenarios for WNW wind. The wind escape increases the ACH 60% more than the 2 side case in which the ACH was increased with 27 % more than the single-side

### 5.2.5. Air flow and indoor temperature

From the above discussion and observations the effectiveness of the natural ventilation mechanisms employed in this building are tangible in terms of air flow and exchange rates. However, the main purpose of the ventilation process is the removal of heat and replacement of the warm air with the fresh cool air, which directly influences the indoor temperature. The indoor temperature were simulated in TRNSYS and simulations are further reinitialized upon the real ACH values, predicted through the CFD modeling, within the next section. However to draw better understanding about the direct relationship between the air flow and temperature it can be more illustrative to visualize this relationship by the CFD modeling.

As previously explained the steady state simulations are not representative for indoor temperature. For instance, a steady state simulation doesn't count for the heat storage capacity of the walls' material along the day as it runs several iterations for a single time step in which all boundary conditions are constant. A transient simulation is likely needed to get more realistic results for diurnal indoor temperature differences. However, running a transient simulation that spans a wide range of hours would not be possible as explained through the configuration of the CFD model and time steps. Therefore, running a single diurnal cycle could fulfill the objective of this simulation. A single day, August 19, was thus selected, in which the wind could be fixed to the prevailing direction along the 24 hour.

According to the weather data the northern wind prevailed along 16 hours and NNE and NNW winds occurred for the rest of the day. The wind hence were blowing over a 45° degrees along the day, which could be therefore combined at the north direction for the 24 hours. Considering the thermal properties of the building material, i.e. heat capacity, a single diurnal cycle would not be representative of the real temperature. However, as previously referred to, this simulation run does not aim to obtain plausible quantifications for indoor temperature, which already achieved in TRNSYS simulations. To count on the potential shading capacity of the actual building design, detailed window screens were added to the model geometry. Polynomial boundary conditions were assigned for 86400 seconds and the CFD solver then ran over 62396 iterations for a 4 seconds-size 20700 time steps.

Interestingly the results show a couple of observations. The first is the high correlation between indoor temperature gradient and the airflow pattern in both halls GH and SH (figs. 5.21-2). This correlation is a direct representation of the free convection and the rise of hot air which finds its path out through the roof wind-escape. The second observation is the influence of variable ventilation options as illustrated in figures 5.23 a-b for GH and SH respectively. The figures show indoor temperature gradient for different situations. First is the three side openings of the halls in the first floor, in which the temperature gradually increases along the way up to the roof from where the warm air escapes. The second situation is the double side cross ventilation in the room right below the GH on the ground floor. The indoor temperature in this room is found to be comparatively higher than in the middle of the hall, 2 °C in average. Nevertheless, this case has expectedly demonstrated better performance than the last one which has a single window overlooking the courtyard for different orientations (a-b). This comparison does not represent actual temperature profile, however it can visually demonstrate the influence of different ventilation options which was previously quantified in terms of air flow and air change rates.

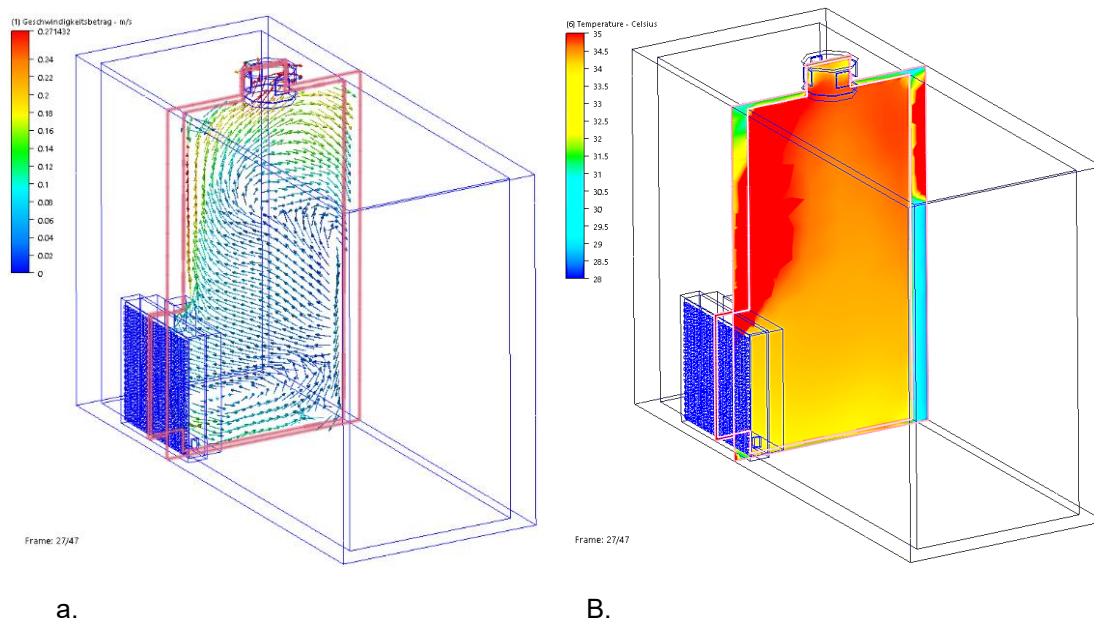


**Figure 5.21 a-b:** GH, correlation between air flow pattern (a) and temperature gradient (b)

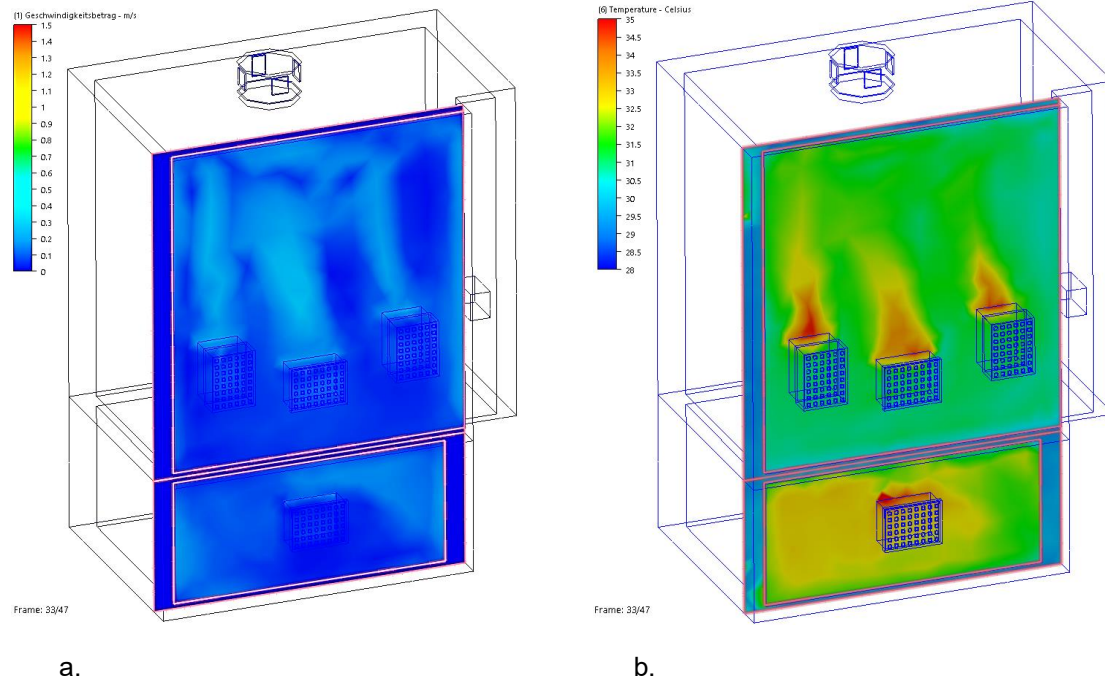


Figure 5.22 a-b: SH, correlation between air flow pattern (a) and temperature gradient (b)

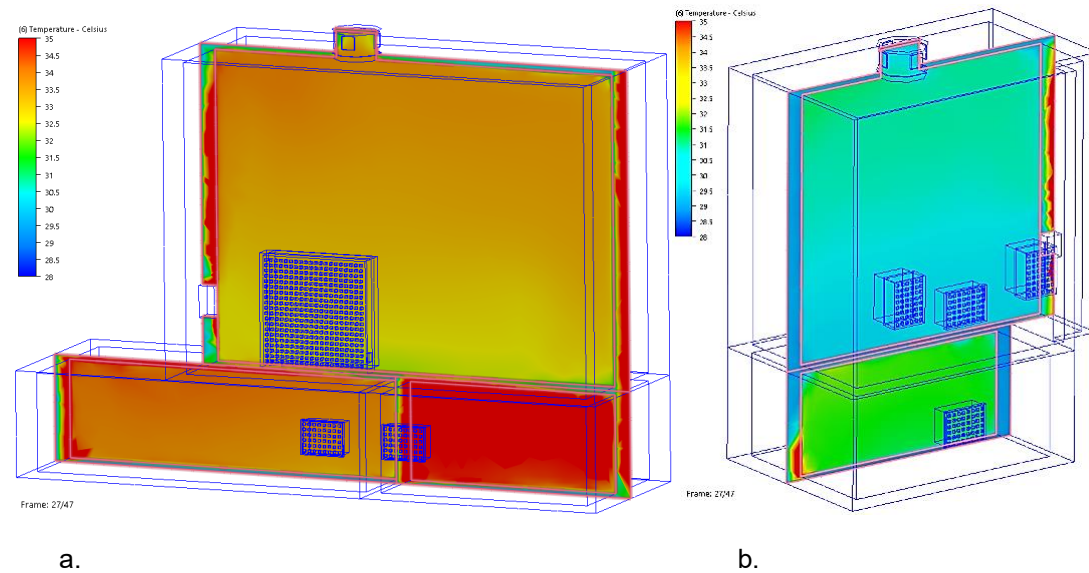


Figure 5.23 a-b: Indoor temperature gradient, different ventilation options for GH (a) and SH (b)

### 5.3. Pattern recognition design and assessment for ACH modeling

This section describes the modeling of ACH (output variable) as a mathematical function/model of ambient conditions (input variables). The model is built inductively using the pattern recognition approach, not deductively using the fluid dynamic equations. For naturally ventilated buildings, the former approach is very feasible while the latter is almost impossible for the following reasons. A deductive model is built from the laws of physics, fluid mechanics, and thermodynamics; then derived equations are either solved in closed form or numerically. This approach is extremely difficult, if not impossible. Complicated equations and different structure and boundary conditions of each building makes it infeasible to derive a mathematical model; this is why simulators, e.g., CFD, are designed. On the other hand, an inductive (inferential) mathematical model is feasibly built if we have a "sufficient" dataset (input-output values). From this dataset the input-output relationship is modeled and its error is estimated. The dataset consists of the ambient conditions at several time steps along with their ACH values calculated from CFD simulations. In this section, the pattern recognition mathematical framework is set up (Section 5.3.1); this framework is followed in model design and assessment procedure (Section 5.3.2).

**Algorithm 5.1:** Model design and assessment to select among possible  $L$  models by estimating their KCV error and choosing the model achieving a minimum estimated error.

```

for 1 = 1 : L
    Divide the n-observation dataset to K partitions, each has n /K observations;

    for k = 1 : K
        Train the model f on all data except partition k;
        Test on partition k;
        Save the n/K predictions;
    end

    Collect the K * n/K predictions;

    Err [1] = RMSE between predicted & true responses;
end

Find the minimum value in the Err & its model;
    
```

#### 5.3.1 Pattern recognition framework

The input  $X$  is called the features, or the predictors; and the output  $Y$  is called the response. It is assumed that the dataset

$$\mathbf{tr} = \{(x_i, y_i) \mid i = 1, 2, \dots, n\}, \quad (5.1)$$

is available, which consists of  $n$  observations and is generated by this input-output dependency. The observation  $(x_i, y_i)$  is the  $i^{th}$  observation consisting of the value  $x_i$  of the input  $X$  and the corresponding value  $y_i$  of the output  $Y$ . Each  $x_i$  is a  $p$  dimensional vector consisting of  $p$  features (predictors). For this research,  $x_i$  is the ambient conditions at the  $i^{th}$  time step comprised of hour, wind speed, direction, and temperature, and obtained by direct experimental measurements; where  $y_i$  is the ACH value (simulated by CFD) at the same time step.

It is required then to “learn” the unknown input-output dependency between  $X$  and  $Y$  that resulted in the dataset  $\mathbf{tr}$ . The dataset  $\mathbf{tr}$  is called the training dataset because it is used to design (or “train”) a function  $f_{tr}$  (also called a model) for the sake of “learning” the input-output dependency between  $X$  and  $Y$ . For any unseen observation, i.e., an observation  $(x_i, y_i) \notin \mathbf{tr}$ , it is required that the prediction  $f_{tr}(x_i)$ , for short denoted by  $\hat{y}_i$ , be as close as possible to the true response  $y_i$ . The error is usually measured in square loss  $L(y_i, \hat{y}_i) = (y_i - \hat{y}_i)^2$ .

Theoretically speaking, infinite number of functions (models) can be trained and designed on the same dataset. Moreover, for a certain class of functions, e.g., Classification and Regression Trees (CART) introduced by Breiman [15], usually there is a tuning parameter  $\lambda$  to be appropriately selected for minimum error. Assessing models, estimating errors, and selecting the best model and parameter from a limited size dataset  $\mathbf{tr}$  are not straightforward. For instance, if the trained function  $f_{tr}$  is tested on the same observations of the training set  $\mathbf{tr}$  the estimated error will be optimistic, since all observations participated in designing the function. In this study, the typical  $K$ -fold cross-validation (KCV) procedure is adopted for both model assessment and selection. In this procedure the training dataset  $\mathbf{tr}$  is partitioned into equally sized  $K$  partitions with  $n/K$  observations per each. The function  $f$  is trained on  $K-1$  partitions; then tested on the remaining observations of the  $K^{th}$  partition. This testing produces  $n/K$  estimated ACH values. The procedure is repeated  $K$  times to account for all the  $K$  partitions and the  $n$  observations. The final Root Mean Square Error (RMSE) estimated from this design and assessment procedure for a particular model  $f_{tr}$  with a particular tuning parameter  $\lambda$  can be elegantly expressed in the following compact mathematical notation

$$\widehat{err}(f_{tr}, \lambda) = \sqrt{\frac{1}{n} \sum_{i=0}^n (y_i - \hat{y}_i)^2}, \quad (5.2)$$

$$\hat{y}_i = f^{-k(i)}(x_i, \lambda), \quad (5.3)$$

where  $f_{tr}^{-k(i)}(x_i, \lambda)$  denotes the prediction of the true response  $y_i$  from the predictors  $x_i$  using the function  $f$  that is trained on all the training dataset  $\mathbf{tr}$  except the partition  $K(i)$  to which the  $i^{th}$  observation belongs. For the family of functions  $f_{tr}(\lambda)$ , e.g., CART with depth  $\lambda$ , the previous KCV procedure is repeated for each value of  $\lambda$ , and the model with minimum error is selected as a final design. The whole design and assessment procedure is summarized in algorithm 5.1. The number of partitions  $K$  is arbitrary and usually a value of 10 is chosen by practitioners. However, a common choice as well is choosing  $K=n$ ; i.e., the number of partitions equals exactly the number of observations. In that case the CV procedure is called leave-one-out CV. In this case, the function is trained on all observations except one left out, on which the function is tested. The procedure is repeated  $n$  times to finally obtain  $n$  tested values.

### 5.3.2 Classification and regression trees (CART) for ACH modeling

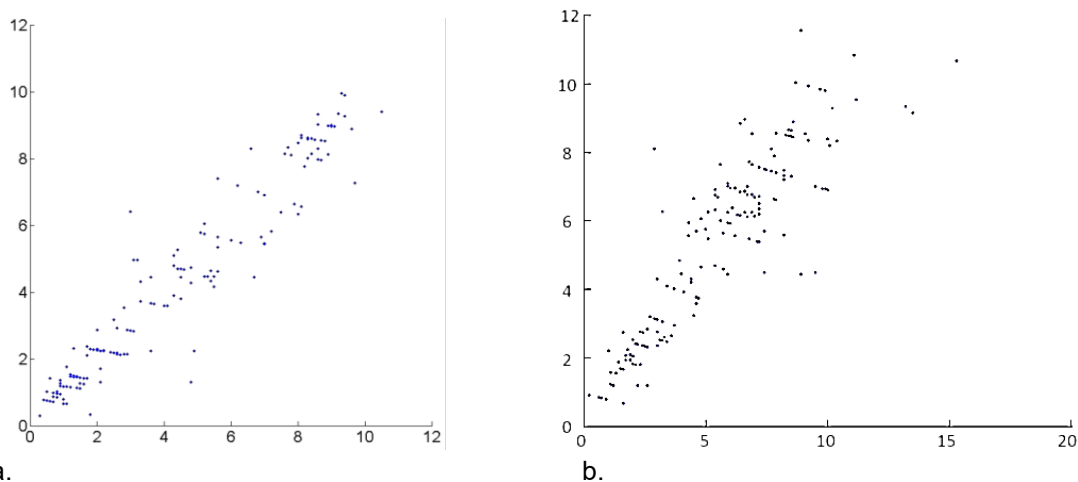
For the purpose of the present study, several models are designed, including neural networks with several number of neurons, linear models, and CART with several depth levels. This section explains the best model discovered by the algorithm 5.1 that gives the minimum error. As previously explained, only 180 observations (time step measurements) were recorded for the ambient conditions; at each time step  $i$  the ambient conditions are denoted by the vector  $x_i$  from which the ACH value  $y_i$  was simulated by CFD. This comprises the training dataset (1), where  $n=180$ . The ambient variables used in designing CART are only three: hour of the day, wind velocity, and wind direction (denoted by  $H$ ,  $V$ , and  $D$  respectively). Since the hour and wind direction are cyclic in nature, it is intuitive to use the sinusoidal transformation as a resolution for adjacent directions with distinct values, e.g.,  $1^\circ$  and  $379^\circ$ . Hence the final variables used to train the CART are four:

$$(x_1, x_2, x_3, x_4) = (\sin(2\pi/24 H), \cos(2\pi/24 H), V, \sin(2\pi/360 D)) \quad (5.4)$$

The other transformation  $\cos(2\pi/360 D)$ , that is parallel to  $\cos(2\pi/24 H)$ , is not needed. This is because all the measured directions already lay in the 3<sup>rd</sup> and 4<sup>th</sup> quadrants.

CART has a tuning parameter  $\lambda$ , which is the depth of the tree. The deeper the tree the lower its error on the training dataset  $\mathbf{tr}$ , but not necessarily on the unseen dataset. For dataset of GH, the optimal value of  $\lambda$  found using the leave-one-out CV procedure of algorithm 5.1 was 9 levels, and produced RMSE of 0.78. For sensing this quantitative error visually, figures 5.24 a-b are plots for the 180 predicted values of ACH produced by CART vs. their actual values simulated by CFD for GH and SH respectively. It is remarkable that the ambient temperature  $T$  is not predictive; i.e., when fed to the tree as an additional variable besides  $H$ ,  $V$ , and  $D$  it did not decrease the RMSE lower than 0.78. This complies with what is expected from the laws of physics and fluid dynamics.

The CART made for each hall, GH and SH, are displayed in appendix (B). Each CART consists of several nodes, symbolized as triangles. Starting at the top node, a binary decision is made to descend right or left based on the features  $x_1$ – $x_4$  of a particular observation  $x_i$ . The decisions continue until reaching a leaf, at the end of the tree, holding the prediction value  $y_i$ . The CART is expressed as explicit decision rules. These rules are fed to TRNSYS in FORTRAN language (Appendix C). For the dataset of SH, the winning model was CART with 7 levels, with exactly the same feature transformation explained above but with RMSE of 1.48.



**5.24 a-b:** ACH values predicted by CART vs. simulated by CFD for GH (a) and SH (b). Each prediction is obtained after training the CART on all the observations except the one to be tested (predicted) through the leave-one-out cross validation.

#### 5.4. Validation of the simulation model upon predicted ACH

The prediction rule obtained through the CART then is given to the TRNSYS environment as an equation where variables defined as algebraic functions to produce an hourly output for the ACH rates, upon which the simulations can be reinitialized. This step was intended to achieve two goals. The first is to consolidate the validation of the simulation model according to realistic variability of ACH. The second goal is accordingly to predict the indoor temperature along the summer and the probable levels of thermal comfort which would definitely be influenced by indoor relative velocity, which will be also variable.

The variables time (H) and direction (D) were introduced as cycles of 24 and 360 respectively in the prediction rule. Accordingly, as referred to in appendix (B), the nomenclatures x1, x2, x3, and x4 stand for: sin (15H), cos (15H), V, and sin (D) respectively. As for the case GH the tree of regression included 39 prediction rules (possible values of ACH). However 50 rules were concluded for SH. Both prediction rules were transferred into equations statements according to the mathematical functions available in TRNSYS (equations in TRNSYS are formulated using the same rules used in FORTRAN). Equation statements for both GH and SH are listed in appendix (C). Air change rate was then redefined as from the equation output and simulation reinitialized for indoor temperature for both halls. Figures 5.25-6 show simulation results for indoor temperature against measured data for two weeks within the measurement period spans from 13 to 26 August. The absolute deviance error (ADE) between simulation results and measured data is found to be  $\pm 0.38$  °C and  $\pm 0.39$  °C for GH and SH respectively (figs. 5.27-8).

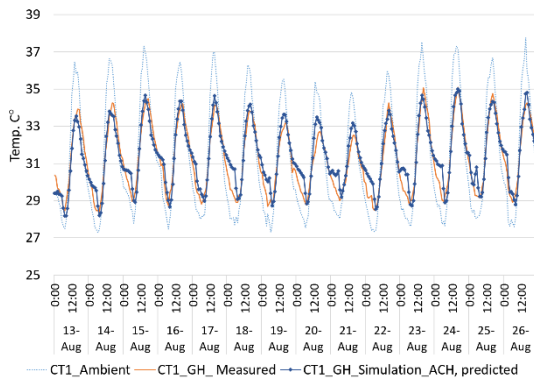


**Figure 5.25:** CT1-GH, simulation results for indoor temperature against measured data upon predicted ACH

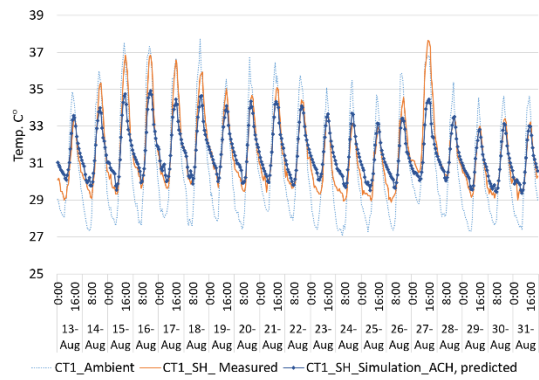


**Figure 5.26:** CT1-SH, simulation results for indoor temperature against measured data upon predicted ACH

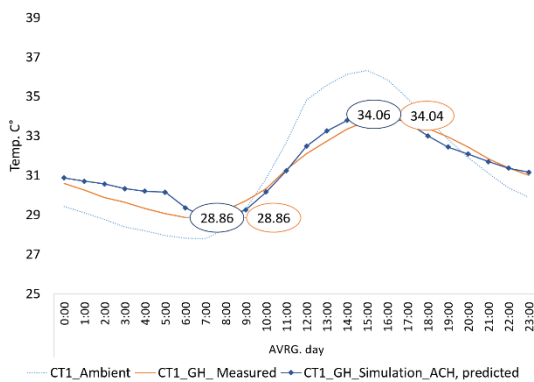


**Figure 5.27:** CT1-GH, simulation results for indoor temperature against measured data upon predicted ACH, average day. ADE  $\pm 0.38$  °C

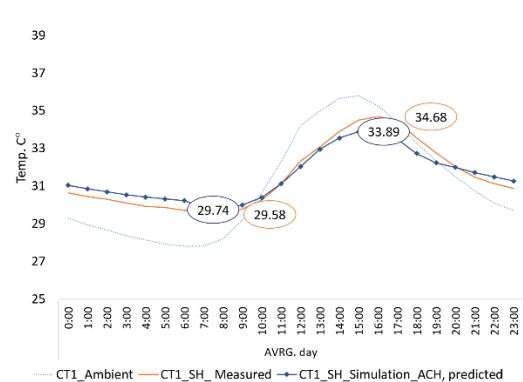


**Figure 5.28:** CT1-SH, simulation results for indoor temperature against measured data upon predicted ACH, average day. ADE  $\pm 0.39$  °C

## 5.5 Conclusion

1. Velocity inside the courtyard remains relatively stable, below 1 m/s. However, solar radiation warm up the ground surface of the courtyard and hot air rises to higher levels through a free convection and being replaced by cooler air from the outside. An area of high pressure is created and the air starts to recirculate and travel to the lower pressure region at the openings, where air flow would be magnified.
2. The courtyard enclosure protects the building against high undesirable wind speeds.
3. The north-west opening overlooking the courtyard usually acts as air inlet regardless of the wind direction and velocity, except for the ENE wind; blowing from behind.
4. As ENE and NNE winds come from the backside of the south-west hall, the courtyard openings act as outlets except with low amount of flow rates in response to N and NNW winds. However these openings act entirely as air inlets with W, WNW and NW winds.
5. The wind-escape acts consistently as an air outlet. The indoor free convection results in the movement of the low dense hot air to rise to the lower pressure region of the roof and therefore escape from the roof device.
6. A matrix compiled the wind directions and percentage of occurrence of air flow at each opening according to its assumed inlet/outlet functionality. The openings' directional flow functionality (ODFF) varied between 83 and 100 %.
7. The orientation and distribution of openings reveal awareness of local wind distribution.
8. The average ACH upon all wind directions is 4.5 /h, quite acceptable according to presumptions in the previous chapter.
9. Best performance in terms of both air flow and indoor temperature is found in the base case, three openings. The wind escape in GH is found to increase the ACH 25% more than the 2 side case in which the ACH was increased with 45 % more than the single-side. In SH however, the differences were 60% and 27 % respectively.
10. A high correlation between indoor temperature gradient and the airflow pattern is found; a direct representation of the free convection and the rise of hot air which finds its path out through the roof wind-escape.
11. Upon statistical learning from 180 pairs of ACH values, for both halls, regression trees (CART) are created, which included 39 and 50 prediction rules (possible values of ACH) for GH and SH respectively. Prediction rules were transferred into equations' statements that redefined the ACH for the simulation model in TRNSYS. ADE between simulation results and measured data is found to be  $\pm 0.38$  °C and  $\pm 0.39$  °C for GH and SH respectively.

## Chapter 6

# Temperature, comfort and energy; conclusive analysis

### 6.1 Introduction

This chapter aims to obtain a conclusive assessment for the potential capabilities of the adopted case study (CT1) to achieve indoor thermal comfort and its possible contribution in terms of energy efficiency. As for further demonstration of the potentiality of this case, a comparative analysis for different alternatives took place. The analysis aims to identify the extent to which can each of the examined features of the building contribute to lowering the indoor temperature, achieving thermal comfort and hence reducing the energy demand for cooling and heating. An assessment obtained through applying a comparative analysis of different options for the same building. The comparison aimed to draw better understanding on the relationship between comfort and energy consumption within the passive method.

Thermal comfort requires stability of the indoor environment and small temperature swings under free running conditions, which can be achieved through adequate heat storage capacity and proper relationship between the solar gains and thermal distribution [21]. As principle factors in the model adopted in this study, the impact of wall material and the window screens on indoor temperature, thermal comfort, and energy demand were demonstrated. The base case CT1 was compared to a couple of modified versions of the simulation model. Each modified model lacks one of the features. In the first model the lime stone wall material was substituted with hollow red brick (with thermal properties as the same as of the modern case CM, previously examined). The second model however represents the same characteristics as the base case but with absence of the window screens. The adaptive thermal comfort standard EN 15251 was adopted for this comparison. Unlike the modified models, the base case achieved accepted operative temperatures along the summer. Both evaluated features had tangible impacts on the indoor temperatures during winter season as well, especially when considering the difference in heat storage capacity between the stones and the hollow bricks which plays a role during the relatively cold winter. Considering the winter sun solstice, the absence of the window screen contributes to a slight increase of indoor temperature and hence decrease of the energy demand required for heating during winter time.

## 6.2 Ventilation Schedule

In order to set the ventilation schedule during summer to correspond to the ambient temperature a conditional function is added to the ACH equation statement. The ACH prediction rule was assigned according to this condition:  $ge(T, 20) * lt(T, 26)$ , where  $ge$  and  $lt$  stand for greater than or equal, and less than respectively, and  $T$  is the ambient temperature. This means that windows will be opened only when ambient temperature ranges between 20 and 26 °C. Figure 6.1 shows the simulation results for indoor temperatures for both halls GH and SH during summer, June-August, upon predicted ACH and ambient temperature-dependent natural ventilation. The maximum indoor temperatures were remarkably reduced, in average of 5.45 °C and 4.19 °C below ambient for GH and SH respectively. The highest maximum values for GH and SH are found to be 31.12 °C and 32.68 during August. This might be quite high considering the required levels of comfort in mechanically cooled buildings. However, as for a naturally ventilated building the indoor operative temperatures in both halls were quite accepted as will be explained within the thermal comfort evaluation in section 6.4. Moreover, these values remain quite acceptable in as much as being 11.88 °C and 10.32 °C below ambient temperature which reaches 43 °C. The wide difference here is attributed to the capacitance of the wall material thermal mass as explained within the regression analysis in chapter 4, and for the reduced amount of absorbed solar radiation through the window screens. The average minimum however was 1.37 °C and 2.01 °C above ambient for GH and SH respectively (fig. 6.2). The average maximum values for GH and SH were 28.79 °C and 30.05 °C.

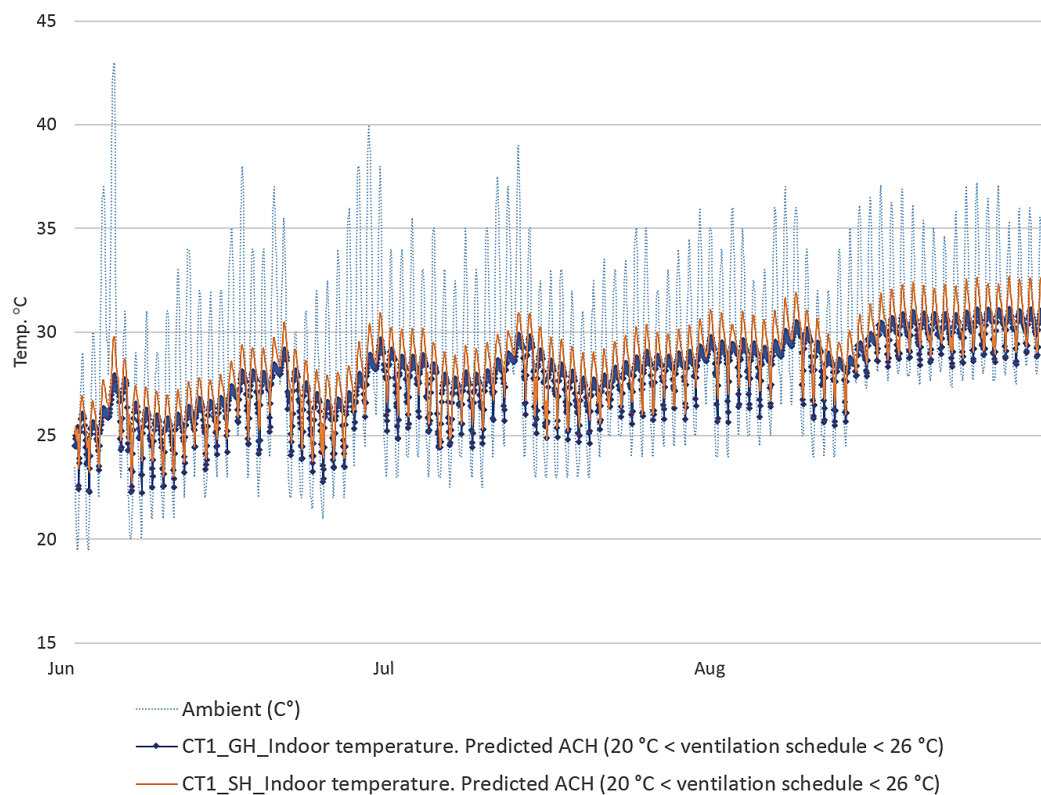


**Figure 6.1:** GH-SH, Simulation results for indoor temperatures upon predicted ACH and ambient temperature-dependent natural ventilation, Jun-Aug.

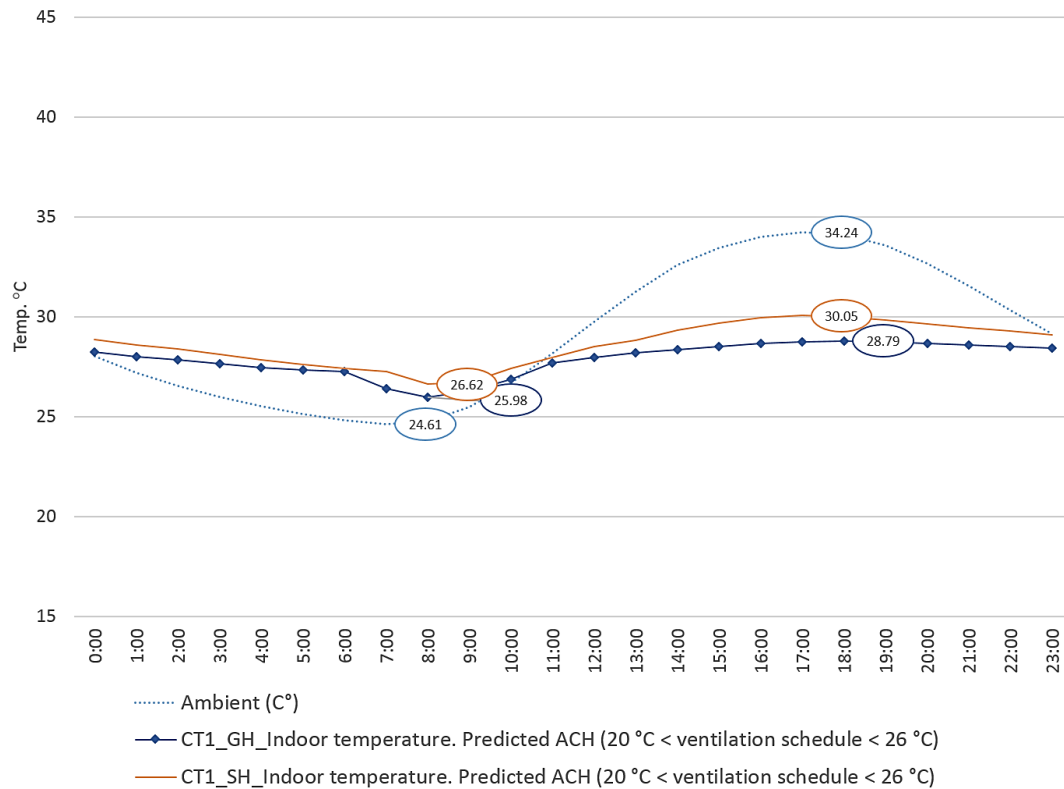


**Figure 6.2:** GH-SH, average summer day indoor temperatures upon predicted ACH and ambient temperature-dependent natural ventilation

### 6.3 Indoor temperature

As for the window screen comparison, the indoor temperatures in the base case were found to be, year-round, significantly lower than in the modified model which lacks the window screens, for both halls GH and SH (figs. 6.3-4). These differences are much significant during summer days in the case of GH where the maximum temperature of an average summer day is found to be 2.95 °C lower than in the no-screen case. For the hall SH however, maximum temperature of an average summer day in the base case was 1.83 °C lower than in the no-screen case. On the contrary and yet expectedly, slight differences are found in minimum temperatures. The indoor space releases the heat gained by radiation, within the absence of the window screen, by ventilation and night time cooling when the window screen plays no role.

With regards to solar geometry the winter sun solstice can be a more decisive factor for temperature differences between both halls. As the windows of the secondary hall (SH) are south-west oriented, they will be facing the sun for a wide time span during daytime, unlike the window of GH due to its orientation north-west. The solar rays will be allowed to penetrate the south-west windows of the secondary hall which will stay warmer during daytime (refer to solar geometry in chapter 2 and solar analysis in chapter 4). Figures 6.5-6 show the winter temperature comparison for both halls.

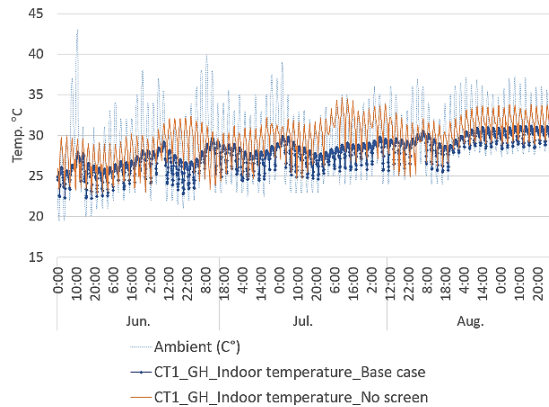


**Figure 6.3:** GH, summer indoor temperature, base case vs. modified model (no-screen)

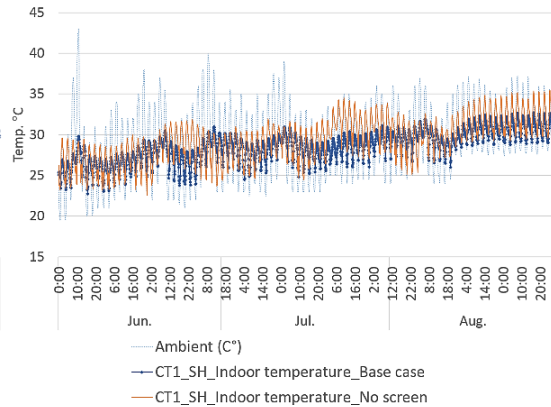


**Figure 6.4:** SH, summer indoor temperature, base case vs. modified model (no-screen)

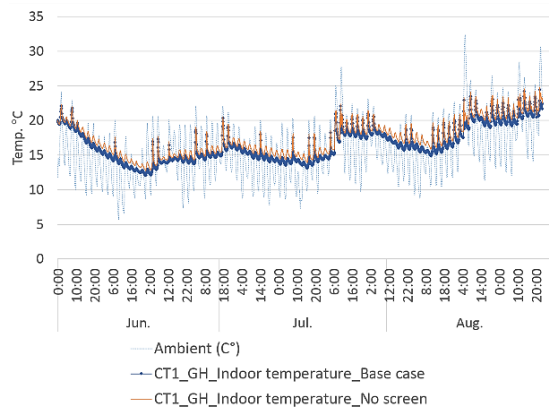


**Figure 6.5:** GH, winter indoor temperature, base case vs. modified model (no-screen)

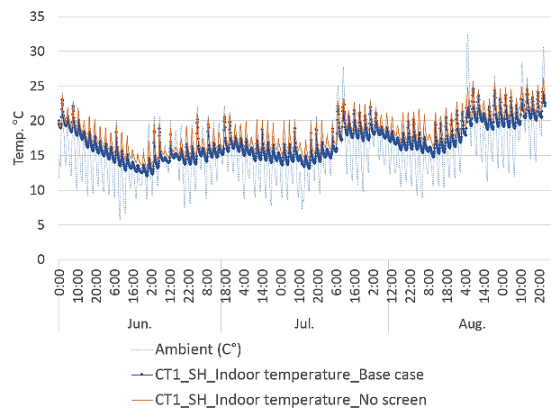


**Figure 6.6:** SH, winter indoor temperature, base case vs. modified model (no-screen)

The second comparison took place between the base case and a modified version for wall material properties where the limestone was replaced with hollow red bricks. Although the efficacy of the higher thermal mass of the stone walls was previously analyzed, it can be more illustrative to demonstrate this impact on the thermal behavior and energy demand of the building along the year. Figures 6.7-8 show annual temperature profiles of this comparison for both halls. For the summer season the indoor temperatures in the brick-walls case are found to be much higher for both maximum and minimum temperature, alike in the previous comparison where the window screens plays no role at night time.

The bricks, due to the lower heat storage capacity, absorb and release heat much faster than the stones do and thus are more influenced by the ambient temperature fluctuations. This behavior can be more tangible in the grand hall than in the secondary hall where the south-west wall is more exposed to solar radiation, in terms of time span, and the secondary hall hence has higher temperatures than the grand hall within all conditions year-round. On the contrary the indoor temperature variation between the two cases in winter is not as wide as in summer, though the energy demand for heating significantly differs due to the lower thermal capacity of the brick walls. This will be described through the discussion of energy demand in section 6.5.

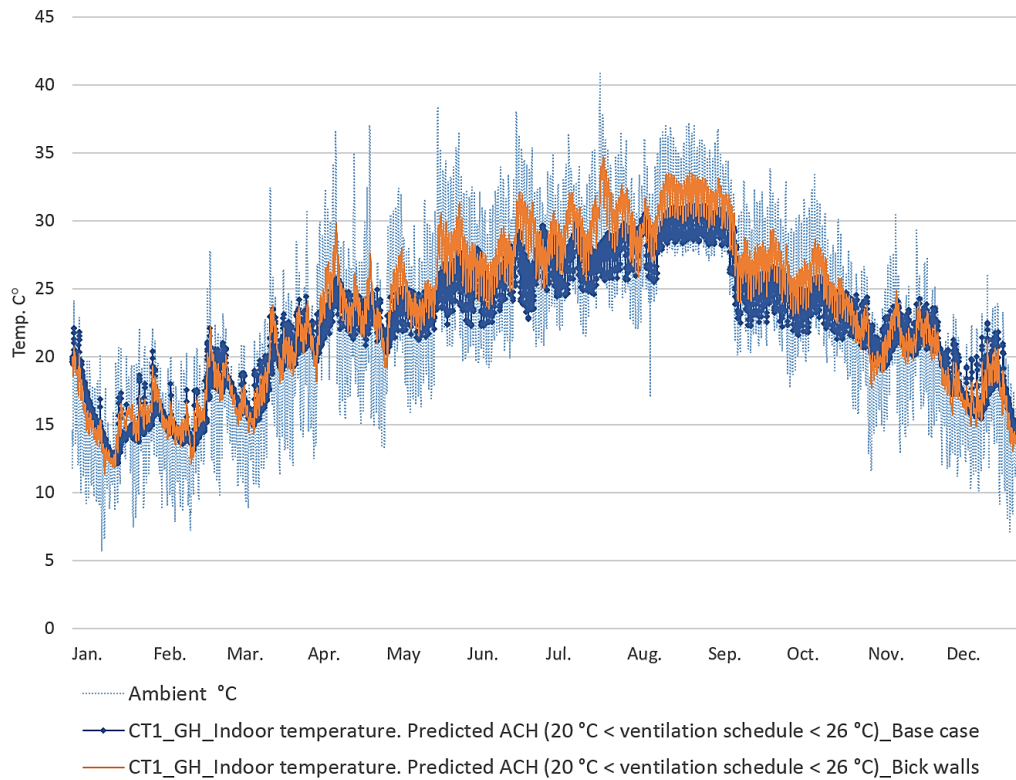


**Figure 6.7:** GH, annual indoor temperature, base case vs. modified model (brick walls)

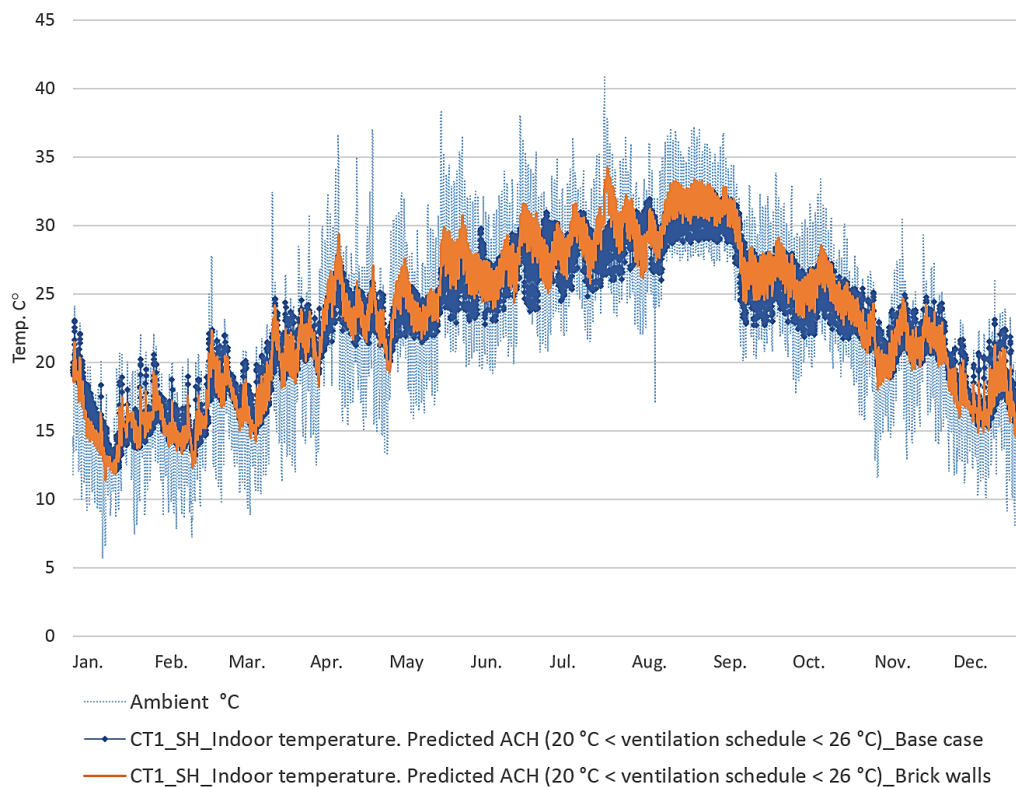


**Figure 6.8:** SH, annual indoor temperature, base case vs. modified model (brick walls)

Generally the base case consistently shows better thermal performance during summer than the two modified models, especially for the grand hall (GH). Figure 6.9 shows temperature differences between the three cases for an average summer day. For an average summer day (Jun-Aug) the base case had a maximum temperature as lower as 3.5 and 1.83 °C than the no-screen and brick-wall models respectively. The differences in minimum temperatures however are relatively smaller, 1.78 and 0.71 °C. Furthermore, the base case showed less correlation to the outdoor temperature fluctuation than the other two cases, which is attributed to a couple of factors. The first is the lower amount of solar radiation transmitted through the windows when compared to the no-screen model which shows obvious increase of indoor temperature in the afternoon as the sun being facing the north-west façade of the hall. The second factor is the higher thermal mass which keeps the indoor temperature more stable when compared to the brick-walls case where the indoor temperature keeps to increase until night time as the heat being transferred to the indoor space rather than to the outside.

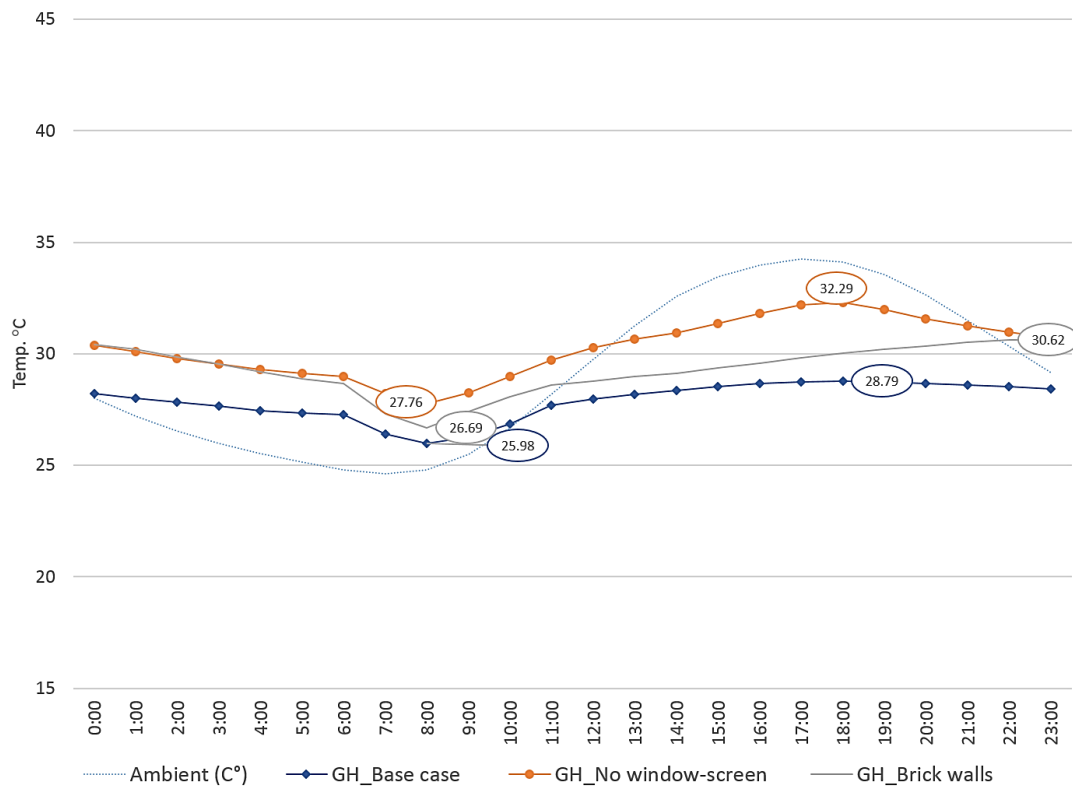


**Figure 6.9:** GH, indoor temperature, base case vs. modified models, average summer day

**Table 6.1:** Average differences of indoor temperature between base case vs modified models

Average indoor temperature variation (Jun-Aug)			
Base case	Modified model	Average difference (°C)	Statistical Significance
	No window-screen	-2.38	1.0
	Brick walls	-1.41	1.0

Table 6.1 provides results of a comparative analysis of the indoor temperatures for the base case against the two modified models. For two different designs X and Y, (average of X)-(average of Y) are computed, which equals to: average of  $(X_i - Y_i)$ , where  $i$  is an index running over all readings. Statistical significance of this difference is then tested. Statistical significance confirms whether the calculated temperature difference occurs only by coincidence or a consequence of the corresponding design. The statistical test used in this analysis is the two-sided t-test, a standard test in statistics literature to measure the difference between the means of two populations (a population here in this context is the readings of inside temperature for a particular design). The hypothesis is tested that the means of the two populations are the same; then the hypothesis either accepted or rejected at some level of significance. For example, at summer time (June-Aug), the first row of average difference in the table reads as follows: The average difference between the indoor temperature for the base case and the no-screen model is -2.38 degrees; and a two-sided t-test that tests the hypothesis that "the two populations of temperature have the same mean value" is rejected at 0.05 level. The 0.05 level means a confidence level of 95% (=  $100 \times (1-0.05)$ ) that what has been concluded about the temperature difference is correct and statistically significant (referred to as 1.0). The same is applied on the average difference between the base case and the brick walls model.

## 6.4 Thermal comfort

A thermally comfort indoor environment is a result of physical influencing factors such as indoor temperature, average ambient temperature, humidity and air movement [35]. As for the indoor temperature, an average maximum temperatures of 28.79 °C and 30.05 °C might be acceptable when considering the relatively high ambient temperatures. However, this should be evaluated in terms of levels of thermal comfort that would be achieved. This study adopts the DIN EN 15251 adaptive comfort standard for naturally ventilated buildings. According to the standard, figure 6.10 shows acceptable ranges of indoor operative temperature for naturally ventilated buildings. The standard proposes three categories of buildings. In this study the third category is considered, which assumes moderate expectations for existing buildings.

The operative temperatures presented in Figure 6.10 are valid for buildings used mainly for human occupancy with sedentary activities and dwelling, where there is easy access to operable windows and occupants can adapt their clothing to both indoor and outdoor thermal conditions [16]. The clothing factor ( $clo$ ) corresponds to clothing insulation which is calculated in  $m^2K/W$ , and metabolic rate ( $met$ ) corresponds to the amount of energy expenditure per  $W/m^2$  at different activities. This study assumes a metabolic rate of 1.2 (seated or light work in homes) along the day and a rate of 1 (seated or relaxed) between 12 and 8 pm. As for the predominant hot climate of Cairo people normally rely on the relatively heavy clothes during the winter season rather than active heating methods. A clothing factor is then scheduled according to temperature range. Three conditional equations were defined in TRNSYS simulation as inputs for clothing factor as:

$$clo_1 = 0.3 * ge(T_{in}, 28), clo_2 = 0.5 * lt(T_{in}, 28) \text{ and } clo_3 = 0.8 * lt(T_{in}, 21)$$

where  $clo$  is the clothing factor,  $T_{in}$  is the indoor temperature, and  $ge$  and  $lt$  stand for greater than or equal and less than respectively. Considered clothing factors and metabolic rates are listed in tables 6.2-3 respectively.

The indoor relative air velocity m/s also influences the persons' feel of thermal satisfaction. The indoor relative velocity was hence defined as hourly input according to the predicted ACH and calculated from the flowing equation:

$$Vel = ACH \cdot V \cdot \frac{A}{3600} \quad (6.1)$$

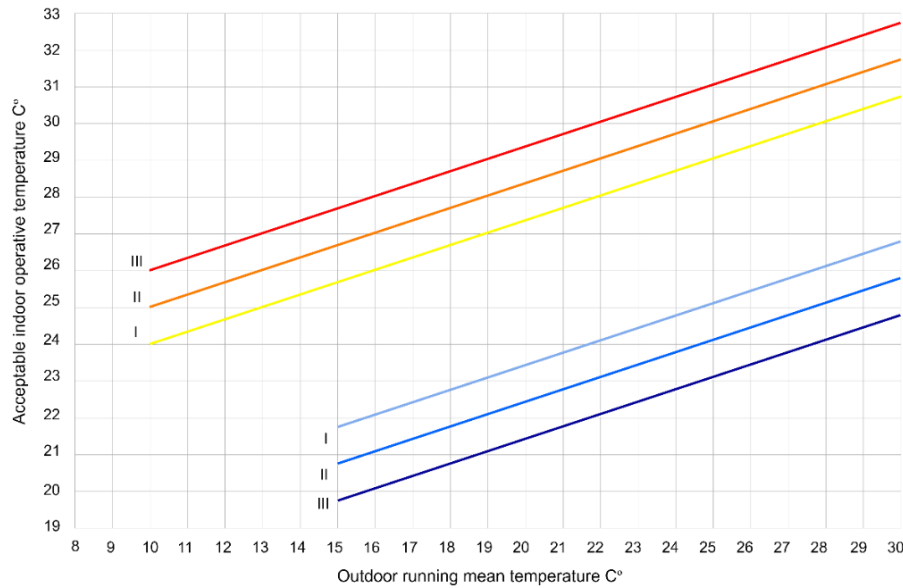
where  $Vel$  is the indoor velocity,  $ACH$  is the air change rate,  $V$  is the volume and  $A$  is the window area.

**Table 6.2:** Assigned clothing factors

Clothing ensemble	Clothing factor (clo)	Condition
clo1- Panties, T-shirt, shorts, light socks, sandals	0.3	$T_{in} \geq 28 \text{ }^\circ\text{C}$
clo2- Underpants, light trousers, light socks, shoes	0.5	$T_{in} < 28 \text{ }^\circ\text{C}$
clo3- Underpants, shirt, boiler suit, socks, shoes	0.8	$T_{in} < 21 \text{ }^\circ\text{C}$

**Table 6.3:** Assigned metabolic rates

Degree of activity	Metabolic rate (met)	Condition
Sedentary, light work	1.2	$0:00 > \text{Time} > 8:00$
Seated, relaxed	1	$0:00 < \text{Time} < 8:00$


**Figure 6.10:** Acceptable indoor operative temperature for buildings without mechanical cooling as a function of the exponentially-weighted running mean of the outdoor temperature [16]

The allowable indoor operative temperatures in figure 6.10 are plotted against the external running mean temperature which is calculated from the following equation:

$$T_{rm} = (1 - \alpha)T_{ed-1} + \alpha \cdot T_{rm-1} \quad (6.2)$$

where  $T_{rm}$  is running mean temperature for today,  $T_{ed-1}$  is the daily mean external temperature for the previous day,  $T_{rm-1}$  is running mean temperature for previous day and  $\alpha$  is a constant between 0 and 1 (0.8 is used in this evaluation)

For category III the upper limit is calculated as:

$$T_{i \max} = 0.33 T_{rm} + 18.8 + 4 \quad (6.3)$$

and the lower limit is calculated as:

$$T_{i \min} = 0.33 T_{rm} + 18.8 - 4 \quad (6.4)$$

where  $T_i$  is the limit value of indoor operative temperature  $^\circ\text{C}$ ,  $T_{rm}$  is the running mean outdoor temperature  $^\circ\text{C}$ . These limits apply when  $10 < T_{rm} < 30 \text{ }^\circ\text{C}$  for upper limit and  $15 < T_{rm} < 30 \text{ }^\circ\text{C}$  for lower limit [16]. However, in this case the running mean temperatures exceeds  $30 \text{ }^\circ\text{C}$  and reach  $38.07 \text{ }^\circ\text{C}$ . The allowable indoor operative temperature  $T_{i \max}$  therefore is considered as  $32.7 \text{ }^\circ\text{C}$  which is the maximum limit corresponding to  $T_{rm}$  of  $30 \text{ }^\circ\text{C}$  according to the above equation.

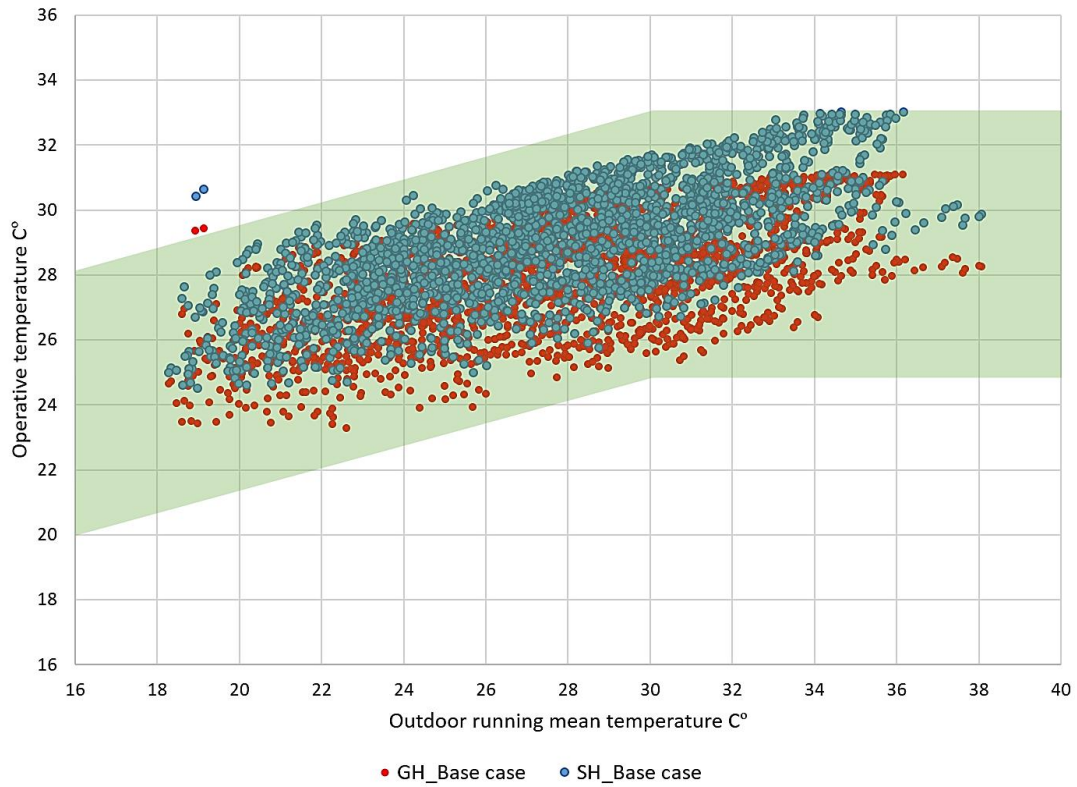


**Figure 6.11:** GH-SH, summer indoor operative temperature, base case (acc. DIN EN 15251)

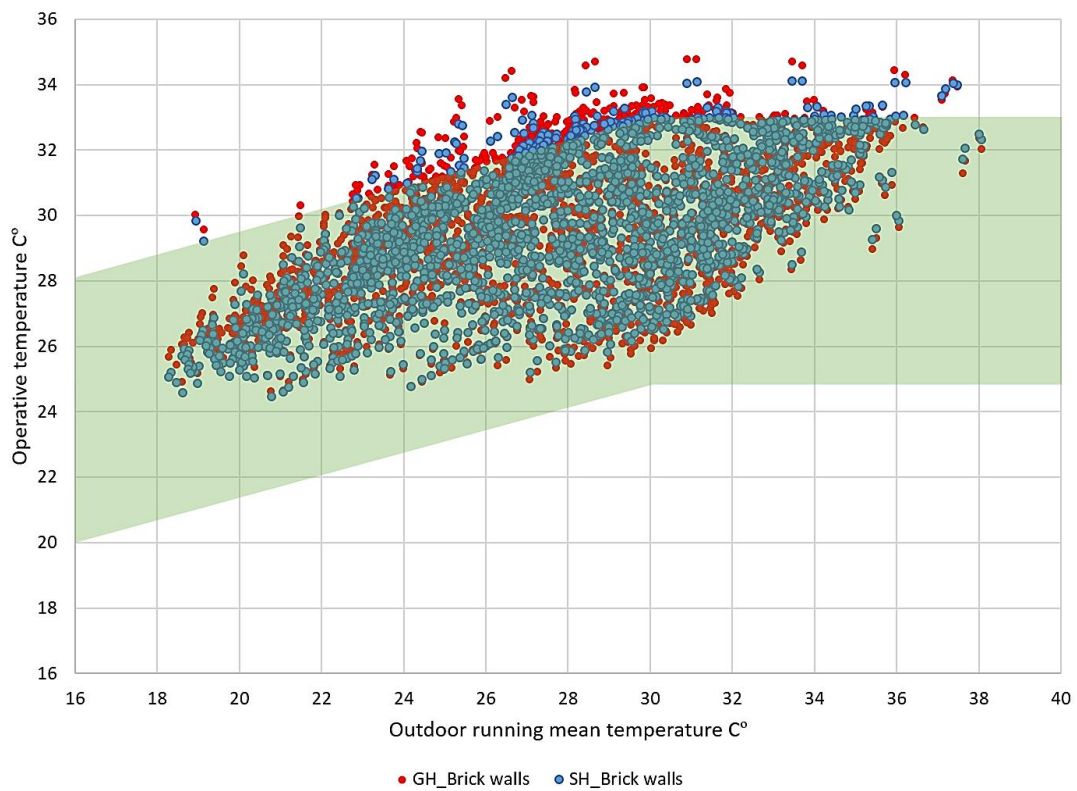


**Figure 6.12:** GH-SH, summer indoor operative temperature, brick walls (acc. DIN EN 15251)

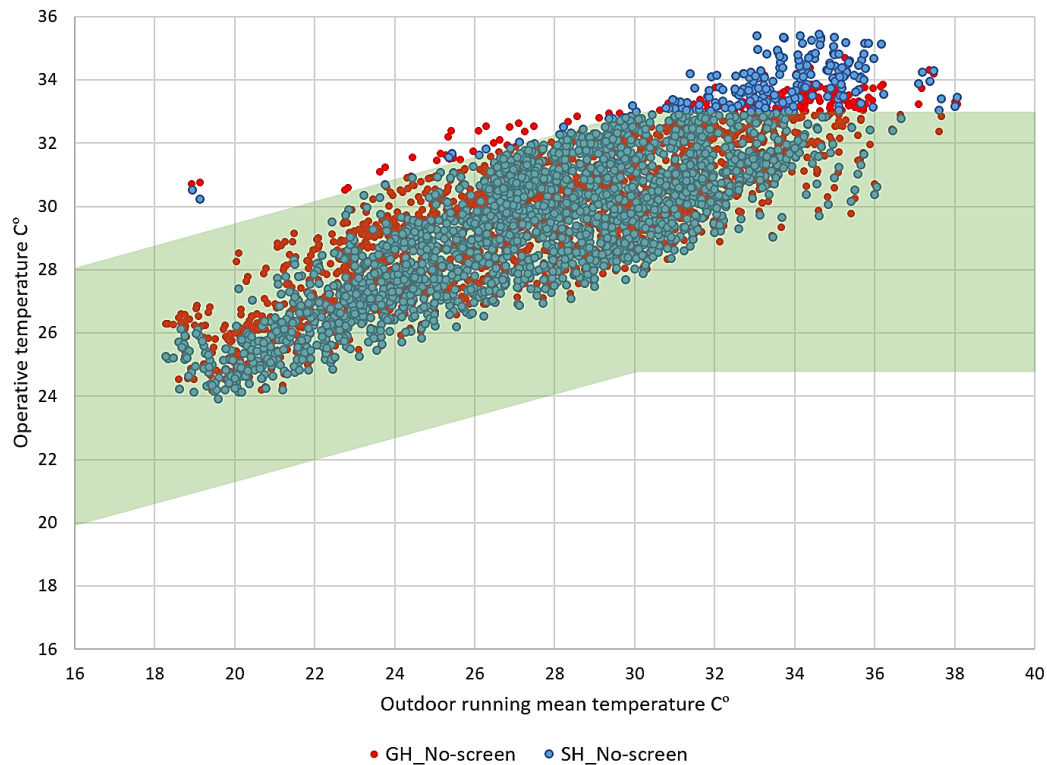


**Figure 6.13:** GH-SH, summer indoor operative temperature, no-screen (acc. DIN EN 15251)

Figures 6.11-3 show the indoor operative temperatures in summer for the base case, brick-walls case, and no-screen case respectively. The figures conclude that the base case complies with the allowable limits for the indoor operative temperatures along the summer and almost unexceptionally. On the contrary in both other cases the indoor operative temperatures exceed the allowable limits, especially when the running mean temperature exceeds  $30\text{ C}^{\circ}$ . In the case where the window screens do not exist and as more solar radiation is transmitted through the unshaded windows, the indoor space would be warmed up during the day time, especially through the south-west windows of the secondary hall, as previously described. In terms of thermal comfort this would be more desirable during the relatively cold winter days and has its direct impact on heating demand as it will be explained. The summer thermal comfort profiles for the three cases are close proportional correspondence to these thermal behaviors.

The adaptive thermal standard DIN EN 15251 will not be suitable to assess the thermal comfort during winter as the outdoor running mean temperature will be far below the presumed range. The operative temperatures in both the base case and the modified model do not fall into the acceptable range, though the no-screen case achieved better levels of acceptance (figs. 6.14-5). The previous presumed clothing factors and metabolic rates were adopted then to simulate the thermal comfort in winter for both cases to get the predicted mean vote according to the EN ISO 7730 standard [41]. The PMV in winter for both halls GH and SH is shown in figures 6.16-7 respectively. Generally the base case achieves a slightly cool indoor environment, which is rather accepted without mechanical heating. However the effect of solar radiation transmitted through the unshaded windows in the no-screen model on warming up the indoor is evident. The absence of window screen mostly provides a neutral indoor environment during the winter season. This effect is more evident in the secondary hall (SH) where the window on the south-west façade is more exposed to solar radiation during daytime than the window on the north-west façade of the grand hall. As the ACH is neglected in winter simulations, except for infiltration rate  $0.4/h$ , the thermal comfort is more temperature-dependent and hence the comparison between the PMV of both cases is more correspondent to the indoor temperatures of both.

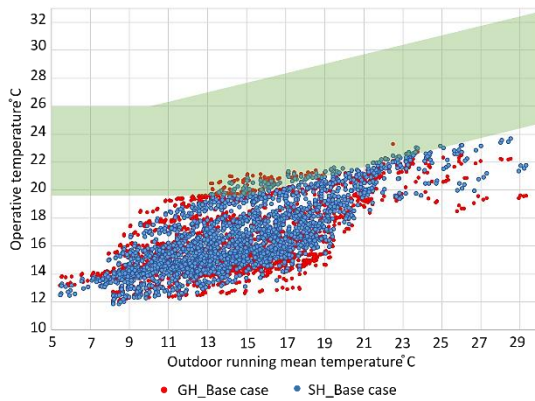


**Figure 6.14:** GH-SH, winter indoor operative temperature, base case (acc. DIN EN 15251)

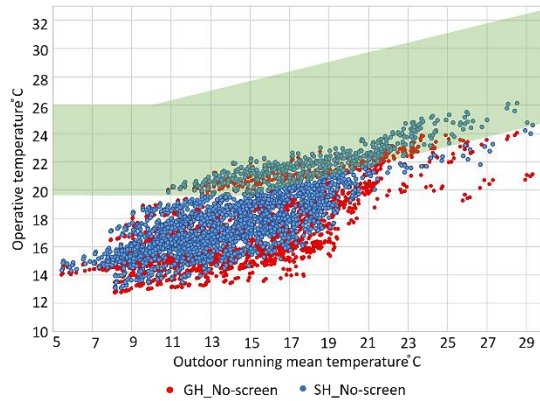


**Figure 6.15:** GH-SH, winter indoor operative temperature, no-screen (acc. DIN EN 15251)

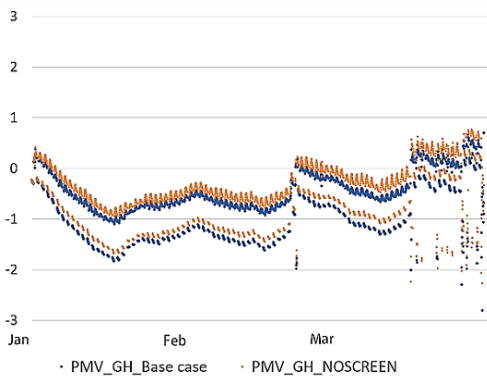


**Figure 6.16.** GH, winter PMV, base case vs. modified model (no-screen) (acc. EN ISO 7730)

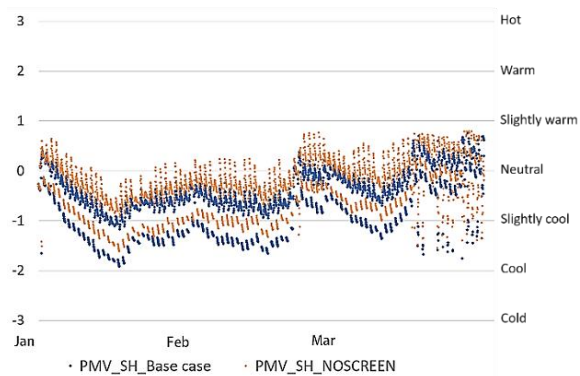


**Figure 6.17.** SH, winter PMV, base case vs. modified model (no-screen) (acc. EN ISO 7730)

### 6.5 Energy efficiency

In naturally ventilated buildings people generally accept greater climate variability. According to the adaptive thermal comfort standard the achieved level of comfort in the base case is quite acceptable along the summer. However, it remains subject to the inhabitants' culture and behavior. In such a relatively harsh hot climate, it remains expected to adopt mechanical cooling devices, as long as they are available, in response to even slight overheating. As considered for the ventilation schedule, a temperature between 20 and 26 °C is adopted as an accepted range of indoor temperature (refer to the psychometric chart of Cairo in chapter 2). Moreover, the ambient temperatures, and hence indoor temperatures, significantly drop during winter time which cause states of dissatisfaction in winter. A rough assessment of the energy needed can therefore be obtained, whether for cooling or heating. Here the heat gains by different factors, i.e. inhabitants and electronic devices, are neglected.

The simulation model was adapted in TRNBuild for both cooling and heating types which would be operated for an indoor temperature above 26 °C and below 20 °C respectively. The ventilation schedule and hence the ACH equation were in reverse disabled. As the windows would be closed during cooling and heating times, a conditional statement was added to the ACH equation as:  $(lt(T, 20) * ge(T, 26))$ .

Figure 6.18 shows the monthly energy demand for cooling (+) and heating (-) for both halls to keep the indoor temperature between 20 and 26 °C. The highest cooling energy demand is found in summer mostly between June and September as the indoor temperature reaches its maximum value. Figure 6.19 shows the total annual energy demand (for cooling and heating) for both halls. It is clear however that the building generally demands more energy for heating than for cooling, especially for the grand hall GH.

Here some basic remarks can be stated. The energy needed in the grand hall (GH) is 3164 kW and 4922 kW/h for cooling and heating respectively, which are apparently great values for one room in a building that adopts a holistic passive design method. However, considering the volume of this hall explains these values. Due to the spaciousness of the hall area and its extreme height its volume is ca. 1125 m<sup>3</sup>. This might exceed the sum of volumes of three medium scale modern apartments where each might demand similar amount of energy.

The second observation is that the grand hall demands more energy than the secondary hall, especially for heating, 4922 kW/h for GH vs. 2835 kW/h for SH. In addition to the greater volume of the grand hall, another fact stands behind this enormous difference in heating energy. According to the discussion in section 6.3, this can be attributed to the orientation of the openings in SH, south-west, which allows the lower sun rays to reach the indoor space in winter, which will be further explained through analyzing the energy demand in absence of the window-screens. However the difference in energy demand for cooling remains comparatively closer; 3164 kW/h vs. 2520 kW/h for GH and SH respectively, especially as the indoor temperature in GH remains almost lower than in SH.

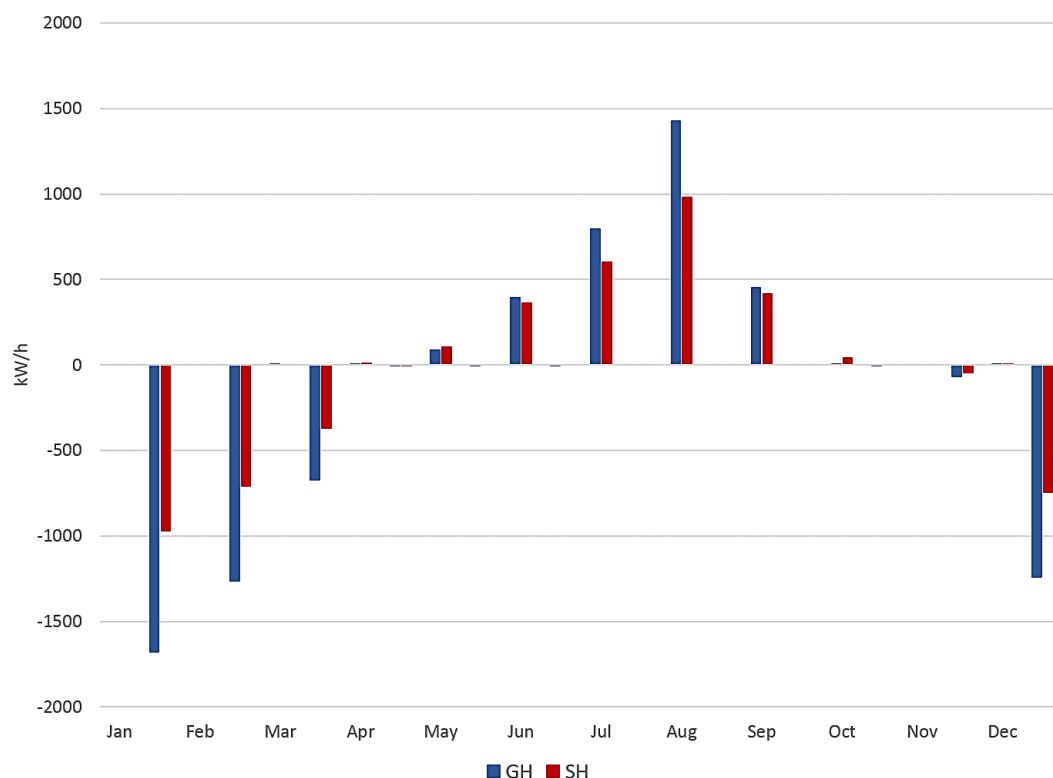


**Figure 6.18:** GH-SH, monthly energy demand (kW) for cooling and heating, operation on 26 and 20 °C respectively

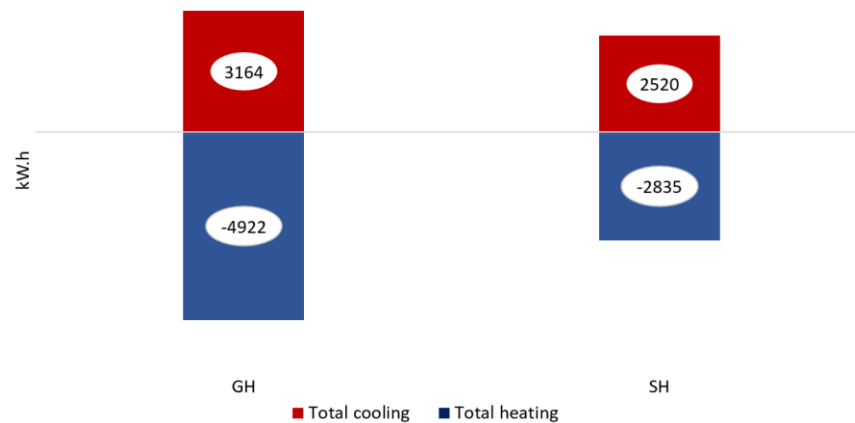


**Figure 6.19:** GH-SH, total annual energy demand (kW/h) for cooling (+) and heating (-)

The energy demand for cooling and heating in the no-screen case can be proportionally expected as corresponding to indoor temperature variation when compared to the base case. As similar as in the base case the cooling energy needed to keep the indoor temperature between 20 and 26 °C is found in summer mostly between June and September as the indoor temperature reaches its maximum value. The amount of energy needed for cooling exceeded that in the base case approximately as proportionally as corresponding to the temperature variation. However, the amount of shading increases the required heating loads in winter more than it decrease the cooling loads in summer [74]. A slight reduction in the sensible energy demand for heating is found, which responds as well to the relatively warmer winter indoor environment when the screens are absent (fig. 6.20).

The use of thermal mass can reduce peak heating or cooling load and hence the energy consumption, especially when it is integrated with night ventilation [76]. For the brick-walls model however, the energy needed for both cooling and heating is significantly higher (fig. 6.21), which can be simply understood in light of the thermal capacity of the wall material. Even in winter time, the indoor temperature variation between this model and the base case is not as wide as in summer. However, the energy needed to keep the indoor environment within the required range is much higher than in the base case as the walls do not reserve the heat as much as in the stone case and hence the indoor space would not be protected against temperature fluctuations.

The differences in energy demand between the base case and both modified models do not proportionally correspond to the differences in indoor temperatures. In other words, despite having lower maximum temperature degrees, the brick-walls model demands more energy for cooling than the stone walls model with no window screens does. This could be explained by following the thermal behavior of both cases. For the grand hall for instance, the absence of the window screens results in a significant rise in indoor temperatures during the afternoon only because of the higher amount of transmitted solar radiation. Nevertheless, the stone walls store the heat during daytime and release it at night to the cooler outdoor. The indoor temperature therefore can significantly drop during nighttime, and therefore mechanical cooling will be switched off. The time-shifting accomplished by the thermal mass can move the energy demand for cooling or heating from the peak hours [69]. On the contrary and despite the openings being protected by the screen in the brick-walls model, the wall material keeps transferring the heat to the indoor environment, which results in the temperature rising continuously even in nighttime. So even if the maximum indoor temperature in the brick wall model is lower than in the no-screen model, the temperature along the day remains higher than the level needed to keep the indoor temperature within the accepted range. Thus, more operational hours are demanded to cool down the space. The same interpretation can, conversely, be valid for the heating process.

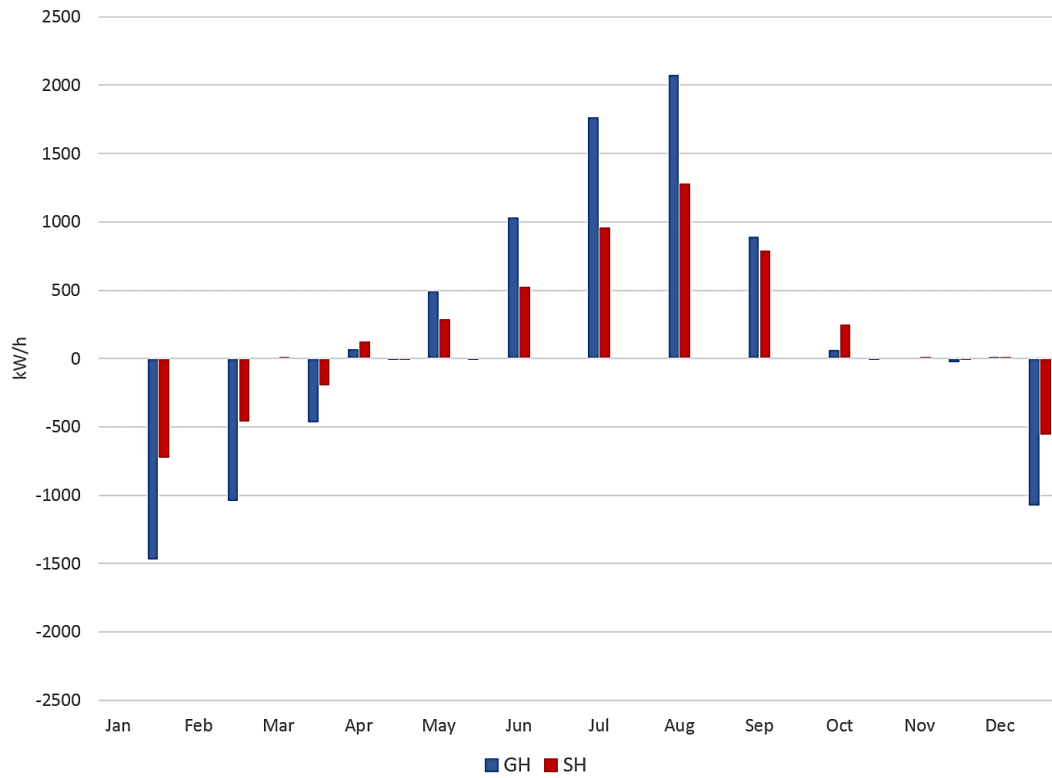


**Figure 6.20:** GH-SH, modified model (no window-screens), monthly energy demand (kW) for cooling and heating, operation on 26 and 20 °C respectively

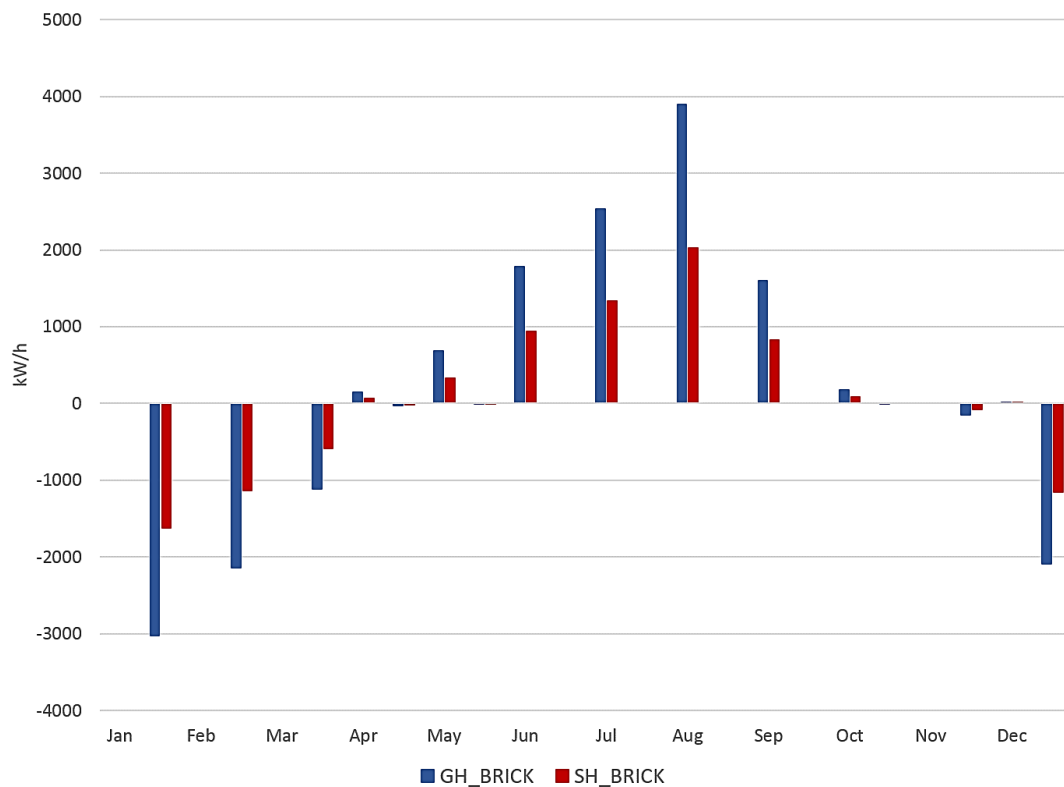


**Figure 6.21:** GH-SH, modified model (brick walls), monthly energy demand (kW) for cooling and heating, operation on 26 and 20 °C respectively

Figure 6.22 shows a comparison between the annual energy demand of cooling and heating between the base case and the two modified models for both halls GH and SH. From the figure it can be concluded that the grand hall (GH) in the base case demands energy as less as 72 % and 49 % than the brick walls model for cooling and heating respectively. This can obviously reflect the impact of the wall material thermal mass on the energy efficiency of the building model, especially in hot weather conditions. This gap between the energy demands for both cases significantly narrows down in the secondary hall to 56 % for cooling. However the difference in energy demand for heating remains too close, 45%, as the secondary hall has higher temperature degrees during the winter in both cases due to the higher amounts of solar radiation transmitted through the south-west windows.

As for the modified model (no-screen) the difference in energy demand for cooling is not as great as in the previous case. However, the base case remains more efficient since the grand hall demands energy as less ca. 50 % than the modified model. The secondary hall however is found to be more efficient with 40 % less in cooling demand. On the contrary within the absence of the window screens the modified model is found to be more efficient in terms of heating demands. The grand hall demands energy as less as 19 % and 31 % than the base case for GH and SH respectively. This can be explained in light of the fact that the space is warmed up by the greater amount of solar radiation transmitted through the unshaded windows, especially in SH due to the south-west orientation and winter sun solstice, as previously discussed. Energy savings of the base case compared to the modified models are concluded in table 6.4.

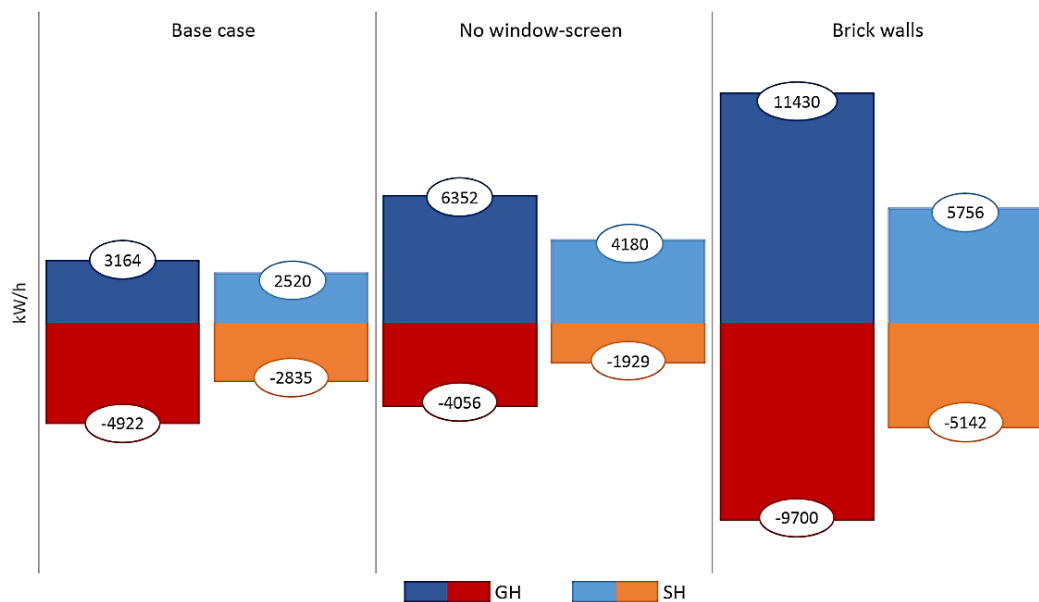


**Figure 6.22:** GH-SH, total annual energy demand (kW/h) for cooling (+) and heating (-), base case vs. modified models, operation on 26 and 20 °C respectively

**Table 6.4:** Energy saving of the base case compared to the modified models

	Base case vs. Brick-wall model		Base case vs. No-screen model	
	GH	SH	GH	SH
Cooling loads	- 72 %	- 56 %	- 50 %	- 40 %
Heating loads	- 49 %	- 45 %	+ 21 %	+ 47 %

## 6.6 Conclusion

1. Upon predicted ACH and ambient temperature dependent, 20-26 °C, natural ventilation, the maximum indoor temperatures were reduced, in average of 5.45 °C and 4.19 °C below ambient for GH and SH respectively.
2. Indoor temperatures in the base case were found to be, year-round, lower than in the modified model which lacks the window screens for both halls GH and SH. Differences where 2.95 and 1.83 °C for average summer midday.
3. For the summer season the indoor temperatures with the brick walls are found to be much higher than stone walls for both maximum and minimum temperature. Due to its lower capacity to heat storage, the bricks absorb and release heat much faster and thus is more influenced with the ambient temperature fluctuations.
4. Generally the base case consistently shows better thermal performance during summer than the two modified models. Upon comparative analysis the temperature differences are found to be statistically significant.
5. In winter the absence of the window screens is more efficient to allow solar radiation to be transmitted and warm up the indoor space, especially for the southwest hall.
6. According to the DIN EN 15251 adaptive thermal comfort standard for naturally ventilated buildings, the base case unexceptionally complies with the allowable limits for the indoor operative temperatures along the summer.
7. According to EN ISO 7730 standard for thermal comfort the model that lacks the window screen achieved higher levels of comfort as it provides warmer indoor environment in winter.
8. The grand hall (GH) in the base case demands energy as less as 72 % than the brick walls model does for cooling and 49 % for heating respectively, which is a direct impact of thermal mass especially in hot weather conditions.
9. The secondary hall (SH) demands cooling energy as less as 56 % than the brick walls model does. However the difference in energy demand for heating remains too close to the grand hall, 45%, as the secondary hall has higher temperature degrees during the winter in both cases due to the higher amounts of transmitted solar radiation due to the windows' south-west orientation.
10. Within the absence of window screens the modified model is found to be more efficient in terms of heating demands, especially for southwest orientation, 31 % lower in cooling demand.

## Potentials for future building practices

In addition to the higher solar heat loads, the utilization of air conditioning systems offset the resulting increase of cooling loads [32]. Active solutions for air cooling does not respond to people's needs and still confined to upper and middle classes due to the higher cost. The limited conservative approach towards contextualization of traditional features and symbolic meanings of regression are the major challenges facing traditional architecture. However, a functionally-oriented approach can add a new progressive dimension to the traditional building practices, which can change the ingrained perception of these features as mere images from the past.

Vernacular architecture responds to both cultural concerns and climatic conditions. Different features employed in the traditional house demonstrate remarkable levels of awareness of heat transfer mechanisms, ways of heat gain/loss in the building, and requirements of indoor thermal comfort. The traditional house adopts a passive cooling strategy for the minimization of heat transferred into the building and disposal of heat. Heat gain is significantly decreased due to the quality of building envelope; i.e. the wall material heat storage capacity, the paucity of openings and shading mechanisms which corresponds as well to the social need for privacy. The disposal of heat takes place as well through a wind driven natural ventilation process that involves different parameters; opening orientation and distribution; the roof wind-escape device; and the microclimate of the courtyard.

In this study simulation models in TRNSYS were validated against real measured data for indoor temperatures for the three selected cases. The first case is a contemporary residential building (CM). The other two cases are historical traditional houses (CT1) and (CT2), the former was adopted as a potential integrated model for passive design as it showed the most efficient thermal performance. Upon statistical learning, a classification and regression tree (CART) was created to infer the relationship between hour, velocity and direction (H, V, D) on one hand and 180 pairs of air change rates (ACH) obtained from CFD simulations, for both halls of the case CT1 on the other hand. Two trees of regression included 39 and 50 prediction rules (possible values of ACH) for both halls. Prediction rules were transferred into equations' statements that redefined the ACH to reinitialize the simulation for indoor temperature in TRNSYS. The average conformity between simulation results and measured data is found to be  $\pm 0.38$  °C and  $\pm 0.39$  °C. Upon the predicted ACH and ambient temperature dependent, 20-26 °C, natural ventilation, the maximum indoor temperatures were reduced, in average of 5.45 °C and 4.19 °C below ambient in the two halls of CT1.

According to the DIN EN 15251 adaptive thermal comfort standard for naturally ventilated buildings, the indoor operative temperatures in the traditional building adopted in this study comply, unexceptionally, with the allowable limits along the summer. The achieved level of comfort in the traditional building is a result of an integrated passive design strategy which incorporates various climatically responsive features. Understanding the measures will help to integrate them into modern architecture. Upon the investigations of the potentiality of the traditional house through the experiments applied in this study, some major remarks to be considered for future building practices can be concluded regarding the following features:

1. The courtyard: The microclimate of the courtyard is found to be comparatively better than that of the modern case in terms of maximum temperature, over 3 °C lower. The amount of shadings resulted on façades within the courtyard enclosure has significant impact on both the amount of solar transmittance and to delay the occurrence of direct solar transmittance for ca. 4 hours during summer, especially for the north-west façade. The summer sun does not hit the north-west façade that remains almost shaded by the other wing of the courtyard (south-east). In winter however, the sun becomes much lower in the sky and can penetrate the courtyard to hit the south-west façade, and hence the incident radiation increases during winter time which is more desirable.

The design of the traditional house responds efficiently to the prevailing winds. Despite the reduction of velocity inside the courtyard the air moves in cyclone manner resulting in the redirection of air flow which supposedly would not otherwise be facing any of the windows, with regards to the given wind directions. Velocity inside the courtyard remains relatively stable, below 1 m/s. However, solar radiation warms up the ground surface of the courtyard and hot air rises to higher levels by free convection and is replaced by cooler air from the outside. An area of high pressure is created and the air starts to recirculate and travel to the lower pressure region at the openings, where air flow would be magnified. The courtyard enclosure protects the building against high undesirable wind speeds.

As for adopting the courtyard form in future buildings, land use and prices hinder the construction of single family houses in town and around. However, two possibilities can then be investigated. The first is in newly constructed cities and urban communities. Multifamily houses remain acceptable in all cases as the apartment buildings represent nearly 90% of the housing projects [19]. Courtyard houses can be applied within the frame of urban planning that maintains same levels of compactness and density of the old town. However a minimum courtyard width should be considered as minimum as regular street width for purposes of privacy. The second possibility is through the understanding and exploitation of the advantages of the courtyard regarding the resulted convective current. An adapted structure can be introduced which might look different as the courtyard being shrunk to a ventilation shaft that can incorporate a solar chimney. The advantages of the stack effect by pulling fresh air and enhance ventilation at night can hence be introduced.

2. Fenestration system: The orientation and distribution of openings reflect a high level of awareness of local wind distribution. The north-west opening overlooking the courtyard usually acts as air inlet regardless of the wind direction and velocity, except for the ENE wind; blowing from behind. For the south-west oriented windows however, as ENE and NNE winds come from the backside of the south-west space, the courtyard openings act as outlets except with low amount of flow rates in response to N and NNW winds. However these openings act entirely as air inlets with W, WNW and NW winds. The wind-escape which acts consistently as an air outlet plays a crucial role in the natural ventilation process and maintains the balance of the indoor flow rates. The ACH average is found to be 4.5/h during summer. The indoor free convection results in the rise of the low dense hot air to the lower pressure region of the roof and therefore escapes from the roof device.

Best performance in terms of both air flow and indoor temperature is found in the base case with three-side opening. The wind escape in the room with north-west oriented window overlooking the courtyard is found to increase the ACH 25% more than the double-side case in which the ACH was increased with 45 % more than the single-side. In a room with south-west oriented windows however, the differences were 60% and 27 % respectively. A high correlation between indoor temperature gradient and the airflow pattern is found as well; a direct representation of the free convection and the rise of hot air which finds its path out through the roof wind-escape. A matrix compiled the wind directions and percentage of occurrence of air flow at each opening according to its assumed inlet/outlet functionality. The openings' directional flow functionality (ODFF) varied between 83 and 100 %.

3. Shading mechanisms: The amount of shading depends mainly on the morphology of the street canyon which results in decrease in the canyon temperature and hence the façade temperature and subsequently the amount of heat transferred by conduction through the walls. The urban fabric of a large city like Cairo is generally characterized by compactness. While the overall structure of the ancient city was formed on the basis of human scale generated by the pedestrian movement, (street width ca. 7 cubits), the contemporary city is influenced mainly by a different scale generated by traffic and movements of variable speeds. However, within the residential quarters streets are mostly narrow and vary between 6 and 10 meter in width [22]. These widths can allow light traffic as well as adequate amounts of cross shading, considering a corresponding street aspect ratio. As the Egyptian code of buildings dictates that building height should not exceed 1.5 of the street width, the average height in residential areas is 4 stories which generally results in medium to deep street canyons with aspect ratio (height to width) of 1.5 to 2.5. The ratio of the length of canyons (length to height) is generally 5 to 7, medium to long. In accordance with the findings in chapter 4 for street cross shading, the exploitation of cross shading mechanisms resulted from the narrow streets canyons remains hence possible.

The incorporation of window screens contributes as well to lower the indoor air temperature in hot climate. The screen acts as a baffle zone between the interior and the exterior, so the glare of sunlight is broken up by the lattice that provides a dark area. By introducing the technique to a contemporary building by running simulations in TRNSYS it is found to be relatively effective in reducing maximum indoor temperature in hot weather. Moreover, indoor temperatures in the base case were found to be, year-round, lower than in the modified model which lacks the window screens for both halls of the case study (CT1). Differences were 2.95 and 1.83 °C for average summer midday. However, the absence of the window screens in winter is more efficient to allow solar radiation to be transmitted and warm up the indoor space, especially for the south-west hall. According to DIN EN 15251 standard, the base case achieved better levels of comfort than the modified model does. However the model that lacks the window screen provides warmer indoor environment in winter. Within the absence of window screens the modified model is found to be more efficient in terms of heating demands, especially for southwest orientation, 31 % lower in cooling demand. This can draw attention to recommend the installation of removable or folded window screens in future buildings to profit by the warm sun ray when it is more desirable in winter time.

4. Material/thermal mass: Upon a regression analysis of indoor temperature on simultaneous outdoor temperature and before 12 hours, the case CT1 showed a relative stability of the indoor temperature. This is a direct result of the capacitance effect of the buildings' high thermal mass. Moreover, a comparative analysis applied between the base case with the limestone walls and a modified version where the wall material was substituted with hollow red brick with lower capacity. For the summer season the indoor temperatures in the brick-walls case are found to be much higher than in the base case for both maximum and minimum temperature. Due to its lower capacity to heat storage, the bricks absorb and release the heat much faster and thus is more influenced by the ambient temperature fluctuations. The grand hall in the base case demands energy as less as 72 % and 49 % than the brick walls model does for cooling and heating respectively, which obviously, a direct impact of the thermal mass, especially in hot weather conditions. The secondary hall however, demands cooling energy as less as 56 % than the brick-walls model. However the difference in energy demand for heating remains too close to the grand hall, 45%, as the secondary hall has higher temperature degrees during the winter in both cases because of the higher amounts of transmitted solar radiation due to the windows' south-west orientation.



# References

- [1] Abdul Rehman. (2002). The Grand Tradition of Islamic Architecture, in Understanding Islamic Architecture (ed.) Petruccioli A & Pirani K. New York. 27-30. (cited on page 7)
- [2] Al-Bakri, U. (1997). Natural Ventilation in Traditional Courtyard Houses in the Central Region of Saudi Arabia. Wales. (cited on page 61)
- [3] Allegrini, J, Dorer, V, & Carmeliet, J. (2012). Analysis of convective heat transfer at building facades in street canyons and its influence on the predictions of space cooling demand in buildings. *Journal of Wind Engineering and Industrial Aerodynamics* 104–106, 464–473. (cited on page 56)
- [4] Al-Sanea, S.A., Zedan, M.F., Al-Hussain, S.N. (2012). Effect of thermal mass on performance of insulated building walls and the concept of energy savings potential. *Applied Energy* 89, 430-442. (cited on page 30)
- [5] Al-Sanea, S.A., Zedan, M.F., Al-Hussain, S.N. (2013). Effect of masonry material and surface absorptivity on critical thermal mass in insulated building walls. *Applied Energy* 102, 1063-1070. (cited on page 27)
- [6] Asfour, O, Gadi, M. (2007). A comparison between CFD and Network models for predicting wind-driven ventilation in buildings. *Building and Environment* 42, 4079–4085. (cited on page 87)
- [7] ASHRAE 2004 ANSI/ASHRAE Standard 55R - Thermal Environmental Conditions for Human Occupancy. American Society of Heating, Refrigerating and Air-Conditioning Engineers, Inc. (cited on page 12)
- [8] Askar, H, Probert, S.D, Batty, W.J. (2001). Windows for Buildings in Hot Arid Countries. *Applied Energy* 70, 77-101. (cited on page 14)
- [9] Bagneid, A. (2006). The Creation of a Courtyard Microclimate Thermal Model for the Analysis of Courtyard Houses. Texas. (cited on page 61)
- [10] Balaras, C.A. (1996). The role of thermal mass on the cooling load of buildings. An overview of computational methods. *Energy and Buildings* 24, 1-10. (cited on page 27)
- [11] Bansal, N.K., Hauser G., Minke, G. (1994). *Passive Building Design, a Handbook of Natural Climate Control*. Amsterdam. (cited on pages 24, 25)
- [12] Bittencourt, L & Peixoto, L. (2001). The Influence of Different Courtyard Configuration on Natural Ventilation through Low-Rise School Buildings. *Building Simulation Seventh International Conference*. Rio de Janeiro. 125-131. (cited on page 29)

- [13] Bourbia, F. & Awbi, H.B. (2004). Building Cluster and Shading in Urban Canyon for Hot Dry Climate, Part 1: Air and Surface Temperature Measurements. *Renewable Energy* 29, 249-262. (cited on page 29)
- [14] Bourbia, F. & Awbi, H.B. (2004). Building Cluster and Shading in Urban Canyon for Hot Dry Climate, Part2: Shading Simulations. *Renewable Energy* 29, 291-301. (cited on page 29)
- [15] Breiman, L, Friedman, J, Stone, C.J. & Olshen, R.A. (1984). *Classification and Regression Trees*. Florida. (cited on page 107)
- [16] CEN Standard EN15251 (2007). Indoor environmental input parameters for design and assessment of energy performance of buildings addressing indoor air quality, thermal environment, lighting and acoustics. European committee for Standardization. Brussels. (cited on pages 12, 117, 118)
- [17] Cook, J. (1989). *Passive Cooling*. Massachusetts. (cited on page 26)
- [18] Crawley, D, Hand, J, Kummert, M & Griffith, B. (2008). Contrasting the Capabilities of Building Energy Performance Simulation Programs. *Building and Environment* 43, 661-673. (cited on page 60)
- [19] Central Agency for Public Mobilization and Statistics (CAPMAS), <http://www.capmas.gov.eg/?lang=2> [Accessed Sep. 2013] (cited on page 128)
- [20] Datta, G. (2001). Effect of Fixed Horizontal Devices on Thermal Performance of Building by TRNSYS Simulation. *Renewable Energy* 23, 497-507. (cited on page 14)
- [21] Douglas Balcomb, J. (1992). *Passive Solar Buildings*. Massachusetts. (cited on page 111)
- [22] El Feky, U. (2006). *Toward Applicable Green Architecture, an Approach to Colonize the Desert in Egypt*. Eindhoven. (cited on page 129)
- [23] Elseragy, A. (2003). *Architectural and Solar Potential of Curved and Flat Roofs in Hot and Arid Regions with Reference to Egypt*. Nottingham. (cited on page 11)
- [24] Etheridge, D. (2004). Natural ventilation through large openings – measurements at model scale and envelope flow theory. *International Journal of Ventilation* 2 (4), 325–342. (cited on page 87)
- [25] Fathy, H. (1986). *Natural Energy and Vernacular Architecture: Principles and Examples with Reference to Hot Arid Climates*. Chicago. (cited on pages 15, 28)
- [26] Georgakis, Ch. & Santamouris, M. (2006). Experimental Investigation of Air Flow and Temperature Distribution in Deep Urban Canyons for Natural Ventilation Purposes. *Energy and Buildings* 38, 367-376. (cited on page 29)
- [27] Givoni, B. (1998). Effectiveness of Mass and Night Ventilation in Lowering the Indoor Daytime Temperatures. *Energy and Buildings* 28, 25-32. (cited on page 30)
- [28] Givoni B. (1976). *Climate & Architecture*. London. (cited on page 8)

- [29] Grabar, O. (1984). The Meaning of History in Cairo. In *The Expanding Metropolis Coping with the Urban Growth of Cairo*. Proceedings of Seminar Nine in the Series *Architectural Transformations in the Islamic World*. The Aga Khan Award for Architecture. Cairo. 1-24. (cited on page 16)
- [30] Gregory, K, Moghtaderi, B, Sugo, H, Page, A. (2008). Effect of thermal mass on the thermal performance of various Australian residential constructions systems. *Energy and Buildings* 40, 459–465. (cited on page 30)
- [31] Hakim, B. (1988). *Arabic-Islamic Cities Building and Planning Principles*. London. (cited on pages 17, 18)
- [32] Hanna, G., Guirguis, N. & Aziz, A. (2011). Energy Efficiency Building Codes for Egypt. *Journal of Energy and Power Engineering* 5, 1134-1141. (cited on page 127)
- [33] Hausladen, G, de Saldanha, M, & Liedl, P. (2006). *Climate Skin, Building-Skin Concepts that can do more with less Energy*. Berlin. (cited on page 13)
- [34] Hausladen, G, de Saldanha, M, & Liedl, P. (2012). *Building to Suit the Climate, a Handbook*. Berlin. (cited on page 76)
- [35] Hegger, M, Fuchs, M, Stark, T & Zeumer, M. (2008). *Energy Manual, Sustainable Architecture*. Munich. (cited on page 117)
- [36] Heiselberg, P. (2004). Natural ventilation design. *International Journal of Ventilation* 2 (4), 295–312. (cited on page 25)
- [37] Hassaan, A. (2011). An analysis of bioclimatic zones and implications for design of outdoor built environments in Egypt. *Building and Environment* 46, 605-620. (cited on page 7)
- [38] Heschong, L. (1979). *Thermal Delight in Architecture*. London. (cited on page 11)
- [39] Hindrichs, D.U. & Daniels, K. (2008). *Plus Minus. 20°/40° latitude* (Eds.). Bielefeld. (cited on pages 12, 14, 24, 27, 28)
- [40] Horan, J, Finn, D. (2008). Sensitivity of air change rates in a naturally ventilated atrium space subject to variations in external wind speed and direction. *Energy and Buildings* 40, 1577–1585. (cited on pages 30, 61)
- [41] ISO 7730 (2005) *Ergonomics of the thermal environment—analytical determination and interpretation of thermal comfort using calculation of the PMV and PPD indices and local thermal comfort criteria*. (cited on page 120)
- [42] James Lo, L, Banks, D, Novoselac, A. (2013). Combined wind tunnel and CFD analysis for indoor airflow prediction of wind-driven cross ventilation. *Building and Environment* 60, 12–23. (cited on page 89)
- [43] James Lo, L, Novoselac, A. (2012). Cross ventilation with small openings: Measurements in a multi-zone test building. *Building and Environment* 57, 377–386. (cited on pages 88, 98)

- [44] Ji, Y, Cook, M, Hanby, V. (2007). CFD modelling of natural displacement ventilation in an enclosure connected to an atrium. *Building and Environment* 42, 1158–1172. (cited on page 27)
- [45] Karava, P, Stathopoulos, T, Athienitis, A. (2006). Wind induced natural ventilation analysis. *Solar Energy* 81, 20–30. (cited on page 25)
- [46] Khan, N, Su, Y, Riffat, S. (2008). A Review on Wind Driven Ventilation Techniques. *Energy and Buildings* 40, 1586–1604. (cited on page 87)
- [47] Koenigsberger, O. H. (1973). *Manual of Tropical housing and Building - Part one: Climatic Design*. London. (cited on page 12)
- [48] Konya, A. A. (1980). *Design Primer for Hot Climates*. London. (cited on page 20)
- [49] Labat, M, Woloszyn, M, Garnier, G, Roux, JJ. (2012). Assessment of the air change rate of airtight buildings under natural conditions using the tracer gas technique. Comparison with numerical modelling. *Building and Environment* 60, 37–44. (cited on page 87)
- [50] Maury, B. & Ravault, J. (1977). *Palais et Maisons du Caire du XIVe au XVIIIe siècles*, vol. 2, Cairo (cited on pages 39, 40, 49)
- [51] MEREONORM: [www.meteonorm.com](http://www.meteonorm.com) [Accessed Sep. 2012] (cited on page 9)
- [52] Mortada, H. (2007). *Traditional Islamic Principles of Built Environment*. London. (cited on page 18)
- [53] National Oceanic and Atmospheric Administration (NOAA) <http://www.noaa.gov/> [accessed Jun-Sep. 2014] (cited on page 36)
- [54] Niles, Ph.W.B. (1992). "Simulation Analysis," in *Passive Solar Buildings*. (ed.) J. Douglas Balcomb. MIT Press. 111-179. (cited on page 82)
- [55] Nour, M.M. (1979). *An Analytical Study of Traditional Arab Domestic Architecture*. Newcastle. (cited on pages 17, 18, 26, 30)
- [56] Ogoli, D.M. (2003). Predicting Indoor Temperatures in Closed Buildings with High Thermal Mass. *Energy and Buildings* 35. 851-862. (cited on page 30)
- [57] Olgyay, V. (1973). *Design with Climate*. Princeton. (cited on pages 11, 12)
- [58] P. La Roche, M. Milne. (2004) Effects of window size and thermal mass on comfort using an intelligent ventilation controller. *Solar Energy* 77, 421–434. (cited on page 27)
- [59] Ragette, F. (2006). *Traditional Domestic Architecture of the Arab Region*. Sharjah. (cited on pages 17, 18, 19)
- [60] Ramponi R, Blocken B. (2012) CFD simulation of cross-ventilation for a generic isolated building: Impact of computational parameters. *Building and Environment* 53, 34–48. (cited on page 26)

- [61] Ratti, C, Raydan, D & Steemers, K. (2003). Building Form and Environmental Performance: Archetypes, Analysis and an Arid Climate. *Energy and Buildings* 35, 49–59. (cited on pages 20, 30)
- [62] Robaa, S.M. (2006). A Study of Solar Radiation Climate at Cairo Urban Area, Egypt and its Environs. *International Journal of Climatology* 26, 1913–1928. (cited on page 10)
- [63] Shaltout, M, Hassan, A and Fathy, A. (2001). Total suspended particles and solar radiation over Cairo and Aswan. *Renewable Energy* 23, 605–619. (cited on page 10)
- [64] Schittich, Ch. (2003). *Solar Architecture, Strategies, Visions, Concepts*. Munich. (cited on page 12)
- [65] Sherif, A, El Zafarany, A & Arafa, R. (2012). External Perforated Window Solar Screens: The Effect of Screen Depth and Perforation on Energy Performance in Extreme Desert Environment. *Energy and Buildings* 52, 1-10. (cited on page 30)
- [66] Shen, X, Zhang, G, Bjerg, B. (2012). Comparison of different methods for estimating ventilation rates through wind driven ventilated buildings. *Energy and Buildings* 54, 297–306. (cited on pages 87, 90)
- [67] Stevens, V, Kotol, M, Grunau, B, Craven, C. (2016). The Effect of Thermal Mass on Annual Heat Load and Thermal Comfort in Cold Climate Construction. *Journal of Cold Regions Engineering* 30, 1-13. (cited on page 30)
- [68] Tablada, A, Blocken, B, Carmeliet, J, De Troyer, F & Verschure, H. (2005). The Influence of Courtyard Geometry on Air Flow and Thermal Comfort: CFD and Thermal Comfort Simulations. *PLEA 2005-The 22<sup>nd</sup> Conference on Passive and Low Energy Architecture*. Beirut. 1-6. (cited on page 29)
- [69] Talyor, R, Miner, M. (2014). A metric for characterizing the effectiveness of thermal mass in building materials. *Applied Energy* 128, 156-163. (cited on page 123)
- [70] Tan, G, Glicksman, L. (2005). Application of integrating multi-zone model with CFD simulation to natural ventilation prediction. *Energy and Buildings* 37, 1049–1057. (cited on page 87)
- [71] Toudert, F & Mayer, H. (2006). Numerical study on the effects of aspect ratio and orientation of an urban street canyon on outdoor thermal comfort in hot and dry climate. *Building and Environment* 41, 94–108. (cited on pages 75, 82)
- [72] Yam, J, Li, Y, Zheng, Z. (2003). Nonlinear coupling between thermal mass and natural ventilation in buildings. *International Journal of Heat and Mass Transfer* 46, 1251–1264. (cited on page 87)
- [73] Yang, L, Li, Y. (2008). Cooling load reduction by using thermal mass and night ventilation. *Energy and Buildings* 40, 2052–2058. (cited on page 72)
- [74] Yaşa. E. & Ok, V. (2014). Evaluation of the Effect of Courtyard Building Shapes on Solar Heat Gains and Energy According to Different Climatic Regions. *Energy and Buildings* 73. 192-199. (cited on page 123)

- [75] Zhai, Z, Previtali, J. (2010). Ancient vernacular architecture: characteristics categorization and energy performance evaluation. *Energy and Buildings* 42, 357–365. (cited on page 7)
- [76] Zhou, J, Zhang, G, Lin, Yaolin, Li, Y. (2008). Coupling of thermal mass and natural ventilation in buildings. *Energy and Buildings* 40, 979–986. (cited on pages 30, 123)

# List of abbreviations

**ACH** Air change rate

**ADE** Absolute deviance error

**AH** Absolute humidity

**AVRG** Average

**CART** Classification and regression tree

**CFD** Computational fluid dynamics

**clo** Clothing factor

**CRT** Courtyard

**DBT** Dry-bulb temperature

**CM** Contemporary case study

**CT1** Traditional case study 1, the adopted model

**CT2** Traditional case study 2

**CV** Cross-validation

**GH** Grand hall in the case CT1

**Hrs** hours

**kg/m<sup>3</sup>** Kilogram/meter<sup>3</sup>

**kJ/hr** Kilojoule per hour

**kJ/hmK** Kilojoule/hour.meter.kalvin

**m** meter

**met** Metabolic rate

**MH** Main hall in the case CT2

**NOAA** National Oceanic and Atmospheric Administration

**ODFF** Openings' directional flow functionality

**QSGI** Solar radiation absorbed on window

**RH** Relative humidity

**RMSE** Root mean square error

**SCHDL** Schedule

**SH** Secondary hall in the case CT1

**TEMP** Temperature

**W/m<sup>2</sup>** Watt/meter<sup>2</sup>

# Appendix A

## CFD simulation scenarios and aggregated results

### A.1. Base-case Model

#### 01\_N\_01\_18\_31Aug

Scenario	Date	Time	Velocity m/s	Wind Dir.	Temp. °C	Zone										Nodal Velocity m/s					
						GH					SH					01_CRT_16m	02_CRT_7m	03_CRT_2m	04_SSW_7m	05_NNE_7m	06_WNW_7m
						Volume = 1125 m <sup>3</sup>					Volume = 577 m <sup>3</sup>										
						Volumetric flow rate (Q) m <sup>3</sup> /s				ACH 1/h	Volumetric flow rate (Q) m <sup>3</sup> /s				ACH 1/h						
						NW Court	NE Side	Roof	Σ		SW Court	SE Side	Roof	Σ							
01N_01Aug_S01	18-Aug	11:00	0.30	N	32	1.29	1.44	-2.73	0	8.7	0.18	1.13	-1.31	0	8.2	0.57	0.85	0.33	0.41	0.43	0.42
01N_01Aug_S02	18-Aug	17:00	3.00	N	34	0.48	0.94	-1.42	0	4.5	-0.17	0.86	-0.69	0	5.4	1.5	0.44	0.37	0.42	1.9	2.22
01N_01Aug_S03	18-Aug	20:00	6.20	N	31	0.95	-0.27	-0.68	0	3	0.41	-0.27	-0.14	0	2.6	3.29	0.18	0.56	1.02	3.6	4.39
01N_01Aug_S04	18-Aug	21:00	3.60	N	31	0.62	-0.19	-0.43	0	2	0.26	-0.18	-0.08	0	1.6	1.91	0.09	0.32	0.59	2.1	2.55
01N_01Aug_S05	19-Aug	1:00	4.10	N	28	0.66	-0.21	-0.45	0	2.1	0.28	-0.19	-0.09	0	1.7	2.18	0.11	0.37	0.66	2.39	2.9
01N_01Aug_S06	19-Aug	3:00	3.60	N	28	0.61	-0.19	-0.42	0	2	0.24	-0.17	-0.07	0	1.5	1.91	0.1	0.32	0.59	2.1	2.55
01N_01Aug_S07	19-Aug	4:00	3.00	N	28	0.51	-0.17	-0.34	0	1.6	0.21	-0.14	-0.07	0	1.3	1.59	0.08	0.26	0.49	1.76	2.13
01N_01Aug_S08	19-Aug	6:00	2.60	N	27	1.18	0.31	-1.49	0	4.8	0.28	0.13	-0.41	0	2.6	1.35	0.07	0.26	0.37	1.68	1.92
01N_01Aug_S09	19-Aug	9:00	2.00	N	30	1.87	1.12	-2.99	0	9.6	0.01	0.68	-0.69	0	4.3	1.02	0.17	0.33	0.29	1.21	1.5
01N_01Aug_S10	19-Aug	10:00	3.00	N	31	1.57	1.19	-2.76	0	8.8	-0.39	0.81	-0.42	0	5.1	1.49	0.14	0.41	0.41	1.81	2.2
01N_01Aug_S11	19-Aug	15:00	3.60	N	36	0.15	1.2	-1.35	0	4.3	-0.4	1.07	-0.67	0	6.7	1.83	0.49	0.58	0.49	2.18	2.63
01N_01Aug_S12	19-Aug	18:00	4.10	N	33	0.7	0.16	-0.86	0	2.8	0.25	0.12	-0.37	0	2.3	2.14	0.14	0.4	0.63	2.51	2.94
01N_01Aug_S13	19-Aug	19:00	5.70	N	32	0.91	-0.27	-0.64	0	2.9	0.4	-0.28	-0.12	0	2.5	3.02	0.16	0.51	0.92	3.32	4.04
01N_01Aug_S14	20-Aug	12:00	0.30	N	34	0.98	1.52	-2.5	0	8	0.22	1.31	-1.53	0	9.5	0.73	0.3	0.55	0.62	0.44	0.46
01N_01Aug_S15	20-Aug	21:00	5.10	N	30	0.81	-0.24	-0.57	0	2.6	0.35	-0.24	-0.11	0	2.2	2.71	0.15	0.46	0.84	2.96	3.61
01N_01Aug_S16	21-Aug	12:00	5.70	N	33	1.12	0.52	-1.64	0	5.2	0.26	0.36	-0.62	0	3.9	2.96	0.15	0.63	0.88	3.45	4.11
01N_01Aug_S17	21-Aug	14:00	2.60	N	35	0.03	1.39	-1.42	0	4.5	-0.48	1.26	-0.78	0	7.9	1.24	0.5	0.37	0.34	1.58	1.94
01N_01Aug_S18	21-Aug	16:00	4.60	N	34	0.42	0.83	-1.25	0	4	-0.14	0.73	-0.59	0	4.6	2.4	0.3	0.55	0.68	2.77	3.31
01N_01Aug_S19	23-Aug	20:00	3.60	N	33	0.61	-0.19	-0.42	0	2	0.25	-0.17	-0.08	0	1.6	1.91	0.1	0.32	0.59	2.1	2.55
01N_01Aug_S20	25-Aug	18:00	5.10	N	35	0.97	-0.12	-0.85	0	3.1	0.38	-0.14	-0.24	0	2.4	2.67	0.11	0.45	0.82	3.09	3.65
01N_01Aug_S21	26-Aug	1:00	0.30	N	30	0.08	-0.04	-0.04	0	0.3	0.03	-0.02	-0.01	0	0.2	0.16	0.01	0.02	0.05	0.18	0.22
01N_01Aug_S22	26-Aug	11:00	1.60	N	33	1.4	1.29	-2.69	0	8.6	0.03	0.94	-0.97	0	6.1	0.86	0.22	0.38	0.34	0.96	1.23
01N_01Aug_S23	27-Aug	23:00	2.60	N	29	0.47	-0.16	-0.31	0	1.5	0.18	-0.14	-0.04	0	1.1	1.38	0.06	0.23	0.41	1.52	1.84

## 01\_N\_02\_Jun\_Aug

Scenario	Date	Time	Velocity m/s	Wind Dir.	Temp. °C	Zone										Nodal Velocity m/s					
						GH					SH					01_CRT_16m	02_CRT_7m	03_CRT_2m	04_SSW_7m	05_NNE_7m	06_WNW_7m
						Volume = 1125 m <sup>3</sup>					Volume = 577 m <sup>3</sup>										
						Volumetric flow rate (Q) m <sup>3</sup> /s				ACH 1/h	Volumetric flow rate (Q) m <sup>3</sup> /s				ACH 1/h						
NW Court	NE Side	Roof	Σ	SW Court	SE Side	Roof	Σ														
01N_02Jun_Aug_S01	1-Jun	23:30	3.61	N	23	0.62	-0.2	-0.42	0	2	0.24	-0.17	-0.07	0	1.5	1.91	0.09	0.32	0.59	2.1	2.55
01N_02Jun_Aug_S02	6-Jun	12:00	3	N	26	0.93	1.04	-1.97	0	3	-0.39	0.72	-0.33	0	4.5	1.48	0.12	0.49	0.38	1.82	2.21
01N_02Jun_Aug_S03	7-Jun	2:00	2.58	N	22	0.47	-0.15	-0.32	0	1.5	0.17	-0.13	-0.04	0	1.1	1.38	0.07	0.23	0.41	1.52	1.84
01N_02Jun_Aug_S04	14-Jun	1:00	2.58	N	25	0.46	-0.15	-0.31	0	1.5	0.19	-0.13	-0.06	0	1.2	1.38	0.07	0.23	0.41	1.52	1.84
01N_02Jun_Aug_S05	14-Jun	13:00	5	N	29	0.61	0.54	-1.15	0	3.7	0.03	0.48	-0.51	0	3.2	2.6	0.2	0.56	0.75	3.04	3.62
01N_02Jun_Aug_S06	22-Jun	22:00	5	N	26	0.81	-0.24	-0.57	0	2.6	0.34	-0.23	-0.11	0	2.1	2.65	0.14	0.45	0.82	2.91	3.54
01N_02Jun_Aug_S07	23-Jun	1:00	4.64	N	23	0.77	-0.23	-0.54	0	2.5	0.31	-0.22	-0.09	0	1.9	2.44	0.12	0.41	0.75	2.68	3.26
01N_02Jun_Aug_S08	24-Jun	22:00	5.67	N	27	0.93	-0.29	-0.64	0	3	0.38	-0.26	-0.12	0	2.4	3.02	0.16	0.51	0.92	3.32	4.04
01N_02Jun_Aug_S09	8-Jul	5:00	1.56	N	23	0.33	-0.12	-0.21	0	1.1	0.12	-0.09	-0.03	0	0.7	0.85	0.03	0.14	0.25	0.94	1.14
01N_02Jun_Aug_S10	13-Aug	1:00	1.56	N	29	0.31	-0.11	-0.2	0	1	0.12	-0.08	-0.04	0	0.7	0.85	0.04	0.14	0.26	0.94	1.14



02\_NNE\_Jun\_Aug

Scenario	Date	Time	Velocity m/s	Wind Dir.	Temp. °C	Zone										Nodal Velocity m/s					
						GH					SH					01_CRT_16m	02_CRT_7m	03_CRT_2m	04_SSW_7m	05_NNE_7m	06_WNW_7m
						Volume = 1125 m³					Volume = 577 m³										
						Volumetric flow rate (Q) m³/s				ACH 1/h	Volumetric flow rate (Q) m³/s				ACH 1/h						
						NW Court	NE Side	Roof	Σ		SW Court	SE Side	Roof	Σ							
02NNE_01Aug_S01	19-Aug	5:00	2.00	NNE	28	0.13	0.03	-0.16	0	0.5	-0.18	0.31	-0.13	0	1.9	0.98	0.08	0.13	0.6	0.15	0.52
02NNE_01Aug_S02	19-Aug	11:00	2.00	NNE	33	1.19	1.39	-2.58	0	8.3	-0.43	1.12	-0.69	0	7	0.93	0.27	0.41	0.85	0.23	0.6
02NNE_01Aug_S03	20-Aug	11:00	2.60	NNE	33	1.13	1.31	-2.44	0	7.8	-0.52	1.06	-0.54	0	6.6	1.18	0.24	0.41	0.93	0.25	0.75
02NNE_01Aug_S04	21-Aug	4:00	1.00	NNE	28	0.07	0.01	-0.08	0	0.3	-0.09	0.14	-0.05	0	0.9	0.49	0.04	0.06	0.3	0.07	0.26
02NNE_01Aug_S05	22-Aug	8:00	1.60	NNE	28	1.7	1.12	-2.82	0	9	-0.2	0.87	-0.67	0	5.4	0.91	0.18	0.38	0.58	0.27	0.46
02NNE_01Aug_S06	30-Aug	10:00	1.00	NNE	31	1.48	1.47	-2.95	0	9.4	-0.01	1.18	-1.17	0	7.4	0.89	0.28	0.45	0.65	0.38	0.37
02NNE_01Aug_S07	30-Aug	15:00	4.10	NNE	35	0.54	1.17	-1.71	0	5.5	-0.47	1.16	-0.69	0	7.2	2.01	0.33	0.43	1.31	0.43	1.12
02NNE_02Jun_Aug_S01	9-Jun	1:00	4.10	NNE	23	0.44	-0.1	-0.34	0	1.4	-0.31	0.5	-0.19	0	3.1	1.99	0.17	0.27	1.21	0.43	1.1
02NNE_02Jun_Aug_S02	10-Jun	22:00	5.70	NNE	27	0.61	-0.17	-0.44	0	2	-0.43	0.72	-0.29	0	4.5	2.79	0.23	0.37	1.7	0.57	1.52
02NNE_02Jun_Aug_S03	11-Jun	0:00	4.10	NNE	26	0.41	-0.08	-0.33	0	1.3	-0.33	0.55	-0.22	0	3.4	1.98	0.17	0.27	1.2	0.42	1.1
02NNE_02Jun_Aug_S04	14-Jun	4:00	1.60	NNE	24	0.11	0.01	-0.12	0	0.4	-0.14	0.25	-0.11	0	1.6	0.78	0.06	0.1	0.48	0.12	0.42
02NNE_02Jun_Aug_S05	16-Jun	9:00	5.00	NNE	26	1.77	0.91	-2.68	0	8.6	-0.59	0.96	-0.37	0	6	2.43	0.24	0.37	1.55	0.44	1.34
02NNE_02Jun_Aug_S06	16-Jun	10:00	5.00	NNE	29	1.84	0.81	-2.65	0	8.5	-0.52	0.86	-0.34	0	5.4	2.44	0.22	0.37	1.52	0.53	1.35
02NNE_02Jun_Aug_S07	17-Jun	2:00	6.70	NNE	25	0.79	-0.22	-0.57	0	2.5	-0.43	0.76	-0.33	0	4.7	3.29	0.28	0.44	2.01	0.7	1.78
02NNE_02Jun_Aug_S08	17-Jun	3:00	5.70	NNE	24	0.64	-0.16	-0.48	0	2	-0.44	0.73	-0.29	0	4.6	2.78	0.23	0.37	1.73	0.58	1.52
02NNE_02Jun_Aug_S09	17-Jun	9:00	7.20	NNE	27	1.98	0.54	-2.52	0	8.1	-0.53	0.94	-0.41	0	5.9	3.54	0.27	0.35	2.19	0.77	1.93
02NNE_02Jun_Aug_S10	22-Jun	8:00	4.60	NNE	23	1.98	0.81	-2.79	0	8.9	-0.47	0.89	-0.42	0	5.6	2.1	0.22	0.32	1.42	0.68	1.33
02NNE_02Jun_Aug_S11	24-Jun	10:00	1.00	NNE	25	1.62	1.31	-2.93	0	9.4	-0.08	0.95	-0.87	0	5.9	0.85	0.26	0.4	0.66	0.32	0.37
02NNE_02Jun_Aug_S12	27-Jun	5:00	2.00	NNE	23	0.15	0.06	-0.21	0	0.7	-0.19	0.32	-0.13	0	2	0.97	0.08	0.13	0.61	0.17	0.53
02NNE_02Jun_Aug_S13	25-Jul	2:00	2.60	NNE	25	0.15	0.04	-0.19	0	0.6	-0.23	0.36	-0.13	0	2.2	1.27	0.1	0.17	0.8	0.21	0.68
02NNE_02Jun_Aug_S14	27-Jul	22:00	4.10	NNE	29	0.41	-0.09	-0.32	0	1.3	-0.32	0.52	-0.2	0	3.2	1.98	0.17	0.27	1.21	0.42	1.1

## 03\_NE\_Jun\_Aug

Scenario	Date	Time	Velocity m/s	Wind Dir.	Temp. °C	Zone										Nodal Velocity m/s					
						GH					SH					01_CRT_16m	02_CRT_7m	03_CRT_2m	04_SSW_7m	05_NNE_7m	06_WNW_7m
						Volume = 1125 m <sup>3</sup>					Volume = 577 m <sup>3</sup>										
						Volumetric flow rate (Q) m <sup>3</sup> /s				ACH 1/h	Volumetric flow rate (Q) m <sup>3</sup> /s				ACH 1/h						
						NW Court	NE Side	Roof	Σ		SW Court	SE Side	Roof	Σ							
03NE_01Aug_S01	20-Aug	7:00	2.60	NE	28	1.16	0.98	-2.14	0	6.8	-0.59	1.06	-0.47	0	6.6	0.52	0.05	0.28	1.6	0.77	0.76
03NE_01Aug_S02	20-Aug	10:00	1.60	NE	31	1.3	1.39	-2.69	0	8.6	-0.4	1.16	-0.76	0	7.2	0.68	0.2	0.41	1.23	0.6	0.33
03NE_01Aug_S03	21-Aug	8:00	3.00	NE	29	1.41	1.1	-2.51	0	8	-0.76	1.15	-0.39	0	7.2	0.54	0.07	0.31	1.75	0.89	0.78
03NE_01Aug_S04	28-Aug	23:00	3.61	NE	30	0.05	0.36	-0.41	0	1.3	-0.83	1.18	-0.35	0	7.4	0.46	0.18	1.09	1.94	1.11	1
03NE_01Aug_S05	29-Aug	0:00	2.60	NE	30	0.01	0.28	-0.29	0	0.9	-0.49	0.75	-0.26	0	4.7	0.32	0.13	0.79	1.41	0.79	0.72
03NE_01Aug_S06	29-Aug	5:00	2.00	NE	29	0.01	0.23	-0.24	0	0.8	-0.44	0.66	-0.22	0	4.1	0.25	0.1	0.61	1.08	0.63	0.56
03NE_01Aug_S07	29-Aug	22:00	4.60	NE	30	0.02	0.47	-0.49	0	1.6	-0.93	1.35	-0.42	0	8.4	0.59	0.22	1.37	2.49	1.39	1.27
03NE_01Aug_S08	30-Aug	7:00	1.60	NE	28	1.17	1.02	-2.19	0	7	-0.49	0.96	-0.47	0	6	0.44	0.06	0.26	1.02	0.56	0.38
03NE_02Jun_Aug_S01	3-Jun	3:00	3.60	NE	23	0.01	0.38	-0.39	0	1.2	-0.72	1.06	-0.34	0	6.6	0.46	0.18	1.07	1.95	1.09	1
03NE_02Jun_Aug_S02	10-Jun	10:00	3.00	NE	26	1.42	1.17	-2.59	0	8.3	-0.84	1.1	-0.26	0	6.9	0.64	0.1	0.32	1.77	0.95	0.72
03NE_02Jun_Aug_S03	12-Jun	0:00	5.00	NE	26	0.01	0.55	-0.56	0	1.8	-1.01	1.46	-0.45	0	9.1	0.65	0.24	1.5	2.71	1.51	1.39
03NE_02Jun_Aug_S04	12-Jun	5:00	1.00	NE	23	0.19	0.37	-0.56	0	1.8	-0.15	0.48	-0.33	0	3	0.32	0.1	0.23	0.77	0.18	0.33
03NE_02Jun_Aug_S05	14-Jun	23:00	5.70	NE	28	0.03	0.56	-0.59	0	1.9	-1.14	1.66	-0.52	0	10.4	0.74	0.27	1.71	3.09	1.73	1.59
03NE_02Jun_Aug_S06	17-Jun	6:00	5.00	NE	23	0.57	0.96	-1.53	0	4.9	-1.12	1.61	-0.49	0	10	0.76	0.29	1.6	2.87	1.47	1.42
03NE_02Jun_Aug_S07	27-Jun	23:00	4.60	NE	29	0.02	0.46	-0.48	0	1.5	-0.94	1.36	-0.42	0	8.5	0.59	0.23	1.38	2.49	1.39	1.27
03NE_02Jun_Aug_S08	28-Jun	5:00	2.00	NE	24	-0.06	0.27	-0.21	0	0.7	-0.42	0.65	-0.23	0	4.1	0.25	0.08	0.66	1.12	0.59	0.56
03NE_02Jun_Aug_S09	11-Jul	9:00	1.00	NE	28	1.6	1.28	-2.88	0	9.2	-0.34	1.11	-0.77	0	6.9	0.72	0.28	0.39	1.01	0.45	0.3

## 04\_ENE\_Jun\_Aug

Scenario	Date	Time	Velocity m/s	Wind Dir.	Temp. °C	Zone										Nodal Velocity m/s					
						GH					SH					01_CRT_16m	02_CRT_7m	03_CRT_2m	04_SSW_7m	05_NNE_7m	06_WNW_7m
						Volume = 1125 m <sup>3</sup>					Volume = 577 m <sup>3</sup>										
						Volumetric flow rate (Q) m <sup>3</sup> /s				ACH 1/h	Volumetric flow rate (Q) m <sup>3</sup> /s				ACH 1/h						
						NW Court	NE Side	Roof	Σ		SW Court	SE Side	Roof	Σ							
04ENE_01Aug_S01	19-Aug	23:00	3.60	ENE	30	-0.01	0.54	-0.53	0	1.7	-0.99	1.58	-0.59	0	9.9	0.77	0.12	0.82	2.57	1.94	1.85
04ENE_01Aug_S02	20-Aug	9:00	3.00	ENE	30	1.34	1.3	-2.64	0	8.4	-0.75	1.52	-0.77	0	9.5	0.8	0.3	0.34	2.33	1.62	1.46
04ENE_01Aug_S03	30-Aug	5:00	2.00	ENE	28	-0.01	0.29	-0.28	0	0.9	-0.54	0.89	-0.35	0	5.6	0.44	0.06	0.46	1.43	1.09	1.04
04ENE_02Jun_Aug_S01	3-Jun	4:00	3.00	ENE	23	-0.02	0.47	-0.45	0	1.5	-0.8	1.31	-0.51	0	8.2	0.64	0.1	0.7	2.14	1.63	1.55
04ENE_02Jun_Aug_S02	4-Jun	0:00	7.70	ENE	29	-0.03	1.12	-1.09	0	3.6	-2.17	3.35	-1.18	0	20.9	1.67	0.25	1.71	5.48	4.14	3.93
04ENE_02Jun_Aug_S03	4-Jun	4:00	6.20	ENE	28	-0.02	0.92	-0.9	0	2.9	-1.74	2.76	-1.02	0	17.2	1.33	0.2	1.43	4.4	3.34	3.15
04ENE_02Jun_Aug_S04	15-Jun	1:00	3.60	ENE	26	-0.03	0.54	-0.51	0	1.7	-0.97	1.57	-0.6	0	9.8	0.78	0.12	0.8	2.56	1.95	1.86
04ENE_02Jun_Aug_S05	15-Jun	2:00	2.00	ENE	26	-0.01	0.29	-0.28	0	0.9	-0.53	0.89	-0.36	0	5.6	0.44	0.06	0.46	1.43	1.09	1.04
04ENE_02Jun_Aug_S06	16-Jun	0:00	5.70	ENE	28	-0.01	0.82	-0.81	0	2.6	-1.5	2.45	-0.95	0	15.3	1.23	0.19	1.25	4.06	3.06	2.92
04ENE_02Jun_Aug_S07	16-Jun	4:00	5.00	ENE	26	-0.03	0.69	-0.66	0	2.2	-1.32	2.11	-0.79	0	13.2	1.1	0.17	1.09	3.55	2.7	2.57
04ENE_02Jun_Aug_S08	16-Jul	5:00	1.00	ENE	23	-0.01	0.16	-0.15	0	0.5	-0.28	0.47	-0.19	0	2.9	0.2	0.03	0.23	0.71	0.54	0.51

## 13\_W\_Jun\_Aug

Scenario	Date	Time	Velocity m/s	Wind Dir.	Temp. °C	Zone										Nodal Velocity m/s					
						GH					SH					01_CRT_16m	02_CRT_7m	03_CRT_2m	04_SSW_7m	05_NNE_7m	06_WNW_7m
						Volume = 1125 m <sup>3</sup>					Volume = 577 m <sup>3</sup>										
						Volumetric flow rate (Q) m <sup>3</sup> /s				ACH 1/h	Volumetric flow rate (Q) m <sup>3</sup> /s				ACH 1/h						
						NW Court	NE Side	Roof	Σ		SW Court	SE Side	Roof	Σ							
13W_01Aug_S01	23-Aug	8:00	2.60	W	28	2.45	0.01	-2.46	0	7.9	1.23	0.16	-1.39	0	8.7	1.33	0.38	0.17	0.26	2.77	2.07
13W_01Aug_S02	27-Aug	14:00	5.10	W	35	2.8	-1.24	-1.56	0	9	1.55	-0.16	-1.39	0	9.7	2.55	0.64	0.41	0.37	5.2	3.84
13W_02Jun_Aug_S01	7-Jun	11:00	3.00	W	26	1.76	-0.91	-0.85	0	5.6	1.5	0.09	-1.59	0	9.9	1.7	0.14	0.35	0.34	3.36	2.67
13W_02Jun_Aug_S02	7-Jun	15:00	5.00	W	29	2.8	-1.28	-1.52	0	9	1.48	-0.36	-1.12	0	9.2	2.35	0.44	0.31	0.59	4.73	3.23
13W_02Jun_Aug_S03	4-Jul	3:00	3.00	W	23	1.35	-0.97	-0.38	0	4.3	0.94	-0.78	-0.16	0	5.9	1.45	0.13	0.19	0.36	2.84	1.93
13W_02Jun_Aug_S04	4-Jul	6:00	2.60	W	24	2.09	-0.21	-1.88	0	6.7	0.94	0.05	-0.99	0	6.2	1.28	0.25	0.19	0.33	2.5	1.68
13W_02Jun_Aug_S05	4-Jul	23:00	5.70	W	25	2.57	-1.88	-0.69	0	8.2	1.78	-1.46	-0.32	0	11.1	2.74	0.23	0.35	0.66	5.42	3.7
13W_02Jun_Aug_S06	5-Jul	2:00	4.60	W	23	2.07	-1.46	-0.61	0	6.6	1.43	-1.18	-0.25	0	8.9	2.21	0.19	0.29	0.54	4.37	2.97
13W_02Jun_Aug_S07	6-Jul	11:00	3.60	W	29	1.94	-1.06	-0.88	0	6.2	1.64	-0.13	-1.51	0	10.2	1.87	0.12	0.35	0.24	3.76	2.79
13W_02Jun_Aug_S08	15-Jul	8:00	1.60	W	25	2.53	-0.15	-2.38	0	8.1	1.52	0.28	-1.8	0	11.2	0.8	0.34	0.32	0.2	1.69	1.03

## 14\_WNW\_Jun\_Aug

Scenario	Date	Time	Velocity m/s	Wind Dir.	Temp. °C	Zone										Nodal Velocity m/s					
						GH					SH					01_CRT_16m	02_CRT_7m	03_CRT_2m	04_SSW_7m	05_NNE_7m	06_WNW_7m
						Volume = 1125 m <sup>3</sup>					Volume = 577 m <sup>3</sup>										
						Volumetric flow rate (Q) m <sup>3</sup> /s				ACH 1/h	Volumetric flow rate (Q) m <sup>3</sup> /s				ACH 1/h						
						NW Court	NE Side	Roof	Σ		SW Court	SE Side	Roof	Σ							
14WNW_01Aug_S01	20-Aug	13:00	3.60	WNW	35	1.58	-0.1	-1.48	0	5.1	1.03	0.31	-1.34	0	8.4	2.72	0.52	0.6	0.47	4.29	2.92
14WNW_01Aug_S02	22-Aug	13:00	3.00	WNW	34	1.34	0.42	-1.76	0	5.6	0.83	0.51	-1.34	0	8.3	2.24	0.64	0.36	0.39	3.6	2.44
14WNW_01Aug_S03	23-Aug	11:00	2.00	WNW	33	2.08	0.84	-2.92	0	9.3	0.89	0.46	-1.35	0	8.4	1.49	0.23	0.54	0.2	2.45	1.63
14WNW_01Aug_S04	23-Aug	13:00	4.10	WNW	36	1.87	-0.46	-1.41	0	6	1.25	0.12	-1.37	0	8.6	3.15	0.57	0.6	0.55	4.9	3.32
14WNW_01Aug_S05	24-Aug	13:00	3.00	WNW	37	1.16	0.45	-1.61	0	5.2	0.87	0.6	-1.47	0	9.2	2.29	0.61	0.43	0.37	3.64	2.43
14WNW_01Aug_S06	24-Aug	21:00	3.60	WNW	31	1.69	-1.04	-0.65	0	5.4	1.27	-0.89	-0.38	0	7.9	2.8	0.49	0.4	0.51	4.3	2.91
14WNW_01Aug_S07	25-Aug	1:00	3.00	WNW	29	1.5	-0.97	-0.53	0	4.8	1.06	-0.72	-0.34	0	6.6	2.33	0.4	0.34	0.42	3.58	2.42
14WNW_01Aug_S08	25-Aug	2:00	2.00	WNW	28	0.98	-0.62	-0.36	0	3.1	0.71	-0.48	-0.23	0	4.4	1.54	0.26	0.22	0.29	2.37	1.61
14WNW_01Aug_S09	27-Aug	12:00	3.60	WNW	34	1.97	0.2	-2.17	0	6.9	1.11	0.16	-1.27	0	7.9	2.72	0.54	0.55	0.47	4.35	2.91
14WNW_01Aug_S10	27-Aug	13:00	4.10	WNW	34	1.96	-0.55	-1.41	0	6.3	1.25	0.11	-1.36	0	8.5	3.1	0.56	0.57	0.54	4.88	3.33
14WNW_02Jun_Aug_S01	5-Jun	3:00	3.60	WNW	26	1.76	-1.12	-0.64	0	5.6	1.25	-0.84	-0.41	0	7.8	2.8	0.47	0.4	0.51	4.3	2.91
14WNW_02Jun_Aug_S02	5-Jun	10:00	4.60	WNW	25	2.94	-0.72	-2.22	0	9.4	1.61	-0.85	-0.76	0	10	3.54	0.55	0.56	0.64	5.51	3.73
14WNW_02Jun_Aug_S03	5-Jun	20:00	6.20	WNW	27	3.02	-1.93	-1.09	0	9.7	2.16	-1.45	-0.71	0	13.5	4.81	0.81	0.69	0.87	7.5	5.04
14WNW_02Jun_Aug_S04	25-Jun	4:00	3.00	WNW	23	1.5	-0.96	-0.54	0	4.8	1.06	-0.73	-0.33	0	6.6	2.33	0.41	0.34	0.42	3.58	2.42
14WNW_02Jun_Aug_S05	4-Jul	5:00	2.00	WNW	23	1	-0.64	-0.36	0	3.2	0.69	-0.47	-0.22	0	4.3	1.55	0.26	0.22	0.29	2.38	1.61
14WNW_02Jun_Aug_S06	4-Jul	9:00	2.60	WNW	26	3.11	0.17	-3.28	0	10.5	1.11	-0.3	-0.81	0	6.9	1.97	0.46	0.14	0.32	3.14	2.13
14WNW_02Jun_Aug_S07	4-Jul	21:00	4.60	WNW	28	2.19	-1.4	-0.79	0	7	1.62	-1.09	-0.53	0	10.1	3.58	0.62	0.52	0.64	5.5	3.73

## 15\_NW\_01\_18\_31\_Aug

Scenario	Date	Time	Velocity m/s	Wind Dir.	Temp. °C	Zone										Nodal Velocity m/s					
						GH					SH					01_CRT_16m	02_CRT_7m	03_CRT_2m	04_SSW_7m	05_NNE_7m	06_WNW_7m
						Volume = 1125 m <sup>3</sup>					Volume = 577 m <sup>3</sup>										
						Volumetric flow rate (Q) m <sup>3</sup> /s				ACH 1/h	Volumetric flow rate (Q) m <sup>3</sup> /s				ACH 1/h						
						NW Court	NE Side	Roof	Σ		SW Court	SE Side	Roof	Σ							
15NW_01Aug_S01	18-Aug	3:00	3.00	NW	28	0.32	-0.23	-0.09	0	1	0.31	0.17	-0.48	0	3	2.71	0.48	0.44	0.34	3.09	2.67
15NW_01Aug_S02	18-Aug	10:00	3.00	NW	31	1.67	1.04	-2.71	0	8.7	0.6	0.43	-1.03	0	6.4	2.34	0.19	0.5	0.33	3.04	2.68
15NW_01Aug_S03	18-Aug	12:00	1.20	NW	35	1.19	1.15	-2.34	0	7.5	0.45	0.78	-1.23	0	7.7	1.1	0.22	0.59	0.12	1.35	1.1
15NW_01Aug_S04	18-Aug	13:00	2.60	NW	35	0.52	1.14	-1.66	0	5.3	0.24	0.91	-1.15	0	7.2	2.21	0.55	0.4	0.33	2.68	2.32
15NW_01Aug_S05	18-Aug	16:00	3.00	NW	36	0.82	0.92	-1.74	0	5.6	0.47	0.78	-1.25	0	7.8	2.71	0.69	0.32	0.41	3.12	2.67
15NW_01Aug_S06	19-Aug	12:00	2.00	NW	34	1.02	1.23	-2.25	0	7.2	0.25	0.86	-1.11	0	6.9	1.7	0.59	0.37	0.19	2.09	1.79
15NW_01Aug_S07	19-Aug	17:00	3.60	NW	34	0.7	0.64	-1.34	0	4.3	0.52	0.6	-1.12	0	7	3.21	0.69	0.43	0.49	3.72	3.23
15NW_01Aug_S08	22-Aug	12:00	1.00	NW	34	1.13	1.2	-2.33	0	7.5	0.49	0.82	-1.31	0	8.2	1.02	0.26	0.54	0.11	1.16	0.93
15NW_01Aug_S09	22-Aug	15:00	4.60	NW	36	0.56	0.71	-1.27	0	4.1	0.6	0.78	-1.38	0	8.6	4.16	0.84	0.68	0.53	4.76	4.1
15NW_01Aug_S10	22-Aug	16:00	4.10	NW	36	0.58	0.78	-1.36	0	4.4	0.5	0.75	-1.25	0	7.8	3.68	0.72	0.55	0.5	4.24	3.65
15NW_01Aug_S11	22-Aug	21:00	4.10	NW	31	0.44	-0.31	-0.13	0	1.4	0.41	0.24	-0.65	0	4.1	3.69	0.64	0.59	0.45	4.22	3.66
15NW_01Aug_S12	23-Aug	0:00	3.60	NW	29	0.35	-0.24	-0.11	0	1.1	0.36	0.22	-0.58	0	3.6	3.23	0.55	0.51	0.4	3.7	3.22
15NW_01Aug_S13	23-Aug	3:00	2.60	NW	28	0.24	-0.17	-0.07	0	0.8	0.25	0.17	-0.42	0	2.6	2.36	0.4	0.39	0.29	2.68	2.32
15NW_01Aug_S14	23-Aug	9:00	1.60	NW	29	1.69	1.12	-2.81	0	9	0.6	0.42	-1.02	0	6.4	1.3	0.2	0.48	0.24	1.7	1.45
15NW_01Aug_S15	24-Aug	16:00	3.60	NW	37	0.61	0.89	-1.5	0	4.8	0.46	0.77	-1.23	0	7.7	3.22	0.66	0.45	0.44	3.73	3.21
15NW_01Aug_S16	24-Aug	22:00	3.60	NW	31	0.38	-0.26	-0.12	0	1.2	0.37	0.21	-0.58	0	3.6	3.24	0.54	0.52	0.4	3.71	3.21
15NW_01Aug_S17	25-Aug	10:00	2.00	NW	31	1.67	1.1	-2.77	0	8.9	0.44	0.57	-1.01	0	6.3	1.54	0.19	0.47	0.26	2.08	1.79
15NW_01Aug_S18	26-Aug	15:00	3.00	NW	38	0.65	1.04	-1.69	0	5.4	0.44	0.87	-1.31	0	8.2	2.72	0.67	0.35	0.43	3.13	2.67
15NW_01Aug_S19	26-Aug	8:00	0.50	NW	28	1.57	1.3	-2.87	0	9.2	0.61	0.4	-1.01	0	6.3	0.52	0.46	0.25	0.15	0.7	0.51
15NW_01Aug_S20	27-Aug	3:00	1.00	NW	29	0.1	-0.08	-0.02	0	0.3	0.1	0.06	-0.16	0	1	0.91	0.17	0.15	0.12	1.02	0.9
15NW_01Aug_S21	27-Aug	10:00	2.60	NW	31	1.57	1.15	-2.72	0	8.7	0.5	0.57	-1.07	0	6.7	2.05	0.21	0.55	0.27	2.66	2.32
15NW_01Aug_S22	27-Aug	15:00	5.70	NW	35	0.6	0.53	-1.13	0	3.6	0.66	0.77	-1.43	0	8.9	5.13	0.94	0.88	0.65	5.91	5.09
15NW_01Aug_S23	31-Aug	5:00	2.00	NW	28	0.18	-0.13	-0.05	0	0.6	0.19	0.13	-0.32	0	2	1.81	0.32	0.29	0.22	2.05	1.79
15NW_01Aug_S24	31-Aug	12:00	3.00	NW	33	1.07	1.11	-2.18	0	7	0.35	0.86	-1.21	0	7.5	2.68	0.6	0.62	0.36	3.14	2.67
15NW_01Aug_S25	31-Aug	17:00	4.10	NW	33	0.53	0.51	-1.04	0	3.3	0.47	0.6	-1.07	0	6.7	3.68	0.69	0.59	0.47	4.24	3.65
15NW_01Aug_S26	31-Aug	19:00	4.60	NW	31	0.47	-0.32	-0.15	0	1.5	0.46	0.28	-0.74	0	4.6	4.14	0.72	0.66	0.5	4.73	4.12

## 15\_NW\_02\_Jun\_Aug

Scenario	Date	Time	Velocity m/s	Wind Dir.	Temp. °C	Zone										Nodal Velocity m/s					
						GH					SH					01_CRT_16m	02_CRT_7m	03_CRT_2m	04_SSW_7m	05_NNE_7m	06_WNW_7m
						Volume = 1125 m <sup>3</sup>					Volume = 577 m <sup>3</sup>										
						Volumetric flow rate (Q) m <sup>3</sup> /s				ACH 1/h	Volumetric flow rate (Q) m <sup>3</sup> /s				ACH 1/h						
						NW Court	NE Side	Roof	Σ		SW Court	SE Side	Roof	Σ							
15NW_02Jun_Aug_S01	1-Jun	10:00	2.60	NW	23	1.43	1.2	-2.63	0	8.4	0.36	0.51	-0.87	0	5.4	2.24	0.21	0.59	0.25	2.7	2.32
15NW_02Jun_Aug_S02	1-Jun	20:00	5.70	NW	27	0.63	-0.41	-0.22	0	2	0.58	0.33	-0.91	0	5.7	5.14	0.88	0.83	0.63	5.87	5.11
15NW_02Jun_Aug_S03	5-Jun	8:00	4.00	NW	23	1.85	0.75	-2.6	0	8.3	0.69	0.26	-0.95	0	5.9	3.53	0.84	0.25	0.49	4.17	3.64
15NW_02Jun_Aug_S04	6-Jun	18:00	5.00	NW	29	0.7	0.15	-0.85	0	2.7	0.59	0.5	-1.09	0	6.8	4.43	0.8	0.7	0.55	5.17	4.5
15NW_02Jun_Aug_S05	6-Jun	20:00	6.20	NW	27	0.7	-0.49	-0.21	0	2.2	0.65	0.34	-0.99	0	6.2	5.55	0.94	0.88	0.68	6.4	5.55
15NW_02Jun_Aug_S06	20-Jun	20:00	7.20	NW	29	0.82	-0.55	-0.27	0	2.6	0.76	0.4	-1.16	0	7.2	6.48	1.1	1.04	0.78	7.43	6.47
15NW_02Jun_Aug_S07	20-Jun	22:00	5.00	NW	25	0.53	-0.38	-0.15	0	1.7	0.51	0.29	-0.8	0	5	4.5	0.79	0.72	0.55	5.15	4.47
15NW_02Jun_Aug_S08	21-Jun	11:00	3.00	NW	26	1.4	0.98	-2.38	0	7.6	0.37	0.44	-0.81	0	5.1	2.53	0.5	0.17	0.35	3.07	2.68
15NW_02Jun_Aug_S09	3-Aug	4:00	2.00	NW	25	0.21	-0.15	-0.06	0	0.7	0.2	0.12	-0.32	0	2	1.82	0.33	0.29	0.23	2.06	1.79

## 16\_NNW\_01\_18\_31\_Aug

Scenario	Date	Time	Velocity m/s	Wind Dir.	Temp. °C	Zone										Nodal Velocity m/s					
						GH					SH					01_CRT_16m	02_CRT_7m	03_CRT_2m	04_SSW_7m	05_NNE_7m	06_WNW_7m
						Volume = 1125 m³					Volume = 577 m³										
						Volumetric flow rate (Q) m³/s				ACH 1/h	Volumetric flow rate (Q) m³/s				ACH 1/h						
						NW Court	NE Side	Roof	Σ		SW Court	SE Side	Roof	Σ							
16NNW_01Aug_S01	18-Aug	8:00	1.60	NNW	28	1.84	0.85	-2.69	0	8.6	0.3	0.34	-0.64	0	4	1.02	0.31	0.29	0.32	1.41	1.49
16NNW_01Aug_S02	18-Aug	14:00	1.60	NNW	36	0.01	1.42	-1.43	0	4.6	-0.53	1.36	-0.83	0	8.5	1.18	0.62	0.31	0.26	1.43	1.52
16NNW_01Aug_S03	18-Aug	15:00	3.00	NNW	36	0.15	1.22	-1.37	0	4.4	-0.24	1.09	-0.85	0	6.8	2.06	0.59	0.26	0.44	2.66	2.79
16NNW_01Aug_S04	18-Aug	18:00	3.60	NNW	34	0.12	0.53	-0.65	0	2.1	0.04	0.49	-0.53	0	3.3	2.53	0.58	0.44	0.45	3.08	3.33
16NNW_01Aug_S05	18-Aug	23:30	3.60	NNW	29	0.02	0.26	-0.28	0	0.9	0.02	0.31	-0.33	0	2.1	2.54	0.54	0.48	0.55	3.04	3.28
16NNW_01Aug_S06	19-Aug	13:00	1.00	NNW	35	0.3	1.32	-1.62	0	5.2	0.06	1.13	-1.19	0	7.2	1.03	0.34	0.76	0.15	0.95	1
16NNW_01Aug_S07	20-Aug	18:00	5.10	NNW	32	0.19	0.46	-0.65	0	2.1	0.09	0.5	-0.59	0	3.7	3.73	0.82	0.63	0.71	4.49	4.67
16NNW_01Aug_S08	21-Aug	13:00	3.00	NNW	34	0.32	1.09	-1.41	0	4.5	-0.12	0.97	-0.85	0	6.1	2.03	0.36	0.31	0.43	2.65	2.79
16NNW_01Aug_S09	21-Aug	17:00	6.70	NNW	33	0.06	0.83	-0.89	0	2.8	0.02	0.75	-0.77	0	4.8	4.72	1	0.88	0.91	5.73	6.13
16NNW_01Aug_S10	22-Aug	14:00	5.10	NNW	35	0.21	0.81	-1.02	0	3.3	0.14	0.81	-0.95	0	5.9	3.68	0.98	0.51	0.69	4.45	4.68
16NNW_01Aug_S11	22-Aug	19:00	4.60	NNW	33	0.03	0.31	-0.34	0	1.1	0.02	0.36	-0.38	0	2.4	3.25	0.68	0.61	0.69	3.92	4.2
16NNW_01Aug_S12	23-Aug	5:00	1.00	NNW	28	0.01	0.08	-0.09	0	0.3	0.01	0.08	-0.09	0	0.6	0.72	0.16	0.13	0.14	0.84	0.91
16NNW_01Aug_S13	23-Aug	16:00	4.60	NNW	37	0.47	0.8	-1.27	0	4.1	0.19	0.73	-0.92	0	5.7	3.3	0.86	0.34	0.64	4.02	4.22
16NNW_01Aug_S14	24-Aug	10:00	2.00	NNW	31	1.82	0.98	-2.8	0	9	0.03	0.74	-0.77	0	4.8	1.3	0.6	0.47	0.36	1.74	1.86
16NNW_01Aug_S15	24-Aug	11:00	1.60	NNW	33	1.16	1.26	-2.42	0	7.7	0.03	0.85	-0.88	0	5.5	1.19	0.29	0.33	0.29	1.43	1.51
16NNW_01Aug_S16	25-Aug	4:00	2.60	NNW	28	0.02	0.21	-0.23	0	0.7	0.01	0.22	-0.23	0	1.4	1.83	0.4	0.35	0.38	2.19	2.36
16NNW_01Aug_S17	26-Aug	14:00	3.60	NNW	37	0.03	1.1	-1.13	0	3.6	0.11	0.96	-1.07	0	6.7	2.45	0.55	0.31	0.49	3.07	3.31
16NNW_01Aug_S18	27-Aug	20:00	3.00	NNW	31	0.03	0.24	-0.27	0	0.9	0.01	0.26	-0.27	0	1.7	2.11	0.45	0.4	0.45	2.53	2.73
16NNW_01Aug_S19	28-Aug	7:00	2.00	NNW	27	1.51	0.67	-2.18	0	7	0.19	0.35	-0.54	0	3.4	1.24	0.27	0.25	0.32	1.76	1.86
16NNW_01Aug_S20	29-Aug	14:00	2.60	NNW	36	0.04	1.33	-1.37	0	4.4	-0.38	1.19	-0.81	0	7.4	1.71	0.7	0.39	0.4	2.25	2.41
16NNW_01Aug_S21	29-Aug	16:00	2.00	NNW	36	0.47	1.24	-1.71	0	5.5	-0.26	1.13	-0.87	0	7.1	1.38	0.5	0.22	0.31	1.8	1.88
16NNW_01Aug_S22	30-Aug	14:00	4.10	NNW	36	0.5	0.91	-1.41	0	4.5	0.19	0.84	-1.03	0	6.4	2.95	0.67	0.31	0.56	3.61	3.76
16NNW_01Aug_S23	31-Aug	8:00	3.00	NNW	28	1.73	0.8	-2.53	0	8.1	0.07	0.53	-0.6	0	3.7	2.02	0.33	0.24	0.47	2.61	2.75
16NNW_01Aug_S24	31-Aug	13:00	2.60	NNW	33	0.12	1.25	-1.37	0	4.4	-0.27	1.1	-0.83	0	6.9	1.71	0.33	0.27	0.4	2.29	2.42
16NNW_01Aug_S25	31-Aug	18:00	4.10	NNW	32	0.15	0.37	-0.52	0	1.7	0.07	0.41	-0.48	0	3	3.01	0.67	0.5	0.54	3.62	3.76
16NNW_01Aug_S26	31-Aug	21:00	4.10	NNW	29	0.03	0.32	-0.35	0	1.1	0.02	0.35	-0.37	0	2.3	2.88	0.61	0.55	0.63	3.47	3.73

16\_NNW\_02\_Jun\_Aug

Scenario	Date	Time	Velocity m/s	Wind Dir.	Temp. °C	Zone										Nodal Velocity m/s					
						GH					SH					01_CRT_16m	02_CRT_7m	03_CRT_2m	04_SSW_7m	05_NNE_7m	06_WNW_7m
						Volume = 1125 m <sup>3</sup>					Volume = 577 m <sup>3</sup>										
						Volumetric flow rate (Q) m <sup>3</sup> /s				ACH 1/h	Volumetric flow rate (Q) m <sup>3</sup> /s				ACH 1/h						
						NW Court	NE Side	Roof	Σ		SW Court	SE Side	Roof	Σ							
16NNW_02Jun_Aug_S01	1-Jun	0:00	3.00	NNW	23	0.02	0.23	-0.25	0	0.8	0.02	0.25	-0.27	0	1.7	2.12	0.46	0.4	0.44	2.54	2.73
16NNW_02Jun_Aug_S02	2-Jun	11:00	0.50	NNW	25	1.16	1.25	-2.41	0	7.7	0.19	0.83	-1.02	0	6.4	0.68	0.15	0.52	0.14	0.56	0.57
16NNW_02Jun_Aug_S03	5-Jun	21:00	5.70	NNW	25	0.02	0.39	-0.41	0	1.3	0.02	0.46	-0.48	0	3	4.01	0.84	0.75	0.86	4.85	5.2
16NNW_02Jun_Aug_S04	6-Jun	19:00	5.70	NNW	28	0.01	0.4	-0.41	0	1.3	0.02	0.45	-0.47	0	2.9	4	0.83	0.75	0.84	4.82	5.2
16NNW_02Jun_Aug_S05	12-Jun	23:00	3.60	NNW	26	0.02	0.28	-0.3	0	1	0.01	0.31	-0.32	0	2	2.54	0.53	0.48	0.54	3.05	3.28
16NNW_02Jun_Aug_S06	13-Jun	9:00	1.60	NNW	23	1.98	0.85	-2.83	0	9.1	0.37	0.34	-0.71	0	4.4	1.02	0.36	0.33	0.31	1.45	1.52
16NNW_02Jun_Aug_S07	22-Jun	21:00	6.20	NNW	27	0.03	0.42	-0.45	0	1.4	0.03	0.49	-0.52	0	3.2	4.35	0.9	0.81	0.98	5.24	5.65
16NNW_02Jun_Aug_S08	23-Jun	23:00	4.60	NNW	25	0.01	0.33	-0.34	0	1.1	0.01	0.38	-0.39	0	2.4	3.24	0.68	0.61	0.7	3.91	4.2
16NNW_02Jun_Aug_S09	24-Jun	21:00	5.00	NNW	29	0.02	0.35	-0.37	0	1.2	0.02	0.41	-0.43	0	2.7	3.53	0.74	0.66	0.75	4.26	4.55

## A.2. Modified Model

### A.2.1. Modified Model (1) side window excluded

#### 14\_WNW\_Jun\_Aug

Scenario	Date	Time	Velocity m/s	Wind Dir.	Temp. °C	Zone							
						GH				SH			
						Volume = 1125 m <sup>3</sup>				Volume = 577 m <sup>3</sup>			
						Volumetric flow rate (Q) m <sup>3</sup> /s			ACH 1/h	Volumetric flow rate (Q) m <sup>3</sup> /s			ACH 1/h
						NW Court	Roof	Σ		SW Court	Roof	Σ	
14WNW_01Aug_S01	20-Aug	13:00	3.60	WNW	35	1.57	-1.57	0	5.024	1.24	-1.24	0	7.73657
14WNW_01Aug_S02	22-Aug	13:00	3.00	WNW	34	1.62	-1.62	0	5.184	1.18	-1.18	0	7.36222
14WNW_01Aug_S03	23-Aug	11:00	2.00	WNW	33	2.98	-2.98	0	9.536	1.05	-1.05	0	6.55113
14WNW_01Aug_S04	23-Aug	13:00	4.10	WNW	36	1.57	-1.57	0	5.024	1.31	-1.31	0	8.17331
14WNW_01Aug_S05	24-Aug	13:00	3.00	WNW	37	1.65	-1.65	0	5.28	1.22	-1.22	0	7.61179
14WNW_01Aug_S06	24-Aug	21:00	3.60	WNW	31	0.77	-0.77	0	2.464	0.78	-0.78	0	4.86655
14WNW_01Aug_S07	25-Aug	1:00	3.00	WNW	29	0.65	-0.65	0	2.08	0.67	-0.67	0	4.18024
14WNW_01Aug_S08	25-Aug	2:00	2.00	WNW	28	0.45	-0.45	0	1.44	0.43	-0.43	0	2.68284
14WNW_01Aug_S09	27-Aug	12:00	3.60	WNW	34	2.26	-2.26	0	7.232	1.23	-1.23	0	7.67418
14WNW_01Aug_S10	27-Aug	13:00	4.10	WNW	34	1.59	-1.59	0	5.088	1.32	-1.32	0	8.2357
14WNW_02Jun_Aug_S01	5-Jun	3:00	3.60	WNW	26	0.83	-0.83	0	2.656	0.8	-0.8	0	4.99133
14WNW_02Jun_Aug_S02	5-Jun	10:00	4.60	WNW	25	2.58	-2.58	0	8.256	1.16	-1.16	0	7.23744
14WNW_02Jun_Aug_S03	5-Jun	20:00	6.20	WNW	27	1.37	-1.37	0	4.384	1.42	-1.42	0	8.85962
14WNW_02Jun_Aug_S04	25-Jun	4:00	3.00	WNW	23	0.67	-0.67	0	2.144	0.67	-0.67	0	4.18024
14WNW_02Jun_Aug_S05	4-Jul	5:00	2.00	WNW	23	0.42	-0.42	0	1.344	0.43	-0.43	0	2.68284
14WNW_02Jun_Aug_S06	4-Jul	9:00	2.60	WNW	26	3.25	-3.25	0	10.4	0.94	-0.94	0	5.86482
14WNW_02Jun_Aug_S07	4-Jul	21:00	4.60	WNW	28	1.04	-1.04	0	3.328	1.02	-1.02	0	6.36395

## A.2.2. Modified Model (2) Wind-escape excluded

### 14\_WNW\_Jun\_Aug

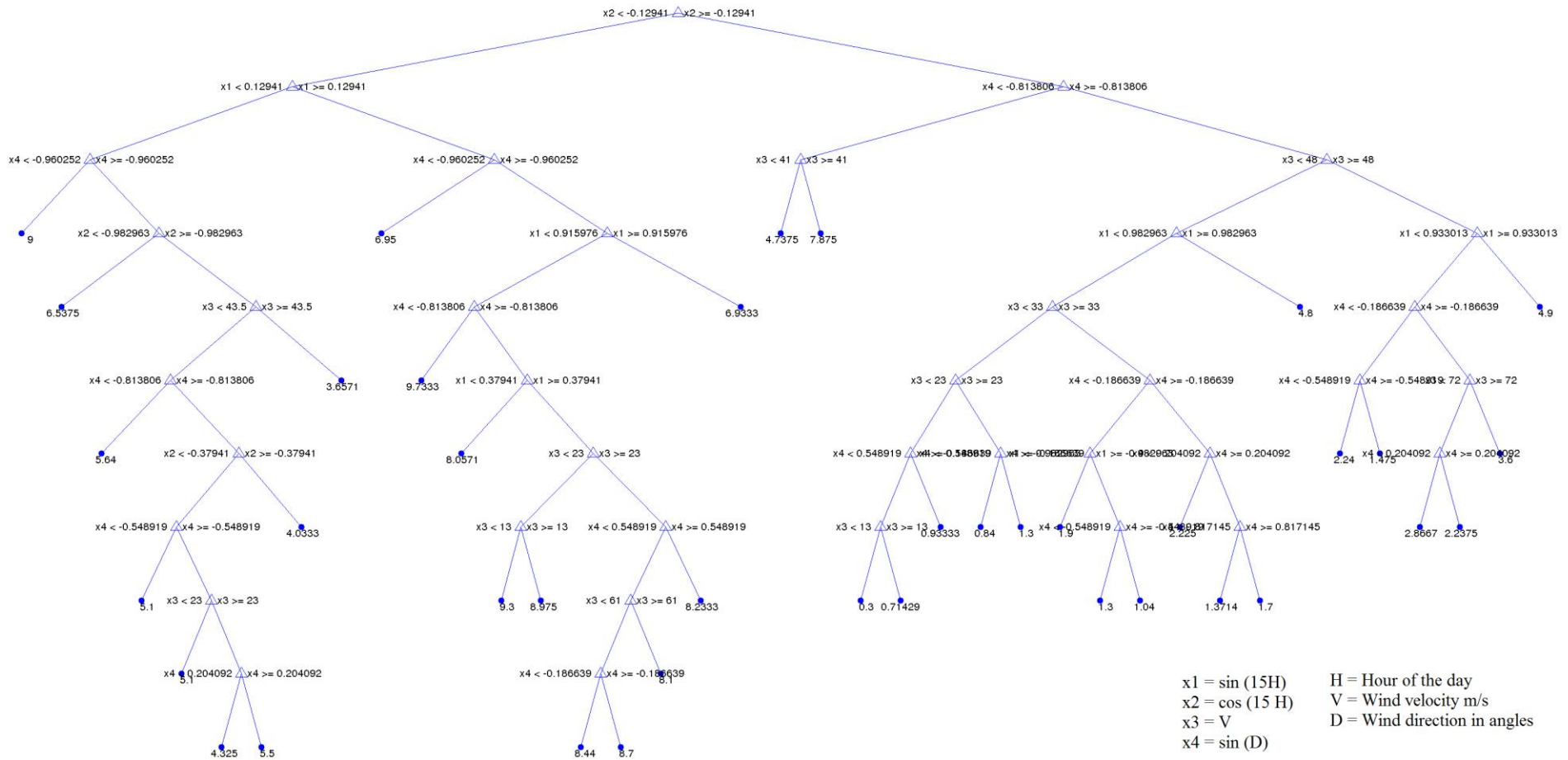
Scenario	Date	Time	Velocity m/s	Wind Dir.	Temp. °C	Zone							
						GH				SH			
						Volume = 1125 m <sup>3</sup>				Volume = 577 m <sup>3</sup>			
						Volumetric flow rate (Q) m <sup>3</sup> /s			ACH 1/h	Volumetric flow rate (Q) m <sup>3</sup> /s			ACH 1/h
						NW Court	Roof	Σ		SW Court	Roof	Σ	
14WNW_01Aug_S01	20-Aug	13:00	3.60	WNW	35	0.39	-0.39	0	1.248	0.33	-0.33	0	2.05893
14WNW_01Aug_S02	22-Aug	13:00	3.00	WNW	34	0.11	-0.11	0	0.352	0.06	-0.06	0	0.37435
14WNW_01Aug_S03	23-Aug	11:00	2.00	WNW	33	0.45	-0.45	0	1.44	0.28	-0.28	0	1.74697
14WNW_01Aug_S04	23-Aug	13:00	4.10	WNW	36	0.71	-0.71	0	2.272	0.6	-0.6	0	3.7435
14WNW_01Aug_S05	24-Aug	13:00	3.00	WNW	37	0.12	-0.12	0	0.384	0.07	-0.07	0	0.43674
14WNW_01Aug_S06	24-Aug	21:00	3.60	WNW	31	1.31	-1.31	0	4.192	1.02	-1.02	0	6.36395
14WNW_01Aug_S07	25-Aug	1:00	3.00	WNW	29	1.04	-1.04	0	3.328	0.83	-0.83	0	5.17851
14WNW_01Aug_S08	25-Aug	2:00	2.00	WNW	28	0.72	-0.72	0	2.304	0.57	-0.57	0	3.55633
14WNW_01Aug_S09	27-Aug	12:00	3.60	WNW	34	0.22	-0.22	0	0.704	0.46	-0.46	0	2.87002
14WNW_01Aug_S10	27-Aug	13:00	4.10	WNW	34	0.91	-0.91	0	2.912	0.68	-0.68	0	4.24263
14WNW_02Jun_Aug_S01	5-Jun	3:00	3.60	WNW	26	1.29	-1.29	0	4.128	0.91	-0.91	0	5.67764
14WNW_02Jun_Aug_S02	5-Jun	10:00	4.60	WNW	25	1.18	-1.18	0	3.776	1.38	-1.38	0	8.61005
14WNW_02Jun_Aug_S03	5-Jun	20:00	6.20	WNW	27	2.26	-2.26	0	7.232	1.74	-1.74	0	10.8562
14WNW_02Jun_Aug_S04	25-Jun	4:00	3.00	WNW	23	0.93	-0.93	0	2.976	0.77	-0.77	0	4.80416
14WNW_02Jun_Aug_S05	4-Jul	5:00	2.00	WNW	23	0.61	-0.61	0	1.952	0.55	-0.55	0	3.43154
14WNW_02Jun_Aug_S06	4-Jul	9:00	2.60	WNW	26	0.11	-0.11	0	0.352	0.71	-0.71	0	4.42981
14WNW_02Jun_Aug_S07	4-Jul	21:00	4.60	WNW	28	1.43	-1.43	0	4.576	1.31	-1.31	0	8.17331



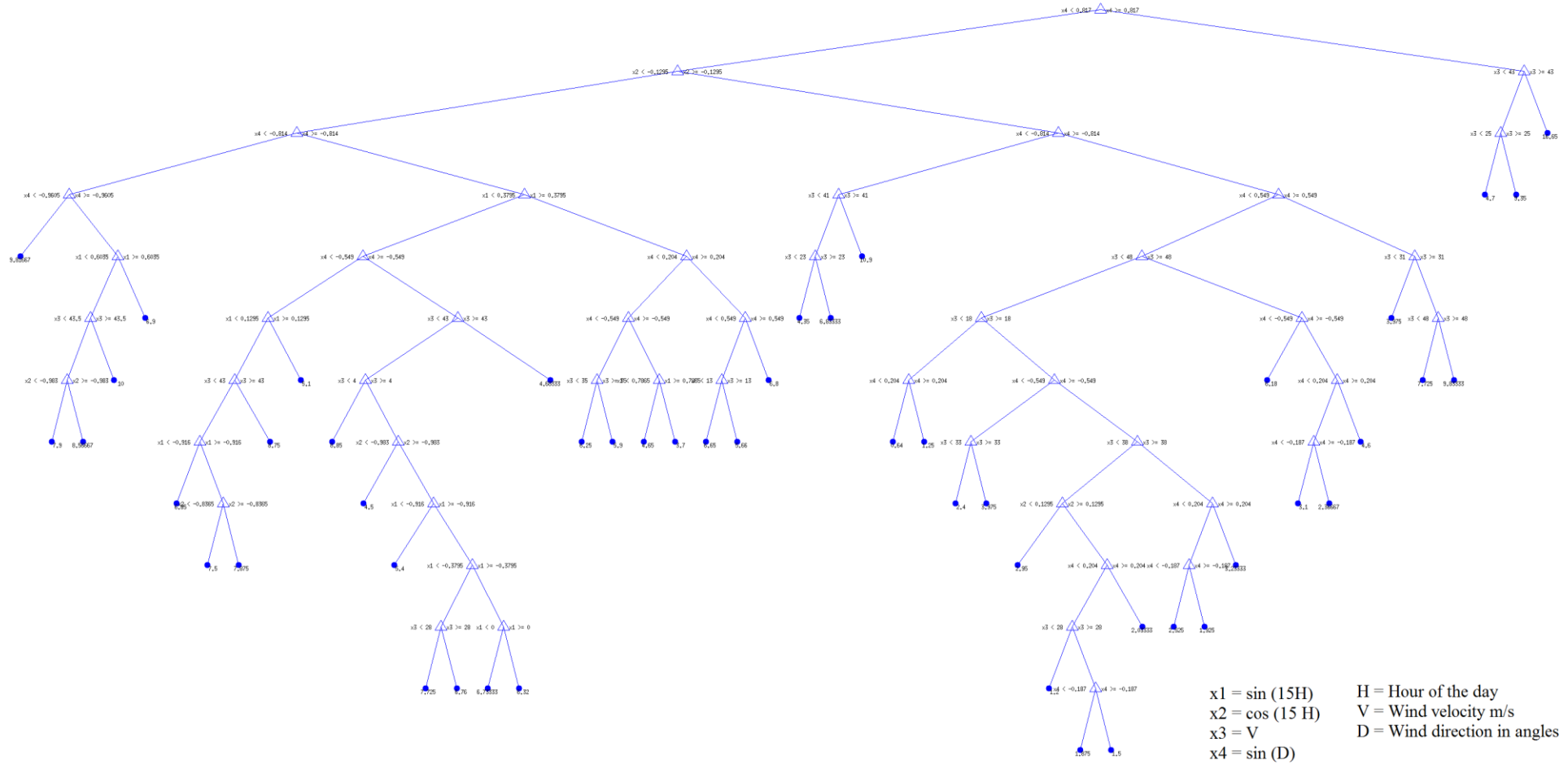
# Appendix B

## Regression trees (CART)

### B.1. GH\_ACH Tree of Regression



## B.2. SH\_ACH Tree of Regression



# Appendix C

## ACH prediction rule

### C.1. GH\_ACH Prediction Rule

ACH\_01 =  $9 * (\text{lt}(\sin(D), -0.960252) * \text{lt}(\sin(15 * H), 0.12941) * \text{lt}(\cos(15 * H), -0.12941))$   
ACH\_02 =  $6.95 * (\text{lt}(\sin(D), -0.960252) * \text{ge}(\sin(15 * H), 0.12941) * \text{lt}(\cos(15 * H), -0.12941))$   
ACH\_03 =  $4.7375 * (\text{lt}(V, 4.1) * \text{lt}(\sin(D), -0.813806) * \text{ge}(\cos(15 * H), -0.12941))$   
ACH\_04 =  $7.875 * (\text{ge}(V, 4.1) * \text{lt}(\sin(D), -0.813806) * \text{ge}(\cos(15 * H), -0.12941))$   
ACH\_05 =  $6.5375 * (\text{lt}(\cos(15 * H), -0.982963) * \text{ge}(\sin(D), -0.960252) * \text{lt}(\sin(15 * H), 0.12941) * \text{lt}(\cos(15 * H), -0.12941))$   
ACH\_06 =  $6.93333 * (\text{ge}(\sin(15 * H), 0.915976) * \text{ge}(\sin(D), -0.960252) * \text{ge}(\sin(15 * H), 0.12941) * \text{lt}(\cos(15 * H), -0.12941))$   
ACH\_07 =  $4.8 * (\text{ge}(\sin(15 * H), 0.982963) * \text{lt}(V, 4.8) * \text{ge}(\sin(D), -0.813806) * \text{ge}(\cos(15 * H), -0.12941))$   
ACH\_08 =  $4.9 * (\text{ge}(\sin(15 * H), 0.933013) * \text{ge}(V, 4.8) * \text{ge}(\sin(D), -0.813806) * \text{ge}(\cos(15 * H), -0.12941))$   
ACH\_09 =  $3.65714 * (\text{ge}(V, 4.35) * \text{ge}(\cos(15 * H), -0.982963) * \text{ge}(\sin(D), -0.960252) * \text{lt}(\sin(15 * H), 0.12941) * \text{lt}(\cos(15 * H), -0.12941))$   
ACH\_10 =  $9.73333 * (\text{lt}(\sin(D), -0.813806) * \text{lt}(\sin(15 * H), 0.915976) * \text{ge}(\sin(D), -0.960252) * \text{ge}(\sin(15 * H), 0.12941) * \text{lt}(\cos(15 * H), -0.12941))$   
ACH\_11 =  $5.64 * (\text{lt}(\sin(D), -0.813806) * \text{lt}(V, 4.35) * \text{ge}(\cos(15 * H), -0.982963) * \text{ge}(\sin(D), -0.960252) * \text{lt}(\sin(15 * H), 0.12941) * \text{lt}(\cos(15 * H), -0.12941))$   
ACH\_12 =  $8.05714 * (\text{lt}(\sin(15 * H), 0.37941) * \text{ge}(\sin(D), -0.813806) * \text{lt}(\sin(15 * H), 0.915976) * \text{ge}(\sin(D), -0.960252) * \text{ge}(\sin(15 * H), 0.12941) * \text{lt}(\cos(15 * H), -0.12941))$   
ACH\_13 =  $2.24 * (\text{lt}(\sin(D), -0.548919) * \text{lt}(\sin(D), -0.186639) * \text{lt}(\sin(15 * H), 0.933013) * \text{ge}(V, 4.8) * \text{ge}(\sin(D), -0.813806) * \text{ge}(\cos(15 * H), -0.12941))$   
ACH\_14 =  $1.46 * (\text{ge}(\sin(D), -0.548919) * \text{lt}(\sin(D), -0.186639) * \text{lt}(\sin(15 * H), 0.933013) * \text{ge}(V, 4.8) * \text{ge}(\sin(D), -0.813806) * \text{ge}(\cos(15 * H), -0.12941))$   
ACH\_15 =  $3.6 * (\text{ge}(V, 7.2) * \text{ge}(\sin(D), -0.186639) * \text{lt}(\sin(15 * H), 0.933013) * \text{ge}(V, 4.8) * \text{ge}(\sin(D), -0.813806) * \text{ge}(\cos(15 * H), -0.12941))$   
ACH\_16 =  $4.03333 * (\text{ge}(\cos(15 * H), -0.37941) * \text{ge}(\sin(D), -0.813806) * \text{lt}(V, 4.35) * \text{ge}(\cos(15 * H), -0.982963) * \text{ge}(\sin(D), -0.960252) * \text{lt}(\sin(15 * H), 0.12941) * \text{lt}(\cos(15 * H), -0.12941))$   
ACH\_17 =  $0.933333 * (\text{ge}(\sin(D), 0.548919) * \text{lt}(V, 2.3) * \text{lt}(V, 3.3) * \text{lt}(\sin(15 * H), 0.982963) * \text{lt}(V, 4.8) * \text{ge}(\sin(D), -0.813806) * \text{ge}(\cos(15 * H), -0.12941))$   
ACH\_18 =  $0.84 * (\text{lt}(\sin(D), -0.186639) * \text{ge}(V, 2.3) * \text{lt}(V, 3.3) * \text{lt}(\sin(15 * H), 0.982963) * \text{lt}(V, 4.8) * \text{ge}(\sin(D), -0.813806) * \text{ge}(\cos(15 * H), -0.12941))$   
ACH\_19 =  $1.3 * (\text{ge}(\sin(D), -0.186639) * \text{ge}(V, 2.3) * \text{lt}(V, 3.3) * \text{lt}(\sin(15 * H), 0.982963) * \text{lt}(V, 4.8) * \text{ge}(\sin(D), -0.813806) * \text{ge}(\cos(15 * H), -0.12941))$   
ACH\_20 =  $2.1 * (\text{lt}(\sin(15 * H), -0.982963) * \text{lt}(\sin(D), -0.186639) * \text{ge}(V, 3.3) * \text{lt}(\sin(15 * H), 0.982963) * \text{lt}(V, 4.8) * \text{ge}(\sin(D), -0.813806) * \text{ge}(\cos(15 * H), -0.12941))$   
ACH\_21 =  $2.225 * (\text{lt}(\sin(D), 0.204092) * \text{ge}(\sin(D), -0.186639) * \text{ge}(V, 3.3) * \text{lt}(\sin(15 * H), 0.982963) * \text{lt}(V, 4.8) * \text{ge}(\sin(D), -0.813806) * \text{ge}(\cos(15 * H), -0.12941))$   
ACH\_22 =  $2.86667 * (\text{lt}(\sin(D), 0.204092) * \text{lt}(V, 7.2) * \text{ge}(\sin(D), -0.186639) * \text{lt}(\sin(15 * H), 0.933013) * \text{ge}(V, 4.8) * \text{ge}(\sin(D), -0.813806) * \text{ge}(\cos(15 * H), -0.12941))$

$ACH_{23} = 2.2375 * (ge(\sin(D), 0.204092) * \text{lt}(V, 7.2) * ge(\sin(D), -0.186639) * \text{lt}(\sin(15 * H), 0.933013) * ge(V, 4.8) * ge(\sin(D), -0.813806) * ge(\cos(15 * H), -0.12941))$   
 $ACH_{24} = 5.1 * (\text{lt}(\sin(D), -0.548919) * \text{lt}(\cos(15 * H), -0.37941) * ge(\sin(D), -0.813806) * \text{lt}(V, 4.35) * ge(\cos(15 * H), -0.982963) * ge(\sin(D), -0.960252) * \text{lt}(\sin(15 * H), 0.12941) * \text{lt}(\cos(15 * H), -0.12941))$   
 $ACH_{25} = 9.3 * (\text{lt}(V, 1.3) * \text{lt}(V, 2.3) * ge(\sin(15 * H), 0.37941) * ge(\sin(D), -0.813806) * \text{lt}(\sin(15 * H), 0.915976) * ge(\sin(D), -0.960252) * ge(\sin(15 * H), 0.12941) * \text{lt}(\cos(15 * H), -0.12941))$   
 $ACH_{26} = 8.975 * (ge(V, 1.3) * \text{lt}(V, 2.3) * ge(\sin(15 * H), 0.37941) * ge(\sin(D), -0.813806) * \text{lt}(\sin(15 * H), 0.915976) * ge(\sin(D), -0.960252) * ge(\sin(15 * H), 0.12941) * \text{lt}(\cos(15 * H), -0.12941))$   
 $ACH_{27} = 8.23333 * (ge(\sin(D), 0.548919) * GE(V, 2.3) * ge(\sin(15 * H), 0.37941) * ge(\sin(D), -0.813806) * \text{lt}(\sin(15 * H), 0.915976) * ge(\sin(D), -0.960252) * ge(\sin(15 * H), 0.12941) * \text{lt}(\cos(15 * H), -0.12941))$   
 $ACH_{28} = 0.3 * (\text{lt}(V, 1.3) * \text{lt}(\sin(D), 0.548919) * \text{lt}(V, 2.3) * \text{lt}(V, 3.3) * \text{lt}(\sin(15 * H), 0.982963) * \text{lt}(V, 4.8) * ge(\sin(D), -0.813806) * ge(\cos(15 * H), -0.12941))$   
 $ACH_{29} = 0.714286 * (ge(V, 1.3) * \text{lt}(\sin(D), 0.548919) * \text{lt}(V, 2.3) * \text{lt}(V, 3.3) * \text{lt}(\sin(15 * H), 0.982963) * \text{lt}(V, 4.8) * ge(\sin(D), -0.813806) * ge(\cos(15 * H), -0.12941))$   
 $ACH_{30} = 1.3 * (\text{lt}(\sin(D), -0.548919) * ge(\sin(15 * H), -0.982963) * \text{lt}(\sin(D), -0.186639) * ge(V, 3.3) * \text{lt}(\sin(15 * H), 0.982963) * \text{lt}(\sin(15 * H), 0.982963) * ge(\sin(D), -0.813806) * ge(\cos(15 * H), -0.12941))$   
 $ACH_{31} = 1.04 * (ge(\sin(D), -0.548919) * ge(\sin(15 * H), -0.982963) * \text{lt}(\sin(D), -0.186639) * ge(V, 3.3) * \text{lt}(\sin(15 * H), 0.982963) * \text{lt}(V, 4.8) * ge(\sin(D), -0.813806) * ge(\cos(15 * H), -0.12941))$   
 $ACH_{32} = 1.37143 * (\text{lt}(\sin(D), 0.817145) * ge(\sin(D), 0.204092) * ge(\sin(D), -0.186639) * ge(V, 3.3) * \text{lt}(\sin(15 * H), 0.982963) * \text{lt}(V, 4.8) * ge(\sin(D), -0.813806) * ge(\cos(15 * H), -0.12941))$   
 $ACH_{33} = 1.7 * (ge(\sin(D), 0.817145) * ge(\sin(D), 0.204092) * ge(\sin(D), -0.186639) * ge(V, 3.3) * \text{lt}(\sin(15 * H), 0.982963) * \text{lt}(V, 4.8) * ge(\sin(D), -0.813806) * ge(\cos(15 * H), -0.12941))$   
 $ACH_{34} = 5.1 * (\text{lt}(V, 2.3) * ge(\sin(D), -0.548919) * \text{lt}(\cos(15 * H), -0.37941) * ge(\sin(D), -0.813806) * \text{lt}(V, 4.35) * ge(\cos(15 * H), -0.982963) * ge(\sin(D), -0.960252) * \text{lt}(\sin(15 * H), 0.12941) * \text{lt}(\cos(15 * H), -0.12941))$   
 $ACH_{35} = 8.1 * (ge(V, 6.1) * \text{lt}(\sin(D), 0.548919) * ge(V, 2.3) * ge(\sin(15 * H), 0.37941) * ge(\sin(D), -0.813806) * \text{lt}(\sin(15 * H), 0.915976) * ge(\sin(D), -0.960252) * ge(\sin(15 * H), 0.12941) * \text{lt}(\cos(15 * H), -0.12941))$   
 $ACH_{36} = 4.325 * (\text{lt}(\sin(D), 0.204092) * GE(V, 2.3) * ge(\sin(D), -0.548919) * \text{lt}(\cos(15 * H), -0.37941) * ge(\sin(D), -0.813806) * \text{lt}(V, 4.35) * ge(\cos(15 * H), -0.982963) * ge(\sin(D), -0.960252) * \text{lt}(\sin(15 * H), 0.12941) * \text{lt}(\cos(15 * H), -0.12941))$   
 $ACH_{37} = 5.5 * (ge(\sin(D), 0.204092) * ge(V, 2.3) * ge(\sin(D), -0.548919) * \text{lt}(\cos(15 * H), -0.37941) * ge(\sin(D), -0.813806) * \text{lt}(V, 4.35) * ge(\cos(15 * H), -0.982963) * ge(\sin(D), -0.960252) * \text{lt}(\sin(15 * H), 0.12941) * \text{lt}(\cos(15 * H), -0.12941))$   
 $ACH_{38} = 8.44 * (\text{lt}(\sin(D), -0.186639) * \text{lt}(V, 6.1) * \text{lt}(\sin(D), 0.548919) * ge(V, 2.3) * ge(\sin(15 * H), 0.37941) * ge(\sin(D), -0.813806) * \text{lt}(\sin(15 * H), 0.915976) * ge(\sin(D), -0.960252) * ge(\sin(15 * H), 0.12941) * \text{lt}(\cos(15 * H), -0.12941))$   
 $ACH_{39} = 8.7 * (ge(\sin(D), -0.186639) * \text{lt}(V, 6.1) * \text{lt}(\sin(D), 0.548919) * ge(V, 2.3) * ge(\sin(15 * H), 0.37941) * ge(\sin(D), -0.813806) * \text{lt}(\sin(15 * H), 0.915976) * ge(\sin(D), -0.960252) * ge(\sin(15 * H), 0.12941) * \text{lt}(\cos(15 * H), -0.12941))$   
 $ACH = (ge(T, 20) * \text{lt}(T, 26)) * (ACH_{01} + ACH_{02} + ACH_{03} + ACH_{04} + ACH_{05} + ACH_{06} + ACH_{07} + ACH_{08} + ACH_{09} + ACH_{10} + ACH_{11} + ACH_{12} + ACH_{13} + ACH_{14} + ACH_{15} + ACH_{16} + ACH_{17} + ACH_{18} + ACH_{19} + ACH_{20} + ACH_{21} + ACH_{22} + ACH_{23} + ACH_{24} + ACH_{25} + ACH_{26} + ACH_{27} + ACH_{28} + ACH_{29} + ACH_{30} + ACH_{31} + ACH_{32} + ACH_{33} + ACH_{34} + ACH_{35} + ACH_{36} + ACH_{37} + ACH_{38} + ACH_{39})$



$ACH\_SH\_27 = 6.83333 * (\text{ge}(V,23) * \text{lt}(V,41) * \text{lt}(\sin(D), -0.814) * \text{ge}(\cos(15 * H), -0.1295) * \text{lt}(\sin(D), 0.817))$   
 $ACH\_SH\_28 = 10.9 * (\text{ge}(V,41) * \text{lt}(\sin(D), -0.814) * \text{ge}(\cos(15 * H), -0.1295) * \text{lt}(\sin(D), 0.817))$   
 $ACH\_SH\_29 = 1.875 * (\text{lt}(\sin(D), -$   
 $0.187) * \text{ge}(V,28) * \text{lt}(\sin(D), 0.204) * \text{ge}(\cos(15 * H), 0.1295) * \text{lt}(V,38) * \text{ge}(\sin(D), -$   
 $0.549) * \text{ge}(V,18) * \text{lt}(V,48) * \text{lt}(\sin(D), 0.549) * \text{ge}(\sin(D), -0.814) * \text{ge}(\cos(15 * H), -0.1295) * \text{lt}(\sin(D), 0.817))$   
 $ACH\_SH\_30 = 1.5 * (\text{ge}(\sin(D), -$   
 $0.187) * \text{ge}(V,28) * \text{lt}(\sin(D), 0.204) * \text{ge}(\cos(15 * H), 0.1295) * \text{lt}(V,38) * \text{ge}(\sin(D), -$   
 $0.549) * \text{ge}(V,18) * \text{lt}(V,48) * \text{lt}(\sin(D), 0.549) * \text{ge}(\sin(D), -0.814) * \text{ge}(\cos(15 * H), -0.1295) * \text{lt}(\sin(D), 0.817))$   
 $ACH\_SH\_31 = 1.2 * (\text{lt}(V,28) * \text{lt}(\sin(D), 0.204) * \text{ge}(\cos(15 * H), 0.1295) * \text{lt}(V,38) * \text{ge}(\sin(D), -$   
 $0.549) * \text{ge}(V,18) * \text{lt}(V,48) * \text{lt}(\sin(D), 0.549) * \text{ge}(\sin(D), -0.814) * \text{ge}(\cos(15 * H), -0.1295) * \text{lt}(\sin(D), 0.817))$   
 $ACH\_SH\_32 = 2.03333 * (\text{ge}(\sin(D), 0.204) * \text{ge}(\cos(15 * H), 0.1295) * \text{lt}(V,38) * \text{ge}(\sin(D), -$   
 $0.549) * \text{ge}(V,18) * \text{lt}(V,48) * \text{lt}(\sin(D), 0.549) * \text{ge}(\sin(D), -0.814) * \text{ge}(\cos(15 * H), -0.1295) * \text{lt}(\sin(D), 0.817))$   
 $ACH\_SH\_33 = 2.95 * (\text{lt}(\cos(15 * H), 0.1295) * \text{lt}(V,38) * \text{ge}(\sin(D), -$   
 $0.549) * \text{ge}(V,18) * \text{lt}(V,48) * \text{lt}(\sin(D), 0.549) * \text{ge}(\sin(D), -0.814) * \text{ge}(\cos(15 * H), -0.1295) * \text{lt}(\sin(D), 0.817))$   
 $ACH\_SH\_34 = 2.525 * (\text{lt}(\sin(D), -0.187) * \text{lt}(\sin(D), 0.204) * \text{ge}(V,38) * \text{ge}(\sin(D), -$   
 $0.549) * \text{ge}(V,18) * \text{lt}(V,48) * \text{lt}(\sin(D), 0.549) * \text{ge}(\sin(D), -0.814) * \text{ge}(\cos(15 * H), -0.1295) * \text{lt}(\sin(D), 0.817))$   
 $ACH\_SH\_35 = 1.925 * (\text{ge}(\sin(D), -0.187) * \text{lt}(\sin(D), 0.204) * \text{ge}(V,38) * \text{ge}(\sin(D), -$   
 $0.549) * \text{ge}(V,18) * \text{lt}(V,48) * \text{lt}(\sin(D), 0.549) * \text{ge}(\sin(D), -0.814) * \text{ge}(\cos(15 * H), -0.1295) * \text{lt}(\sin(D), 0.817))$   
 $ACH\_SH\_36 = 3.23333 * (\text{ge}(\sin(D), 0.204) * \text{ge}(V,38) * \text{ge}(\sin(D), -$   
 $0.549) * \text{ge}(V,18) * \text{lt}(V,48) * \text{lt}(\sin(D), 0.549) * \text{ge}(\sin(D), -0.814) * \text{ge}(\cos(15 * H), -0.1295) * \text{lt}(\sin(D), 0.817))$   
 $ACH\_SH\_37 = 2.4 * (\text{lt}(V,33) * \text{lt}(\sin(D), -0.549) * \text{ge}(V,18) * \text{lt}(V,48) * \text{lt}(\sin(D), 0.549) * \text{ge}(\sin(D), -$   
 $0.814) * \text{ge}(\cos(15 * H), -0.1295) * \text{lt}(\sin(D), 0.817))$   
 $ACH\_SH\_38 = 3.975 * (\text{ge}(V,33) * \text{lt}(\sin(D), -0.549) * \text{ge}(V,18) * \text{lt}(V,48) * \text{lt}(\sin(D), 0.549) * \text{ge}(\sin(D), -$   
 $0.814) * \text{ge}(\cos(15 * H), -0.1295) * \text{lt}(\sin(D), 0.817))$   
 $ACH\_SH\_39 = 0.64 * (\text{lt}(\sin(D), 0.204) * \text{lt}(V,18) * \text{lt}(V,48) * \text{lt}(\sin(D), 0.549) * \text{ge}(\sin(D), -0.814) * \text{ge}(\cos(15 * H), -$   
 $0.1295) * \text{lt}(\sin(D), 0.817))$   
 $ACH\_SH\_40 = 1.25 * (\text{ge}(\sin(D), 0.204) * \text{lt}(V,18) * \text{lt}(V,48) * \text{lt}(\sin(D), 0.549) * \text{ge}(\sin(D), -0.814) * \text{ge}(\cos(15 * H), -$   
 $0.1295) * \text{lt}(\sin(D), 0.817))$   
 $ACH\_SH\_41 = 3.1 * (\text{lt}(\sin(D), -0.187) * \text{lt}(\sin(D), 0.204) * \text{ge}(\sin(D), -$   
 $0.549) * \text{ge}(V,48) * \text{lt}(\sin(D), 0.549) * \text{ge}(\sin(D), -0.814) * \text{ge}(\cos(15 * H), -0.1295) * \text{lt}(\sin(D), 0.817))$   
 $ACH\_SH\_42 = 2.36667 * (\text{ge}(\sin(D), -0.187) * \text{lt}(\sin(D), 0.204) * \text{ge}(\sin(D), -$   
 $0.549) * \text{ge}(V,48) * \text{lt}(\sin(D), 0.549) * \text{ge}(\sin(D), -0.814) * \text{ge}(\cos(15 * H), -0.1295) * \text{lt}(\sin(D), 0.817))$   
 $ACH\_SH\_43 = 4.6 * (\text{ge}(\sin(D), 0.204) * \text{ge}(\sin(D), -0.549) * \text{ge}(V,48) * \text{lt}(\sin(D), 0.549) * \text{ge}(\sin(D), -$   
 $0.814) * \text{ge}(\cos(15 * H), -0.1295) * \text{lt}(\sin(D), 0.817))$   
 $ACH\_SH\_44 = 6.18 * (\text{lt}(\sin(D), -0.549) * \text{ge}(V,48) * \text{lt}(\sin(D), 0.549) * \text{ge}(\sin(D), -0.814) * \text{ge}(\cos(15 * H), -$   
 $0.1295) * \text{lt}(\sin(D), 0.817))$   
 $ACH\_SH\_45 = 7.725 * (\text{lt}(V,48) * \text{ge}(V,31) * \text{ge}(\sin(D), 0.549) * \text{ge}(\sin(D), -0.814) * \text{ge}(\cos(15 * H), -$   
 $0.1295) * \text{lt}(\sin(D), 0.817))$   
 $ACH\_SH\_46 = 3.975 * (\text{lt}(V,31) * \text{ge}(\sin(D), 0.549) * \text{ge}(\sin(D), -0.814) * \text{ge}(\cos(15 * H), -$   
 $0.1295) * \text{lt}(\sin(D), 0.817))$   
 $ACH\_SH\_47 = 9.83333 * (\text{ge}(V,48) * \text{ge}(V,31) * \text{ge}(\sin(D), 0.549) * \text{ge}(\sin(D), -0.814) * \text{ge}(\cos(15 * H), -$   
 $0.1295) * \text{lt}(\sin(D), 0.817))$   
 $ACH\_SH\_48 = 4.7 * (\text{lt}(V,25) * \text{lt}(V,43) * \text{ge}(\sin(D), 0.817))$   
 $ACH\_SH\_49 = 9.35 * (\text{ge}(V,25) * \text{lt}(V,43) * \text{ge}(\sin(D), 0.817))$   
 $ACH\_SH\_50 = 16.65 * (\text{ge}(V,43) * \text{ge}(\sin(D), 0.817))$   
 $ACH\_SH =$   
 $(\text{ge}(T,20) * \text{lt}(T,26)) * (ACH\_SH\_01 + ACH\_SH\_02 + ACH\_SH\_03 + ACH\_SH\_04 + ACH\_SH\_05 + ACH\_SH\_06$   
 $+ ACH\_SH\_07 + ACH\_SH\_08 + ACH\_SH\_09 + ACH\_SH\_10 + ACH\_SH\_11 + ACH\_SH\_12 + ACH\_SH\_13 + ACH\_SH\_14 + ACH\_SH\_15 + ACH\_SH\_16 + ACH\_SH\_17 + ACH\_SH\_18 + ACH\_SH\_19 + ACH\_SH\_20 + ACH\_SH\_21 + ACH\_SH\_22 + ACH\_SH\_23 + ACH\_SH\_24 + ACH\_SH\_25 + ACH\_SH\_26 + ACH\_SH\_27 + ACH\_SH\_28 + ACH\_SH\_29 + ACH\_SH\_30 + ACH\_SH\_31 + ACH\_SH\_32 + ACH\_SH\_33 + ACH\_SH\_34 + ACH\_SH\_35 + ACH\_SH\_36 + ACH\_SH\_37 + ACH\_SH\_38 + ACH\_SH\_39 + ACH\_SH\_40 + ACH\_SH\_41 + ACH\_SH\_42 + ACH\_SH\_43 + ACH\_SH\_44 + ACH\_SH\_45 + ACH\_SH\_46 + ACH\_SH\_47 + ACH\_SH\_48 + ACH\_SH\_49 + ACH\_SH\_50)$

